# Molecular Drivers of Aerobic Glycolysis in the Mammalian Retina

Cameron David Haydinger

A thesis submitted in fulfilment of the requirements of the degree of Doctor of Philosophy (Science)

July 2022

Discipline of Molecular and Biomedical Science

School of Biological Sciences


THE UNIVERSITY of ADELAIDE

# Contents

# Abstract

The retinas of various mammalian species exhibit aerobic glycolysis, a metabolic scheme wherein glucose is catabolised to lactate which is excreted, rather than being oxidised to carbon dioxide in mitochondria, despite ample oxygen availability. The retina is also uncommonly vulnerable to diseases that affect its supply of glucose and oxygen, and these diseases cause significant human morbidity. Recent studies have demonstrated the roles of key enzymes in the glycolytic pathway in facilitating aerobic glycolysis in the retina, but very little is known about the transcriptional programs or signalling pathways that drive the expression and activity of these enzymes. Improved understanding of the molecular mechanisms that drive aerobic glycolysis in the retina will inform the development of therapeutic strategies for retinal diseases in which metabolism is dysfunctional.

The primary aim of this project was to elucidate molecular drivers of aerobic glycolysis in the mammalian retina. Initial work focussed on Müller glial cells. Treatment of the rMC-1 immortalised rat Müller glial cell line with small-molecule inhibitors of phosphoinositide 3-kinase (PI3K), the mitogen-activated protein kinase kinase MEK1 or the small GTPase Rac1 was found to decrease lactate production.

Over the course of the project, it became increasingly evident that photoreceptors, rather than Müller cells, were responsible for most lactate production in the mammalian retina *in vivo*. Published RNA-sequencing data from photoreceptors and Müller cells were analysed for expression of genes involved in glucose metabolism and the findings corroborated this perspective and shed light on novel differences at the RNA level between the metabolism of these two cell types.

Later work utilised whole rat retinal explants as an experimental model. Small-molecule inhibitors were used to treat explants. Several proteins and pathways were investigated, including those where an effect was observed in rMC-1 cells, but no pathway was identified that unambiguously drove lactate production in explants. The results nevertheless ruled out many likely candidate pathways. New hypotheses are proposed based on analyses of RNA-seq data, and ideas regarding the fundamental reason for aerobic glycolysis in the retina, which is an open question, are discussed in detail.

# Declaration

I certify that this work contains no material which has been accepted for the award of any other degree or diploma in my name, in any university or other tertiary institution and, to the best of my knowledge and belief, contains no material previously published or written by another person, except where due reference has been made in the text. In addition, I certify that no part of this work will, in the future, be used in a submission in my name, for any other degree or diploma in any university or other tertiary institution without the prior approval of the University of Adelaide and where applicable, any partner institution responsible for the joint-award of this degree.

I acknowledge that copyright of published works contained within this thesis resides with the copyright holder(s) of those works.

I also give permission for the digital version of my thesis to be made available on the web, via the University's digital research repository, the Library Search and also through web search engines, unless permission has been granted by the University to restrict access for a period of time.

I acknowledge the support I have received for my research through the provision of an Australian Government Research Training Program Scholarship.

09/07/2022

Cameron Haydinger Date

# Acknowledgements

Thank you to my supervisor Dan Peet for taking me on as a student and providing an amazing environment in which to do a PhD as well as a thoroughly interesting project. I greatly appreciate the balance of freedom and direction you offered. Thank you to my co-supervisors Robert Casson and Murray Whitelaw for advice, resources and suggestions on project direction and experiments. I could not have asked for a more knowledgeable and supportive group of supervisors.

Thank you to past and present members of the Peet Lab for all being fantastic people who made the Peet lab such a great place to work. Thanks Ali for being so supportive and generally amazing – the lab has a very bright future, Dave H for the retina biology deep-dives and for taking the project to new and exciting places, Ice for the excellent initial work on the project and for teaching me many lab techniques, and Nat, Jay, Josh (thanks for getting us into bouldering), Mogana, Josiah, Alex, Luke, Nick, Carla and Rachel for the help and advice with the project, and the fun times.

Thank you to past and present members of the Whitelaw lab: Joe for the highly productive, strictly scientific discussions, Tim for being boisterous but generally benevolent, and Alexis, Emily, Adrienne, Dave B, Akhil, Yesha and Toan for the helpful advice and suggestions, and the fun times.

Thank you to the members of the Casson lab, in particular John and Teresa, for their willingness to share their knowledge on all things retina, and their willingness to teach and share equipment and resources.

Thank you to laboratory animal services, in particular Rosanna, for their assistance with the scavenging of rat retinal explants.

Thank you to others in the MLS building: Michael, Mel, Nick, Kylie, Byron, Rosa, Emily, Brooke, Tom, Ornella, Brandon, Simon and all others who helped with the project in various ways and who made the MLS building a productive, fun and social place to work.

Finally, and importantly, thank you to my family, especially my parents for their invaluable support throughout the PhD.

# List of publications arising from this thesis

**Paper 1**: Included in body of introduction

Haydinger CD, Kittipassorn T, Peet DJ. Power to see-Drivers of aerobic glycolysis in the mammalian retina: A review. Clin Exp Ophthalmol. 2020 Nov;48(8):1057-1071. doi: 10.1111/ceo.13833. Epub 2020 Aug 16. PMID: 32710505.

**Paper 2**: Included in Appendix 2

Kittipassorn T, Haydinger CD, Wood JPM, Mammone T, Casson RJ, Peet DJ. Characterization of the novel spontaneously immortalized rat Müller cell line SIRMu-1. Exp Eye Res. 2019 Apr;181:127-135. doi: 10.1016/j.exer.2019.01.013. Epub 2019 Jan 21. PMID: 30677389.

**Paper 3**: Included in Appendix 3

Kittipassorn T, Haydinger CD, Wood JPM, Mammone T, Casson RJ, Peet DJ. RNA sequencing data of cultured primary rat Müller cells, the spontaneously immortalized rat Müller cell line, SIRMu-1, and the SV40-transformed rat Müller cell line, rMC-1. Data Brief. 2019 Mar 7;23:103721. doi: 10.1016/j.dib.2019.103721. PMID: 31372389; PMCID: PMC6660449.

# Abbreviations

| | |
|---|---|
| ADP | Adenosine diphosphate |
| AMD | Age-related macular degeneration |
| ANLS | Astrocyte-neuron lactate shuttle |
| ATP | Adenosine triphosphate |
| cGMP | Cyclic guanidine monophosphate |
| DTT | Dithiothreitol |
| DMEM | Dulbecco's modified Eagle's medium |
| DMSO | Dimethyl sulfoxide |
| ECAR | Extracellular acidification rate |
| EDTA | Ethylenediaminetetraacetic acid |
| ETC | Electron transport chain |
| EtOH | Ethanol |
| ERK | Extracellular signal-regulated kinase |
| ERR/ERRβ/Esrrb | Estrogen-related receptor (beta isoform) |
| ERRE | Estrogen-related response element |
| FACS | Fluorescence-activated cell sorting |
| FAD/$FADH_2$ | Flavine adenine dinucleotide (oxidised/reduced, respectively) |
| FBS | Foetal bovine serum |
| FCCP | Carbonyl cyanide-p-trifluoromethoxyphenylhydrazone |
| FGF2 | Fibroblast growth factor 2 (basic fibroblast growth factor) |
| FGFR | Fibroblast growth factor receptor |
| FRS2 | Fibroblast receptor substrate 2 |
| GCL | Ganglion cell layer |
| glycoPER | Proton efflux rate attributable to glycolysis |
| HBSS | Hank's balanced salt solution |
| HIF | Hypoxia-inducible factor |
| HK/HK1/HK2 | Hexokinase (isoform 1 or 2) |
| HRP | Horseradish peroxidase |
| INL | Inner nuclear layer |

| | |
|---|---|
| IPL | Inner plexiform layer |
| LDH/LDHA/LDHB | Lactate dehydrogenase (subunit A or B) |
| MAS | Malate aspartate shuttle |
| MEK | Mitogen-activated protein kinase kinase (also abbreviated as MAPKK) |
| MEM | Minimal essential medium |
| mRNA | Messenger ribonucleic acid |
| mTOR | Mammalian target of rapamycin |
| $NAD^+$/NADH | Nicotinamide adenine dinucleotide (oxidised/reduced, respectively) |
| OCR | Oxygen consumption rate |
| ONL | Outer nuclear layer |
| OPL | Outer plexiform layer |
| OXPHOS | Oxidative phosphorylation |
| PBS | Phosphate buffered saline |
| PBS-T | Phosphate buffered saline with tween-20 |
| PER | Proton efflux rate |
| PI3K | Phosphoinositide 3-kinase |
| PK/PKM/PKM2 | Pyruvate kinase / PK muscle isoform / PKM isoform 2 |
| PMSF | Phenylmethylsulphonyl fluoride |
| rpm | Revolutions per minute |
| RPE | Retinal pigment epithelium |
| RT | Room temperature |
| SD | Standard deviation |
| SDS | Sodium dodecyl sulphate |
| SEM | Standard error of the mean |
| shRNA | Short hairpin ribonucleic acid |
| SV40 | Simian virus 40 |
| TMM | Trimmed mean of M-values |
| TCA cycle | Tricarboxylic acid cycle/ Krebs cycle / Citric acid cycle |
| VEGF | Vascular endothelial growth factor |
| Wnt | Wingless/Int-1 |

# 1. Introduction

# 1.1 Overview

The retina is a complex neural tissue, responsible for the absorption of light and initial stages of visual processing, that lines the inner surface at the back of the eye. It is an exceptionally energy-demanding tissue in terms of both ATP consumption and macromolecular biosynthesis; demand which is met by rapid consumption of both glucose and oxygen[4-6]. The metabolic requirements of the retina have been likened to those of cancer cells, and it is interesting that the mammalian retina is one of few non-proliferative physiological tissues to predominantly catabolise glucose via aerobic glycolysis, an enigmatic type of metabolism common in cancer cells and other proliferating cells[6-10]. Studies using retinal explants have demonstrated that glucose deprivation and glycolytic inhibition cause rapid loss of electrical function, and cell death[6,10-12]. In addition, there is mounting evidence to implicate metabolic dysfunction, either primary or as a secondary consequence of ischemia, as a unifying aspect of the pathology of diverse major retinal diseases including retinitis pigmentosa[13,14], age-related macular degeneration[15,16], glaucoma[17,18] and diabetic retinopathy[19]. Treatments for these diseases are often inadequate to prevent damage to or loss of vision. Current understanding of retinal glucose metabolism, in particular the fundamental reason for aerobic glycolysis and the molecular pathways that drive aerobic glycolysis in the retina, is inadequate to develop targeted treatments that modulate metabolism. The aim of this project was therefore to elucidate molecular drivers of aerobic glycolysis in the mammalian retina.

# 1.2 Glucose metabolism

## *Glycolysis and oxidative phosphorylation*

Glycolysis is a series of cytoplasmic enzyme-catalysed reactions that results in the breakdown one mole of glucose to two moles of pyruvate for the purpose of generating ATP[20]. Alone, it generates, on net, two moles of ATP and two moles of NADH per mole of glucose (Figure 1A). In most cells, when oxygen is available, pyruvate is imported into the mitochondrial matrix where it is sequentially oxidised to $CO_2$ in the tricarboxylic acid (TCA) cycle, producing ATP or GTP, NADH and $FADH_2$. The NADH and $FADH_2$ pass electrons to complex I and complex II of the electron transport chain (ETC), respectively, in the inner mitochondrial membrane. In the ETC, electrons are transferred sequentially through a series of acceptors of increasing electron affinity, finally reducing molecular oxygen to $H_2O$. An electrochemical proton gradient is generated across the inner mitochondrial membrane as a result of these exergonic reactions. The potential energy of the gradient is captured by the phosphorylation of ADP to ATP as protons return from the intermembrane space to the matrix through $F_0F_1$ ATP

synthase. This process of ATP generation through the complete oxidation of pyruvate to $CO_2$ is termed oxidative phosphorylation (OXPHOS) (Figure 1B). Including the ATP from glycolysis, the whole process yields approximately 30-32 moles of ATP per mole of glucose fully oxidised. Note that the NADH produced by glycolysis in the cytoplasm cannot cross the inner mitochondrial membrane to pass electrons directly to the ETC. Instead, the malate-aspartate shuttle and the glycerol phosphate shuttle indirectly transfer reducing equivalents into mitochondria via intermediates.

## *Anaerobic glycolysis and aerobic glycolysis*

Under physiological hypoxia (when oxygen demand exceeds supply), oxygen becomes limiting as a final electron acceptor in the ETC, leading to insufficient oxidation of mitochondrial NADH to support ATP production by OXPHOS. In this case, cytosolic pyruvate is reduced to lactate, with NADH oxidised to $NAD^+$, by lactate dehydrogenase (LDH), with the $NAD^+$ produced enabling glycolysis to continue. Lactate is then exported from the cell as waste, although it can be taken up and oxidised to produce energy in other cells. This is termed anaerobic glycolysis and yields only two moles of ATP per mole of glucose. Curiously, in some cells, usually highly proliferative cells such as cancer cells[7,9] and many cell types of the immune system[21-24], most pyruvate produced by glycolysis is reduced to lactate despite adequate oxygen availability to support OXPHOS. This is termed aerobic glycolysis or, eponymously, the Warburg effect[25]. Warburg's paradigm-shifting findings regarding glucose metabolism in proliferating cells led to his hypothesis that defective respiration caused aerobic glycolysis and cancer[25,26], but it is now accepted that not all cancer cells undertake aerobic glycolysis (although many do) and most cells that undertake aerobic glycolysis have functional mitochondria[25,27-34]. Rather than a complete switch from OXPHOS to glycolysis, in most cases, aerobic glycolysis involves increased glucose uptake and conversion of pyruvate to lactate in the presence of continued respiration.

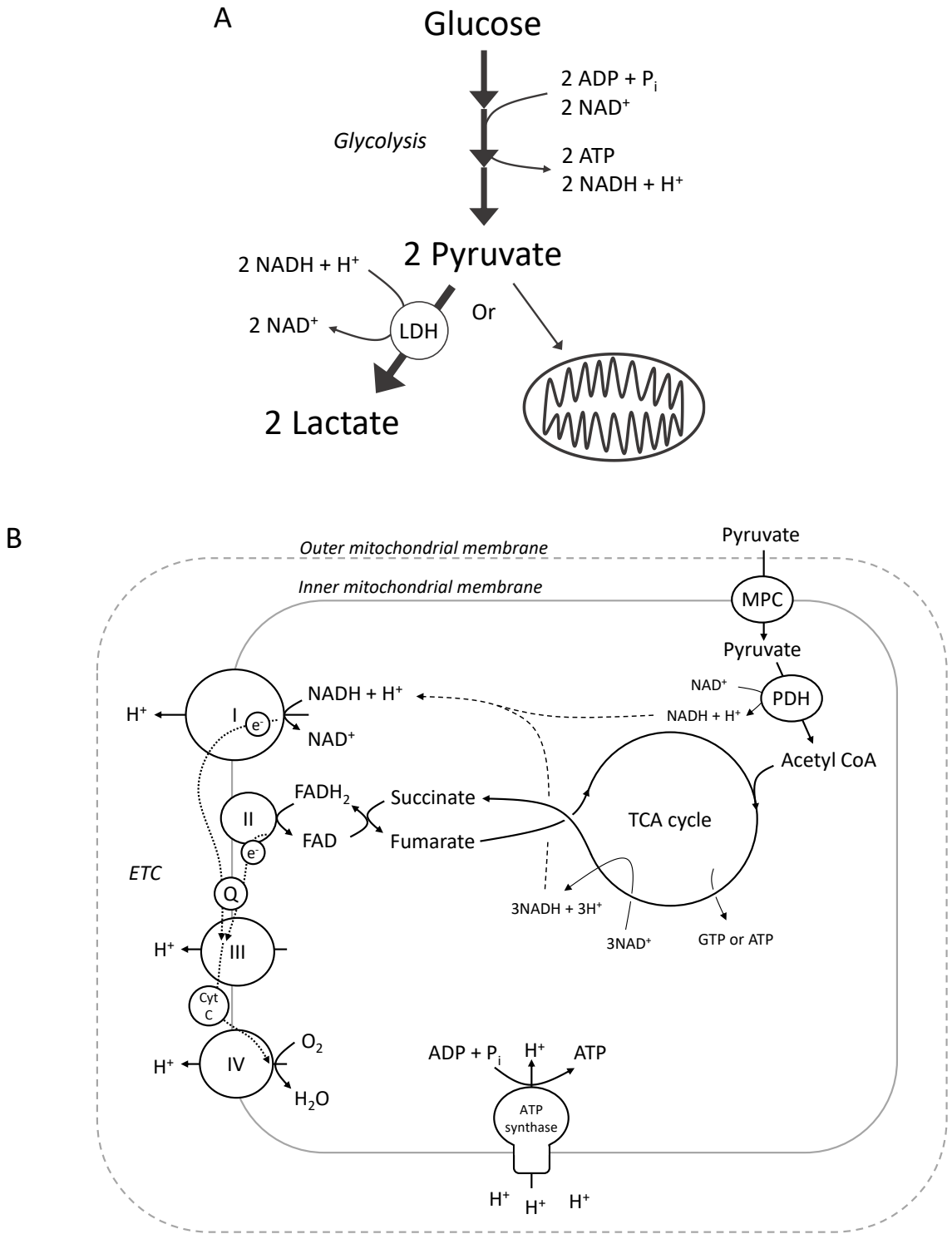


**Figure 1: Pathways of glucose catabolism. A.** Glycolysis occurs in the cytoplasm and results in catabolism of one mole of glucose to two moles of pyruvate. Pyruvate is usually imported into mitochondria, but in the case of either anerobic glycolysis or aerobic glycolysis (the Warburg effect) it is mostly converted to lactate and exported from the cell. **B.** In oxidative phosphorylation (OXPHOS), pyruvate enters mitochondria where it fuels the tricarboxylic acid (TCA) cycle. Via the electron transport chain (ETC), reducing equivalents power generation of a proton gradient across the inner mitochondrial membrane (IMM). ATP synthase leverages the energy of the gradient to phosphorylate ADP to ATP. LDH: Lactate dehydrogenase, MPC: Mitochondrial pyruvate carrier, PDH: Pyruvate dehydrogenase, Q: Coenzyme Q, Cyt C: Cytochrome C.

The reasons why cells undertake aerobic glycolysis are incompletely understood, although many hypotheses have been proposed[35-37]. Among the most prevalent is the idea that high flux through glycolysis supports pools of glycolytic intermediates that can be readily syphoned into pathways for the synthesis of macromolecular precursors such as nucleotides, amino acids and triglycerides[37]. This idea is contested, however, with evidence indicating that only a minor proportion of biomass derives from glucose in at least some cell types that undertake aerobic glycolysis[38]. Another proposed reason is that ATP can be produced more rapidly by aerobic glycolysis than by oxidative phosphorylation despite its relative inefficiency in terms of the amount of ATP produced per mole of glucose, which may allow cancer cells to operate ATP-demanding ion and substrate transporters at high rates[39,40]. In addition, in the context of cancer, the acidic environment promoted by aerobic glycolysis is proposed to modulate immune responses and advantage the development and growth of cancer cells[36,41]. A very recent proposal suggests that aerobic glycolysis reflects a metabolic state in which $NAD^+$ demand outweighs the requirement for ATP hydrolysis[42]. Hypotheses regarding the reason for aerobic glycolysis specifically in the retina are discussed in detail in Chapter 7.

## *1.3 The retina*

### *Basic structure and metabolism*

The retina comprises three neuronal layers separated by two synaptic layers, and its constituent cell classes and general structure are broadly conserved among vertebrates[43]. The side of the retina nearest incoming light, adjacent to the vitreous humour which fills the eye, is termed the inner retina. The side furthest incoming light is termed the outer retina. The outer nuclear layer (ONL) contains the outermost cells of the retina, the photoreceptors (Figure 2A). These specialised neurons transmit neurochemical signals in response to light. In the synaptic outer plexiform layer (OPL), signals are received by secondary neurons, namely bipolar cells and horizontal cells. Bipolar cells are responsible for radial transmission whereas horizontal cells mediate lateral communication. The somas of these cell types are situated in the inner nuclear layer (INL). Bipolar cells synapse onto retinal ganglion cells in the inner plexiform layer (IPL). In this layer, amacrine cells mediate lateral communication. The ganglion cell bodies form the ganglion cell layer (GCL), and their axons traverse the innermost surface of the retina, convening at a point to form the optic nerve, which transmits to the brain. The major type of glial cell in the retina is the Müller cell, which spans all layers of the retina.

Photoreceptors and Müller cells, in separate hypotheses, have each been proposed to be responsible for the major portion of aerobic glycolysis in the retina[44,45]. Photoreceptors are the most energetically

demanding retinal cell type and the classical perspective was therefore that they consume most glucose and are largely responsible for retinal aerobic glycolysis[45]. However, an alternative hypothesis proposed that Müller cells are responsible for the major portion of aerobic glycolysis in order to provide lactate as a metabolic substrate to photoreceptors[44,46]. The latter hypothesis had widespread (although not unanimous[45]) support during the early stages of this project[46-49], but more recent studies favour the classical perspective[14,50-54]. Photoreceptors and Müller cells were therefore both of particular focus in this project due to their proposed roles in retinal aerobic glycolysis, so these cell types are reviewed in detail below. General introductions and summaries of key functions for these two specific cell types are provided, then metabolism is discussed in context of their known roles.

## *Photoreceptors*

Photoreceptors are classified into two broad types, rods and cones. Rods are highly photosensitive. Specialised for low-light vision, they can signal the detection of even a single photon. Cones facilitate high-acuity vision in bright light. In the retinas of most mammals, including all species pertinent to this work, rods far outnumber cones. They comprise over 95% of photoreceptors in human and mouse retinas[55]. The proportions of photoreceptor types vary by region within the retina, however, with cones much more prevalent in central focal zones. Overall, rod photoreceptors are not only the predominant type of photoreceptor but are the most abundant cell type in most mammalian retinas. In humans, for example, approximately 74% of all retinal cells are rods[56], with a similar proportion reported for mouse and rat[57,58].

Morphologically, photoreceptors are highly polarised (Figure 2B). Outermost is the outer segment, a stack of membrane-bound discs that contain visual opsin proteins and downstream components of the phototransduction cascade. The outer segment is joined to the inner segment by a narrow connecting cilium. The ellipsoid region of the inner segment is densely packed with mitochondria and metabolic enzymes, a hub for ATP production by OXPHOS[59]. The myoid region of the inner segment is the main site of protein synthesis and contains ribosomes, endoplasmic reticulum and the Golgi complex from which proteins are trafficked throughout the cell[60]. The inner segment connects to the cell body, which contains the nucleus, and inward from the cell body is the synaptic terminal, where signals are transmitted to second order neurons in the OPL.

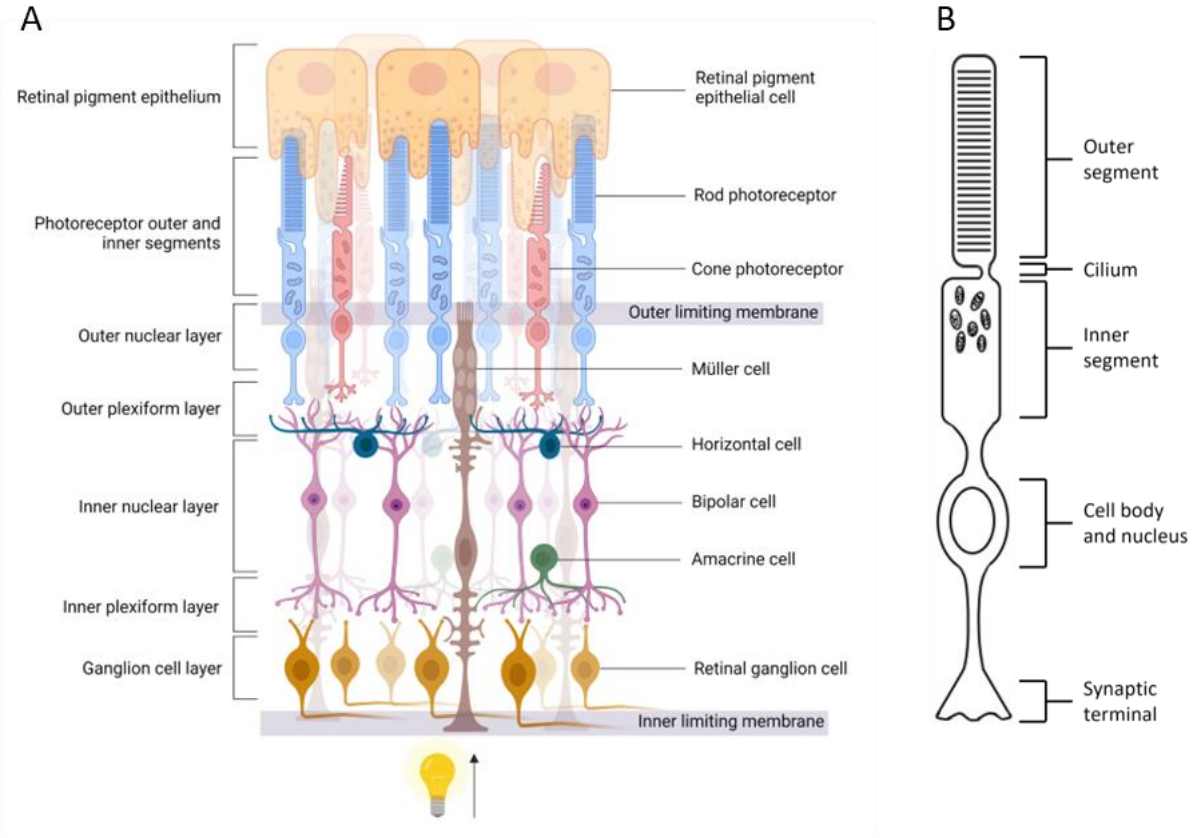


**Figure 2: The mammalian retina. A.** Diagram of a mammalian retina and retinal pigment epithelium. (Created with BioRender.com) **B.** Diagram of a rod photoreceptor.

Unlike most neurons, photoreceptors do not fire action potentials but rather continuously modulate release of glutamate, the dominant excitatory neurotransmitter in the retina, in response to tonic changes in their membrane potential. The phototransduction cascade is a series of rapid reactions leading from the absorption of light in the outer segment to changes in membrane potential and glutamate release from the synaptic terminal[61]. Located abundantly in the outer segment membranes, visual opsins are responsible for light detection. Opsins are G protein-coupled receptors comprised of a protein covalently linked to the chromophore, retinal. The absorption of a photon by retinal results in its isomerisation from *11-cis* to *all-trans* retinal which induces a series of changes in conformation of the opsin. This leads to the activation of the cytoplasmic G-protein, transducin, which subsequently activates the PDE6 cGMP phosphodiesterase complex. PDE6 hydrolyses cGMP, causing a drop in its concentration and closure of cGMP-gated cation channels in the outer segment plasma membrane[62]. Positively charged ions are occluded from entering the cell, which hyperpolarises due to the continued activity of ion transporters such as the Na,K ATPase pump. Hyperpolarisation inhibits $Ca^{2+}$ influx at the synaptic terminal, decreasing $Ca^{2+}$-dependent fusion of synaptic vesicles with the plasma membrane. The resulting drop in glutamate release is recognised by bipolar cells in type-specific ways and signalled through successive layers of retinal circuitry.

Requisite for this process is that, in darkness, photoreceptors constantly maintain a partially depolarised state in which positive charge is exported, notably by Na,K ATPase pumps located in the inner segment membranes[63], but re-enters through cGMP-gated cation channels in the outer segments. This is termed the dark current and is exceptionally energy demanding. It is the most ATP-expensive process undertaken by photoreceptors[5].

In addition to ATP demand, photoreceptors face significant biosynthetic demand. The retinal pigment epithelium (RPE) is a cell monolayer that borders the outer retina adjacent to the photoreceptors and forms the outer blood-retina barrier. RPE cells surround the ends of photoreceptors and phagocytose a portion of the outer segments daily[64,65]. As such, photoreceptors must resynthesise their outer segments, with new discs added at the cilial end while mature discs are shed[66]. Both rods and cones shed and resynthesise their outer segments[64,67,68]. Approximately 60% of the dry weight of outer segments is protein, predominantly opsin, and 40% is lipid[69,70]. The myoid region of the inner segment of photoreceptors is the major site of synthesis of both protein and phospholipid which is incorporated into new outer segment discs[60,71]. Once opsin proteins are incorporated into an outer segment disc, most remain in the disc through shedding until phagocytosis by the RPE; however, exchange of fatty acids and replacement of phospholipid molecules throughout the outer segment occurs continually[60,71].

The rate of outer segment renewal depends on the species. Many early experiments were performed in the frog, where turnover of the full rod outer segments takes approximately six weeks[64]. In the rat and mouse, it takes approximately ten days[64], and in the rhesus monkey, the photoreceptors of which are very similar to human photoreceptors, it takes nine to thirteen days[72]. In vertebrate rods, outer segment shedding is induced by light onset after darkness, but in most species is also subject to a local circadian rhythm that induces shedding at subjective light onset even in darkness[73-76]. Disc shedding is also light-responsive and rhythmic in cones, but the timing varies between species[76].

## *Müller cells*

In mammalian retinas, Müller cells are the most abundant, and in some species the only, type of glial cell. They maintain the function and survival of retinal neurons and are essential. When Müller cells are ablated from young or adult mice, photoreceptors degenerate and vision is lost[77,78]. Müller cell dysfunction is an aspect of the pathophysiology of retinal degenerative diseases including diabetic retinopathy, macular oedema, and certain types of retinitis pigmentosa, so improved understanding of Müller cells is likely to have significant therapeutic benefit[48,79,80].

Müller cells possess nuclei in the INL, and they extend processes radially in both directions, spanning almost the full thickness of the retina[81] (Figure 2A). Outward, their processes extend to the outer limiting membrane, located just inward of the photoreceptor inner segments. This is not a basement membrane, just a distinct line at which Müller cell processes terminate, forming junctions with adjacent Müller cells and photoreceptors[82]. Müller cells project microvilli partway into the subretinal space – the extracellular milieu surrounding the photoreceptor inner and outer segments – granting them direct access to nutrients that pass through the RPE. Inward from their nuclei, Müller cells extend processes to the inner limiting membrane adjacent to the vitreous (Figure 2A). This is a true basement membrane. The cone-shaped Müller cell endfeet abut an extracellular matrix of collagen and proteoglycans which separates the retina from the vitreous, but which permits exchange of molecules with the large fluid volume[83].

During development, Müller cells arise in clonal columnar units from a common progenitor along with a specific number – which differs by species – of rod photoreceptors, bipolar cells, and amacrine cells[84]. Müller cells differentiate late in retinal development in comparison to other retinal cell types. They are softer than neurons, which they fluidly surround and ensheath in all layers, separating them from direct contact with adjacent neurons except at synapses[80,85].

The overarching role of Müller cells is to increase the signal-to-noise ratio of visual perception, and many functions contribute to this[80]. Most directly, by virtue of their morphology, Müller cells act as fibres to limit scattering of light as it passes through all layers of the retina before reaching the photoreceptors[86]. Biochemical mechanisms are also at play. Retinal glutamate homeostasis is tightly regulated to maintain control of neuronal signalling and prevent excitotoxicity. Müller cells express the glutamate and aspartate transporter, GLAST (also called EAAT1), and are responsible for most extracellular glutamate uptake in the retina[87-90]. Uptake of glutamate is dependent on the active maintenance of the transmembrane $Na^+$ gradient and strong negative membrane potential of Müller cells. It decreases interference between neighbouring neurons and influences the kinetics of neuronal signalling[91,92]. Müller cell glutamate uptake is particularly important for normal signalling in the inner retina but largely dispensable at the synapses between rods and bipolar cells, where most glutamate is recovered by the rods[93].

Müller cells are the only retinal cells to express glutamine synthetase, which catalyses the ATP-dependent formation of glutamine from glutamate and ammonium. Cyclically, glutamine is returned to neurons and converted to back glutamate for neurotransmission[94]. Bipolar cells and retinal ganglion cells are fully reliant on glial-derived glutamine for synthesis of glutamate[95]. Photoreceptors can import or synthesise a portion of glutamate by other means, but Müller cell-derived glutamine is also an important substrate for glutamate production in these cells[95,96].

Müller cells spatially buffer potassium ions released by neurons during their normal activity. Müller cell endfeet are highly conductive to potassium, and potassium uptake from sites of high concentration is matched by its immediate release from endfeet, where the large volume of vitreous humour acts as an ion sink[97]. This process is more efficient than extracellular diffusion for spatial potassium buffering. The direction of potassium flow is determined by the distributions of rectifying channels in the Müller cell membrane[80]. These channels require ATP hydrolysis for maximal activity[98]. Another role of Müller cells, related to the potassium currents, is the efflux of water, which is needed to maintain osmotic homeostasis. Water co-transported into the retina with osmolytes or produced by oxidative phosphorylation is removed into the blood and vitreous through aquaporin 4 channels expressed by Müller cells[99].

Müller cells synthesise and store glycogen. The level of glycogen present differs by species and is generally inversely proportional to the degree of retinal vascularisation[100]. The distribution of mitochondria in Müller cells is also affected by the vasculature. In avascular retinas, Müller cells contain mitochondria essentially only at their scleral ends, closest to the choroid, their exclusive blood supply[101]. In contrast, in vascular retinas, mitochondria are distributed along the length of Müller cells,

including at the endfeet. In culture, mitochondria in Müller cells derived from avascular retinas redistribute throughout the cells in response to uniform oxygen availability[102].

## *Differences between species*

All vertebrate retinas structurally comprise three neuronal layers separated by two synaptic layers. However, there are many aspects on which retinas differ between species[43]. These include the number of cell subtypes within each neural class, the relative proportions of cell types and their spatial distributions in the retina, the thickness of synaptic layers and interconnectedness of neural processes, the density of retinal ganglion cells, and the degree of intraretinal vascularisation[43]. The end-goal of the research in this project is to develop treatments for human diseases. Model systems and species should therefore closely represent the human retina from a metabolic perspective.

Firstly, and importantly, the ratio of rod to cone photoreceptors and the overall proportion of photoreceptors relative to other cell types are similar between human, mouse and rat retinas[56-58]. Oxygen and nutrient availability are important determinants of metabolic fluxes in a tissue, so another very important consideration for metabolism is the degree of retinal vascularisation. The outer retina of all mammals is avascular. It is supplied with oxygen and nutrients by diffusion from the choroidal vascular bed[4]; however, the inner retina may be vascularised to a degree greatly variable between species. For example, the guinea pig retina is avascular whereas the inner layers of mouse, rat, primate and human retinas are vascular. The oxygen distribution through the full depth of retinas of many species has been measured *in vivo* using microelectrodes[4]. In the avascular guinea pig retina, the choroid is the only source of oxygen and nutrients for the whole retina, which renders the inner retina anoxic[103]. The rabbit retina is mostly avascular, yet the oxygen level does not fall to anoxic levels; rather, the inner retina has adapted to use a tiny amount of oxygen compared to the outer[4]. In vascular retinas, oxygen tension drops steeply with distance from the choroidal and retinal vessels and may reach very low levels during darkness when oxygen consumption is highest[104]. The oxygen profile through the retinal depth is similar between many species with vascularised retinas, including the mouse, rat, cat, pig and primate[4,105-110].

As a point of difference between species, the human retina and many primate retinas possess a macula, a pigmented area with high photoreceptor density, which is not present in lower mammals[111]. The centre of the macula contains a very high density of cone photoreceptors in an area called the fovea centralis, which is avascular, very thin in its centre, and comprises simplified neuronal circuitry[112]. Outside the fovea is a zone of high rod density. The elastic lamina of Bruch's membrane, a basement membrane between the RPE and the choroidal vasculature, is thinner adjacent to the

macula than adjacent to the peripheral retina which presumably allows more efficient diffusion of substrates to this area of high metabolic demand[113]. The macula is particularly susceptible to degenerative disease[111]. Although rodents do not possess a macula, the assumption was made for this thesis that metabolism at the cellular level is unlikely to differ greatly from higher mammals, especially when studying the whole retina including the periphery.

## *1.4 Retinal glucose metabolism*

### *Review paper: Power to see: Drivers of aerobic glycolysis in the mammalian retina*

The following published review discusses retinal glucose metabolism in detail, focussing on the whole retina and photoreceptors. Especially relevant to the aims of this project is the discussion of signalling pathways that potentially drive aerobic glycolysis. The thesis subsequently continues with background on glucose metabolism in Müller cells, and consideration of different perspectives regarding the major cellular source of lactate in the retina.

# Statement of Authorship

| | |
|---|---|
| Title of Paper | Power to see-Drivers of aerobic glycolysis in the mammalian retina: A review |
| Publication Status | ☑ Published ☐ Accepted for Publication<br>☐ Submitted for Publication ☐ Unpublished and Unsubmitted work written in manuscript style |
| Publication Details | Haydinger CD, Kittipassorn T, Peet DJ. Power to see-Drivers of aerobic glycolysis in the mammalian retina: A review. Clin Exp Ophthalmol. 2020 Nov;48(8):1057-1071. doi: 10.1111/ceo.13833. Epub 2020 Aug 16. PMID: 32710505. |

## Principal Author

| | | | |
|---|---|---|---|
| Name of Principal Author (Candidate) | Cameron D Haydinger | | |
| Contribution to the Paper | Conceived of the content of the review, including collation of relevant data and ideas in the literature, and generation of original ideas and connections. Wrote the full manuscript. Generated both figures. Edited the manuscript. | | |
| Overall percentage (%) | 85 | | |
| Certification: | This paper reports on original research I conducted during the period of my Higher Degree by Research candidature and is not subject to any obligations or contractual agreements with a third party that would constrain its inclusion in this thesis. I am the primary author of this paper. | | |
| Signature | | Date | 12/04/2022 |

## Co-Author Contributions

By signing the Statement of Authorship, each author certifies that:

i. the candidate's stated contribution to the publication is accurate (as detailed above);

ii. permission is granted for the candidate in include the publication in the thesis; and

iii. the sum of all co-author contributions is equal to 100% less the candidate's stated contribution.

| | | | |
|---|---|---|---|
| Name of Co-Author | Thaksaon Kittipassorn | | |
| Contribution to the Paper | Contributed ideas and provided feedback and insight relating to the scientific content of the manuscript. Edited the manuscript. | | |
| Signature | | Date | 18/5/2022 |

| | | | |
|---|---|---|---|
| Name of Co-Author | Daniel J Peet | | |
| Contribution to the Paper | Conceived of the review topic. Contributed ideas and provided feedback and insight relating to the scientific content of the manuscript. Edited the manuscript. | | |
| Signature | | Date | 12/4/2022 |

Please cut and paste additional co-author panels here as required.

Received: 26 March 2020 | Revised: 3 July 2020 | Accepted: 20 July 2020

DOI: 10.1111/ceo.13833

INVITED REVIEW

Clinical & Experimental Ophthalmology WILEY

# Power to see—Drivers of aerobic glycolysis in the mammalian retina: A review

**Cameron D. Haydinger BSc(Hons)[1] | Thaksaon Kittipassorn MD, PhD[1,2] | Daniel J. Peet PhD[1]**

[1]School of Biological Sciences, University of Adelaide, Adelaide, South Australia, Australia

[2]Department of Physiology, Faculty of Medicine Siriraj Hospital, Mahidol University, Mahidol, Thailand

**Correspondence**
Associate Professor Daniel J. Peet, Department of Molecular and Biomedical Science, School of Biological Sciences, University of Adelaide, Adelaide, SA, 5005, Australia.
Email: daniel.peet@adelaide.edu.au

**Funding information**
National Health and Medical Research Council, Grant/Award Number: Project Grant 1099932

**Abstract**

The mammalian retina converts most glucose to lactate rather than catabolizing it completely to carbon dioxide via oxidative phosphorylation, despite the availability of oxygen. This unusual metabolism is known as aerobic glycolysis or the Warburg effect. Molecules and pathways that drive aerobic glycolysis have been identified and thoroughly studied in the context of cancer but remain relatively poorly understood in the retina. Here, we review recent research on the molecular mechanisms that underly aerobic glycolysis in the retina, focusing on key glycolytic enzymes including hexokinase 2 (HK2), pyruvate kinase M2 (PKM2) and lactate dehydrogenase A (LDHA). We also discuss the potential involvement of cell signalling and transcriptional pathways including phosphoinositide 3-kinase (PI3K) signalling, fibroblast growth factor receptor (FGFR) signalling, and hypoxia-inducible factor 1 (HIF-1), which have been implicated in driving aerobic glycolysis in the context of cancer.

**KEYWORDS**

biochemistry, metabolism, retina

## 1 | AEROBIC GLYCOLYSIS/THE WARBURG EFFECT IN THE RETINA

In most non-dividing mammalian cells, pyruvate produced by glycolysis is predominantly oxidized in mitochondria via the tricarboxylic acid (TCA) cycle, fuelling efficient ATP production by oxidative phosphorylation (OXPHOS). However, in proliferating cells, notably in many types of cancer cells, glucose uptake is increased, the rate of glycolysis is elevated, and most pyruvate is instead reduced to lactate that is exported from the cell, a much less efficient method of generating ATP.[1,2] This metabolic reprogramming occurs even in cells with functional mitochondria and ample oxygen availability, and is hence termed aerobic glycolysis, or the Warburg effect.[3,4]

The mammalian retina is one of few non-proliferative tissues to exhibit aerobic glycolysis.[4-8] For example, in adult rat retinal explants, approximately 90% of the glucose that is consumed is exported as lactate, even when the explants are incubated in highly oxygenated medium.[8] High rates of aerobic lactate production and export have also been demonstrated ex vivo in species including mouse,[9] rabbit,[10,11] cattle[12] and ox.[13] Similar findings in vivo in anesthetized cats and pigs, by measurement of retinal arteriovenous lactate, glucose and oxygen differences, have confirmed the physiological translation of observations of aerobic glycolysis made in explants.[14,15]

Many studies have investigated the effects of glycolytic inhibition on retinal function and survival. Ames

and Gurian showed the importance of aerobic glycolysis for retinal function with the omission of glucose from medium leading to a rapid decrease in electrical responses of rabbit retinas ex vivo.[16] Likewise, Winkler found in rat retinas that glucose deprivation, or treatment with the glycolysis inhibitors iodoacetate or 2-deoxyglucose, caused the loss of fast PIII wave amplitude.[7,8] In mouse explants, Chertov et al showed that glycolysis was necessary for photoreceptor survival, and that the supply of alternative mitochondrial fuels could delay but not prevent the increased cell death caused by glucose deprivation.[17] Altogether, these data demonstrate that glycolysis is essential for retinal function and survival, and why disruption of retinal glucose metabolism is an expected cause of visual disease. There are now growing bodies of evidence to suggest that altered glucose metabolism contributes to the pathology of age-related macular degeneration and retinitis pigmentosa.[18-23]

It should be recognized that oxygen is rapidly consumed by the retina, and is essential for ATP production and retinal function regardless of glucose availability.[11,16] In vascular mammalian retinas, such as those of the cat, pig and rat, microelectrode measurements of oxygen tension throughout the retina have demonstrated that the photoreceptors are well-oxygenated by the choroid, and that the inner layers are oxygenated by the retinal vasculature.[24-27] This is consistent with lactate production via aerobic glycolysis. Furthermore, the fact that rat retinas incubated ex vivo with medium saturated with 95% oxygen convert approximately 90% of glucose to lactate is further evidence that lactate production in the rat retina is not predominantly driven by hypoxia.[8] Similarly, experiments in vivo in anesthetized cats showed that only a portion of retinal lactate production was lost under conditions of hyperoxia compared to normoxia, supporting the conclusion that most lactate is produced aerobically in normoxia.[14]

However, not all of the retina is well oxygenated. For example, the outer nuclear and outer plexiform layers may reach almost anoxic conditions in darkness, when oxygen consumption by photoreceptors is highest. Similarly, in avascular retinas such as those of the rabbit and guinea pig, the choroid supplies oxygen to the whole retina via diffusion, so the distant inner retinal layers operate at low oxygen tension.[28] It is therefore possible that a small proportion of lactate production in vivo is due to anaerobic glycolysis. In this case, hypoxia-inducible factors (HIFs) would be the most likely candidates in driving lactate production. Their putative role in retinal glycolysis, discussed in this review, is relevant when considering conditions of either hypoxia or normoxia, and would only differ in their mode of activation.

While it is now well-established that aerobic glycolysis is essential for normal retinal function, the benefits conferred by aerobic glycolysis to offset its apparent inefficiency in ATP production remain incompletely resolved. Possible reasons for aerobic glycolysis in the retina include the generation of metabolites for the biosynthesis of photoreceptor outer segments,[5,9] supplementary ATP production to meet demand that may exceed oxidative capacity,[29] production of lactate as a fuel for particular cell types, including Müller glia or retinal pigment epithelial cells,[30] or rapid ATP production to meet fluctuating energy demand in stimulated neurons, as has been postulated in the brain.[31] This fundamental question may be more conclusively addressed with improved understanding of the molecular mechanisms that drive aerobic glycolysis in the retina.

In this review, we discuss selected molecules and signalling pathways that commonly drive aerobic glycolysis in cancer cells, and what is known regarding the involvement of these pathways in retinal metabolism and function, with a focus on recent findings. Several studies have begun to reveal or call into question roles for key molecules in driving retinal glycolysis, filling in important pieces of the puzzle, but we still lack a complete picture. Understanding the drivers of aerobic glycolysis may provide the basis for development of novel therapeutic approaches for retinal diseases of metabolic cause. In addition, if the roles of these pathways are conserved between cancer and the retina, then, the implications for cancer therapies designed to target glucose metabolism need to be carefully considered in light of potential damage to the retina.

## 2 | DRIVERS OF AEROBIC GLYCOLYSIS IN THE RETINA

A switch in glucose metabolism from OXPHOS to aerobic glycolysis typically involves increased expression and activity of glucose transporters, glycolytic enzymes, enzymes converting pyruvate to lactate, and lactate exporters, together with a decrease in the activity of enzymes converting pyruvate into acetyl CoA and promoting its entry into the TCA cycle, in mitochondrial activity and oxygen consumption. Expression and activity of individual proteins directly involved in these pathways, as well as their control by various signalling pathways, specific kinases and transcription factors have been postulated to control aerobic glycolysis in cancer (reviewed in References [1,32]), and a number of these have been directly examined for their roles in retinal glycolysis or visual function. The following discussion focusses on analyses of some of these postulated drivers

in the context of aerobic glycolysis in the mammalian retina.

## 3 | LACTATE DEHYDROGENASE A

Lactate dehydrogenases (LDH) are enzymes that catalyze the reduction of pyruvate to lactate, which is coupled to the oxidation of NADH to $NAD^+$. They can also catalyze the reverse reaction. The two most widely-expressed LDH isoforms in mammals are lactate dehydrogenase (LDHA) and lactate dehydrogenase (LDHB), which are encoded by separate genes.[33,34] LDHA and LDHB homo- or hetero-tetramerise to form five possible complexes distinguished by the number of A and B subunits. Some evidence indicates that LDHA, to a greater extent than LDHB, favours the reduction of pyruvate to lactate over the reverse reaction, enabling it to support higher rates of glycolysis through faster regeneration of $NAD^+$, especially at high pyruvate concentrations.[35-37] In general, expression of LDHA is high in highly glycolytic physiological tissues, such as skeletal muscle, whereas LDHB dominates in aerobic tissues, such as the heart.[38] LDHA is also commonly upregulated in cancers, often due to HIF-1-mediated transcription as a result of intratumoural hypoxia or aberrant HIF activation.[33,39]

By immunohistochemistry (IHC) and in situ hybridization (ISH), LDHA expression has been detected in all layers of the mouse retina, except the inner plexiform layer, with the strongest expression in the photoreceptors, especially their inner segments.[9,40] The same pattern was observed in rat, marmoset and human retinas and, assuming that LDHA expression correlates with lactate production, suggests that photoreceptors are the dominant, although possibly not exclusive, producers of lactate in the retinas of most tested mammals.[41] The concept of photoreceptors being the main source of lactate production is supported by the work of Lindsay et al who found that retinas from $AIPL1^{-/-}$ mice, which lack photoreceptors, contained 74% less lactate than retinas from normal mice.[42] Surprisingly, however, in one study, LDHA was not detected in the rod photoreceptors of the avascular rabbit retina.[41]

In rats with inherited retinal degeneration, it was shown that there was a shift in the proportions of tetrameric LDH isozymes from LDHA-dominant to LDHB-dominant forms.[43] This isozyme-shift slightly preceded both a decrease in the overall retinal LDH activity and the onset of morphological signs of retinal degeneration, indicating that it may have been a causative factor in the degeneration. The regional or cell type-specific requirement for LDHA in this study was unclear. Recently, Chinchore et al performed a series of experiments that tested the function of several potential drivers of aerobic glycolysis in mouse retinas, including LDHA.[9] Pharmacological inhibition specific for LDHA in retinal explants decreased lactate production by approximately 70%. The researchers also used the LMOPC1 mouse,[44] which harbours Cre recombinase driven by a 4.1 kb rhodopsin promoter, to achieve the knockout of LDHA in 50% to 90% of rod photoreceptors. They found that lactate production in retinal explants from these mice was approximately half that of control mice. These data show that LDHA is necessary for normal lactate production in the mouse retina, and confirm the notion that rods are prodigious lactate producers. There were also morphological consequences of LDHA disruption; in vivo electroporation of shRNA targeting LDHA caused a large decrease in rod outer segment (OS) length over 45 days, and maintenance of the OS was dependent on LDHA catalytic activity.[9]

It is evident that LDHA is required for preservation of photoreceptor morphology and consequently probably retinal function, although to our knowledge, retinal function after LDHA inhibition has not been directly tested. The necessity of LDHA in particular cell types, especially of the inner retina, remains relatively unexplored, as do the factors that control its expression. Furthermore, while high LDHA expression is required for lactate production, LDHA expression alone is not thought to be sufficient to drive aerobic glycolysis, which is dependent on upregulated glucose uptake and conversion of glucose to pyruvate. In cancer cells, these processes are contingent upon transcriptional and cell signalling programs that direct the expression and activities of numerous upstream components of glucometabolic pathways, in addition to LDHA. So, although LDHA is necessary for aerobic glycolysis in the retina, it is unlikely a driver per se.

## 4 | HEXOKINASE 2

Hexokinases (HKs) catalyze the ATP-dependent phosphorylation of glucose to form glucose-6-phosphate in the first step of glycolysis (Figure 1). There are four hexokinase isoforms in mammals, denoted HK1-4. HK1-3 have a high affinity for glucose, and especially HK1 and HK2 are able to support the elevated rates of glucose phosphorylation demanded by highly glycolytic tissues.[45,46] This efficiency of HK-mediated glucose phosphorylation by HK1 and HK2 is largely due to their ability to bind voltage-dependent anion channels (VDAC) on the outer mitochondrial membrane, an interaction which spatially links glycolysis and OXPHOS by providing HK1 and HK2 with immediate access to mitochondrially-produced ATP (Figure 1).[47] The

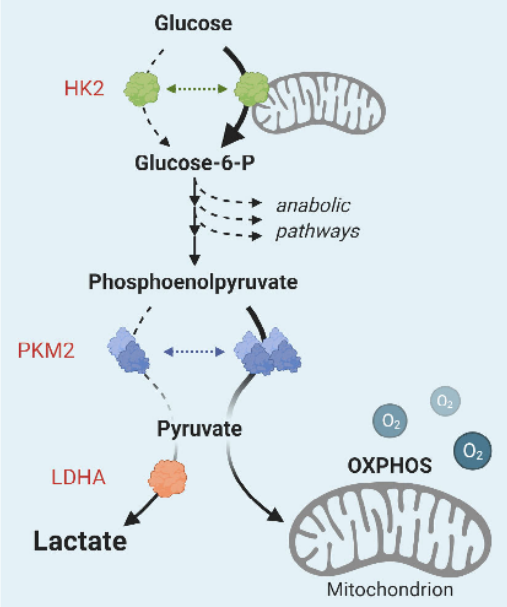


**FIGURE 1** Glycolysis can be modulated by multiple mechanisms. Mitochondrial localisation of hexokinase 2 (HK2) can increase glucose phosphorylation. The glycolytic enzyme pyruvate kinase M2 (PKM2) can adopt a highly active tetrameric form or a less active dimeric form. The dimeric form is, somewhat paradoxically, associated with increased rates of aerobic glycolysis in cancer cells. It can promote the siphoning of upstream glycolytic metabolites into anabolic pathways for the production of nucleotides, lipids and amino acids. Tetramerisation of PKM2 is positively regulated by the glycolytic metabolite fructose-1,6-bisphosphate, and negatively regulated by high tyrosine kinase activity. Downstream of PKM2, expression of lactate dehydrogenase A (LDHA) can favour lactate production over oxidative phosphorylation (OXPHOS)

interaction is governed in part by phosphoinositide 3-kinase (PI3K)/Akt signalling.[48,49]

HK1 is the isoform most widely expressed in adult mammals, with expression of HK2 being much more restricted, generally to insulin-sensitive tissues.[45] HK2, however, is most commonly upregulated in cancer, where it promotes aerobic glycolysis. In various cancer types, including glioblastoma multiforme, medulloblastoma and pancreatic ductal adenocarcinoma, HK2 expression has been shown to promote lactate production and tumour growth.[50-52] HK2, given that it catalyzes the first step of the glycolytic pathway, cannot via its known enzymatic functions directly divert the fate of pyruvate from mitochondrial oxidation to reduction to lactate. Rather, it facilitates aerobic glycolysis by promoting high glycolytic flux. The differential expression of HK2 between normal and cancerous tissues and its role in cancer metabolism and growth renders it a promising target for selective anti-cancer therapies.

In the mouse and rat retina, HK2 is most strongly expressed in the inner segments of both rod and cone photoreceptors, and also the perinuclear region, specifically in cones.[21,40,53,54] This pattern is consistent with localization to mitochondria. Reports of HK2 expression in the outer plexiform layer vary from as strong as its expression in photoreceptors,[40] to weak,[53] or undetectable.[21,54] HK1 is the dominant HK isoform in the inner retina, expressed from the outer plexiform layer to the ganglion cell layer, but like HK2 it is also detectable in photoreceptor inner segments, albeit relatively weakly.[40,53]

Petit et al used the iCre75 mouse[55] which, similar to the LMOPC1 mouse, expresses Cre recombinase under the control of a 4 kb rhodopsin promoter, to conditionally knock out HK2 in mouse rod photoreceptors.[21] They achieved knockout in almost 90% of rods. Explants of heterozygous and homozygous knockout mice produced 25% and 33% less lactate than control retinas, respectively. They did not display decreased glucose uptake, however, supporting a genuine shift in the metabolic balance from aerobic glycolysis to OXPHOS. Mechanistically, this shift may have been enabled by the observed increase of greater than 4-fold in the number of mitochondria in the outer nuclear layer, specifically the rod perinuclear regions. Expression of Glucose Transporter 1 (GLUT1) and HK1 were also higher in total retinal extracts of homozygous rod HK2 knockout mice.[21]

Functionally, the rod HK2 knockout mice displayed diminished scotopic a- and b-wave amplitudes, and the b-wave implicit time was higher compared to controls, evident after 1 month of age.[21] HK2 is therefore required for normal rod function. However, neither rod survival nor morphology was affected by HK2 knockout over a period of 12 months. This was surprising given the earlier report of Chinchore et al which, although not directly studying HK2, demonstrated the importance of aerobic glycolysis in the maintenance of rod outer segments.[9] The discrepancies may be reconcilable in the activation of compensatory mechanisms unique to disruption of particular genes. An example of such a putative compensatory mechanism is the increase in rod perinuclear mitochondria in the HK2 knockout mice.[21] Petit et al proposed that these mitochondria provide an alternative means of NADPH production to the pentose phosphate pathway (PPP), and they may provide an alternative source of energy for rod terminal processes which have been proposed to normally be supplied with ATP from glycolysis.[21,40,56] These hypotheses will require direct investigation to be confirmed or disproven.

Cone-specific knockout of HK2 in mice by utilizing Cre recombinase under the control of the human red/-green pigment promoter (HRGP) did not induce cone cell

death, or result in any detectable functional change in the retina.[21,57] HK2 is therefore required for normal function in rods but not cones. Interestingly, simultaneous deletion of HK2 from rods and cones resulted in reduced cone function.[21] This is consistent with the hypothesis that cones rely on lactate produced by rods, but the exclusion of other possible mechanisms requires further research. For example, cone function could conceivably be diminished due to altered availability of another metabolite such as glutamine, decreased oxygen availability due to the increased OXPHOS activity in rods, or impaired production of rod-derived cone viability factor (RdCVF), a protein secreted by rods that stimulates aerobic glycolysis in cones.[20]

Rajala et al found that in both light- and dark-adapted rat and mouse retinas, HK2 associated with mitochondria, and more HK2 was present in mitochondrial extracts from light-adapted than dark-adapted retinas.[54] The light-associated increase in mitochondrial HK2 was dependent on insulin receptor signalling, which is primarily mediated by PI3K. Consistent with this, treatment with the PI3K inhibitor, LY294002, decreased the amount of HK2 in mitochondrial extracts from both light- and dark-adapted retinas. Further experiments elucidated a mechanism involving activation of Akt1 followed by deactivation of GSK-3β, dephosphorylation of VDAC, and therefore, increased mitochondrial HK2 binding. It should be noted that LY294002 has inhibitory activity against multiple PI3K-related kinases including GSK3 at the concentration used.[58] Interestingly, the authors found less mitochondrial HK2 in type 1 diabetic mouse retinas compared to wild type. It remains to be confirmed whether this observation contributes to retinopathy in the mouse model, or indeed whether the subcellular localization of HK2 has a significant effect on retinal metabolism, for example, in modulating the glycolytic rate or fate of glucose.

Given that its enzymatic role is far upstream of the point at which pyruvate diverges to either lactate or OXPHOS, HK2 cannot alone be considered a driver of aerobic glycolysis. However, HK2 is necessary to maintain a normal level of aerobic glycolysis in mouse rod photoreceptors. It is not required in cones for function or survival, and its metabolic role in cones remains unclear. Its necessity in other retinal cell types and mammalian species is also unknown.

## 5 | PYRUVATE KINASE M2

Pyruvate kinases (PKs) are enzymes that catalyze the final step of glycolysis, the conversion of phosphoenolpyruvate to pyruvate (Figure 1), which is coupled to the phosphorylation of ADP to ATP. There are four PK isoforms in mammals, pyruvate kinase (PKM1) (muscle 1), pyruvate kinase (PKM2) (muscle 2), PKL (liver) and PKR (erythrocytes). Expression of PKL is confined to the liver and kidney, whereas PKR is expressed exclusively in erythrocytes. PKM1 and PKM2 are alternatively spliced products of the same gene, *Pkm*, that differ by a single exon,[59] but they nevertheless have broad but unique expression patterns and significant functional differences.[60,61] PKM2 expression is widespread during embryonic development, and in most adult tissues, whereas PKM1 is expressed predominantly in highly catabolic tissues such as heart, brain and skeletal muscle. PKM1 and PKM2 both exist as enzymatically active tetramers, but PKM2 can also exist in a much less active dimeric form.[62] The enzymatic activity of PKM2 is lower than PKM1, and is also subject to complex regulation. For example, tetramerization of PKM2 is allosterically promoted by the glycolytic metabolite fructose-1,6-bisphosphate (FBP) and negatively regulated by high tyrosine kinase activity due to the capacity of PKM2 to bind phospho-tyrosine residues, as well as direct phosphorylation of PKM2.[62-65] In proliferating cells, the low activity of the dimer is proposed to promote growth by facilitating the accumulation of glycolytic metabolites, which can be siphoned into pathways for the biosynthesis of macromolecular precursors such as amino acids and nucleotides, whereas expression of PKM1 even in the presence of PKM2 can inhibit growth.[66] In the retina, it has been proposed that PKM2 promotes anabolic activity necessary for the maintenance of photoreceptor outer segments, which are shed and re-synthesized at a rate of approximately 10% of their length per day.[9,41,67]

PKM2 is the dominant PKM isoform expressed in most cancers, consistent with a role in supporting anabolism. Christofk et al knocked down PKM2 in highly glycolytic cancer cell lines and then expressed either recombinant PKM1 or PKM2.[68] Compared to PKM1, PKM2 expression resulted in higher lactate production, lower oxygen consumption, and lower dependence on OXPHOS for growth. It seems paradoxical that PKM2 expression is associated with increased lactate production given that is acts upstream of LDH and is less active than PKM1. This can be explained in part by the ability of PKM2 to act as a coactivator of HIF-1α and other transcription factors independently of its enzymatic activity, thereby promoting lactate production over OXPHOS through activation of pro-glycolytic target genes such as LDHA.[69,70]

The roles of PK isoforms in the retina are complex (recently reviewed by Rajala[71]). Both PKM1 and PKM2 are expressed in mouse retinas. In mouse, total retinal extracts Lindsay et al observed over 5-fold more PKM2

than PKM1 protein on a molar basis, with PKM levels approximately 25% of rhodopsin, the most abundant photoreceptor protein.[42] In mouse and rat retinas, PKM2 is most highly expressed in photoreceptor inner segments, but it is also detectable in the inner nuclear layer in a population of bipolar cells, and in the inner plexiform layer.[9,41,42,72] In marmosets, PKM2 localization is similar to rodent, except for weak expression in Müller cells, which was not detectable by immunohistochemical analysis in mice, and for a lack of expression in the inner nuclear layer.[41] PKM1 expression in mouse and rat retinas is, however, more widespread than PKM2, especially in the inner retina. An important point given its potential to inhibit anabolic pathways is whether PKM1 is co-expressed with PKM2 in photoreceptors; indeed, the overexpression of PKM1 in the presence of endogenous PKM2 has been demonstrated to slightly reduce OS length.[9] Most studies show relatively weak PKM1 expression in photoreceptors based on IHC,[41,42,73,74] with one reporting it as undetectable by IHC and ISH but detectable in rods by quantitative polymerase chain reaction.[9] In all cases, expression of PKM2 in the photoreceptor layer was much stronger, and this observation was consistent in both rod and cone-dominant retinas.[41,73]

Wubben et al crossed the LMOPC1 mouse with floxed PKM2 mice to knock out PKM2 in rods.[74] Only the PKM2-specific exon 10 of the *Pkm* gene is floxed in these mice, which enables PKM2 to be knocked out in rod photoreceptors, while leaving the PKM1-encoding sequence intact. No obvious functional consequences were observed upon rod-specific PKM2 deletion except for a slight decrease in scotopic a-wave amplitude after 24 to 28 weeks.[74] The researchers described a minor degenerative phenotype characterized by a small reduction in outer retinal volume and cell number, but no significant TUNEL staining indictive of cell apoptosis. Chinchore et al had previously used the LMOPC1 mouse to generate rod-specific PKM2 knockout mice and most importantly only found a small but significant decrease in lactate production in retinal explants in knockout mice compared to controls.[9] This small decrease is consistent with only a minor role for PKM2 in aerobic glycolysis in rods.

Rajala et al used the iCre75 mouse to also knock out PKM2 in rods.[55,72] These knockout mice showed decreases in scotopic a and b-wave amplitudes at 5 months old. Similar to the other studies, there was only a slight morphological change noted in the form of decreased thickness of the photoreceptor end tips. While in this model there was significantly more TUNEL staining in the photoreceptor layer of the knockout compared to control, only a minute fraction of photoreceptors stained positively in either. Importantly, lactate production in the rod PKM2 knockout retinas was slightly lower than in control retinas, consistent with the earlier observation that PKM2 plays a minor role in aerobic glycolysis in the mouse retina.[9,72]

When the PKM2-specific exon 10 is deleted, PKM1 expression often dramatically increases, an observation common to all discussed rod PKM2 knockout studies.[9,72,74] However, there was considerable variation in this regard between the results of each mouse model. Wubben et al directly measured total PK activity in retinal homogenates and found that it was higher in PKM2 knockouts due to increased PKM1 expression.[74] In contrast, Rajala et al inferred decreased total PK activity from measurements showing higher levels of glycolytic metabolites and lower levels of TCA cycle metabolites in the knockout, but PK activity was not directly measured.[72] The effects of PKM2 knockout on the balance of anabolic activity and oxidative energy production may therefore be specific to each mouse model, and interpretation requires careful consideration of the residual PK activity. It is not clear why either an increase or apparent decrease in PK activity in each case resulted in a decrease in lactate production. Taken together, the results show that either heightened or lowered PK activity in rods can be damaging, and this circumstantially indicates that PKM2, being highly regulatable, may be preferred over PKM1 to dynamically control the glycolytic rate.

In addition to their knockout, Chinchore et al also used electroporation of shRNA to specifically target PKM2 in mice, and surprisingly in this case found a much greater decrease in rod OS length compared to the PKM2 knockout. The utility of functional analyses following knockdown is limited by inefficient and mosaic construct penetrance inherent to the technique, but the substantial morphological changes hint that PKM2 may play a more significant role in photoreceptors than is apparent in the knockouts. As shRNA-mediated knockdown acts post-splicing, it did not result in an increase in PKM1 levels. PKM1 may therefore be able to partly compensate for the absence of PKM2 in the knockouts, resulting in milder phenotypes. However, the OS loss caused by knockdown of PKM2 could not be rescued by co-electroporation of transcript encoding PKM1, so either PKM1 alone is not protective when PKM2 is acutely lost in mature rods, or is only protective when present within a discrete range of protein expression levels which by chance or regulation was reached in the knockouts.[9] Alternatively, there may be other compensatory effects that protect photoreceptors when PKM2 is absent throughout rod development, which would not be present when shRNA is used acutely on adult mice. For example, Wubben et al observed increased expression of glycolytic, PPP and TCA cycle genes in their homozygous PKM2 knockouts.[74] Finally, the phenotypic differences

between PKM2 knockout and shRNA-mediated knockdown might due to off-target activities of the PKM2 shRNA. The severity of morphological changes to rods upon PKM2 disruption, therefore, remains unclear.

PKM2 has also been conditionally knocked out in cones using the HGRP-Cre mouse.[57,75] This resulted in an age-related decrease in photopic b-wave amplitude and flicker-ERG amplitude, which was used to specifically assess cone function. The number of S- and M-opsin cones was also significantly lower in the knockout, evident at 12 weeks of age and more widespread at 28 and 56 weeks. A surprising observation was that total retinal *Pkm2* RNA in the knockout was less than 40% of wild type levels, and RNA expression of a number of genes involved in glycolysis and fatty acid synthesis was also lower in the PKM2 knockout by a magnitude of approximately 50%. Cones only comprise 2.8% of photoreceptors in mice.[76] Therefore, either cones account for over 60% of retinal *Pkm2* RNA, or cone PKM2 is required for normal metabolism and PKM2 expression in other retinal cell types. In favour of the second hypothesis, PKM2 RNA expression does not appear to be elevated in cones, as evidenced by ISH.[9] In any case, from this study, there is a clear cell-autonomous requirement of PKM2 in cones for their survival, as the observed decrease in the number of cones did not occur in rod-specific knockout models. Due to the small proportion of cones in the mouse retina, no analysis of rates of lactate production and aerobic metabolism were reported for the PKM2 cone-specific knockouts, so the role in cone-mediated aerobic glycolysis is unclear.

In cancer cells, tyrosine phosphorylation of PKM2 at position Y105 decreases PK activity by sterically hindering binding of the PKM2 activator FBP, and thereby promotes anabolism.[65] Fibroblast growth factor receptor 1 (FGFR1) is able to directly catalyze this phosphorylation.[65] Chinchore et al showed that FGFR signalling may modulate Y105 phosphorylation and lactate production in mouse explants, although a causal link between PKM2 phosphorylation state and retinal lactate production remains unconfirmed.[9] Rajala et al had earlier demonstrated light-induced PI3K-dependent Y105 phosphorylation of PKM2 and found that PK activity was lower in retinas of light-adapted compared to dark-adapted mice.[73] Whether light- and FGFR-dependent PKM2 phosphorylation are related processes is unknown. It should be noted that an earlier study reported no difference in PK activity or PKM2 phosphorylation between light- and dark-adapted retinas.[42] Clearly, further research is needed to establish whether PKM2 phosphorylation is functionally important in the control of retinal metabolism, but if so then it is likely a regulatory node at which multiple upstream pathways converge to modulate the glycolytic rate and the fate of glucose.

The specific role of PKM2 in retinal metabolism and function is difficult to distinguish from the role of PKM1 as the knockout of a single exon results in artificial changes to PKM1 expression. The fact that knockout of PKM2 in rods resulted in functional and morphological changes to the retina in multiple studies utilizing different mouse strains is consistent with a role for PKM2 in retinal function and morphology. The observed decreases in lactate production and changes in metabolic pathways upon PKM2 knockout in rods suggest that PKM2 also plays a role in glucose metabolism in rods. However, the fact that changes in retinal lactate production were only small upon knockout supports the notion that, while it may contribute to aerobic glycolysis, it is not a major driver of aerobic glycolysis in rods. Its role in aerobic glycolysis in other cell types of the inner retina is largely unexplored.

## 6 | PHOSPHOINOSITIDE 3-KINASE /AKT SIGNALLING

Phosphoinositide 3-kinases (PI3K) comprise a large family of proteins that phosphorylate inositol-containing lipids in the plasma membrane and mediate signal transduction in many growth factor signalling pathways.[77] There are three classes of PI3K in mammals. Extensively studied and most relevant to metabolism are the class I PI3Ks that are heterodimers comprising a catalytic and a regulatory subunit (detailed reviews of structure and subunit composition in References [78,79]). Class I PI3Ks are activated upon binding of growth factors to cognate receptor tyrosine kinases (RTKs) or G protein-coupled receptors (GPCRs) (Figure 2). Active class I PI3Ks phosphorylate the lipid substrate phosphatidylinositol-4,-5-bisphosphate ($PIP_2$), generating the second messenger phosphatidylinositol-3,4,5-trisphosphate ($PIP_3$), which then recruits a subset of pleckstrin homology (PH) domain-containing effector proteins to the plasma membrane.[80] The dominant, but not exclusive, effector protein is the serine/threonine kinase Akt.[77,81,82] There are three isoforms in mammals, Akt1, Akt2 and Akt3. Upon binding to $PIP_3$, Akt is specifically phosphorylated on two residues, T308 and S473 on Akt1 or homologous residues on Akt2 and Akt3.[83] T308 phosphorylation is catalyzed by phosphoinositide-dependent kinase 1 (PDK1) and is sufficient for partial activity of Akt.[84] S473 phosphorylation, which is catalyzed by the mammalian target of rapamycin complex 2 (mTORC2), completes activation of Akt and stabilizes T308 phosphorylation.[85]

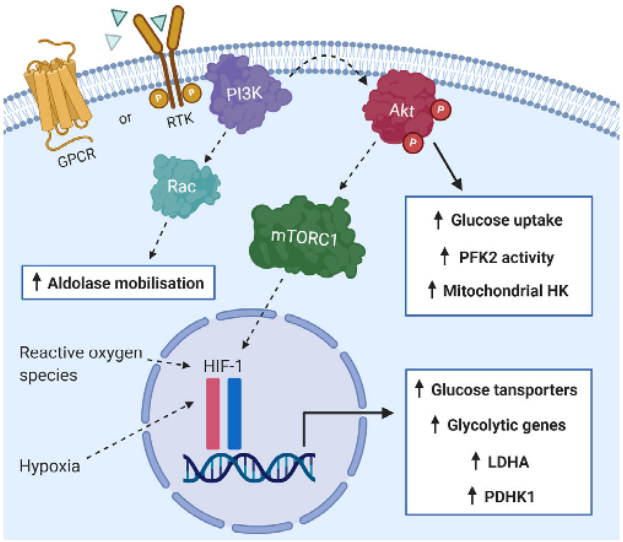


**FIGURE 2** In cancer and proliferating cells, signalling through phosphoinositide 3-kinase (PI3K) can promote glycolysis by various means, both dependent on and independently of the serine/threonine kinase Akt or hypoxia-inducible factor 1 (HIF-1). It remains unknown whether signalling through any of these pathways is required to drive glycolysis in the mammalian retina. GPCR: G protein-coupled receptor, RTK: receptor tyrosine kinase, PFK2: phosphofructokinase 2, HK: hexokinase, mTORC1: mammalian target of rapamycin complex 1, LDHA: lactate dehydrogenase A, PDHK1: pyruvate dehydrogenase kinase 1

Many target proteins with roles in diverse aspects of cell biology including cell growth, survival and metabolism are modulated in response to phosphorylation by Akt.[77]

The PI3K signalling pathway is one of the most commonly mutated pathways in cancer and its aberrant activation is cancer-promoting in diverse ways, including via the direct and indirect upregulation of glycolysis.[77,86] There is a direct evidence in multiple cancer cell types for the requirement of active PI3K/Akt signalling for aerobic glycolysis and growth.[87-89] Active Akt can induce the expression of the glucose transporter GLUT1 and its translocation to the plasma membrane, facilitating increased glucose uptake.[90,91] It can increase the binding of HK1 and HK2 to mitochondria via multiple mechanisms.[48,49] Akt also phosphorylates and activates phosphofructokinase 2 (PFK2), increasing production of fructose-2,6-bisphosphate, a positive regulator of the glycolytic enzyme phosphofructokinase 1 (PFK1).[92] Phosphorylation of tuberous sclerosis complex 2 (TSC2) by Akt relieves inhibition of mTORC1, leading to a diverse set of effects including a context-dependent increase in HIF-1 levels.[93-95] HIF-1, as discussed below, is able to reprogram metabolism toward increased glycolysis and lactate production.

Phosphoinositide signalling in the mammalian retina is active and has been well studied (reviewed by Rajala [96]). In mice, the global knockout of insulin receptor substrate 2 (IRS-2), an activator of PI3K signalling downstream of the insulin receptor, resulted in loss of up to 50% of photoreceptors within 2 weeks after birth, and secondary age-related retinal degeneration.[97] All three isoforms of Akt are expressed in the mouse retina and global knockout of Akt2 was shown to potentiate rods to light-stress induced degeneration. Although in contrast, knockout of Akt1 caused no obvious change to the retina, indicating the existence of isoform-specific roles of Akt in the retina.[98] In rod OS, the insulin receptor is activated by physiological light independently of insulin by a mechanism requiring photobleaching of rhodopsin, leading to the activation of PI3K and Akt.[99] These studies suggest that the activation of PI3K signalling is neuroprotective in light stress and decreases apoptosis.

There is evidence that PI3K may be particularly important for function, survival and glucose metabolism in cones. Knockout of either the p110α catalytic subunit or all isoforms of the p85α regulatory subunit of PI3K in mouse cones using the HGRP-Cre mouse resulted in cone degeneration and significant defects in cone function.[100,101] In each case, cones developed normally, with degeneration commencing after 1 month of age, indicating a requirement for PI3K signalling in adult cones. Rajala et al also utilized neural retina leucine zipper (NRL) knockout mice, which only develop cone photoreceptors, to assess the role of PI3K in cones. HGRP-Cre-mediated knockout of the p85α subunit of PI3K in the cone-dominant $NRL^{-/-}$ mouse retina resulted in significant defects in cone survival and function.[102] Importantly, further study showed that the $NRL^{-/-}$ $p85\alpha^{-/-}$ mice exhibited decreased levels of NADPH, and diminished expression of many glycolysis-related genes at the mRNA level, including those encoding GLUT1, HK2, PKM2 and HIF-1α, compared to $NRL^{-/-}$ mice.[73] These studies support a role for PI3K in driving glycolysis in cones, however, no data on lactate production or other measures of glycolytic flux were reported.

Although there has been minimal investigation, there is presently no evidence that PI3K signalling drives aerobic glycolysis more broadly throughout the retina. One study in rat retinal explants showed that pharmacological inhibition of pan-Akt resulted in no change in lactate production rate, although Akt3 inhibition caused decreased protein synthesis.[103] Given that these experiments were performed after 2.5 hours of treatment with inhibitors, indirect effects mediated by HIF-1-dependent transcription and protein translation, for example, would only be minimal over this relatively short incubation.

Even if Akt does not play a role, PI3K may be able to drive aerobic glycolysis via Akt-independent mechanisms. For example, an important mechanism through which PI3K can upregulate glycolysis is by freeing the glycolytic enzyme, aldolase, from the actin cytoskeleton. This is mediated through the small GTPase, Rac, independently of Akt[104] (Figure 2).

To summarize, PI3K/Akt signalling is basally active in the retina and is upregulated by light. Circumstantial evidence in favour of a role in modulating aerobic glycolysis includes the PI3K-dependent phosphorylation of PKM2, high levels of mitochondrial HK2 and, as discussed below, the possible involvement of FGFR signalling. Evidence against the role includes the reported lack of effect of Akt inhibition on lactate production with retinal explants. PI3K may be a driver of aerobic glycolysis specifically in cones, but the lack of direct evidence for changes in lactate production following disruption of PI3K signalling renders this unconfirmed. A definitive conclusion on the role of PI3K signalling in aerobic glycolysis in the retina, and any differences in its roles between cell types and species, will ultimately require more direct investigation.

## 7 | FIBROBLAST GROWTH FACTOR RECEPTOR

There are four transmembrane RTKs in the fibroblast growth factor receptor (FGFR) family in mammals, denoted FGFR1-4, involved in cellular processes including development, growth, survival and metabolism.[105] Binding of a fibroblast growth factor (FGF) to the extracellular domain of an FGFR induces dimerization, cytoplasmic autophosphorylation and activation of the FGFR. There are 18 FGFs known to directly bind and activate FGFRs with both overlapping and distinct expression patterns, receptor specificities and downstream effects. Most FGFs act in an autocrine or paracrine manner, and three are secreted endocrine hormones. Active FGFRs are able to context-dependently activate the MAPK, PI3K/Akt, PLCγ/PKC and JAK/STAT signalling pathways, giving rise to their diverse battery of cellular roles. FGFR signalling is commonly dysregulated in cancer, and is a therapeutic target.[106] It is therefore important to understand its potential roles in normal retinal physiology.

FGFRs can drive aerobic glycolysis, and there are context-specific mechanisms through which they control glucose metabolism. As discussed above, FGFR1 can phosphorylate residue Y105 on PKM2 which inhibits its tetramerization and thereby decreases PK activity to promote anabolism.[65] FGFR can phosphorylate four tyrosine residues on LDHA, which increases its stability and activity.[107,108] FGFR1 can phosphorylate and activate pyruvate dehydrogenase kinase 1 (PDHK1) that negatively regulates pyruvate dehydrogenase (PDH), resulting in decreased pyruvate entry into OXPHOS.[109] In human lymphatic endothelial cells, FGFR1 knockdown decreased levels of glycolytic metabolites and lactate, and treatment with FGF2 had the opposite effect.[110] These observations were attributed to changes in the expression of HK2, which was induced by FGF2 and lowered by knockdown of FGFR1 in a manner transcriptionally dependent on c-Myc. Treatment of FGF2-stimulated squamous cell lung cancer cells with inhibitors of FGFR decreased glucose uptake and expression of GLUT1, reduced PK activity, and hampered HIF-1α induction in both hypoxia and normoxia.[111] In this context, the PI3K/Akt/mTOR pathway was the key mediator of the effects of FGFR signalling. In human prostate cancer cells, ablation of FGFR1 decreased glucose uptake and lactate production, and increased oxygen consumption, consistent with a switch from glycolysis to oxidative OXPHOS.[108] Expression of LDHB mRNA and protein was higher whereas expression of LDHA protein was lower but mRNA was unchanged, indicating no link between FGFR1 and LDHA transcription in this context. Similar results were obtained in mouse embryonic fibroblasts (MEFs). The endocrine hormone FGF19 has been shown to modulate glucose metabolism in the brain, lowering glucose levels independently of insulin by increasing conversion of glucose to lactate.[112] Altogether, these studies highlight the diverse nature of the mechanisms through which FGFRs can control glucose metabolism. One study in cancer-associated fibroblasts even presented evidence for FGF2 driving OXPHOS and downregulating glycolysis.[113]

Chinchore et al reported that FGFR drives aerobic glycolysis in the mouse retina.[9] The researchers treated mouse retinal explants with the FGFR inhibitor PD173074 or the multi-kinase inhibitor TKI258, and found significantly lower lactate production rates and less of the phosphorylated forms of LDHA and PKM2. It should, however, be noted that PD173074 was used at concentrations orders of magnitude above that which is typically effective in cell culture.[114-117] Leaving the RPE attached to the retina raised the lactate production rate by a similar amount to supplementing medium with FGF2, leading to the authors' proposal that FGF2 secreted by the RPE stimulates aerobic glycolysis in the retina.[9] Some evidence is consistent with a role for FGFRs in retinal neuronal survival and therefore potentially glucose metabolism. A study in mice found that expression of a dominant negative form of FGFR2, but interestingly not FGFR1, under the control of an exogenous rhodopsin promoter resulted in progressive

photoreceptor degeneration.[118] On the other hand, global knockout of FGF2 in mice reportedly causes no morphological changes to the retina.[119,120] Possibly, there is redundancy with other FGFs in driving retinal glycolysis. Interestingly, FGFR1 and FGF2 are upregulated and neurotrophic in response to light damage or retinal detachment, but whether modulation of glycolysis is important for this effect is unclear.[121-124] Altogether, current data show that exogenous FGF2 can drive aerobic glycolysis in the mouse retina, while a role in glucose metabolism in the basal state is plausible but will require a more detailed investigation to confirm.

## 8 | HYPOXIA-INDUCIBLE FACTOR 1

Hypoxia-inducible factor 1 (HIF-1) is a heterodimeric transcription factor comprising an oxygen-regulated α subunit, HIF-1α, and a stable β subunit, HIF-1β, more commonly known as the aryl hydrocarbon receptor nuclear translocator (ARNT).[70] In most cells, HIF-1α and ARNT are constitutively transcribed. However, when oxygen is available, HIF-1α is enzymatically hydroxylated on specific proline residues and an asparagine, which mark it for rapid proteasomal degradation and prevent interaction with transcriptional coactivators, respectively.[125-127] In hypoxia, the hydroxylation reactions cannot proceed and so HIF-1α escapes degradation, translocates to the nucleus, binds to ARNT and activates the expression of hundreds of target genes. These genes function to maintain oxygen homeostasis by various mechanisms including directing the metabolic switch from OXPHOS to glycolysis. HIF-1α is able to orchestrate this switch by initiating transcription of genes encoding glucose transporters such as GLUT1, and an array of glycolytic enzymes including HK2 and LDHA.[128] HIF-1α also activates the transcription of PDHK1 which phosphorylates and decreases the activity of PDH, thereby limiting entry of pyruvate into the TCA cycle.[129] A second HIF-α isoform, HIF-2α, is regulated by hypoxia in a similar manner to HIF-1α, although it has a more discrete set of target genes and plays less of a role in regulating metabolism.

In cancers, HIF-1α has been found to be stable and transcriptionally active and can, among other tumour-promoting effects, drive aerobic glycolysis.[70] Stabilization of HIF-1α in the context of cancer occurs in a number of ways. Hypoxic microenvironments in solid tumours facilitate stabilization via the mechanism described above. Genetic mutations in key components of the regulatory machinery such as the von Hippel-Lindau protein (VHL), which facilitates HIF-1α proteasomal degradation, can cause aberrant stabilization in normoxic conditions. HIF-1α can also be stabilized in the presence of oxygen by high levels of reactive oxygen species such as nitric oxide, and its stability can be modulated context-dependently, including in some cancer cells, via signalling pathways such as the PI3K/Akt/mTORC1 axis.[94,130,131] Interestingly, a feed-forward mechanism also exists whereby high levels of pyruvate and lactate can contribute to HIF stabilization.[130] Given its key role in driving glycolysis and lactate production in cancer, it is logical that HIF-1α could drive aerobic glycolysis in the retina, especially given the established involvement of many of its transcriptional targets.

The role of HIF-1α in retinal lactate production in the adult retina to our knowledge has not been directly tested but evidence indicates that it may not be an essential player. While HIF-1α is important in certain cell types for retinal vascular development, there is limited evidence to support the idea that it is stably expressed and required in the normal adult mammalian retina, especially, in the photoreceptors which appear largely responsible for lactate production. Studies have shown that HIF-1α is expressed at the RNA level but protein is scarcely detectable by western blot in normoxic mouse retinas, consistent with rapid degradation.[132-134] Okano et al showed that expression of HIF-1α rapidly declines in mouse retinas after birth, correlating with increased oxygenation.[135] HIF-1α expression was retained in the ganglion cell layer, however. A separate study that compared HIF-1α expression in adult normoxic and hypoxic mouse retinas found similar results, reporting weak expression in normoxia that was limited to the ganglion cell layer.[133] One study presented immunohistochemical evidence for widespread HIF-1α expression in rat and human retinas, but it is difficult to confidently interpret without validation of antibody specificity or a negative control for expression.[136] It is possible that there are species-specific differences in expression, but together the evidence does not support high levels of HIF-1α protein expression in photoreceptor cells in aerobic or nonpathological conditions.

Importantly, conditional knockout of HIF-1α in mouse rod or cone photoreceptors resulted in no detectable functional change under non-stressed conditions, nor did dual knockout of both HIF-1α and HIF-2α. These results suggest that either aerobic glycolysis is not required for normal retinal function, or more likely that the HIFs are not required for aerobic glycolysis in the mature mouse retina, although this has not been directly confirmed as lactate production or other aerobic analyses of glycolysis were not assessed.[137,138] Given that HIF-1α has been implicated in the pathogenesis of several ischaemic retinal diseases where stabilization results in

neovascularisation and neurodegeneration, its inhibition or deletion is a promising avenue for disease treatments.[139,140] It is worth noting, however, that the converse is possibly true during development. In a hyperoxic mouse model of retinopathy of prematurity, elevated aerobic glycolysis in response to pharmacological HIF activation may contribute to retinal neuroprotection.[141,142] Whether endogenous HIF is important in driving glycolysis during development is unclear.

It is possible that HIF-1 plays a minimal or redundant role in retinal metabolism in the mature retina, but this needs to be directly analysed. The current evidence is convincing that ablation of HIFs in normal mouse photoreceptors is not overtly damaging, and provisionally rules out HIF-1 as a key driver of aerobic glycolysis in the mammalian retina, pending direct metabolic investigations.

## 9 | CONCLUDING REMARKS

Recent findings have highlighted the importance of the expression of LDHA, PKM2 and HK2 in the maintenance of aerobic glycolysis in the retina, and in general, the roles of these enzymes in the retina mirrors their roles in cancer cells. Whether the reported post-translational modifications or changes in subcellular localization of these enzymes are important for retinal metabolism or function is still unclear, and the upstream signalling pathways or transcriptional programs that control their expression and regulation are also largely unknown. Evidence for the PI3K/Akt pathway, FGFRs and HIF-1 driving aerobic glycolysis in the retina is less convincing, with more specific investigations required to determine whether they also make an important contribution. Finally, it is possible that other factors yet to be investigated may prove to be key drivers, including factors common to cancer cells or novel photoreceptor-specific drivers. Ultimately, the identification and characterization of the key drivers of aerobic glycolysis will enable a clearer understanding of normal retinal function, as well as provide valuable tolls to decipher the role of altered metabolism in retinal disease.

## ACKNOWLEDGEMENT

This work was supported by a Project Grant (1099932) from the National Health and Medical Research Council of Australia.

## CONFLICT OF INTEREST

None declared.

## ORCID

*Daniel J. Peet* https://orcid.org/0000-0002-6085-8936

## REFERENCES

1. Lunt SY, Vander Heiden MG. Aerobic glycolysis: meeting the metabolic requirements of cell proliferation. *Annu Rev Cell Dev Biol*. 2011;27:441-464.
2. Liberti MV, Locasale JW. The Warburg effect: how does it benefit cancer cells? *Trends Biochem Sci*. 2016;41:211-218.
3. Koppenol WH, Bounds PL, Dang CV. Otto Warburg's contributions to current concepts of cancer metabolism. *Nat Rev Cancer*. 2011;11:325-337.
4. Warburg O, Posener K, Negelein E. On the metabolism of carcinoma cells. *Biochem Z*. 1924;152:309-344.
5. Ng SK, Wood JP, Chidlow G, et al. Cancer-like metabolism of the mammalian retina. *Clin Experiment Ophthalmol*. 2015;43:367-376.
6. Warburg O. The metabolism of carcinoma cells. *J Can Res*. 1925;9:148-163.
7. Winkler BS. Glycolytic and oxidative metabolism in relation to retinal function. *J Gen Physiol*. 1981;77:667-692.
8. Winkler BS. A quantitative assessment of glucose metabolism in the rat retina. In: Christen Y, Doly M, Droy-Lefaix MT, eds. *Les Seminaries ophthalmologiques d'IPSEN 1995*; tome 6. Paris: Elsevier. 1995;78-96.
9. Chinchore Y, Begaj T, Wu D, Drokhlyansky E, Cepko CL. Glycolytic reliance promotes anabolism in photoreceptors. *Elife*. 2017;6:e25946.
10. Cohen LH, Noell WK. Glucose catabolism of rabbit retina before and after development of visual function. *J Neurochem*. 1960;5:253-276.
11. Ames A 3rd, Li YY, Heher EC, Kimble CR. Energy metabolism of rabbit retina as related to function: high cost of Na+ transport. *J Neurosci*. 1992;12:840-853.
12. Futterman S, Kinoshita JH. Metabolism of the retina. I. Respiration of cattle retina. *J Biol Chem*. 1959;234:723-726.
13. Hopkinson L, Kerly M. The effect of monoiodoacetate on the aerobic metabolism of ox retina in vitro. *Biochem J*. 1959;72:22-27.
14. Wang L, Kondo M, Bill A. Glucose metabolism in cat outer retina. Effects of light and hyperoxia. *Invest Ophthalmol Vis Sci*. 1997;38:48-55.
15. Wang L, Tornquist P, Bill A. Glucose metabolism in pig outer retina in light and darkness. *Acta Physiol Scand*. 1997;160:75-81.
16. Ames A 3rd, Gurian BS. Effects of glucose and oxygen deprivation on function of isolated mammalian retina. *J Neurophysiol*. 1963;26:617-634.
17. Chertov AO, Holzhausen L, Kuok IT, et al. Roles of glucose in photoreceptor survival. *J Biol Chem*. 2011;286:34700-34711.
18. Cheng SY, Cipi J, Ma S, et al. Altered photoreceptor metabolism in mouse causes late stage age-related macular degeneration-like pathologies. *Proc Natl Acad Sci U S A*. 2020;117:13094-13104.
19. Léveillard T, Philp NJ, Sennlaub F. Is retinal metabolic dysfunction at the Center of the Pathogenesis of age-related macular degeneration? *Int J Mol Sci*. 2019;20:762.

20. Aït-Ali N, Fridlich R, Millet-Puel G, et al. Rod-derived cone viability factor promotes cone survival by stimulating aerobic glycolysis. *Cell*. 2015;161:817-832.
21. Petit L, Ma S, Cipi J, et al. Aerobic glycolysis is essential for Normal rod function and controls secondary cone death in retinitis Pigmentosa. *Cell Rep*. 2018;23:2629-2642.
22. Narayan DS, Chidlow G, Wood JP, Casson RJ. Glucose metabolism in mammalian photoreceptor inner and outer segments. *Clin Experiment Ophthalmol*. 2017;45:730-741.
23. Morohoshi K, Ohbayashi M, Patel N, Chong V, Bird AC, Ono SJ. Identification of anti-retinal antibodies in patients with age-related macular degeneration. *Exp Mol Pathol*. 2012; 93:193-199.
24. Wangsa-Wirawan ND, Linsenmeier RA. Retinal oxygen: fundamental and clinical aspects. *Arch Ophthalmol*. 2003;121: 547-557.
25. Linsenmeier RA. Effects of light and darkness on oxygen distribution and consumption in the cat retina. *J Gen Physiol*. 1986;88:521-542.
26. Pournaras CJ, Riva CE, Tsacopoulos M, Strommer K. Diffusion of O2 in the retina of anesthetized miniature pigs in normoxia and hyperoxia. *Exp Eye Res*. 1989;49:347-360.
27. Cringle SJ, Yu DY, Alder VA. Intravitreal and intraretinal oxygen tension in the rat eye. *Adv Exp Med Biol*. 1992;316: 113-117.
28. Yu DY, Cringle SJ. Oxygen distribution and consumption within the retina in vascularised and avascular retinas and in animal models of retinal disease. *Prog Retin Eye Res*. 2001;20: 175-208.
29. Kooragayala K, Gotoh N, Cogliati T, et al. Quantification of oxygen consumption in retina ex vivo demonstrates limited reserve capacity of photoreceptor mitochondria. *Invest Ophthalmol Vis Sci*. 2015;56:8428-8436.
30. Kanow MA, Giarmarco MM, Jankowski CS, et al. Biochemical adaptations of the retina and retinal pigment epithelium support a metabolic ecosystem in the vertebrate eye. *Elife*. 2017;6: e28899.
31. Díaz-García CM, Yellen G. Neurons rely on glucose rather than astrocytic lactate during stimulation. *J Neurosci Res*. 2019;97:883-889.
32. Yu L, Chen X, Wang L, Chen S. The sweet trap in tumors: aerobic glycolysis and potential targets for therapy. *Oncotarget*. 2016;7:38908-38926.
33. Valvona CJ, Fillmore HL, Nunn PB, Pilkington GJ. The regulation and function of lactate dehydrogenase a: therapeutic potential in brain tumor. *Brain Pathol*. 2016;26:3-17.
34. Markert CL, Shaklee JB, Whitt GS. Evolution of a gene. Multiple genes for LDH isozymes provide a model of the evolution of gene structure, function and regulation. *Science*. 1975;189: 102-114.
35. Cahn RD, Zwilling E, Kaplan NO, Levine L. Nature and development of lactic dehydrogenases: the two major types of this enzyme form molecular hybrids which change in makeup during development. *Science*. 1962;136:962-969.
36. Latner AL, Siddiqui SA, Skillen AW. Pyruvate inhibition of lactate dehydrogenase activity in human tissue extracts. *Science*. 1966;154:527-529.
37. Kaplan NO, Everse J, Admiraal J. Significance of substrate inhibition of dehydrogenases. *Ann N Y Acad Sci*. 1968;151:400-412.
38. Dawson DM, Goodfriend TL, Kaplan NO, Kaplan NO. Lactic dehydrogenases: functions of the two types. *Science*. 1964;143: 929-933.
39. Firth JD, Ebert BL, Ratcliffe PJ. Hypoxic regulation of lactate dehydrogenase a. interaction between hypoxia-inducible factor 1 and cAMP response elements. *J Biol Chem*. 1995;270: 21021-21027.
40. Rueda EM, Johnson JE Jr, Giddabasappa A, et al. The cellular and compartmental profile of mouse retinal glycolysis, tricarboxylic acid cycle, oxidative phosphorylation, and ~P transferring kinases. *Mol Vis*. 2016;22:847-885.
41. Casson RJ, Wood JPM, Han G, Kittipassorn T, Peet DJ, Chidlow G. M-type pyruvate kinase isoforms and lactate dehydrogenase a in the mammalian retina: metabolic implications. *Invest Ophthalmol Vis Sci*. 2016;57:66-80.
42. Lindsay KJ, Du J, Sloat SR, et al. Pyruvate kinase and aspartate-glutamate carrier distributions reveal key metabolic links between neurons and glia in retina. *Proc Natl Acad Sci U S A*. 2014;111:15579-15584.
43. Bonavita V, Ponte F, Amore G. Neurochemical studies on the inherited retinal degeneration of the rat I lactate dehydrogenase in the developing retina. *Vision Res*. 1963;61: 271-280.
44. Le YZ, Zheng L, Zheng W, et al. Mouse opsin promoter-directed Cre recombinase expression in transgenic mice. *Mol Vis*. 2006;12:389-398.
45. Roberts DJ, Miyamoto S. Hexokinase II integrates energy metabolism and cellular protection: Akting on mitochondria and TORCing to autophagy. *Cell Death Differ*. 2015;22: 248-257.
46. Patra KC, Wang Q, Bhaskar PT, et al. Hexokinase 2 is required for tumor initiation and maintenance and its systemic deletion is therapeutic in mouse models of cancer. *Cancer Cell*. 2013;24:213-228.
47. Arora KK, Pedersen PL. Functional significance of mitochondrial bound hexokinase in tumor cell metabolism. Evidence for preferential phosphorylation of glucose by intramitochondrially generated ATP. *J Biol Chem*. 1988;263: 17422-17428.
48. Pastorino JG, Hoek JB, Shulga N. Activation of glycogen synthase kinase 3β disrupts the binding of hexokinase II to mitochondria by phosphorylating voltage-dependent anion channel and potentiates chemotherapy-induced cytotoxicity. *Cancer Res*. 2005;65:10545-10554.
49. Roberts DJ, Tan-Sah VP, Smith JM, Miyamoto S. Akt phosphorylates HK-II at Thr-473 and increases mitochondrial HK-II association to protect cardiomyocytes. *J Biol Chem*. 2013; 288:23798-23806.
50. Wolf A, Agnihotri S, Micallef J, et al. Hexokinase 2 is a key mediator of aerobic glycolysis and promotes tumor growth in human glioblastoma multiforme. *J Exp Med*. 2011;208: 313-326.
51. Gershon TR, Crowther AJ, Tikunov A, et al. Hexokinase-2-mediated aerobic glycolysis is integral to cerebellar neurogenesis and pathogenesis of medulloblastoma. *Cancer Metab*. 2013;1:2.
52. Anderson M, Marayati R, Moffitt R, Yeh JJ. Hexokinase 2 promotes tumor growth and metastasis by regulating lactate production in pancreatic cancer. *Oncotarget*. 2017;8:56081-56094.

53. Reidel B, Thompson JW, Farsiu S, Moseley MA, Skiba NP, Arshavsky VY. Proteomic profiling of a layered tissue reveals unique glycolytic specializations of photoreceptor cells. *Mol Cell Proteomics*. 2011;10:M110.002469.
54. Rajala A, Gupta VK, Anderson RE, Rajala RVS. Light activation of the insulin receptor regulates mitochondrial hexokinase. A possible mechanism of retinal neuroprotection. *Mitochondrion*. 2013;13:566-576.
55. Li S, Chen D, Sauve Y, McCandless J, Chen YJ, Chen CK. Rhodopsin-iCre transgenic mouse line for Cre-mediated rod-specific gene targeting. *Genesis*. 2005;41:73-80.
56. Adler L, Chen C, Koutalos Y. Mitochondria contribute to NADPH generation in mouse rod photoreceptors. *J Biol Chem*. 2014;289:1519-1528.
57. Le YZ, Ash JD, Al-Ubaidi MR, Chen Y, Ma JX, Anderson RE. Targeted expression of Cre recombinase to cone photoreceptors in transgenic mice. *Mol Vis*. 2004;10:1011-1018.
58. Gharbi SI, Zvelebil MJ, Shuttleworth SJ, et al. Exploring the specificity of the PI3K family inhibitor LY294002. *Biochem J*. 2007;404:15-21.
59. Noguchi T, Inoue H, Tanaka T. The M1- and M2-type isozymes of rat pyruvate kinase are produced from the same gene by alternative RNA splicing. *J Biol Chem*. 1986;261:13807-13812.
60. Israelsen WJ, Vander Heiden MG. Pyruvate kinase: function, regulation and role in cancer. *Semin Cell Dev Biol*. 2015;43:43-51.
61. Hsu M-C, Hung W-C. Pyruvate kinase M2 fuels multiple aspects of cancer cells: from cellular metabolism, transcriptional regulation to extracellular signaling. *Mol Cancer*. 2018;17:35.
62. Ashizawa K, Willingham MC, Liang CM, Cheng SY. In vivo regulation of monomer-tetramer conversion of pyruvate kinase subtype M2 by glucose is mediated via fructose 1,6-bisphosphate. *J Biol Chem*. 1991;266:16842-16846.
63. Dombrauckas JD, Santarsiero BD, Mesecar AD. Structural basis for tumor pyruvate kinase M2 allosteric regulation and catalysis. *Biochemistry*. 2005;44:9417-9429.
64. Christofk HR, Vander Heiden MG, Wu N, Asara JM, Cantley LC. Pyruvate kinase M2 is a phosphotyrosine-binding protein. *Nature*. 2008;452:181-186.
65. Hitosugi T, Kang S, Vander Heiden MG, et al. Tyrosine phosphorylation inhibits PKM2 to promote the Warburg effect and tumor growth. *Sci Signal*. 2009;2:ra73.
66. Lunt SY, Muralidhar V, Hosios AM, et al. Pyruvate kinase isoform expression alters nucleotide synthesis to impact cell proliferation. *Mol Cell*. 2015;57:95-107.
67. Young RW. The renewal of photoreceptor cell outer segments. *J Cell Biol*. 1967;33:61-72.
68. Christofk HR, Vander Heiden MG, Harris MH, et al. The M2 splice isoform of pyruvate kinase is important for cancer metabolism and tumour growth. *Nature*. 2008;452:230-233.
69. Luo W, Hu H, Chang R, et al. Pyruvate kinase M2 is a PHD3-stimulated coactivator for hypoxia-inducible factor 1. *Cell*. 2011;145:732-744.
70. Semenza GL. Regulation of metabolism by hypoxia-inducible factor 1. *Cold Spring Harb Symp Quant Biol*. 2011;76:347-353.
71. Rajala RVS. Aerobic glycolysis in the retina: functional roles of pyruvate kinase isoforms. *Front Cell Dev Biol*. 2020;8:266.
72. Rajala A, Wang Y, Brush RS, et al. Pyruvate kinase M2 regulates photoreceptor structure, function, and viability. *Cell Death Dis*. 2018;9:240.
73. Rajala RV, Rajala A, Kooker C, Wang Y, Anderson RE. The Warburg effect mediator pyruvate kinase M2 expression and regulation in the retina. *Sci Rep*. 2016;6:37727.
74. Wubben TJ, Pawar M, Smith A, Toolan K, Hager H, Besirli CG. Photoreceptor metabolic reprogramming provides survival advantage in acute stress while causing chronic degeneration. *Sci Rep*. 2017;7:17863.
75. Rajala A, Wang Y, Soni K, Rajala RVS. Pyruvate kinase M2 isoform deletion in cone photoreceptors results in age-related cone degeneration. *Cell Death Dis*. 2018;9:737.
76. Jeon CJ, Strettoi E, Masland RH. The major cell populations of the mouse retina. *J Neurosci*. 1998;18:8936-8946.
77. Fruman DA, Chiu H, Hopkins BD, Bagrodia S, Cantley LC, Abraham RT. The PI3K pathway in human disease. *Cell*. 2017;170:605-635.
78. Vanhaesebroeck B, Guillermet-Guibert J, Graupera M, Bilanges B. The emerging mechanisms of isoform-specific PI3K signalling. *Nat Rev Mol Cell Biol*. 2010;11:329-341.
79. Martini M, De Santis MC, Braccini L, Gulluni F, Hirsch E. PI3K/AKT signaling pathway and cancer: an updated review. *Ann Med*. 2014;46:372-383.
80. Auger KR, Serunian LA, Soltoff SP, Libby P, Cantley LC. PDGF-dependent tyrosine phosphorylation stimulates production of novel polyphosphoinositides in intact cells. *Cell*. 1989;57:167-175.
81. Burgering BM, Coffer PJ. Protein kinase B (c-Akt) in phosphatidylinositol-3-OH kinase signal transduction. *Nature*. 1995;376:599-602.
82. Franke TF, Yang SI, Chan TO, et al. The protein kinase encoded by the Akt proto-oncogene is a target of the PDGF-activated phosphatidylinositol 3-kinase. *Cell*. 1995;81:727-736.
83. Alessi DR, Andjelkovic M, Caudwell B, et al. Mechanism of activation of protein kinase B by insulin and IGF-1. *EMBO J*. 1996;15:6541-6551.
84. Alessi DR, James SR, Downes CP, et al. Characterization of a 3-phosphoinositide-dependent protein kinase which phosphorylates and activates protein kinase Balpha. *Curr Biol*. 1997;7:261-269.
85. Sarbassov DD, Guertin DA, Ali SM, Sabatini DM. Phosphorylation and regulation of Akt/PKB by the rictor-mTOR complex. *Science*. 2005;307:1098-1101.
86. Lawrence MS, Stojanov P, Mermel CH, et al. Discovery and saturation analysis of cancer genes across 21 tumour types. *Nature*. 2014;505:495-501.
87. Elstrom RL, Bauer DE, Buzzai M, et al. Akt stimulates aerobic glycolysis in cancer cells. *Cancer Res*. 2004;64:3892-3899.
88. Ran C, Liu H, Hitoshi Y, Israel MA. Proliferation-independent control of tumor glycolysis by PDGFR-mediated AKT activation. *Cancer Res*. 2013;73:1831-1843.
89. Makinoshima H, Takita M, Saruwatari K, et al. Signaling through the phosphatidylinositol 3-kinase (PI3K)/mammalian target of rapamycin (mTOR) Axis is responsible for aerobic glycolysis mediated by glucose transporter in epidermal growth factor receptor (EGFR)-mutated lung adenocarcinoma. *J Biol Chem*. 2015;290:17495-17504.

90. Barthel A, Okino ST, Liao J, et al. Regulation of GLUT1 gene transcription by the serine/threonine kinase Akt1. *J Biol Chem*. 1999;274:20281-20286.
91. Rathmell JC, Fox CJ, Plas DR, Hammerman PS, Cinalli RM, Thompson CB. Akt-directed glucose metabolism can prevent Bax conformation change and promote growth factor-independent survival. *Mol Cell Biol*. 2003;23:7315-7328.
92. Deprez J, Vertommen D, Alessi DR, Hue L, Rider MH. Phosphorylation and activation of heart 6-phosphofructo-2-kinase by protein kinase B and other protein kinases of the insulin signaling cascades. *J Biol Chem*. 1997;272:17269-17275.
93. Inoki K, Li Y, Zhu T, Wu J, Guan K-L. TSC2 is phosphorylated and inhibited by Akt and suppresses mTOR signalling. *Nat Cell Biol*. 2002;4:648-657.
94. Zhong H, Chiles K, Feldser D, et al. Modulation of hypoxia-inducible factor 1alpha expression by the epidermal growth factor/phosphatidylinositol 3-kinase/PTEN/AKT/FRAP pathway in human prostate cancer cells: implications for tumor angiogenesis and therapeutics. *Cancer Res*. 2000;60:1541-1545.
95. Jiang BH, Jiang G, Zheng JZ, Lu Z, Hunter T, Vogt PK. Phosphatidylinositol 3-kinase signaling controls levels of hypoxia-inducible factor 1. *Cell Growth Differ*. 2001;12:363-369.
96. Rajala RV. Phosphoinositide 3-kinase signaling in the vertebrate retina. *J Lipid Res*. 2010;51:4-22.
97. Yi X, Schubert M, Peachey NS, et al. Insulin receptor substrate 2 is essential for maturation and survival of photoreceptor cells. *J Neurosci*. 2005;25:1240-1248.
98. Li G, Anderson RE, Tomita H, et al. Nonredundant role of Akt2 for neuroprotection of rod photoreceptor cells from light-induced cell death. *J Neurosci*. 2007;27:203-211.
99. Rajala RVS, Anderson RE. Rhodopsin-regulated insulin receptor signaling pathway in rod photoreceptor neurons. *Mol Neurobiol*. 2010;42:39-47.
100. Ivanovic I, Anderson RE, Le YZ, Fliesler SJ, Sherry DM, Rajala RV. Deletion of the p85alpha regulatory subunit of phosphoinositide 3-kinase in cone photoreceptor cells results in cone photoreceptor degeneration. *Invest Ophthalmol Vis Sci*. 2011;52:3775-3783.
101. Rajala RV, Ranjo-Bishop M, Wang Y, Rajala A, Anderson RE. The p110alpha isoform of phosphoinositide 3-kinase is essential for cone photoreceptor survival. *Biochimie*. 2015;112:35-40.
102. Rajala A, Dighe R, Agbaga MP, Anderson RE, Rajala RV. Insulin receptor signaling in cones. *J Biol Chem*. 2013;288:19503-19515.
103. Gardner TW, Abcouwer SF, Losiewicz MK, Fort PE. Phosphatase control of 4E-BP1 phosphorylation state is central for glycolytic regulation of retinal protein synthesis. *Am J Physiol Endocrinol Metab*. 2015;309:E546-E556.
104. Hu H, Juvekar A, Lyssiotis CA, et al. Phosphoinositide 3-kinase regulates glycolysis through mobilization of aldolase from the Actin cytoskeleton. *Cell*. 2016;164:433-446.
105. Ornitz DM, Itoh N. The fibroblast growth factor signaling pathway. *Wiley Interdiscip Rev Dev Biol*. 2015;4:215-266.
106. Babina IS, Turner NC. Advances and challenges in targeting FGFR signalling in cancer. *Nat Rev Cancer*. 2017;17:318-332.
107. Fan J, Hitosugi T, Chung TW, et al. Tyrosine phosphorylation of lactate dehydrogenase a is important for NADH/NAD(+) redox homeostasis in cancer cells. *Mol Cell Biol*. 2011;31:4938-4950.
108. Liu J, Chen G, Liu Z, et al. Aberrant FGFR tyrosine kinase signaling enhances the Warburg effect by reprogramming LDH isoform expression and activity in prostate cancer. *Cancer Res*. 2018;78:4459-4470.
109. Hitosugi T, Fan J, Chung TW, et al. Tyrosine phosphorylation of mitochondrial pyruvate dehydrogenase kinase 1 is important for cancer metabolism. *Mol Cell*. 2011;44:864-877.
110. Yu P, Wilhelm K, Dubrac A, et al. FGF-dependent metabolic control of vascular development. *Nature*. 2017;545:224-228.
111. Fumarola C, Cretella D, La Monica S, et al. Enhancement of the anti-tumor activity of FGFR1 inhibition in squamous cell lung cancer by targeting downstream signaling involved in glucose metabolism. *Oncotarget*. 2017;8:91841-91859.
112. Morton GJ, Matsen ME, Bracy DP, et al. FGF19 action in the brain induces insulin-independent glucose lowering. *J Clin Invest*. 2013;123:4799-4808.
113. Kumar D, New J, Vishwakarma V, et al. Cancer-associated fibroblasts drive glycolysis in a targetable signaling loop implicated in head and neck squamous cell carcinoma progression. *Cancer Res*. 2018;78:3769-3782.
114. Gudernova I, Vesela I, Balek L, et al. Multikinase activity of fibroblast growth factor receptor (FGFR) inhibitors SU5402, PD173074, AZD1480, AZD4547 and BGJ398 compromises the use of small chemicals targeting FGFR catalytic activity for therapy of short-stature syndromes. *Hum Mol Genet*. 2016;25:9-23.
115. Turner N, Pearson A, Sharpe R, et al. FGFR1 amplification drives endocrine therapy resistance and is a therapeutic target in breast cancer. *Cancer Res*. 2010;70:2085-2094.
116. Mohammadi M, Froum S, Hamby JM, et al. Crystal structure of an angiogenesis inhibitor bound to the FGF receptor tyrosine kinase domain. *EMBO J*. 1998;17:5896-5904.
117. Skaper SD, Kee WJ, Facci L, Macdonald G, Doherty P, Walsh FS. The FGFR1 inhibitor PD 173074 selectively and potently antagonizes FGF-2 neurotrophic and neurotropic effects. *J Neurochem*. 2000;75:1520-1527.
118. Campochiaro PA, Chang M, Ohsato M, et al. Retinal degeneration in transgenic mice with photoreceptor-specific expression of a dominant-negative fibroblast growth factor receptor. *J Neurosci*. 1996;16:1679-1688.
119. Ozaki H, Okamoto N, Ortega S, et al. Basic fibroblast growth factor is neither necessary nor sufficient for the development of retinal neovascularization. *Am J Pathol*. 1998;153:757-765.
120. Foletti A, Ackermann J, Schmidt A, Hummler E, Beermann F. Absence of fibroblast growth factor 2 does not prevent tumor formation originating from the RPE. *Oncogene*. 2002;21:1841-1847.
121. Guillonneau X, Regnier-Ricard F, Laplace O, et al. Fibroblast growth factor (FGF) soluble receptor 1 acts as a natural inhibitor of FGF2 neurotrophic activity during retinal degeneration. *Mol Biol Cell*. 1998;9:2785-2802.
122. Cao W, Wen R, Li F, Lavail MM, Steinberg RH. Mechanical injury increases bFGF and CNTF mRNA expression in the mouse retina. *Exp Eye Res*. 1997;65:241-248.
123. Wen R, Cheng T, Song Y, et al. Continuous exposure to bright light upregulates bFGF and CNTF expression in the rat retina. *Curr Eye Res*. 1998;17:494-500.

124. Ozaki S, Radeke MJ, Anderson DH. Rapid upregulation of fibroblast growth factor receptor 1 (flg) by rat photoreceptor cells after injury. *Invest Ophthalmol Vis Sci*. 2000;41:568-579.
125. Bruick RK, McKnight SL. A conserved family of prolyl-4-hydroxylases that modify HIF. *Science*. 2001;294:1337-1340.
126. Mahon PC, Hirota K, Semenza GL. FIH-1: a novel protein that interacts with HIF-1alpha and VHL to mediate repression of HIF-1 transcriptional activity. *Genes Dev*. 2001;15:2675-2686.
127. Lando D, Peet DJ, Whelan DA, Gorman JJ, Whitelaw ML. Asparagine hydroxylation of the HIF transactivation domain a hypoxic switch. *Science*. 2002;295:858-861.
128. Iyer NV, Kotch LE, Agani F, et al. Cellular and developmental control of O2 homeostasis by hypoxia-inducible factor 1 alpha. *Genes Dev*. 1998;12:149-162.
129. Papandreou I, Cairns RA, Fontana L, Lim AL, Denko NC. HIF-1 mediates adaptation to hypoxia by actively down-regulating mitochondrial oxygen consumption. *Cell Metab*. 2006;3:187-197.
130. Lu H, Forbes RA, Verma A. Hypoxia-inducible factor 1 activation by aerobic glycolysis implicates the Warburg effect in carcinogenesis. *J Biol Chem*. 2002;277:23111-23115.
131. Kaelin WG. ROS: really involved in oxygen sensing. *Cell Metab*. 2005;1:357-358.
132. Grimm C, Wenzel A, Groszer M, et al. HIF-1-induced erythropoietin in the hypoxic retina protects against light-induced retinal degeneration. *Nat Med*. 2002;8:718-724.
133. Thiersch M, Lange C, Joly S, et al. Retinal neuroprotection by hypoxic preconditioning is independent of hypoxia-inducible factor-1α expression in photoreceptors. *Eur J Neurosci*. 2009;29:2291-2302.
134. Lange C, Heynen SR, Tanimoto N, et al. Normoxic activation of hypoxia-inducible factors in photoreceptors provides transient protection against light-induced retinal degeneration. *Invest Ophthalmol Vis Sci*. 2011;52:5872-5880.
135. Kurihara T, Kubota Y, Ozawa Y, et al. von Hippel-Lindau protein regulates transition from the fetal to the adult circulatory system in retina. *Development*. 2010;137:1563-1571.
136. Hughes JM, Groot AJ, van der Groep P, et al. Active HIF-1 in the normal human retina. *J Histochem Cytochem*. 2010;58:247-254.
137. Kast B, Schori C, Grimm C. Hypoxic preconditioning protects photoreceptors against light damage independently of hypoxia inducible transcription factors in rods. *Exp Eye Res*. 2016;146:60-71.
138. Samardzija M, Barben M, Todorova V, Klee K, Storti F, Grimm C. Hif1a and Hif2a can be safely inactivated in cone photoreceptors. *Sci Rep*. 2019;9:16121.
139. Peet DJ, Kittipassorn T, Wood JP, Chidlow G, Casson RJ. HIF signalling: the eyes have it. *Exp Cell Res*. 2017;356:136-140.
140. Vadlapatla RK, Vadlapudi AD, Mitra AK. Hypoxia-inducible factor-1 (HIF-1): a potential target for intervention in ocular neovascular diseases. *Curr Drug Targets*. 2013;14:919-935.
141. Singh C, Hoppe G, Tran V, et al. Serine and 1-carbon metabolism are required for HIF-mediated protection against retinopathy of prematurity. *JCI Insight*. 2019;4:e129398.
142. Hoppe G, Yoon S, Gopalan B, et al. Comparative systems pharmacology of HIF stabilization in the prevention of retinopathy of prematurity. *Proc Natl Acad Sci U S A*. 2016;113:E2516-E2525.

**How to cite this article:** Haydinger CD, Kittipassorn T, Peet DJ. Power to see—Drivers of aerobic glycolysis in the mammalian retina: A review. *Clin Experiment Ophthalmol*. 2020;1–15. https://doi.org/10.1111/ceo.13833

## *Müller cell glucose metabolism*

The cellular source of lactate in the retina is debated. The perspective presented in the review above, that photoreceptors produce the majority of lactate, was termed the classical view by Winkler and colleagues, as it was the original view of early researchers of retinal metabolism[45]. However, an alternative hypothesis proposed in the 1990s stated that Müller cells are the major producers of lactate, which is transported into photoreceptors to fuel oxidative phosphorylation[44]. This model is sometimes termed the astrocyte-neuron lactate shuttle (ANLS), especially in the context of the brain, where astrocytes produce lactate that is taken up and oxidised by neurons to generate ATP. Evidence from retinal studies ostensibly supports both hypotheses. So, what is the evidence, and is there yet enough to confirm or reject either idea?

Several observations favour the ANLS model. Poitry-Yamate and colleagues showed that acutely isolated guinea pig Müller cells alone released more lactate into the bathing medium than complexes of photoreceptors and Müller cells[44]. The implication was that photoreceptors consumed lactate released by Müller cells, although this flow was not shown directly. Müller cells in culture – both primary cells and immortalised cell lines – strongly exhibit aerobic glycolysis[47,114]. For example, under aerobic conditions, cultured human primary Müller cells convert 99% of the glucose they consume to lactate[47]. In addition, Müller cells *in vivo* lack the aspartate glutamate carrier, thus cannot engage the malate aspartate shuttle to transfer reducing equivalents from the cytoplasm to the mitochondria[115]. They may therefore have an impaired capacity to oxidise glucose fully, although investigation of the activity of the glycerol phosphate shuttle in Müller cells, which may be able to compensate, has not been reported.

There is also evidence against the ANLS model. Autoradiographic studies show no preferential uptake of glucose into Müller cells in rat or guinea pig retinas, with highest uptake observed in the photoreceptor layer[45]. As discussed in our review above, the importance of key glycolytic enzymes classically involved in aerobic glycolysis has been demonstrated in photoreceptors and is consistent with these cells being lactate producers[116]. Mouse retinas that lack photoreceptors produce 70% less lactate than controls[54]. Müller cells comprise a far smaller proportion of retinal cells than photoreceptors[45,57], and Müller cells are positioned further from the choroidal vasculature which supplies glucose to the outer retina via the RPE, so it is unlikely that Müller cells alone consume a large enough proportion of glucose to account for the high rate of whole retinal aerobic glycolysis.

In addition, it has been reported that mouse Müller cells *in vivo* lack, or only very lowly express, any isoform of pyruvate kinase (PK), and therefore have an impaired ability to undertake complete glycolysis from glucose to pyruvate[54]. Previous work in our laboratory has shown that cultured rat

Müller cells do express PK[114], indicating either a difference between mouse and rat Müller cells or a difference between Müller cells *in vivo* and *in vitro*. It is possible that PK expression is gained rapidly as Müller cells adapt to cell culture conditions. Finally, as highlighted in the review above, LDH-A expression is higher in the photoreceptors than Müller cells *in vivo*[50,117], supporting their predominant role in lactate production over Müller cells.

In summary, the conflicting data regarding the cellular sources of lactate in the retina are yet to be fully explained, but the weight of evidence indicates that photoreceptors are net lactate producers. Most evidence indicates that Müller cells are also likely lactate producers, but if so, their apparent lack of PK *in vivo* is yet to be reconciled with this perspective.

## *Metabolism and retinal disease*

Retinal metabolic dysfunction is linked to disease in multiple ways. Firstly, primary metabolic dysfunction can cause disease. Retinitis pigmentosa, for example, is a heterogeneous group of genetic diseases characterised by photoreceptor degeneration and the appearance of retinal pigment deposits[118]. Mutations in several genes directly involved in metabolism can cause retinitis pigmentosa in humans, including in isocitrate dehydrogenase 3A (*IDH3A*)[119] or 3B (*IDH3B*)[120], hexokinase 1 (*HK1*)[121] and hexokinase domain-containing protein 1 (*HDKC1*)[122].

Secondly, ischemia is a pathological feature of many retinal diseases of major clinical importance, including glaucoma, diabetic retinopathy, age-related macular degeneration (AMD), and retinal vascular occlusion[17,19,123,124]. Metabolic dysfunction due to ischemia is proposed to be a unifying pathological feature of many retinal diseases[125]. Under ischemic conditions, oxygen and nutrient supplies are limited, which induces changes in the retina. For example, expression of hexokinase 2 (HK2) and pyruvate kinase M2 (PKM2) are higher in the retinas of patients with AMD, which is proposed to reflect a decrease in glucose supply[15]. Similar changes have been found in mouse models of retinitis pigmentosa[14,126]. Excess metabolic demand relative to supply can cause an ATP shortage and ultimately lead to dysfunction and excitotoxic death of retinal neurons[123]. In diabetic retinopathy and AMD, ischemia induces upregulation of angiogenic pathways leading to neovascularisation driven by factors such as vascular endothelial growth factor (VEGF)[127]. Neovascularisation is pathogenic as new vessels are prone leaking and haemorrhaging, resulting in retinal oedema and loss of vision. As such, anti-VEGF therapy is a common and useful treatment for these diseases, but it is not effective in all cases, with anti-VEGF-resistant disease a major problem[127]. Given the unifying role of metabolism in many retinal diseases, improved understanding of retinal metabolism is urgently needed so that new targets may be discovered for treatment of debilitating visual diseases.

## *1.5 Aims and approaches*

It is clear that many aspects of retinal energy metabolism require further research to understand comprehensively, including the metabolic relationships between cell types, and the molecular drivers of aerobic glycolysis. In this project, the main experimental focus was elucidating molecular mechanisms that drive aerobic glycolysis at the level of cell signalling pathways and transcriptional programs.

**Hypothesis:** Conserved signalling pathways that drive aerobic glycolysis in the contexts of cancer and proliferation also drive aerobic glycolysis in the mammalian retina.

**Overall Aim:** Determine molecular drivers of aerobic glycolysis in the mammalian retina.

**Sub-aims:**

1. Determine molecular drivers of aerobic glycolysis in the rMC-1 rat Müller cell line.
2. Probe RNA-sequencing (RNA-seq) datasets to investigate metabolic characteristics of Müller cells and photoreceptors.
3. Determine molecular drivers of aerobic glycolysis in rat retinal explants.

A targeted approach was taken to discover drivers of aerobic glycolysis. Initially, molecules and pathways were chosen for study based on their well-established roles in driving aerobic glycolysis in the context of cancer. Small-molecule inhibitors were commercially available specifically targeting components of many such pathways, the effects of which were tested on retinal glucose metabolism using lactate production assays, glucose consumption assays and Seahorse extracellular flux assays.

In this thesis, experiments were performed on cell lines and retinal explants from the rat due to the practical availability of rats and relevant cell lines, and because rats possess similar vasculature and oxygen distribution to primate and human retinas[106]. Cultured Müller cells are widely used and known to exhibit aerobic glycolysis, and readily manipulated experimentally. In addition, our laboratory possessed a strong set of experimental tools and experience that made these cells an excellent starting point for experiments. Later work utilised explanted whole rat retinas, which offered several advantages in modelling *in vivo* metabolism, including complex cell-cell interactions, and the presence of photoreceptors which cannot be cultured alone.

Publicly available RNA-seq datasets were regularly queried to answer questions that arose over the course of the project. A major aim in the analyses of RNA-seq data was to determine metabolic differences between retinal cell types, notably Müller cells and rod photoreceptors, at the transcriptomic level.

# 2. Materials and Methods

## 2.1 Reagent tables

**Inhibitors**

| Inhibitor | Target | Working conc. (µM) | Manufacturer |
|---|---|---|---|
| LY294002 | Class I PI3K (pan) | 30 or 60 | Cayman Chemical |
| ZSTK-474 | Class I PI3K (pan) | 2 or 4 | Cayman Chemical |
| MK-2206 | Akt (pan) | 10 | Cayman Chemical |
| PD98059 | MEK1 | 30 | Cayman Chemical |
| NSC23766 | Rac | 50 | Sigma |
| AZD 8055 | mTOR | 0.3 | Cayman Chemical |
| Rapamycin | mTOR | 0.1 | Cayman Chemical |
| XAV939 | Tankyrase | 10 | Sigma |
| PD173074 | FGFR1 and 3 | 0.1, 5 or 20 | Adooq Bioscience |
| Diethylstilbestrol | ERRs | 20 | Sigma |
| 4-hydroxy tamoxifen | ERRs | 10 | Sigma |
| Sodium oxamate | LDH | 50,000 or 100,000 | Sigma |
| Antimycin A | ETC Complex III | 0.5 | Sigma |
| Rotenone | ETC Complex I | 0.5 | Sigma |
| 2-deoxy-D-glucose | Hexokinase | 50,000 | Sigma |

**Primary antibodies**

| Target | Working dilution | Manufacturer | Catalogue no. | Lot no. |
|---|---|---|---|---|
| Akt (total) | 1:1000 | Cell Signaling Technology | 9272 | 24 |
| P-Akt (S473) | 1:1000 | Cell Signaling Technology | 4051 | 13 |
| P-Akt (T308) | 1:1000 | Cell Signaling Technology | 9275 | 19 |
| ERK1/2 | 1:1000 | Cell Signaling Technology | 4695 | 21 |
| P-ERK1/2 | 1:2000 | Cell Signaling Technology | 4370 | 17 |
| FRS2 | 1:1000 | R & D Systems | MAB4069 | CAEN0220021 |
| P-FRS2 | 1:500 | R & D Systems | AF5126 | CBOS031905A<br>CBOS0319091 |

**Secondary antibodies**

| Target | Working dilution | Manufacturer | Catalogue no. | Lot no. |
|---|---|---|---|---|
| Goat anti-mouse (HRP) | 1:10 000 | Sigma | A4416 | SLCD0197 |
| Goat anti-rabbit (HRP) | 1:10 000 | Pierce | - | - |

**Whole cell extract (WCE) buffer**

| | |
|---|---|
| HEPES pH 7.5 | 20 mM |
| NaCl | 420 mM |
| IGEPAL (NP-40) | 0.5% v/v |
| Glycerol | 25% v/v |
| EDTA | 500 mM |
| $MgCl_2$ | 1.5 mM |
| PhosSTOP (Roche) phosphatase inhibitor | 1 tablet per 10 mL of buffer |
| DTT | 50 mM |
| PMSF | 1 mM |
| Protease inhibitor cocktail (Sigma P8340) | 1X |

Added fresh before use

**Urea lysis buffer**

| | |
|---|---|
| Urea | 6.7 M |
| SDS | 1% w/v |
| Tris-HCl pH 6.8 | 10 mM |
| DTT | 1 mM |
| Glycerol | 10% v/v |

**4X load buffer**

| | |
|---|---|
| Glycerol | 36% v/v |
| SDS | 4% w/v |
| Tris-HCl pH 7 | 100 mM |
| Bromophenol Blue | 0.04% w/v |
| β-mercaptoethanol | 10% v/v |

**4X low-SDS load buffer**

| | |
|---|---|
| Glycerol | 36% v/v |
| SDS | 1% w/v |
| Tris-HCl pH 7 | 100 mM |
| Bromophenol Blue | 0.04% w/v |
| β-mercaptoethanol | 10% v/v |

**Wet transfer buffer**

| | |
|---|---|
| Tris | 48 mM |
| Glycine | 14.5% w/v |
| SDS | 0.1% w/v |

**1X phosphate buffered saline (PBS)**

| | |
|---|---|
| $KH_2PO_4$ | 1.5 mM |
| $Na_2HPO_4$ | 8.1 mM |
| NaCl | 136.9 mM |
| KCl | 2.5 mM |

**PBS-Tween (PBS-T)**

| | |
|---|---|
| $KH_2PO_4$ | 1.5 mM |
| $Na_2HPO_4$ | 8.1 mM |
| NaCl | 136.9 mM |
| KCl | 2.5 mM |
| Tween 20 (Sigma) | 0.1% |

**Ponceau stain**

| | |
|---|---|
| Ponceau S | 0.1% w/v |
| Acetic acid | 5% |

**Krebs-Ringer solution**

| | |
|---|---|
| NaCl | 98.5 mM |
| KCl | 4.9 mM |
| $CaCl_2$ | 2.6 mM |
| $MgSO_4$ | 1.2 mM |
| $KH_2PO_4$ | 1.2 mM |
| $NaHCO_3$ | 26 mM |
| HEPES | 20 mM |
| D-glucose | 5 mM |

**Plasmids**

| | |
|---|---|
| pGL3-promoter Empty/3xERRE | Plasmid encoding firefly luciferase gene under the control of an SV40 promoter and 3xERRE enhancer (or no enhancer for the empty plasmid). 3xERRE-luciferase (called pGL3-promoter 3xERRE in the text and figure) was a gift from Rebecca Riggins (Addgene plasmid # 37851 ; http://n2t.net/addgene:37851 ; RRID:Addgene_37851).<br><br>The pGL3 promoter empty plasmid was a product from Promega. |
| pTwist EF1α puro Empty/rEsrrb | Mammalian expression plasmid encoding rat ERRβ (or no protein for the empty plasmid) under the control of a constitutive EF1α promoter. The plasmid was ordered from Twist Bioscience. The full rEsrrb insert sequence, which was ordered cloned into the EcoRI and BamHI sites of pTwist EF1α puro, can be found in Appendix 5.<br><br>pTwist EF1α puro Empty was generated in-house. Briefly, rEsrrb was removed by digestion with EcoRI and BamHI. The linear plasmid was purified, ends were blunted with Klenow polymerase, and blunt ends were re-ligated. The final plasmid was verified as empty by Sanger sequencing using an EF1α promoter primer (TCAAGCCTCAGACAGTGGTTC) (at the Australian Genome Research Facility). |
| pRL-TK | Plasmid encoding Renilla luciferase under the control of a constitutively active thymidine kinase promoter. This plasmid was a product from Promega. |

**Other reagents**

| | |
|---|---|
| hFGF2 | Abcam ab9596 Lot: GR3332259-1 |
| DMSO | Sigma D8418 |

## 2.2 Experimental methods

### *Routine cell culture*

rMC-1 cells were cultured in DMEM (Gibco 11885) containing 5.56 mM D-glucose, supplemented with 2 mM GlutaMAX (Thermo Fisher) and 10% foetal bovine serum (FBS). HEK 293T, HeLa, N2A, PC3, U2OS, and H4IIE cells were maintained in DMEM (Gibco 12430) containing 25 mM D-glucose, supplemented with 2 mM GlutaMAX and 10% FBS. PC12 cells were maintained in DMEM (Gibco 12430) containing 25 mM D-glucose, supplemented with 5% FBS, 5% horse serum and 2 mM GlutaMAX. All cell lines were maintained in a humidified 37 °C incubator in an atmosphere of 5% $CO_2$ in air.

Experiments using primary rat Müller cells and SIRMu-1 cells were performed by Dr Thaksaon Kittipassorn. See ref[128] for procedures used for isolation and culture of these cells.

### *Signalling inhibitor experiments on rMC-1 cells*

The day before the experiment, rMC-1 cells were seeded at 1.66 x $10^6$ cells per dish in 60 mm dishes in 4 mL of DMEM (Gibco 11885) containing 5.56 mM D-glucose, supplemented with 2 mM GlutaMAX and 10% FBS. 3 dishes were used per treatment group per experiment. The following day, medium was aspirated and replaced with 3.5 mL of medium containing inhibitor (or DMSO) (see 2.1 Reagent tables). Cells were treated for 2 h, then medium was replaced (with the same) and cells were treated for a further 6 h. Samples of media were taken and either used immediately for measurement of lactate or frozen immediately at -80 °C until the time of lactate measurement (see method below). After taking media samples, the remaining medium was aspirated, cells were rinsed once with ice-cold 1X phosphate buffered saline (PBS), and 250 µL of ice-cold whole cell extract (WCE) buffer (see 2.1 Reagent tables) was added to each dish. Cells were scraped from the bottom of each dish and transferred to microcentrifuge tubes. The tubes were placed on a rotating wheel at 4 °C for 30 min then centrifuged at 14,000 rpm for 30 min. Supernatant containing soluble protein was transferred to fresh tubes and stored at -20 °C until the time of protein quantification and western blots. Protein was quantified by Bradford assay[129] (Bio-Rad Protein Assay). Experiments were performed three times independently, and presented as mean ± SD. Data were statistically analysed by Dunnet's multiple comparisons test with significant change defined as $P < 0.05$.

## *PI3K/Akt inhibitor experiments on cell line panel*

The day before the experiment, cell lines were seeded in DMEM (Gibco 11885) containing 5.56 mM D-glucose, supplemented with 2 mM GlutaMAX and 10% FBS. Each cell line was seeded in 2 mL of medium in three wells of a 6-well plate. HeLa cells were seeded at 2 x $10^5$ cells per well. HEK 293T, N2A, PC3, PC12 and U2OS cells were seeded at 3 x $10^5$ cells per well. rMC-1 and H4IIE cells were seeded at 4 x $10^5$ cells per well. Seeding density was decided based on visual assessment of cell size/confluence in preliminary experiments. The following day, medium was aspirated and replaced with 1.5 mL of the same medium containing inhibitor (or DMSO) (see 2.1 Reagent tables) Cells were treated for 6 h, then medium was replaced with the same except containing 0.5% FBS (to ensure lactate production was well above the background level present in serum), and cells were treated for a further 2 h. Samples of media were stored immediately at -80 °C until measurement of lactate (see method below). The experiment was performed three times independently, and presented as mean ± SD. Data were statistically analysed by two-way ANOVA and post-hoc multiple comparisons test, with significant change defined as $P < 0.05$.

## *Lactate and glucose assays*

The concentration lactate or glucose in samples of culture medium was determined using a Biovision Lactate Colorimetric Assay kit II or a Biovision Glucose Colorimetric Assay kit II, respectively, according to the manufacturer's protocol. The volume of medium used for a given assay varied and was determined empirically by performing test measurements before the main assay. A background control well containing no cells or tissue was included in each experiment and subtracted in calculations of lactate production or glucose consumption. Where stated in the figure legend, lactate production was normalised to total protein collected and quantified after the experiment.

## *Seahorse extracellular flux assays*

The day before the assay rMC-1 cells were seeded into a gelatin-coated Seahorse XF96 cell culture microplate at 2.5 x $10^4$ cells per well in 80 µL of routine culture medium. The top and bottom rows were left without cells for either background measurements (corner wells) or for determining the buffer factor of the assay medium. A seahorse XF96 sensor cartridge was hydrated with 200 µL per well of MQ water overnight. The following day, medium was aspirated from all wells and replaced with 80 µL of routine culture medium containing inhibitor as described in the figure (see also 2.1 Reagent tables). Cells were incubated in a humidified 37 °C, 5% $CO_2$ incubator for 3.5 h. Then, medium

was carefully removed (leaving 20 µL to avoid disturbing cells) from all wells and cells were gently washed twice with 200 µL per well of 1X PBS (leaving 20 µL on the first wash and removing all PBS on the second). 180 µL of Seahorse XF base medium supplemented with 5.56 mM D-glucose and 5 mM HEPES, pH-adjusted to 7.4 at 37 °C in air, and containing inhibitor (or DMSO), was added per well, and the culture plate was placed in a 37 °C incubator in air (no added $CO_2$) for 1 h.

All drug ports in the sensor cartridge except those for buffer factor determination (see below) were loaded with the following drugs made up in Seahorse assay medium. A: 5 µM each (0.5 µM final conc.) rotenone and antimycin A (20 µL per port). B: 500 mM (50 mM final conc.) 2-deoxy-D-glucose (2-DG) (22 µL per port). C: 50 mM 2-DG (25 µL per port). D: NucBlue live cell stain (Invitrogen) at 3:2 ratio of stain to medium in port (25 µL per port).

The assay was run in a Seahorse XFe96 extracellular flux analyser. After the assay, an ArrayScan XTA Live High Content imaging system (Thermo Fisher) was used to image nuclear fluorescence of the NucBlue stain in all cells in all wells, and cells were counted using HSC Studio™ for normalisation of Seahorse assay data.

The buffer factor (BF) is a value specific for the medium and conditions that relates changes in pH to molar production of protons. For BF determination, drug ports A, B and C of wells without cells were loaded with 5 mM HCl in Seahorse assay medium. The Seahorse XF Buffer Factor Calculator (part of the Seahorse XF Glycolytic Rate Assay Report Generator download) was downloaded from the Agilent website (https://www.agilent.com/en/products/cell-analysis/xf-glycolytic-rate-assay-report-generator) and used to calculate the buffer factor per the manufacturer's instructions.

The Seahorse assay experiments comparing different Müller cell types were performed by Dr Thaksaon Kittipassorn and detailed methods can be found in her PhD thesis[114].

## *Seahorse assay calculations*

The buffer factor was inputted to Seahorse Wave software to obtain proton efflux rate (PER) data from measurements of extracellular acidification rate (ECAR) according to equation 1 (performed by Wave software):

1. $$PER(pmol/min) = ECAR(mpH/min) * BF(mmol/L/pH) * Vol\ measurement\ chamber\ (\mu L) * Kvol$$

Where BF is determined empirically for the assay according to the procedure described above, Vol measurement chamber is 2.28 µL and Kvol, the volume scaling factor, is 1.60 for the XFe96 instrument.

The Seahorse XF Glycolytic Rate Assay Report Generator, available online, was used to calculate the PER specifically due to glycolysis (glycoPER) according to equation 2:

$$2. \qquad glycoPER(pmol/min) = PER(pmol/min) - CCF * mitoOCR(pmol/min)$$

Where CCF is the $CO_2$ contribution factor, an empirically determined value relating the mitochondrial OCR to the mitochondrial PER, and mitoOCR is the ratio of basal OCR to OCR after injection of rotenone and antimycin A. Agilent has determined the CCF to be 0.61 ± 0.13 for 20 different cell lines across different instruments and the value of 0.61 was used in all calculations.

Glycolytic reserve as a percentage of basal glycolysis was calculated according to equation 3:

$$3. \qquad glycolytic\ reserve(\%) = \frac{glycoPER(rot/AA)(pmol/min)*100}{glycoPER(basal)(pmol/min)}$$

Where glycoPER(rot/AA) (also termed glycolytic capacity or compensatory glycolysis) is the PER due to glycolysis after injection of rotenone and antimycin A, and glycoPER(basal) is the basal PER due to glycolysis.

More information on calculations is available in the Agilent document "Improving Quantification of Cellular Glycolytic Rate Using Agilent Seahorse XF Technology" available online.

## *Western blots*

30-80 µg of protein (equal mass for every lane on any given gel) was mixed with 4X load buffer (or 4X low-SDS load buffer for samples in urea lysis buffer) (See 2.1 Reagent tables) to 1X final concentration. Proteins were separated by electrophoresis in a denaturing 10% polyacrylamide gel run at 140 V for approximately 1 h. Proteins were transferred to a nitrocellulose membrane using a wet transfer technique in a Mini Trans Blot tank (Bio-Rad) filled with 1X wet transfer buffer (see 2.1 Reagent tables). The transfer was run at 250 mA at 4 °C for 2 h. Then, the membrane was rinsed with RO water and incubated with Ponceau stain for 30 min and rinsed again to assess the quality of protein transfer. The membrane was then blocked with 10% skim milk in PBS-T for 1 h at room temperature (RT) with gentle rocking. Primary antibody was applied (see 2.1 Reagent tables for catalogue numbers and dilutions) for approximately 16 h at 4 °C on a rotating wheel. The membrane was washed 3 times for 5 min each with PBS-T. HRP-conjugated secondary antibody was applied (see 2.1 Reagent tables for catalogue numbers and dilutions) at RT for 1 h. The membrane was washed 3 times for 5 min each with PBS-T. The membrane was developed using Clarity Western ECL Substrate (Bio-Rad). Equal parts luminol and peroxide solutions were mixed, and drops were pipetted onto parafilm. The membrane was placed

face-down on the drops and incubated for 5 min, then imaged using a Bio-Rad ChemiDoc MP Imaging System.

Representative examples of full western blots for each of the proteins targeted in this thesis are shown in Appendix 1, Figure A.1 and A.2, to indicate size and appearance of blots.

## *Isolation of retinas and eyecups*

All animals used in experiments were scavenged from The University of Adelaide Laboratory Animal Services (LAS). Animals were not genetically modified and were healthy, without conditions that would affect ocular processes to our knowledge (although this was not assessed on an individual basis), and were euthanised for reasons unrelated to these experiments. Outbred Sprague Dawley rats were euthanised by $CO_2$ asphyxiation (by LAS staff). Experiments used either male or female rats, but all rats in each individual experiment were of a single sex. Male rats were 8 weeks old and females were 6 weeks old. Eyes were enucleated no longer than fifteen minutes after death and placed immediately into ice-cold HBSS containing 100 U/mL penicillin and 100 µg/mL streptomycin. Retinas were isolated by making an initial incision 1-2 mm posterior to the ora serata then hemisecting the eye with fine scissors. The cornea and lens were removed and discarded, and the retina was carefully separated from the sclera and RPE (together referred to as the eyecup) in a drop of HBSS using two pairs of curved forceps. Immediately upon isolation, retinas were placed into a 100 mm dish containing 10 mL of MEM (Gibco 11090) containing 5.56 mM D-glucose, supplemented with 0.8 mM L-glutamine, 100 U/mL penicillin and 100 µg/mL streptomycin, at RT. Where isolated eyecups or intact eyecups and retinas together were used for experiments, the general method up until isolation of the required tissue was the same as for retinas alone.

## *Standard retinal explant inhibitor treatment experiments*

Once all retinas for an experiment had been isolated (< 1 h total duration – often less time when fewer retinas were needed for an experiment), they were transferred to wells of a 12-well plate containing 1 mL of the same MEM formulation used during isolation, plus inhibitor (or DMSO/EtOH) (see 2.1 Reagent tables) which had been equilibrated in an incubator at 37 °C, in an atmosphere of 5% $CO_2$ in air. Retinas were incubated under these conditions in darkness without agitation for 5 h. After this time, under ambient room light, medium was gently removed from all wells with a pipette and replaced with the same medium. Retinas were incubated with inhibitors for a further 11 h in darkness. After this incubation, 200 µL samples of medium were collected from each well and stored

immediately at -80 °C until the time of measurement of glucose or lactate. Remaining medium from each well was discarded. Retinas were washed once with 1 mL of ice-cold 1X PBS. Each retina was transferred to a microcentrifuge tube containing 400 µL of ice-cold WCE buffer. Retinas were homogenised with a plastic pestle, then tubes were incubated for 30 min at 4 °C on a rotating wheel. Tubes were centrifuged for 30 min at 14,000 rpm at 4 °C. Supernatant containing soluble protein was transferred to fresh tubes and stored at -20 °C. Protein concentration was determined by Bradford assay (Bio-Rad Protein Assay) and used to normalise glucose and lactate assay data. Experiments were performed three times independently, and presented as mean ± SD. Data were statistically analysed by Dunnet's multiple comparisons test with significant change defined as $P < 0.05$.

### *Retina inhibitor treatment experiments in 95% oxygen*

Retinas were isolated as described above and placed immediately into a 100 mm dish with 10 mL of Neurobasal A medium (Gibco 10888) containing 25 mM D-glucose, supplemented with 2 mM glutaMAX, 0.2% B-27 supplement (Gibco) and 0.1% N-2 supplement (Gibco). Once all retinas for an experiment had been isolated (approx. 40 min duration) they were transferred to wells of a 12-well plate containing 1 mL of the Neurobasal A formulation plus inhibitor (or DMSO/EtOH). The plate for the high-oxygen groups had been placed in a sealed box filled with 95% $O_2$, 5% $CO_2$ for 1 h prior to isolation of retinas to equilibrate the media. The normoxic group plate had been placed in a regular incubator (5% $CO_2$ in air) for the same period. The high-oxygen group plate was placed into the box which was sealed and filled with a 95% $O_2$, 5% $CO_2$ mixture via a pair of valves in the lid. The oxygen level in the box was monitored throughout the experiment using an oxygen sensor at the bottom of the box, and it while it slowly decreased over time, it never fell below 90% (except when changing media – see below). A tray of water was included to humidify the box. Once filled, the box was placed inside a 37 °C incubator to maintain the required temperature. The plate for the normoxic group was placed directly into a 37 °C, 5% $CO_2$-in-air incubator. Retinas were treated for 6 h, then the medium was gently removed from all retinas by pipetting (this step was performed outside of the hyperoxic box) and replaced with 1 mL of Krebs-Ringer solution. For the high-oxygen group, this solution had been equilibrated by bubbling through 95% $O_2$, 5% $CO_2$ mixture for 3 min, and for the standard-oxygen group the media had been equilibrated in the normal 5% $CO_2$ in air incubator for 30 min. Retinas were placed back in the hyperoxic/normoxic environment and incubated for a further 30 min in the absence of inhibitor. After this, samples of media were collected and stored immediately at -80 °C until the time of lactate measurement. Protein extracts were made for normalisation as described above for standard inhibitor treatment experiments. The experiment was performed three times independently,

and presented as mean ± SD. Data were statistically analysed by Dunnet's multiple comparisons test with significant change defined as $P < 0.05$.

## *Extracts from rat retinal explants and eyecups for western blots*

Retinal explants, eyecups and intact eyecup/retinas were isolated as described above. They were incubated for 1 h in the culture medium and conditions described for the standard retinal explant inhibitor treatment experiments in the presence of human fibroblast growth factor 2 (hFGF2) at the concentration stated in the figure (Figure 5.3 C) (0, 100, 500 or 2000 ng/mL). After incubation, medium was removed with a pipette and tissues were washed once with 1 mL of 1X PBS. Intact eyecup/retinas which were incubated together were separated before making extracts. Tissues were transferred into microcentrifuge tubes containing 100 µL of ice-cold urea lysis buffer, homogenised with a plastic pestle and stored at -20 °C. At the time of western blotting, extracts were thawed and sonicated using a Diagenode Bioruptor on high for 20 cycles of 30 sec on, 30 sec off. This was to decrease the viscosity of samples, which were otherwise extremely thick when using urea lysis buffer. Protein was quantified by bicinchoninic acid (BCA) assay (Pierce) according to the manufacturer's instructions.

For the positive control rMC-1 sample, $6.6 \times 10^5$ cells were seeded in a 60 mm dish in routine culture medium. After 24 h, medium was aspirated, and cells were washed three times with PBS. 4 mL of MEM 11090 containing 5.56 mM D-glucose, supplemented with 2 mM GlutaMAX and 250 µg/mL BSA was added (no serum). After 24 h of incubation, medium was replaced with the same serum-free medium plus 10 ng/mL hFGF2. After 1 h, extracts were made for western blots. Medium was aspirated and cells were washed once with ice-cold 1X PBS. 100 µL of cold urea lysis buffer was added, cells were scraped and transferred to a microcentrifuge tube, then sonicated and quantified as described for explant extracts above.

## *Dual luciferase reporter assays for estrogen-related receptor (ERR) inhibitors*

rMC-1 cells were seeded at $4.8 \times 10^4$ cells per well and 293T cells were seeded at $1.4 \times 10^4$ cells per well in 24-well plates in their respective routine culture media. 24 h later, cells were transfected with 500 ng of pTwist EF1α puro rEsrrb (or empty), 300 ng of RL-TK and 50 ng of pGL3-promoter 3xERRE (or empty) using polyethyleneimine (PEI) at a 3:1 mass ratio. At the same time, cells were treated with diethylstilbestrol (DES) or 4-hydroxytamoxifen (4-OHT) where indicated and at the concentrations stated in the figure. After 16 h, a dual luciferase assay (Promega) was performed according to the manufacturer's instructions. Briefly, medium was aspirated and cells were washed once with 1X PBS.

100 µL of 1X passive lysis buffer was added to each well and trays were rocked gently at RT for 15 min. 20 µL of lysate was transferred to an all-white 96-well plate. Luciferase reagents (50 µL each per well) were injected and luminescence was measured using a Promega Glomax 96 microplate luminometer. Experiments were performed three times independently. Each experiment was normalised to the first control group, and data presented show mean ± SD of the three normalised experiments.

### *RNA-seq on cultured Primary Müller cells, rMC-1 cells and SIRMu-1 cells*

For this experiment, Dr. Kittipassorn cultured cells and isolated RNA for sequencing. Sequencing was performed at the Australian Cancer Research Foundation (ACRF) Cancer Genomics Facility, and initial bioinformatic processing including read trimming, alignment and counting was performed by staff at the facility. I analysed the results for functionally relevant findings and generated figures. The full methodology for these experiments including initial data processing can be found in the articles in Appendix 2 and Appendix 3 (refs[128,130]). Data from these experiments are publicly available from Gene Expression Omnibus (GEO) under accession number GSE123161.

### *RNA-seq analysis – comparison of rMC-1, SIRMu-1 and primary rat Müller cells*

All RNA-seq analyses in this thesis were performed using R[131].

A table of counts was obtained as described in refs[128,130]. Lowly expressed genes were filtered out of downstream analyses using the filterByExpr function in edgeR (version 3.36.0)[132] as default. For normalisation of count data, scaling factors were calculated accounting for library size and composition using the trimmed mean of M-values method[133] in edgeR, and these were supplied in a call to lcpm() to calculate normalised $\log_2$ counts per million mapped reads (lcpm). Genes of interest were selected for generation of heatmaps. Gene sets relating to glycolysis and gluconeogenesis (KEGG_GLYCOLYSIS_GLUCONEOGENESIS), the TCA cycle (KEGG_CITRATE_CYCLE_TCA_CYCLE) and oxidative phosphorylation (KEGG_OXIDATIVE_PHOSPHORYLATION) were obtained by searching the Gene Set Enrichment Analysis (GSEA) Molecular Signatures Database (MSigDB). Variations of gene names were added on an ad hoc basis to these lists to capture as many genes as possible across datasets from different species which used different gene names or identification conventions. As genes vary widely in absolute expression levels, visualisation of changes in expression in heatmaps was improved by calculating z-scores across each row (gene) from the normalised lcpm values. Differential gene expression above the fold-change thresholds specified in the text was tested using

limma (version 3.50.0)[134]. A Benjamini-Hochberg corrected P-value < 0.05 was used to define whether a gene was differentially expressed.

### *RNA-seq analysis – P2 to P28 rod data of Kim et al. 2016*

Data were generated by Kim et al. 2016[1]. The table of transcript-level effective counts was downloaded from GEO under accession number GSE74660 (GSE74660_Seq_eXpress_counts). Samples were separated into individual files then re-imported into R using the tximport package (version 1.22.0) which summarises transcript-level counts to gene-level counts in a manner which accounts for differential usage of transcripts of different lengths between samples[135]. Lowly expressed genes were filtered out using edgeR::filterByExpr as default. Effective counts were then normalised using the trimmed mean of M-values (TMM) method and $\log_2$-transformed using edgeR. Relevant groups were selected and heatmaps were generated using row-wise z-scores calculated from normalised lcpm. Lists of metabolic genes were the same as described for the comparison of Müller cell types. Differential expression by greater than 2-fold between the P2 and P28 groups (P28 - P2) was tested using limma, leveraging the full dataset in modelling (i.e., using all groups, not just those presented in heatmaps). A Benjamini-Hochberg corrected P-value < 0.05 was used to define whether a gene was differentially expressed. Fold-change from P2 to P28 was calculated by taking $2^{(\text{P28 lcpm - P2 lcpm})}$. Values between 0 and 1, which indicated lower expression at P28, were then converted to negative fold-change values by taking the negative inverse.

### *RNA-seq analysis – P2 to adult Müller cell data of VandenBosch et al. 2020*

Data were generated by VandenBosch et al. 2020[2]. The table of counts was downloaded from GEO under accession number GSE137318 (GSE137318_P2GFP_P8_P12_thinned_countstable), and data were processed for generation of heatmaps and tables as described for the developing rod data above. No differential expression analysis was performed due to the absence of replicates of each age group.

### *RNA-seq analysis – comparison of developing rods and Müller cells.*

Normalised lcpm values were obtained as described above. For the rod dataset, the mean lcpm was calculated for each age group. Scatterplots were generated comparing P2 Müller cell (retinal progenitor cell) lcpm values with mean P2 rod lcpm values and comparing adult Müller cell values with mean P28 rod values for the genes stated. The list of metabolic genes combined all three KEGG sets

defined above in the comparison of Müller cell types. For the list of overall most divergent genes, the difference between the fold-change for each gene in each study was calculated, and all genes were ordered by absolute fold-change difference. For the lists of divergent metabolic genes, the data were filtered for the complete list of KEGG metabolic genes and the top 10 genes with largest positive (relatively upregulated in rods) or largest negative (relatively upregulated in Müller cells) fold-change difference were determined.

### *RNA-seq analysis – comparison of Müller and non-Müller cells in data of Hoang et al. 2020.*

Data were generated by Hoang et al. 2020[136]. The table of fragments per kilobase per million mapped reads (FPKM) values was downloaded from GEO under accession number GSE135406 (GSE135406_Fpkm_expression_values_of_all_RNA-seq_samples). Data were filtered to retain the undamaged control P60 GFP-positive (Müller cells) and GFP-negative (other retinal cells) groups. Heatmaps were generated using row-wise z-scores calculated from FPKM values. The mean FPKM for each gene within each group was calculated and presented as a table.

# 3. Results: Müller cells

## *3.1 PI3K drives lactate production in rMC-1 cells independently of Akt*

The first aim of the project was to determine molecular drivers of aerobic glycolysis in Müller cells, specifically the immortalised rMC-1 rat Müller cell line[137]. An immortalised cell line was chosen in favour of primary Müller cells due to particular disadvantages of primary cells. Namely, they senesce after a small number of passages, only a limited number of cells can be obtained from a single retina, and cultures often contain a small proportion of non-Müller cell types such as microglia and astrocytes[137]. In the setting of screening many potential candidate drivers of aerobic glycolysis, these factors would necessitate the use of a large number of eyes and animals. For these reasons, we used the rMC-1 cell line. This line was derived from an adult rat Müller cell culture transduced with simian virus 40[137]. It expresses adult Müller cell markers, but most importantly, like cultured primary Müller cells, it has been shown to exhibit aerobic glycolysis[114,138] and has been used previously in studies of Müller cell metabolism[138-140].

In the present experiments, candidate drivers of aerobic glycolysis were targeted based on their known well-established roles in driving aerobic glycolysis in the context of cancer. Inhibitors were commercially available to many such targets and provided an effective means to screen potential drivers. Lactate production by rMC-1 cells was measured after treatment with small-molecule inhibitors of several common glycolysis-promoting signalling pathways (Figure 3.1). rMC-1 cells were treated with inhibitors at concentrations previously shown to be effective with cultured cells in published studies. An initial 2 h treatment was performed to allow time for the inhibitors to enter cells, inhibit their targets, and for downstream effects to begin to take place. Medium was then changed and the cells were incubated for a further 6 h in the presence of inhibitors before secreted lactate was measured in the medium.

The PI3K/Akt signalling pathway has been well-demonstrated to drive glycolysis in cancer cells[116]. MEK signalling is also linked to glycolysis and is often activated downstream of the same cell membrane receptors as PI3K[141]. Both signalling pathways have important roles in cell growth and proliferation and are commonly dysregulated in cancers. To specifically test the contribution of these pathways to aerobic glycolysis in Müller cells, rMC-1 cells were treated with the PI3K inhibitor LY294002, the Akt inhibitor MK-2206, or the MEK1 inhibitor PD98059 (Figure 3.1).

Treatment of the rMC-1 cells with the PI3K inhibitor LY294002 decreased lactate production by 50% (Figure 3.2 A). Surprisingly, treatment with an inhibitor of Akt, the canonical downstream effector of PI3K, resulted in no change in lactate production. Treatment with the MEK1 inhibitor PD98059

decreased lactate production by 23%. Two control inhibitors were also included. Treatment of the rMC-1 cells with oxamate, which inhibits LDH, decreased lactate production by approximately 75%, as expected. Antimycin A inhibits complex III of the ETC, preventing ATP production by OXPHOS. As expected, treatment of the rMC-1 cells with antimycin A induced an increase in lactate production, nearly 2-fold above the basal level. This shows that the cells had reserve glycolytic capacity in their basal state.

Western blots were performed to confirm basal activity of the pathways targeted and to ensure the inhibitors used had the expected effects on pathway activity (Figure 3.2 B). Example un-cropped western blots are included in Appendix 1 for each protein targeted. PI3K activity is routinely determined by the phosphorylation state of two residues of Akt, namely S473 and T308 in Akt1 or equivalent residues in Akt2 and 3; a greater level of phosphorylation indicates higher pathway activity. The activity of Akt itself is also determinable by the phosphorylation of these two residues. In the untreated state, both S473 and T308 of Akt were phosphorylated in rMC-1 cells (Figure 3.2 B), indicating PI3K pathway activation. As expected, treatment with LY294002 and MK-2206 which target PI3K and Akt, respectively, abolished phosphorylation of S473 and T308 of Akt. MEK1 activity is routinely determined by the phosphorylation state of its substrates, extracellular signal-regulated kinase 1 (ERK1), at positions T202 and Y204, and ERK2, at positions T185 and Y187. Western blots for phosphorylated ERK1 and 2 demonstrated that the MEK/ERK pathway was also active in the basal state and, as expected, treatment with PD98059, which targets MEK1, greatly reduced phosphorylation of ERK1 and 2.

The PI3K inhibitor, LY294002, has been shown to have off-target effects[142]. To mitigate the chance that the observed decrease in lactate production was due to off-target effects, rMC-1 cells were treated with another unrelated PI3K inhibitor, ZSTK474. It caused approximately the same decrease in lactate production, confirming the change was likely due to inhibition of PI3K (Figure 3.2 C). Inhibition of PI3K by ZSTK474 was also confirmed by western blot for phosphorylated Akt (Figure 3.2 D).

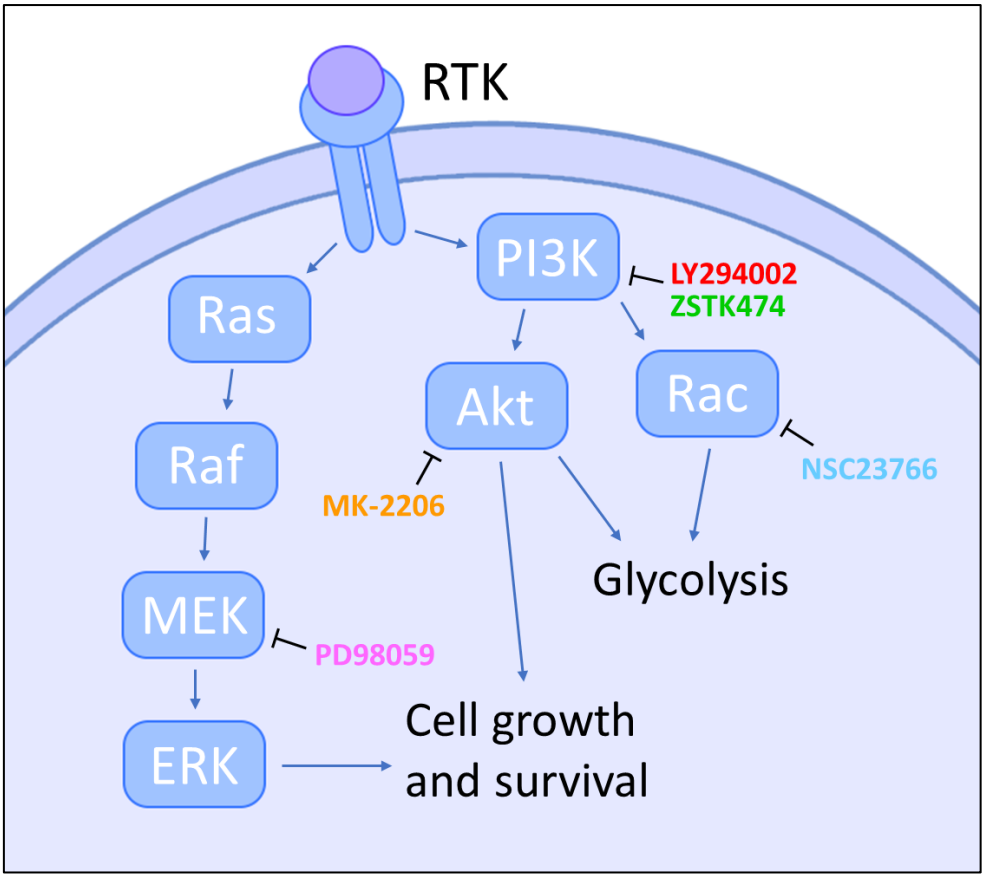


**Figure 3.1 Signalling pathways and inhibitors. A.** Activation of receptor tyrosine kinases (RTK) induces activation of the PI3K/Akt and MEK/ERK signalling pathways. Akt is the canonical mediator of effects on glycolysis downstream of PI3K, but an Akt-independent pathway via Rac1 activation can also upregulate glycolysis. The MEK/ERK pathway has well-established roles in cell growth and survival. Small-molecule inhibitors used to treat rMC-1 cells are indicated.

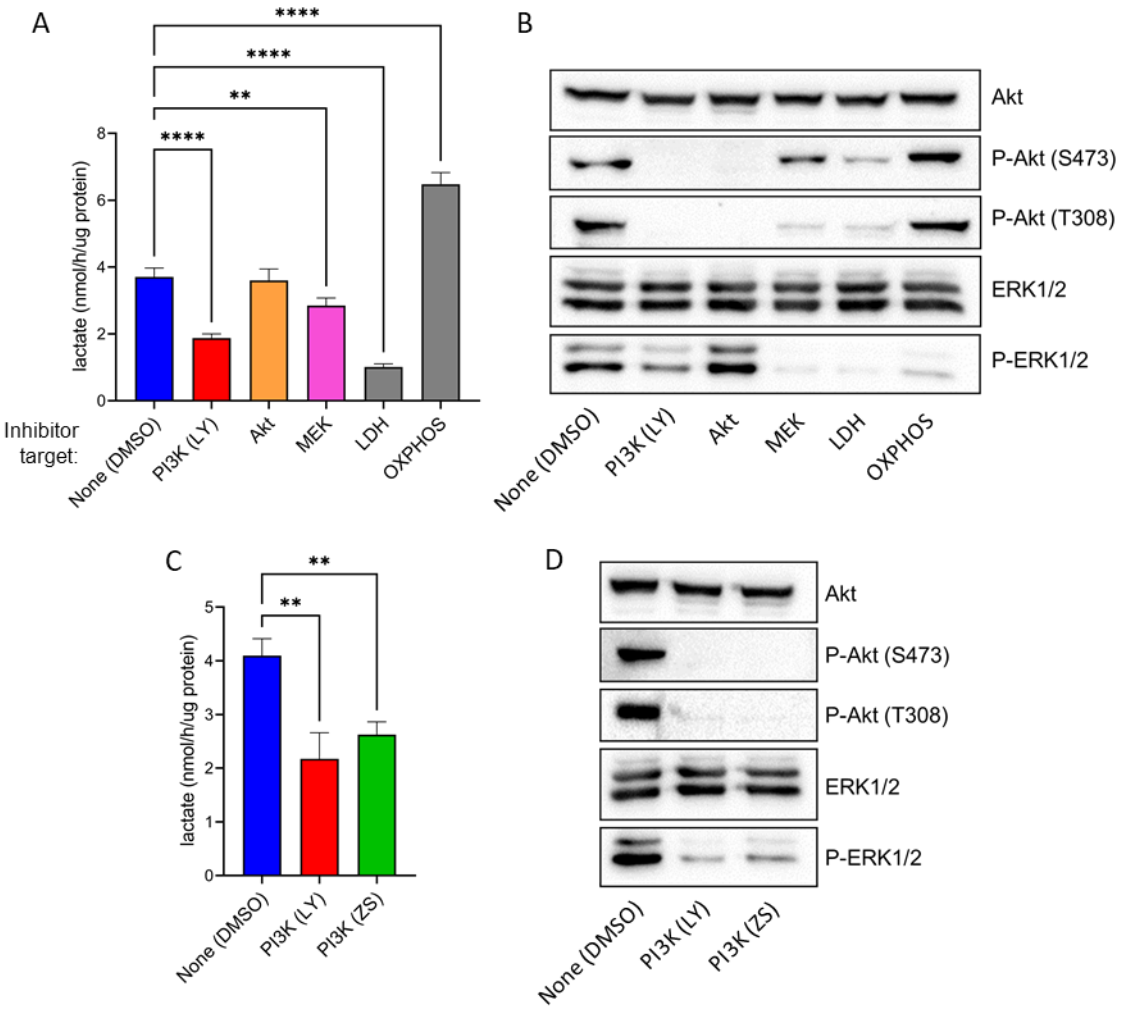


**Figure 3.2 Effects of signalling inhibitors on lactate production in rMC-1 cells. A.** rMC-1 cells were treated with PI3K inhibitor LY294002 (LY) (30 µM), Akt inhibitor MK-2206 (10 µM), MEK1 inhibitor PD98059 (30 µM), lactate dehydrogenase (LDH) inhibitor oxamate (50 mM), oxidative phosphorylation (OXPHOS) inhibitor Antimycin A (1 µM), or vehicle (DMSO, 1:1000) for 2 h, then culture medium was changed, and cells treated for a further 6 h before lactate was measured in media. Data normalised to total protein. **B.** Western blots using extracts collected after a lactate assay experiment in A. P-Akt indicates detection of phosphorylation of Akt at the positions stated. P-ERK1/2 indicates detection of phosphorylation of ERK1, at positions T202 and Y204, and ERK2, at positions T185 and Y187 **C.** Same as A, but treatment with one of the PI3K inhibitors LY294002 (LY) (30 µM) or ZSTK474 (ZS) (2 µM), or vehicle (DMSO, 1:1000). **D.** Western blots using extracts collected after a lactate assay experiment in C. Data in A and C each show the mean ± SD from three independent experiments and were analysed by Dunnet's multiple comparisons tests. Blots in B and D are representative of three independent experiments.

## 3.2 Rac1 drives lactate production in rMC-1 cells

Given the decrease in lactate upon inhibition of PI3K, the lack of any effect upon inhibition of Akt was unexpected. Akt is the canonical downstream effector of PI3K, and it has been shown to drive glycolysis in other cell types via multiple mechanisms[143-148]; however, there is at least one reported mechanism via which PI3K can drive glycolysis independently of Akt[149]. This alternative pathway involves the small GTPase, Rac1, which promotes cytoskeletal remodelling. This remodelling releases the glycolytic enzyme, aldolase, from the actin cytoskeleton, increasing its activity and flux through glycolysis. It should be noted that in the MCF10a cells used in the study by Hu and colleagues where this mechanism was elucidated, glycolysis was also sensitive to Akt inhibition separately to Rac1 inhibition[149]. This is in contrast to the results obtained here in rMC-1 cells, where an inhibitor of Akt caused no decrease in lactate production.

To assess whether Rac1 drives aerobic glycolysis in rMC-1 cells, cells were treated with the Rac1 inhibitor, NSC23766 (Figure 3.3 A). Un-normalised lactate production decreased by 37%. However, measurements of total protein were lower in cells treated with Rac1 inhibitor such that there was no difference in lactate production when normalised to protein (Figure 3.3 B). This would normally indicate that the inhibitor was toxic to cells. However, there was no visual difference in morphology between treated and untreated cells to indicate NSC23766 toxicity (data not shown). The measured change in protein content was also too large to be caused solely by a difference in growth rate over 8 h. Furthermore, the NSC23766 treatment caused no detectable difference in cell counts (Figure 3.3 C). It is therefore likely that the decrease in lactate production upon inhibition of Rac1 does actually reflect a decrease in glycolytic rate per cell rather than a general toxic effect. It is possible the decrease in protein content was simply due to experimental variation. Alternatively, inhibition of Rac1 may decrease protein content in rMC-1 cells; however, there was no similar decrease in protein observed when PI3K (or any other of the tested molecules) was inhibited, so this interpretation is unlikely unless Rac1 drives lactate production via a mechanism independent of PI3K in rMC-1 cells.

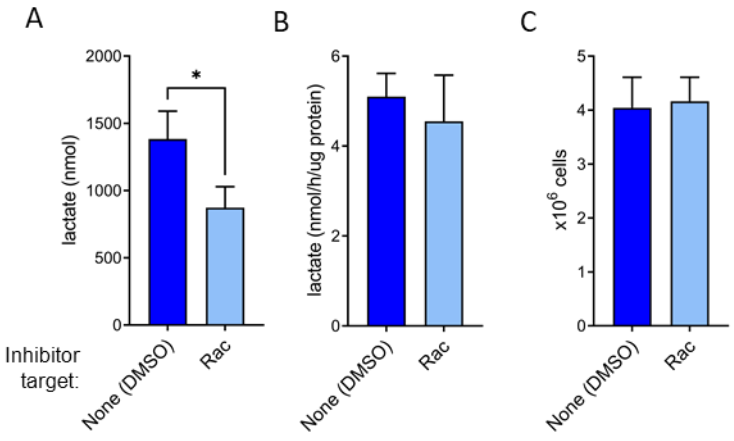


**Figure 3.3 Effects of Rac1 inhibition on lactate production in rMC-1 cells. A.** rMC-1 cells were treated with Rac1 inhibitor NSC23766 (50 µM) or vehicle (DMSO, 1:600) for 2 h, then culture medium was changed and cells treated for a further 6 h before lactate was measured in medium. **B.** Results from A normalised to total protein. **C.** rMC-1 cells treated as described in A were trypsinised and counted (from 60 mm dishes). Data in A and B each show the mean ± SD from three independent experiments and were analysed by unpaired Student's t-tests (No significant difference in B). Data in C are from a single experiment without fully independent replicates, so a statistical test was not performed.

## 3.3 Analysis of oxygen consumption and extracellular acidification rates

Greater detail was sought regarding the effects of the signalling inhibitors on rMC-1 cell metabolism beyond the single parameter of extracellular lactate production. Seahorse extracellular flux assays measure the oxygen consumption rate (OCR) and extracellular acidification rate (ECAR) of a cell monolayer in real-time in a multiple-well plate format, enabling calculation of rates of glycolysis and OXPHOS. Drugs that modulate specific aspects of metabolism can be injected throughout the assay, enabling derivation of parameters such as glycolytic capacity, glycolytic reserve or spare respiratory capacity, depending on the sequence of drugs injected. For example, a glycolytic rate assay begins by taking basal measurements of OCR and ECAR, then a mix of the respiratory chain inhibitors, rotenone and antimycin A, are injected. In order to maintain ATP levels, cells respond by increasing their rate of glycolysis, usually, albeit not necessarily, to its maximal level, which enables determination of the glycolytic capacity and glycolytic reserve (Figure 3.4 A). 2-deoxyglucose (2-DG) is then injected to inhibit glycolysis, confirming that the basal acidification was due to glycolysis. Note that ECAR is often converted to proton efflux rate (PER), a stoichiometric unit of proton release, by its relation to the buffering capacity of the assay medium, which is determined empirically.

In any assay, a proportion of acidification arises from processes other than glycolysis. Notably, respiration produces $CO_2$, some of which hydrates to form carbonic acid, resulting in a mitochondrial PER (mitoPER). MitoPER is related to OCR by a value called the $CO_2$ contribution factor (CCF), and mitoPER can therefore be calculated from OCR and subtracted from total PER to obtain the PER specifically due to glycolysis (glycoPER). The manufacturer of the Seahorse instrument, Agilent, has empirically determined the CCF for 20 cell lines, and the value is constant and approximately equal ($0.61 \pm 0.13$) for cases when the percentage of acidification due to glycolysis is high (> 50%) (Agilent Seahorse XF $CO_2$ Contribution Factor Protocol User Guide, accessed 2022). This was true for rMC-1 cells (see the assay below); therefore, the default CCF value of 0.61 was used in calculations of mitoPER and glycoPER. The CCF can be determined empirically but this is only recommended by Agilent for highly oxidative cells (where the percentage acidification due to glycolysis is less than 50%).

To determine the metabolic effects of PI3K, Akt and MEK1 inhibition in more detail, rMC-1 cells were subjected to a glycolytic rate assay. The Rac1 inhibitor, NSC23766, was found to directly interfere with pH measurements recorded by the Seahorse instrument and was therefore excluded from these assays. Cells were treated with inhibitors for a total of five hours before the start of the assay. This treatment time aligned the start of the assay with the midpoint of the incubation period of the lactate assay experiments in Figure 3.2.

Consistent with lactate assays, a decrease in basal glycolysis was observed upon treatment of rMC-1 cells with the two different PI3K inhibitors (Figure 3.4 B, C). Inhibitors of Akt and MEK1 also decreased basal glycolysis (Figure 3.4 B, D, E); however, these changes were not always consistent between Seahorse assays (data for multiple experiments not shown*). Note, however, that Inhibitors of PI3K produced a decrease in basal PER with greater consistency between experiments than inhibitors of Akt or MEK. For all inhibitors in this particular assay, the glycolytic capacity decreased in proportion with the decrease in basal glycolysis, as shown by the equal percentage glycolytic reserve among treatments (Figure 3.4 F). It can be concluded from Seahorse assays that PI3K is likely a driver of aerobic glycolysis in rMC-1 cells.

The result of Akt inhibition in this assay was not consistent with the results of lactate assays in Figure 3.2. Inconsistencies with this inhibitor between Seahorse experiments makes it difficult to draw conclusions about the involvement of Akt in lactate production in rMC-1 cells. The greater number of cells in experimental samples, less manipulation of cells and media, and better consistency between assays means the lactate assays are probably more reliable – although they provide less detailed information. The reason for inter-assay inconsistency is unclear but may relate to minor differences in conditions between experiments, such as treatment time, glucose concentration, presence or absence of buffer, serum batch, passage number, or cell density. A genuine and physiologically important driver of aerobic glycolysis, however, should be robust to such changes. It is also possible that the shock of the removal of serum when general culture medium (10% serum) was switched for Seahorse assay medium (no serum) approximately 1 h before the start of an assay may have induced metabolic changes in a relatively random or stochastic manner. In one assay, inclusion of serum in assay medium produced OCR and ECAR values much greater than those in its absence (data not shown), so it is possible that rMC-1 cells were in an unstable metabolic state when assayed shortly after serum removal. In contrast, the lactate assays in Figures 3.2 and 3.3 were performed using medium containing 10% FBS. The Seahorse instrument manufacturer recommends against the inclusion of serum in assay media.

In summary, lactate assays and Seahorse extracellular flux assays showed that PI3K drives aerobic glycolysis in rMC-1 cells. The downstream players in this process remain uncertain, but lactate assays indicate that it is likely that Rac1 is required and that Akt is not.

*The reason for presenting this particular dataset was due to the type of Seahorse assay performed – the glycolytic rate assay – as it provides the most direct measurement of parameters of glycolysis. Other assays performed were mitochondrial stress tests which differ only in the drug injections. The conditions up to and including basal glycolysis measurements are otherwise identical between the two experiment types. Only basal glycolysis is considered when comparing between experiments.

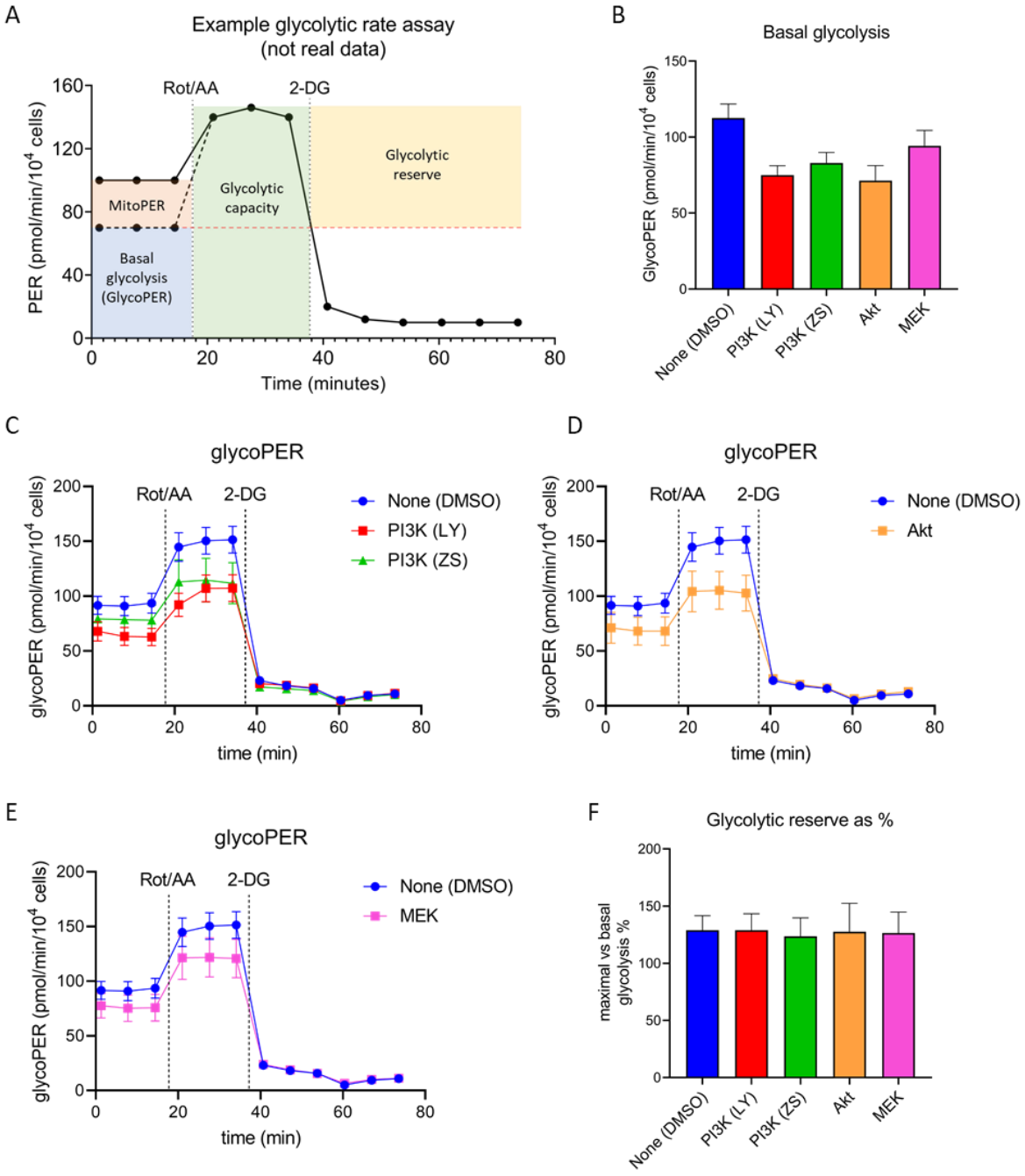


**Figure 3.4 PI3K likely drives acid production in rMC-1 cells. A.** Fabricated example proton efflux rate (PER) data from a Seahorse glycolytic rate assay. Basal glycolysis (basal glycoPER) is the PER in the basal state which is specifically attributable to glycolysis. This is calculated by subtracting mitochondrial PER, which is derived from corresponding readings of oxygen consumption rate, from total basal PER. **B-F.** rMC-1 cells were subjected to a Seahorse glycolytic rate assay after treatment with the PI3K inhibitor LY294002 (LY) (30 µM) or ZSTK474 (ZS) (2 µM), Akt inhibitor MK-2206 (10 µM), MEK1 inhibitor PD98059 (30 µM), or vehicle (DMSO, 1:1000) for 5 h. Basal glycolysis is displayed in **B**, glycoPER traces are displayed in **C-E**, and the glycolytic reserve is represented in **F** as maximal vs basal glycolysis. Data are from a single experiment with 6 replicate wells per group, showing the mean ± SEM of the replicates.

## *3.4 Analysis of rMC-1 cells as an accurate model of retinal or Müller cell metabolism*

In comparison to *in vivo* methods, *in vitro* models such as immortalised cell lines, especially when used in the study of metabolism, balance the benefits of rapid, unlimited growth, and straightforward experimental manipulation, with the downside of potential changes from natural physiology. The necessity of serum for growth and survival of cultured cells is particularly relevant when investigating growth factor signalling pathways, which may be activated by serum components. These considerations raised questions as to whether the observed role of PI3K and Rac signalling in aerobic glycolysis was a true reflection of the metabolic profile of Müller cells *in vivo* or was typical of other immortalised cell lines. We sought answers to two specific questions: 1. How does the response of rMC-1 cells to PI3K and Akt inhibitors compare to the response of other immortal cell types such as cancer cell lines? 2. How does the response compare to other Müller cell types, including primary Müller cells?

To gauge how unique the metabolism of rMC-1 cells was in response to PI3K and Akt inhibition, a panel of common immortal rat, mouse and human cell lines was treated with the PI3K inhibitor, ZSTK474, and the Akt inhibitor, MK-2206, and lactate production was measured (Figure 3.5 A-H). HEK 293T and PC3 cells exhibited responses consistent with both PI3K and Akt being major drivers of aerobic glycolysis. N2A exhibited a similar trend but the changes were not statistically significant. Interestingly PC12 cells and HeLa cells responded with trends similar to rMC-1 cells, with the PI3K inhibition reducing lactate production but little change induced by Akt inhibition. U2OS exhibited a similar trend without statistical significance. This shows that rMC-1 cells are probably not unique in their response to PI3K and Akt inhibition and that PI3k and Akt are perhaps not as inseparably linked in their regulation of metabolism as much literature suggests. An important conclusion from these results is that Akt-independent PI3K signalling may be a novel and beneficial approach to target aerobic glycolysis in some cancers.

Importantly, the fact that rMC-1 cells exhibited a response that was similar to other cell lines, and that PI3K drove lactate production in almost all lines tested, casted doubt on the physiological relevance of rMC-1 cell metabolism; it is probable that serum-mediated activation of growth factor signalling pathways in rMC-1 cells drives proliferation and glycolysis in a manner similar to other immortal cell lines without necessarily reflecting glucose metabolism in a physiological setting.

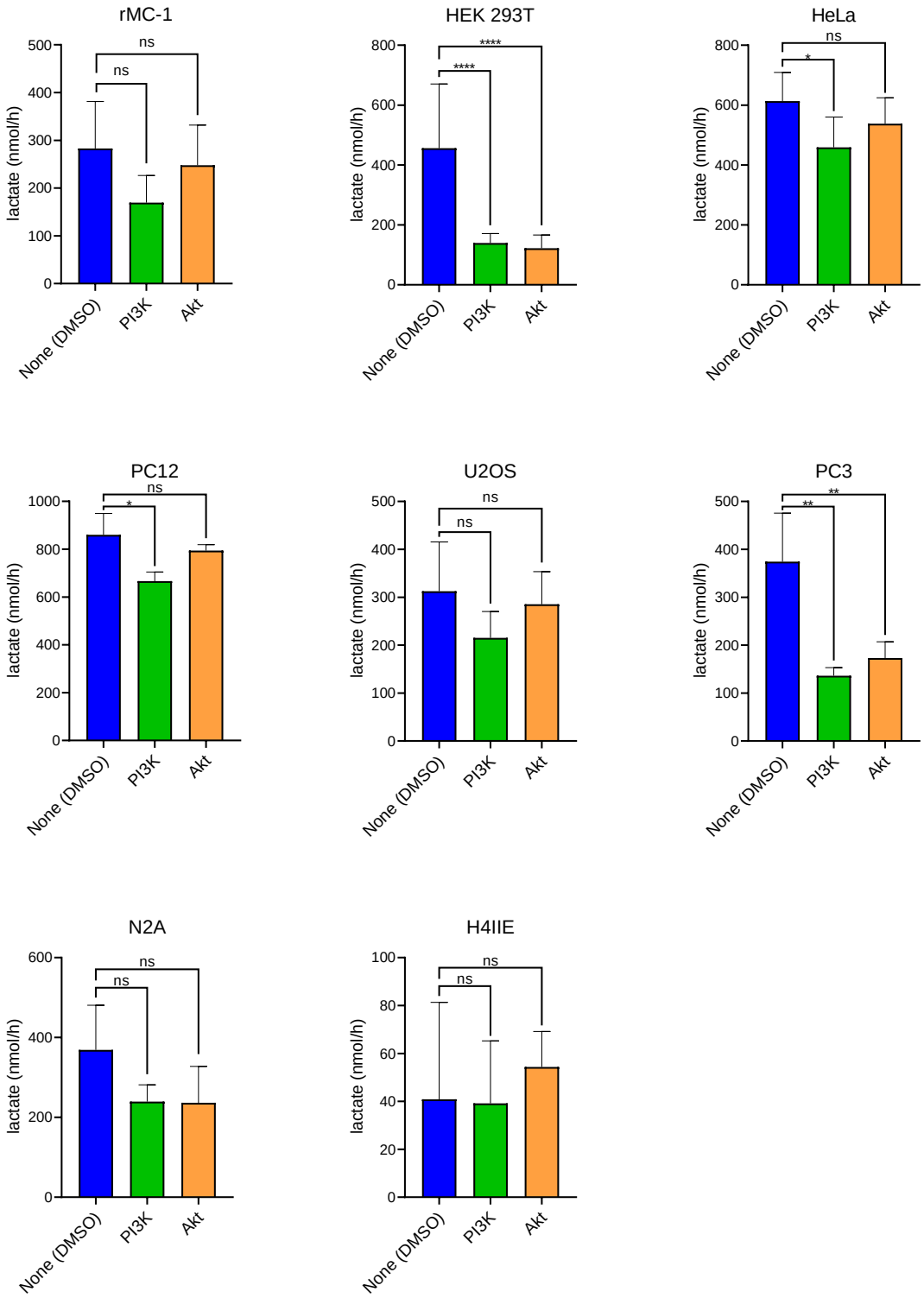


**Figure 3.5 Effects of PI3K or Akt inhibition on lactate production in various cell lines. A-H.** Cell lines indicated were treated with PI3K inhibitor ZSTK474 (2 µM), Akt inhibitor MK-2206 (10 µM), or vehicle (DMSO, 1:1000) for 2 h, culture medium was changed, and cells were treated for a further 6 h before lactate was measured in media. Data show mean ± SD from three independent experiments. Data were statistically analysed using two-way ANOVA and post-hoc multiple comparisons test to compare the mean of each inhibitor-treated group with the mean of the DMSO-treated group for each cell line.

The metabolism of rMC-1 cells was then compared to other cultured Müller cell types. Our laboratory, in collaboration with the laboratory of Prof. Robert Casson, set out to characterise three types of Müller cells: The viral oncogene-immortalised rMC-1 rat cell line, the novel spontaneously immortalised SIRMu-1 rat cell line, and cultured primary rat Müller cells. It is generally assumed that primary cells represent *in vivo* physiology more accurately than immortalised cell lines. However, primary cells also have disadvantages. For Müller cells, these include slow growth rate, poor transfection efficiency, and heterogeneity between batches. The SIRMu-1 cell line was derived from primary Müller cells spontaneously without the transduction of a viral oncogene, so it was potentially a better physiological model than rMC-1 cells. It was therefore useful to determine whether it was metabolically similar to primary cells. All three cell types express Müller cell marker genes, but rMC-1 cells are morphologically very distinct from SIRMu-1 cells and primary rat Müller cells, which share a similar "ghost-like" cell morphology. A general characterisation of these cell types, excluding metabolism, has been published, with the full paper included in Appendix 2[128].

A previous PhD student in our laboratory, Dr. Thaksaon Kittipassorn, compared the metabolism of these three Müller cell types using Seahorse extracellular flux assays. The results have been previously reported in her PhD thesis[114], and select results have been reproduced here (Figure 3.6 A-C). While both rMC-1 and SIRMu-1 cells displayed ECAR lower than primary Müller cells, reflecting a lower rate of aerobic glycolysis (Figure 3.6 A), SIRMu-1 cells displayed a more oxidative phenotype overall. This is shown by their relatively high basal OCR (Figure 3.6 B), and corresponding low percentage-contribution of glycolysis to basal PER (Figure 3.6 C). Although primary Müller cells consumed more oxygen and produced more acid per cell than rMC-1 cells, the proportion of glucose directed into oxidative phosphorylation vs lactate production was similar in both; this is consistent with both displaying aerobic glycolysis. Despite their morphological differences, this metabolic characterisation lends credence to the use of rMC-1 cells as a model of primary Müller cell glucose metabolism and indicates that they are a better model than the SIRMu-1 cells.

As part of a broad characterisation of the three cell types, RNA-sequencing (RNA-seq) was undertaken to compare overall transcriptomic profiles. For this experiment, Dr. Kittipassorn cultured cells and isolated RNA for sequencing. Sequencing was performed at the Australian Cancer Research Foundation (ACRF) Cancer Genomics Facility, and initial bioinformatic processing including read trimming, alignment and counting was performed by staff at the facility. I contributed to an initial published analysis (Appendix 2)[128], without metabolic focus, and the data analysis in a related data-in-brief article (Appendix 3)[130].

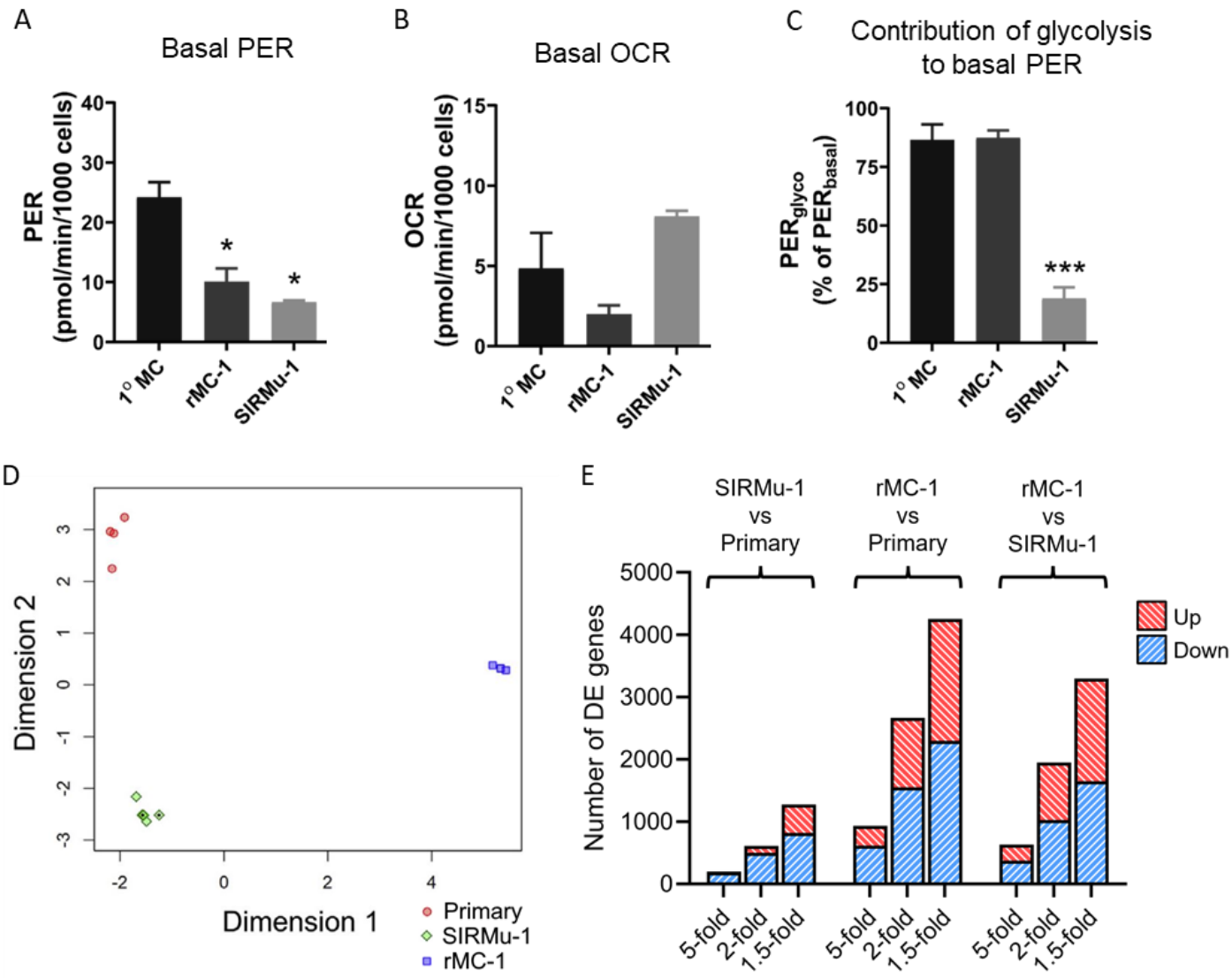


**Figure 3.6 Comparison of cultured rat Müller cell types. A-C.** [*Experiments for A-C were performed by Dr. Thaksaon Kittipassorn and have previously been presented in her PhD thesis.*] Seahorse cell mito stress tests were performed on the indicated cultured rat Müller cell types. Basal proton efflux rate (PER), basal oxygen consumption rate (OCR) and the percentage contribution of glycolysis to basal PER were calculated from Seahorse assay measurements. Data shown are the mean ± SD from two independent experiments and were analysed by Dunnet's multiple comparisons tests comparing each immortal line to primary Müller cells. **D, E.** RNA-sequencing was performed on mRNA isolated from the three cultured Müller cell types indicated. **D.** A multidimensional scaling plot was generated after normalisation of counts. **E.** Genes that were differentially expressed (DE) by greater than the indicated fold-change between each pair of cell types were determined using limma. Significance was defined as a Benjamini-Hochberg corrected P-value of <0.05. The number of DE genes at each tested fold-change was plotted. "Up" indicates significantly higher expression in the first-named cell type. "Down" indicates significantly lower expression in the first-named cell type.

A multidimensional scaling (MDS) plot was generated to assess differences in overall transcriptome between cell types; this has been reproduced from our publication[128] for convenience (Figure 3.6 D). It showed tight clustering of replicates of each cell type, indicating technical and biological consistency, but there was clear separation between different clusters, indicating the presence of transcriptomic differences between cell types. Next, genes differentially expressed between cell types were determined (Hereafter, the data presented extend the published analysis). Differential expression may be statistically significant but biologically unimportant if the fold-change in expression is small between two groups. As such, it is necessary to test for changes above a specified fold-change. The choice of fold-change is arbitrary and decided based on the biological question at hand. Initially, differential expression was tested above three different fold-change cut-offs, 1.5, 2 and 5-fold (Figure 3.6 E). In each case, the greatest number of differentially expressed genes was detected between rMC-1 cells and primary Müller cells. Far fewer genes were differentially expressed between SIRMu-1 and primary Müller cells. Similar relative numbers of genes were differentially expressed in each line when no fold-change cut-off was applied (data not shown).

Differences in expression of metabolic genes between the three cell types that may explain the metabolic differences observed in Seahorse assays were of particular interest. Sets of genes involved in glycolysis/gluconeogenesis, the TCA cycle, and OXPHOS were obtained from the Gene Set Enrichment Analysis (GSEA) Molecular Signatures Database (MSigDB). Heatmaps were generated showing differences in expression of each gene between samples (Figure 3.7) (Note: the heatmaps cannot be used to compare expression of genes in the same sample as the data have not been normalised to gene length and the values displayed are z-scores). The results of differential expression testing above a fold-change cut-off of 2 are displayed as categorical heatmaps alongside each expression heatmap. This fold-change was chosen to balance the detection of likely biologically important differences with the exclusion of likely unimportant differences; it is similar in magnitude to the changes in metabolic parameters measured in the lactate assay and Seahorse assay experiments presented above.

Considering the transcriptomic profile of the metabolic genes between the three cell lines overall, the greatest number of differentially expressed genes was detected between rMC-1 cells and primary Müller cells. It was shown in Figure 3.6 that these differences did not result in differences in the relative levels of acid production and oxygen consumption as measured in Seahorse assays, with these two cell lines showing the most similar metabolic profiles. However, this does not rule out the existence of significant differences in the utilisation of glucose or differing flux through various branches of glucometabolic pathways which sums to a similar proportion of fates in lactate and OXPHOS.

The specific metabolic differences between rMC-1 cells, which were used to investigate aerobic glycolysis, and primary Müller cells were of particular interest to gauge the physiological relevance of immortalised rMC-1 cells as a model of Müller cell metabolism.

Importantly, only two genes in the classic Embden-Meyerhof-Parnas glycolytic pathway were differentially expressed between rMC-1 cells and primary Müller cells, *Ldhb* and *Eno3* (Figure 3.7 A). Expression of *Ldhb* was downregulated in rMC-1 cells compared to both primary Müller cells and SIRMu-1 cells. *Ldhb* encodes a subunit of lactate dehydrogenase typically thought to favour conversion of lactate to pyruvate over the reverse reaction – the opposite is thought to be true of *Ldha*. A higher *Ldha:Ldhb* ratio in rMC-1 cells may therefore contribute to the higher proportion of glucose converted to lactate in rMC-1 cells than SIRMu-1 cells, although this interpretation is confounded by the fact that no such difference in glucose fate was observed between rMC-1 cells and primary Müller cells. *Eno3* encodes enolase beta, which is one of three enzymes that catalyses the reversible interconversion of 2-phosphoglycerate and phosphoenolpyruvate. This is not a rate-limiting step of glycolysis and implications of *Eno3* differential expression are not immediately obvious.

Only two genes in the TCA cycle set were differentially expressed in any comparison, *Idh1* and *Ogdhl* (Figure 3.7 B). The product of *Idh1* is not strictly a TCA cycle enzyme. It is a cytosolic $NADP^+$-dependent isocitrate dehydrogenase which catalyses the reversible decarboxylation of isocitrate to α-ketoglutarate – the same reaction is catalysed in mitochondria in the TCA cycle by different enzymes[150]. Idh1 is situated at a metabolic crossroads; its downregulation in rMC-1 cells relative to primary Müller cells and to SIRMu-1 cells likely has significant metabolic consequences which would require detailed investigation to fully characterise. The other differentially expressed gene in the TCA gene set was *Ogdhl*. It encodes a tissue-restricted component of the oxoglutarate dehydrogenase complex which catalyses the $NAD^+$-dependent decarboxylation of α-ketoglutarate, producing succinyl-CoA and $CO_2$ in the TCA cycle[151]. It was relatively lowly expressed in rMC-1 cells, moderately expressed in SIRMu-1 cells, and relatively highly expressed in primary Müller cells. This inversely correlates with the proliferation rates of the three cell types (primary < SIRMu-1 < rMC-1), which is interesting as *Ogdhl* expression is inversely correlated with rates of cancer cell proliferation and prognosis for multiple cancer types[152-155]. Its downregulation is associated with increased PI3K/Akt pathway activity[152], hence its differential expression may reflect differences in PI3K signalling in the three cell types.

In the OXPHOS gene set, differentially expressed genes were all components of vacuolar ATPase, and were downregulated in rMC-1 cells relative to each of the other two cell types (Figure 3.7 C). Vacuolar ATPase is an evolutionarily ancient enzyme with diverse roles. It consumes ATP to acidify organelles.

Given its wide-ranging roles, consequences of its differential expression would require direct investigation to determine. Despite the high oxygen consumption relative to glycolysis observed in SIRMu-1 cells in Seahorse assays, no genes were differentially expressed (by at least 2-fold) between SIRMu-1 cells and primary Müller cells in the OXPHOS gene set. It is possible that the metabolic differences observed are due to post-transcriptional or post-translational mechanisms.

Finally, the expression of genes involved in the insulin signalling pathway, which incorporates PI3K/Akt signalling, was assessed. The full set of genes is extensive, and data are shown in Figure A.3 in Appendix 4. A heatmap showing only the differentially expressed genes out of the full list is displayed in Figure 3.7 D. The greatest number of differentially expressed genes was again found between rMC-1 cells and primary Müller cells. Immediately concerning were the upregulation of *Pik3cb* and the downregulation of *Inpp5d* in rMC-1 cells. *Pik3cb* encodes the catalytic subunit of one of the isoforms of PI3K, and *Inpp5d* encodes the protein SHIP1, which catalyses dephosphorylation of the 5' position of phosphatidylinositol-3,4,5-trisphosphate, the product of PI3K activity (this is not a direct reversal of the PI3K reaction, which results in phosphorylation of the 3' site). By modifying the membrane inositol lipid composition, SHIP1 activity can alter PI3K signalling.

To summarise, while rMC-1 cells and primary Müller cells displayed similar metabolic profiles in Seahorse assays, the expression of metabolic genes indicates that SIRMu-1 cells and primary Müller cells are more similar transcriptomically than the rMC-1 and primary Müller cells. The differentially expressed metabolic genes do not obviously explain the differences observed in Seahorse assays and neither immortal cell line appears to be a perfect model of primary Müller cell metabolism. Differences in expression of key PI3K signalling-related genes between rMC-1 cells and primary Müller cells cast further doubt on whether the dysregulation of lactate production by PI3K inhibition in section 3.1 is an accurate reflection of the role of PI3K in driving aerobic glycolysis in Müller cells in vivo. For these reasons, and the emerging evidence supporting the photoreceptors as the major producer of lactate *in vivo*, it was decided not to proceed further with metabolic analysis using rMC-1 cells or other types of cultured Müller cells, but instead a more physiological model of retinal metabolism was sought to test the pathway inhibitors used above, and to increase the direct clinical relevance of our findings.

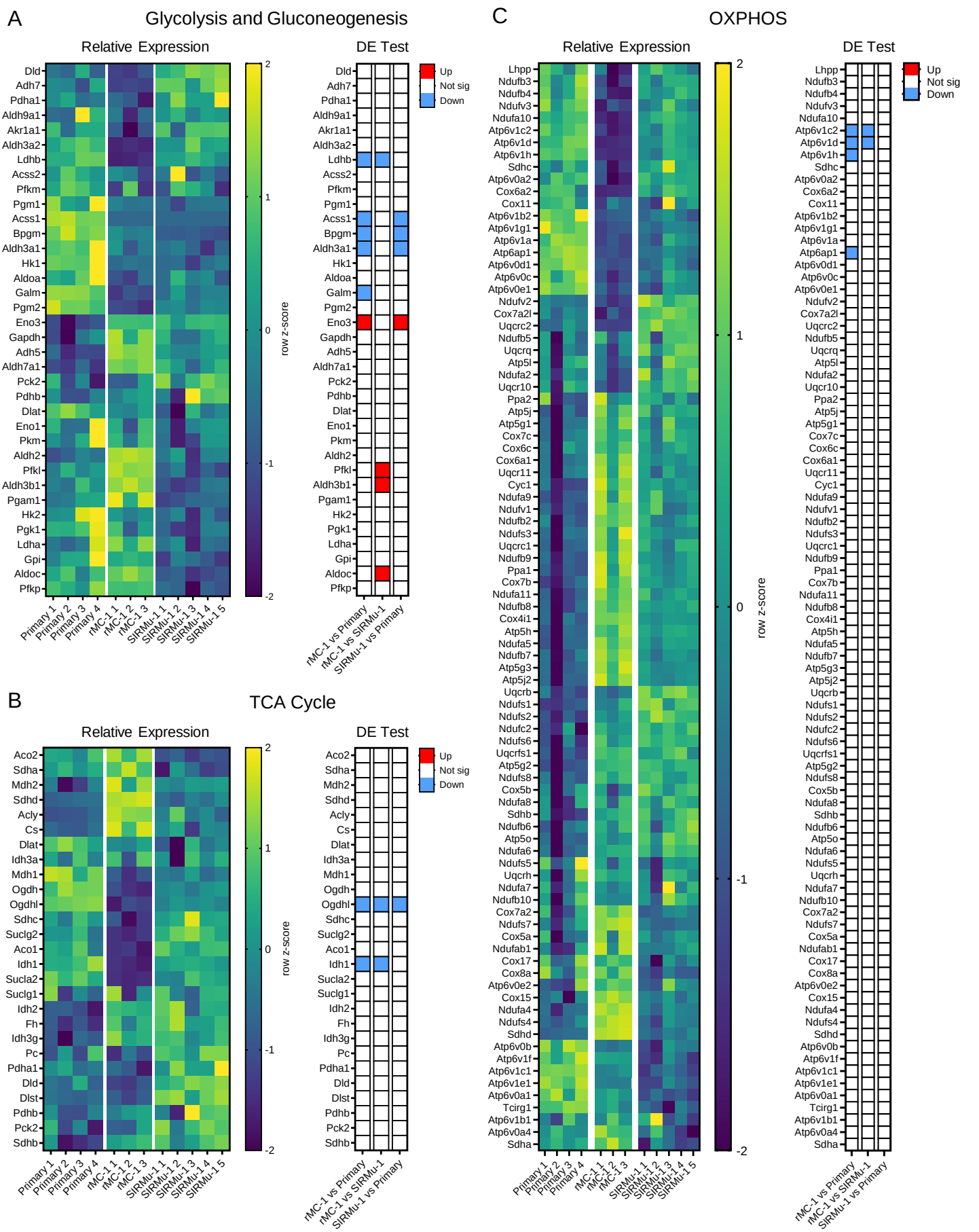
A
Glycolysis and Gluconeogenesis
Relative Expression
DE Test
Dld
Adh7
Pdha1
Aldh9a1
Akr1a1
Aldh3a2
Ldhb
Acss2
Pfkm
Pgm1
Acss1
Bpgm
Aldh3a1
Hk1
Aldoa
Galm
Pgm2
Eno3
Gapdh
Adh5
Aldh7a1
Pck2
Pdhb
Dlat
Eno1
Pkm
Aldh2
Pfkl
Aldh3b1
Pgam1
Hk2
Pgk1
Ldha
Gpi
Aldoc
Pfkp
row z-score
2
1
0
-1
-2
Up
Not sig
Down
Primary 1
Primary 2
Primary 3
Primary 4
rMC-1 1
rMC-1 2
rMC-1 3
SIRMu-1 1
SIRMu-1 2
SIRMu-1 3
SIRMu-1 4
SIRMu-1 5
rMC-1 vs Primary
rMC-1 vs SIRMu-1
SIRMu-1 vs Primary
B
TCA Cycle
Relative Expression
DE Test
Aco2
Sdha
Mdh2
Sdhd
Acly
Cs
Dlat
Idh3a
Mdh1
Ogdh
Ogdhl
Sdhc
Suclg2
Aco1
Idh1
Sucla2
Suclg1
Idh2
Fh
Idh3g
Pc
Pdha1
Dld
Dlst
Pdhb
Pck2
Sdhb
row z-score
2
1
0
-1
-2
Up
Not sig
Down
Primary 1
Primary 2
Primary 3
Primary 4
rMC-1 1
rMC-1 2
rMC-1 3
SIRMu-1 1
SIRMu-1 2
SIRMu-1 3
SIRMu-1 4
SIRMu-1 5
rMC-1 vs Primary
rMC-1 vs SIRMu-1
SIRMu-1 vs Primary
C
OXPHOS
Relative Expression
DE Test
Lhpp
Ndufb3
Ndufb4
Ndufv3
Ndufa10
Atp6v1c2
Atp6v1d
Atp6v1h
Sdhc
Atp6v0a2
Cox6a2
Cox11
Atp6v1b2
Atp6v1g1
Atp6v1a
Atp6ap1
Atp6v0d1
Atp6v0c
Atp6v0e1
Ndufv2
Cox7a2l
Uqcrc2
Ndufb5
Uqcrq
Atp5l
Ndufa2
Uqcr10
Ppa2
Atp5j
Atp5g1
Cox7c
Cox6c
Cox6a1
Uqcr11
Cyc1
Ndufa9
Ndufv1
Ndufb2
Ndufs3
Uqcrc1
Ndufb9
Ppa1
Cox7b
Ndufa11
Ndufb8
Cox4i1
Atp5h
Ndufa5
Ndufb7
Atp5g3
Atp5j2
Uqcrb
Ndufs1
Ndufs2
Ndufc2
Ndufs6
Uqcrfs1
Atp5g2
Ndufs8
Cox5b
Ndufa8
Sdhb
Ndufb6
Atp5o
Ndufa6
Ndufs5
Uqcrh
Ndufa7
Ndufb10
Cox7a2
Ndufs7
Cox5a
Ndufab1
Cox17
Cox8a
Atp6v0e2
Cox15
Ndufa4
Ndufs4
Sdhd
Atp6v0b
Atp6v1f
Atp6v1c1
Atp6v1e1
Atp6v0a1
Tcirg1
Atp6v1b1
Atp6v0a4
Sdha
row z-score
2
1
0
-1
-2
Up
Not sig
Down
Primary 1
Primary 2
Primary 3
Primary 4
rMC-1 1
rMC-1 2
rMC-1 3
SIRMu-1 1
SIRMu-1 2
SIRMu-1 3
SIRMu-1 4
SIRMu-1 5
rMC-1 vs Primary
rMC-1 vs SIRMu-1
SIRMu-1 vs Primary

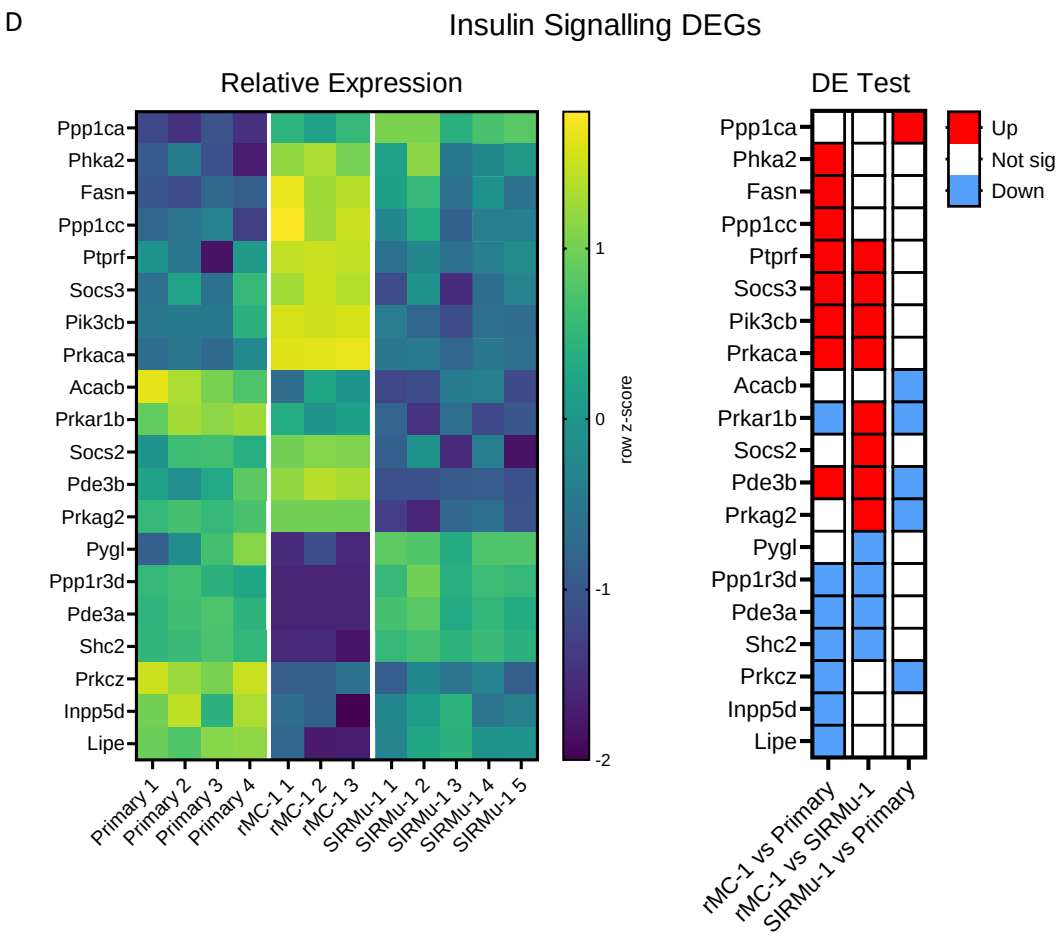


**Figure 3.7 RNA-seq: Differences in expression of metabolic genes between cultured Müller cell types. A-C. Left panels:** Heatmaps were generated from log2 normalised counts per million (with z-scores calculated across each row) to show differences in expression of genes involved in **A.** glycolysis and gluconeogenesis, **B.** the tricarboxylic acid (TCA) cycle, and **C.** oxidative phosphorylation (OXPHOS) between cultured Müller cell types. **Right Panels:** Genes that were significantly differentially expressed (Benjamini-Hochberg corrected P-value of < 0.05) by greater than 2-fold between each pair of cell types are indicated. **D.** Same as A-C but only the genes that were differentially expressed from a larger list of insulin signalling-related genes are presented. Lists of genes under each heading were obtained from the Gene Set Enrichment Analysis (GSEA) Molecular Signatures Database (MSigDB). "Up" indicates significantly higher expression in the first-named cell type. "Down" indicates significantly lower expression in the first-named cell type. DEGs: Differentially expressed genes.

# 4. Results: RNA-seq analyses

The general utility of cultured Müller cells as a model of physiological Müller cell metabolism or broader whole-retinal metabolism was at this time becoming increasingly questionable. This was in part due to a study by Lindsay et al. which showed that mouse Müller cells *in vivo* lack or only minimally express any isoform of pyruvate kinase[54]; therefore, they would not be able to undertake rapid glycolysis in a physiological context. It is abundantly clear that cultured Müller cells strongly exhibit aerobic glycolysis. Together, these observations indicate rapid metabolic changes may occur as Müller cells adapt to culture, and consequently the metabolic profile of cultured Müller cells, either primary or immortalised, do not reflect the metabolic profile of Müller cells in the context of a functioning mammalian retina.

There were also an increasing number of studies reporting expression of key glycolytic enzymes in photoreceptors[14,50,54,117,156,157]. Modulation of these enzymes had significant metabolic and functional effects and indicated that photoreceptors, rather than Müller cells were likely the major lactate-producing retinal cells *in vivo*[14,45,50,53]. However, photoreceptors cannot be cultured in a physiologically normal state, especially for metabolic analyses, which makes them more difficult to study, and as discussed above, dissociated cell types in culture (where culturing is possible) can display metabolic differences to their states *in vivo*. The metabolic relationships between retinal cell types were far from clear, and it is difficult to measure metabolic fluxes in specific cell types in an intact tissue such as the retina.

The best option for further metabolic experiments was to use whole retinal explants, which can survive *ex vivo* for sufficiently long to measure effects of metabolic interventions, and which have been used extensively by other groups in past metabolic studies of the retina[5,6,10,11,50]. Before undertaking these experiments, however, I sought to examine newly published RNA-seq datasets with the aims to characterise key metabolic differences between retinal cell types at the transcriptomic level, and provide further evidence for the photoreceptors, Müller cells or other cell types in the retina being major producers of lactate. In particular, we were interested in analysing the expression of glycolytic and other metabolic genes in Müller cells as compared to photoreceptors, as well as gaining an initial insight into potential pathways that may drive expression of some of these key genes *in vivo.*

## *4.2 Single-cell RNA-seq analyses*

In 2015, Macosko and colleagues published a seminal paper which introduced the Drop-seq method of single-cell RNA-seq (scRNA-seq)[57]. Using the mouse retina as an example of analysis of a complex tissue due to the extensive existing knowledge of its numerous distinct cell populations, they profiled

the transcriptomes of over 44,000 individual cells. The cells were clustered into groups *in silico* based on their transcriptomes. Thirty-nine groups were generated, and each was assigned a cell type label based on expression of known marker genes. Importantly, all previously defined retinal cell types formed unique groups based on their specific transcriptomes, including rods, cones and Müller cells. Differences in glucose metabolism between cell types were not analysed in the original paper, which was mostly an introduction of the Drop-seq technique. So, to interrogate metabolic differences, I downloaded and analysed the publicly available dataset and compared the relative expression of genes related to glucose metabolism between each of the major cell types.

There were limitations to this approach, however. Firstly, there is always a low depth of sequencing of each cell in scRNA-seq (approximately 2000 reads per cell on average in Macosko et al.[57]) compared to a population in bulk RNA-seq (approximately 3 x $10^7$ reads) as the limited reads are often spread across RNA derived from tens of thousands of cells. For most scRNA-seq technologies, only the most abundant transcripts in a given cell are likely to be read, with most genes recording zero reads in most cells – a phenomenon termed gene dropout[158]. Many scRNA-seq studies expressly trade-off sequencing depth for a greater number of cells, as this improves the detection of rare cell types, which is desirable when the aim of the study is cell type classification[159]. Secondly, lowly abundant cell types are particularly susceptible to stochastic noise at the single-gene level, which was not a large problem when considering rods (>29,000 cells) or Müller cells (1,624 cells) but was when considering rare cell types such as astrocytes (54 cells). Finally, and specifically relating to this dataset, known rod-specific transcripts such as *Rho* and *Nrl* were identified in all cell types. This was explained by the authors as likely due to the solubilisation of high-abundance transcripts at the cell suspension stage before the microfluidic separation of cells. This rod-contamination, combined with low sequencing depth, in many cases made it difficult to know whether a given gene was truly expressed in a cell type. For these reasons, no strong conclusions could be made regarding the expression of individual metabolic genes, and the data are not presented.

I recently revisited the dataset after the publication of a new method for normalisation of scRNA-seq data by the same group, termed sctransform, which improves dimensionality reduction and differential expression analysis[160]. The count data were normalised using sctransform and cells were clustered following the process described in the original paper. Marker genes were determined, and cell types were assigned. Expression of genes related to glucose metabolism was then assessed again. Unfortunately, this new normalisation method did not adequately overcome the limitations of the data for our purposes in terms of high variability at the level of single genes.

Since the original Drop-seq paper, other scRNA-seq studies have been published using whole retinas, retinal organoids or acutely isolated retinal cell types, from various species, and across developmental stages and aging, but, for differing reasons relating to experimental design or sequencing depth, none have been ideally suited to the purpose of assessing glucose metabolism in normal adult retinal tissue. As technology and sequencing depth improves, it may become useful to perform scRNA-seq at greater depth or to revisit this type of analysis as new datasets become available.

## *4.3 Bulk RNA-seq analyses*

Although not encompassing the same breadth of cell types, bulk RNA-seq data have no depth problem at the single-gene level. Therefore, publicly available bulk RNA-seq datasets from different isolated retinal cell types were analysed for expression of genes involved in glycolysis, the TCA cycle and OXHPOS.

### *Developing photoreceptors*

A very relevant and high-quality dataset was published by Kim et al. in 2016[1]. As part of this study, GFP-tagged rod cells were FACS-isolated from *Nrl*p-GFP mouse retinas at various developmental stages from postnatal day 2 (P2) to P28. In the mouse, photoreceptors develop postnatally over this period, which includes the growth of outer segments and gain of normal electrical function[161-163]. The dataset could therefore be used to observe the changes in expression of metabolic genes associated with the development and functional maturation of photoreceptors, which provided a better insight into functionally important metabolic genes than any single-age snapshot.

Transcript-level count data were downloaded from GEO (accession number: GSE74660), aggregated to gene-level counts, log-transformed and normalised to library size and composition. The data were filtered to retain groups relevant for our purposes (Nrl-positive groups). Expression of the same sets of metabolic genes as analysed in our Müller cell data above were visualised in heatmaps (Figure 4.1). Differential expression by at least 2-fold was tested between the P28 group and the P2 group. A table alongside each heatmap indicates which genes exhibited statistically significant changes, as well as showing the expression level at P2 and P28, and fold-change between these ages. Note that the $\log_2$ cpm values are not normalised to gene length so expression of genes cannot strictly be compared to one another.

There was widespread upregulation of genes across all three metabolic sets from P2 to P28. This was not due to any error or artifact; across the whole transcriptome, more genes decreased (3938 out of 19,615) than increased in expression (2,181 out of 19,615) from P2 to P28. This is further evidence for

rod photoreceptors being highly metabolically active cells and likely responsible for most retinal aerobic glycolysis – If rods mainly relied on oxidising lactate released by Müller cells rather than autonomous glycolysis, as was proposed by Poitry-Yamate et al.[44] it would make little sense for them to upregulate expression of glycolytic genes so strongly.

Considering the glycolysis and gluconeogenesis gene set, between P2 and P28, rods significantly upregulated, by at least 2-fold, expression of at least one isoform of an enzyme at every step of glycolysis (Figure 4.1 A, C). The two genes that exhibited the greatest increase from P2 to P28 were *Hk1* and *Hk2*, with fold-changes of 70 and 175, respectively. Expression of both of these isoforms in rods is consistent with immunofluorescence data[14]. As discussed in the introduction, both *Hk1* and *Hk2* are able to sustain high rates of glycolysis, with *Hk2* being particularly implicated in supporting aerobic glycolysis in the context of cancer[116,164-167]. Mouse rod *Hk2* knockout retinas exhibit decreased lactate production and functional defects but do not exhibit increased cell death[14]. *Hk1* has been relatively less studied, which is surprising given that a mutation in *HK1*, but not *HK2*, has been found to be associated with retinitis pigmentosa[121], although this mutation did not clearly change the enzymatic function of the protein. This nevertheless suggests non-redundant functions for each isoform in the retina. Given it is upregulated over maturation in a similarly dramatic manner as *Hk2*, the role of *Hk1* in rods warrants investigation. It may be equally important as *Hk2*.

**Figure 4.1 Metabolic gene expression in RNA-seq data from developing mouse photoreceptors (data from Kim et al. 2016).** Kim et al.[1] performed RNA-seq on *Nrlp*-GFP rod photoceptors FACS-isolated from retinas at several stages of development from postnatal day 2 (P2) to P28. The table of effective counts was downloaded from Gene Expression Omnibus under accession number GSE74660. Counts were summed to the gene level in a transcript-aware manner using tximport in R, then were TMM-normalised using EdgeR. Groups were filtered to retain only Nrl-positive groups for heatmap generation. **A, B, D Left panels:** Heatmaps were generated from log2 normalised counts per million (with z-scores calculated across each row) to show differences in expression of genes involved in **A.** glycolysis and gluconeogenesis, **B.** the tricarboxylic acid (TCA) cycle, and **D.** oxidative phosphorylation (OXPHOS). **Right Panels:** Tables are presented showing the normalised log2 counts per million (cpm) at P2 and P28, the fold-change between these two groups, and whether the change was statistically significantly greater than 2-fold. Differential expression (DE) testing was performed using limma to compare the P2 and P28 groups (fold-change threshold of 2, Benjamini-Hochberg corrected P-value of < 0.05). Lists of genes under each heading were obtained from the Gene Set Enrichment Analysis (GSEA) Molecular Signatures Database (MSigDB). **C.** Diagram of the Embden-Meyerhof-Parnas glycolytic pathway with genes that were statistically significantly upregulated by greater than 2-fold over rod development highlighted in bold red.

A

## Glycolysis and Gluconeogenesis

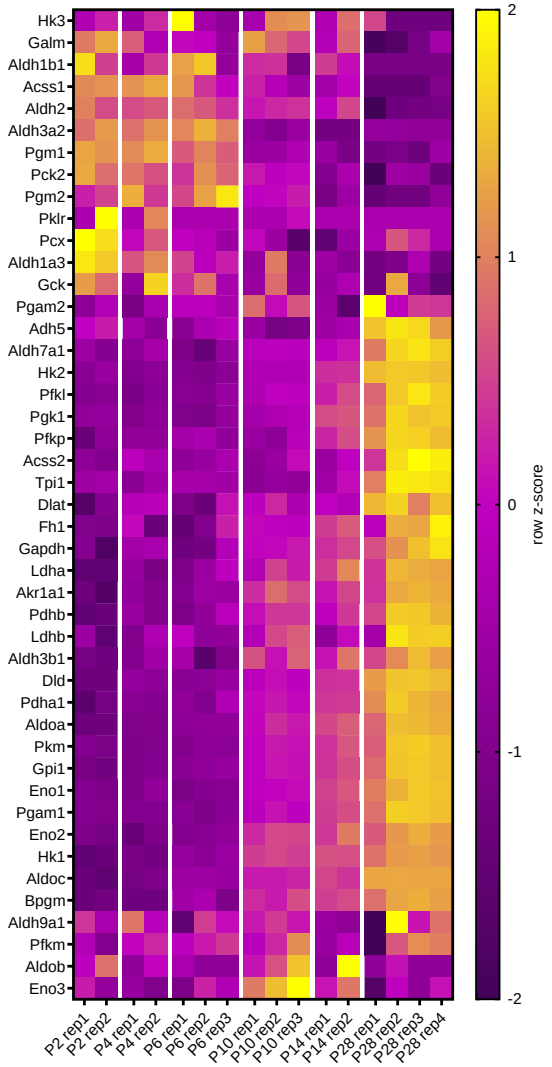


| | P2 Avg log2 cpm | P28 Avg log2 cpm | Fold change | Significant > 2-fold DE |
|---|---|---|---|---|
| Hk3 | -2.0 | -2.4 | -1.4 | no |
| Galm | 1.1 | -0.5 | -3.0 | no |
| Aldh1b1 | -1.2 | -2.7 | -2.9 | no |
| Acss1 | 0.6 | -2.6 | -8.9 | Yes |
| Aldh2 | 3.3 | -0.2 | -12 | Yes |
| Aldh3a2 | 6.0 | 4.4 | -3.0 | no |
| Pgm1 | 4.4 | 2.5 | -3.7 | Yes |
| Pck2 | 3.2 | 1.4 | -3.5 | no |
| Pgm2 | 6.5 | 6.0 | -1.4 | no |
| Pklr | -1.6 | -2.7 | -2.1 | no |
| Pcx | 3.9 | 3.0 | -1.9 | no |
| Aldh1a3 | 3.3 | -2.1 | -43 | Yes |
| Gck | 1.4 | -0.1 | -2.8 | no |
| Pgam2 | -2.0 | -0.9 | 2.0 | no |
| Adh5 | 6.5 | 7.0 | 1.4 | no |
| Aldh7a1 | 5.0 | 6.6 | 3.1 | Yes |
| Hk2 | 3.6 | 11.0 | 170 | Yes |
| Pfkl | 6.5 | 9.4 | 7.0 | Yes |
| Pgk1 | 8.0 | 9.8 | 3.5 | Yes |
| Pfkp | 5.8 | 8.7 | 7.5 | Yes |
| Acss2 | 5.0 | 6.3 | 2.4 | no |
| Tpi1 | 7.9 | 9.5 | 2.9 | Yes |
| Dlat | 5.4 | 7.0 | 2.9 | no |
| Fh1 | 4.8 | 6.3 | 2.9 | no |
| Gapdh | 7.6 | 11.8 | 18 | Yes |
| Ldha | 10.4 | 11.6 | 2.2 | no |
| Akr1a1 | 7.3 | 8.8 | 2.8 | Yes |
| Pdhb | 6.7 | 7.9 | 2.3 | no |
| Ldhb | 6.1 | 6.7 | 1.5 | no |
| Aldh3b1 | -1.5 | 0.8 | 4.8 | no |
| Dld | 6.6 | 8.7 | 4.3 | Yes |
| Pdha1 | 5.4 | 7.3 | 3.6 | Yes |
| Aldoa | 8.4 | 12.3 | 15 | Yes |
| Pkm | 10.2 | 13.2 | 8.1 | Yes |
| Gpi1 | 7.7 | 10.5 | 7.0 | Yes |
| Eno1 | 9.5 | 13.0 | 11 | Yes |
| Pgam1 | 7.6 | 11.0 | 10 | Yes |
| Eno2 | 6.0 | 8.7 | 6.5 | Yes |
| Hk1 | 5.5 | 11.6 | 70 | Yes |
| Aldoc | 3.6 | 8.8 | 36 | Yes |
| Bpgm | 4.8 | 7.8 | 8.0 | Yes |
| Aldh9a1 | 5.1 | 5.1 | 1.0 | no |
| Pfkm | 4.8 | 4.9 | 1.1 | no |
| Aldob | -2.0 | -2.6 | -1.5 | no |
| Eno3 | 4.3 | 4.1 | -1.2 | no |

B

## TCA Cycle

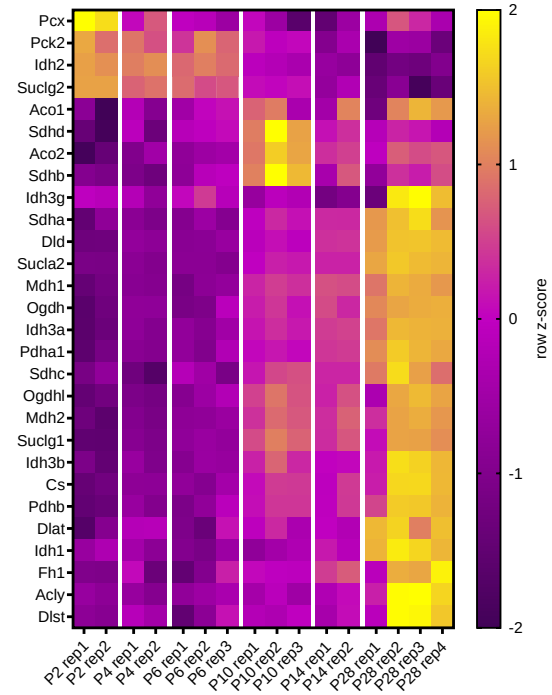


| | P2 Avg log2 cpm | P28 Avg log2 cpm | Fold change | Significant > 2-fold DE |
|---|---|---|---|---|
| Pcx | 3.9 | 3.0 | -1.9 | no |
| Pck2 | 3.2 | 1.4 | -3.5 | no |
| Idh2 | 5.9 | 2.0 | -15 | Yes |
| Suclg2 | 4.0 | -1.4 | -42 | Yes |
| Aco1 | 5.7 | 6.1 | 1.3 | no |
| Sdhd | 6.1 | 6.6 | 1.4 | no |
| Aco2 | 7.1 | 8.4 | 2.5 | no |
| Sdhb | 5.7 | 6.0 | 1.2 | no |
| Idh3g | 6.4 | 6.7 | 1.2 | no |
| Sdha | 7.6 | 9.7 | 4.5 | Yes |
| Dld | 6.6 | 8.7 | 4.3 | Yes |
| Sucla2 | 5.2 | 7.9 | 6.4 | Yes |
| Mdh1 | 7.4 | 10.1 | 6.3 | Yes |
| Ogdh | 6.6 | 8.3 | 3.1 | Yes |
| Idh3a | 5.5 | 7.8 | 5.0 | Yes |
| Pdha1 | 5.4 | 7.3 | 3.6 | Yes |
| Sdhc | 6.0 | 8.0 | 3.7 | Yes |
| Ogdhl | 5.7 | 7.3 | 3.0 | no |
| Mdh2 | 7.2 | 9.2 | 3.9 | Yes |
| Suclg1 | 5.6 | 7.1 | 2.8 | Yes |
| Idh3b | 6.5 | 7.8 | 2.4 | no |
| Cs | 6.9 | 8.3 | 2.5 | no |
| Pdhb | 6.7 | 7.9 | 2.3 | no |
| Dlat | 5.4 | 7.0 | 2.9 | no |
| Idh1 | 6.4 | 7.4 | 1.9 | no |
| Fh1 | 4.8 | 6.3 | 2.9 | no |
| Acly | 8.2 | 9.1 | 1.9 | no |
| Dlst | 6.3 | 6.9 | 1.5 | no |

C

Glycolytic genes upregulated over rod development

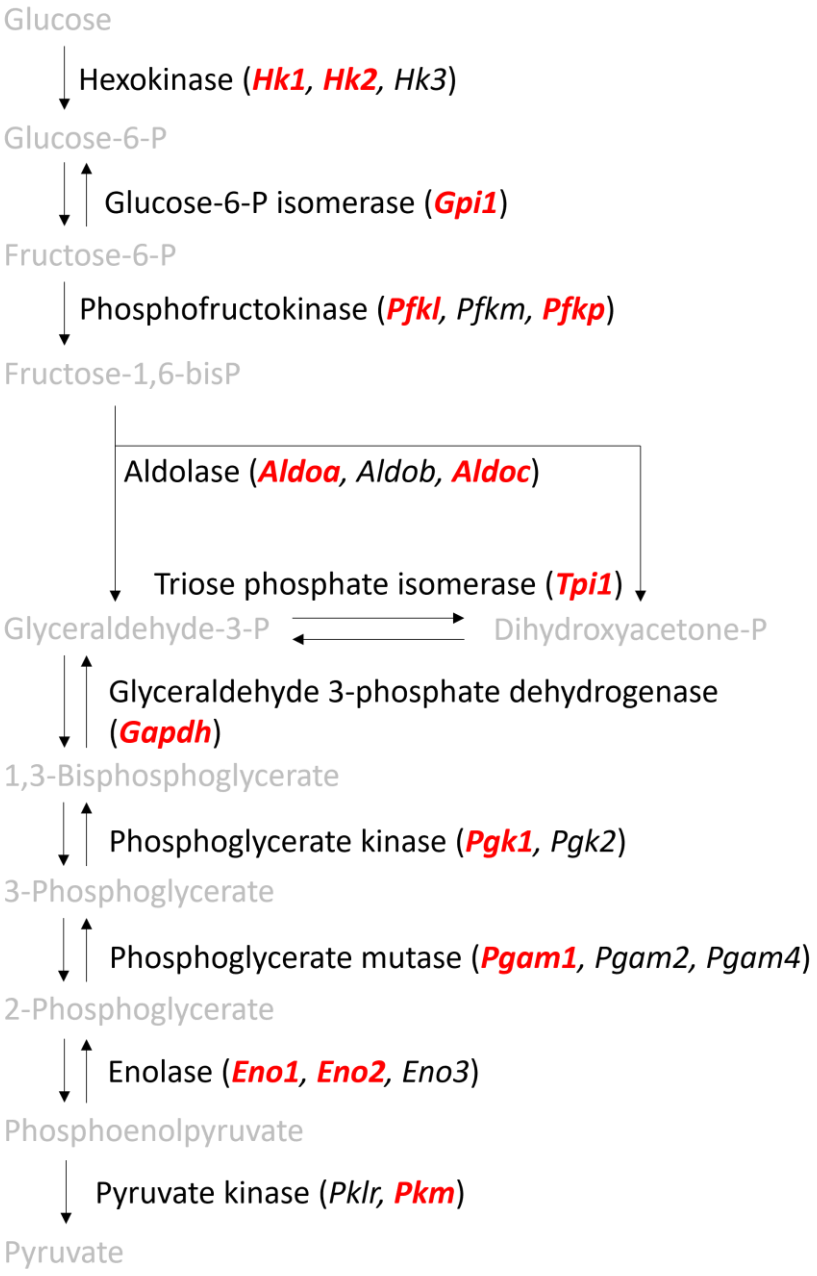

D

# OXPHOS

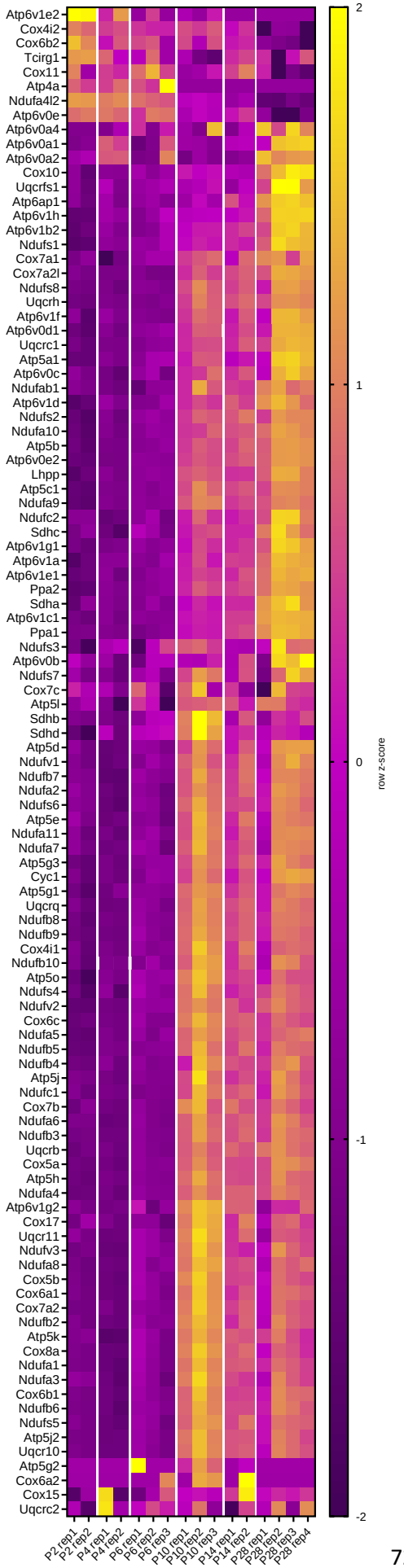


| | P2 Avg log2 cpm | P28 Avg log2 cpm | Fold change | Significant > 2-fold DE |
|---|---|---|---|---|
| Atp6v1e2 | 0.2 | -2.7 | -7.7 | Yes |
| Cox4i2 | 4.1 | -0.5 | -24 | Yes |
| Cox6b2 | 2.5 | -1.2 | -13 | Yes |
| Tcirg1 | 3.1 | 1.6 | -2.8 | no |
| Cox11 | 3.9 | 3.5 | -1.3 | no |
| Atp4a | -1.1 | -2.7 | -3.0 | no |
| Ndufa4l2 | 6.1 | -1.6 | -210 | Yes |
| Atp6v0e | 3.8 | 1.0 | -7.0 | Yes |
| Atp6v0a4 | -2.7 | -0.4 | 5.1 | Yes |
| Atp6v0a1 | 7.4 | 8.3 | 1.8 | no |
| Atp6v0a2 | 4.6 | 4.9 | 1.3 | no |
| Cox10 | 3.3 | 4.7 | 2.7 | no |
| Uqcrfs1 | 6.5 | 7.3 | 1.7 | no |
| Atp6ap1 | 6.5 | 9.3 | 7.1 | Yes |
| Atp6v1h | 6.2 | 7.7 | 2.9 | Yes |
| Atp6v1b2 | 8.0 | 10.0 | 4.0 | Yes |
| Ndufs1 | 6.2 | 7.9 | 3.2 | Yes |
| Cox7a1 | -0.8 | 0.9 | 3.3 | no |
| Cox7a2l | 7.0 | 8.9 | 3.8 | Yes |
| Ndufs8 | 4.6 | 6.6 | 3.9 | Yes |
| Uqcrh | 6.7 | 9.1 | 5.3 | Yes |
| Atp6v1f | 5.3 | 6.4 | 2.3 | no |
| Atp6v0d1 | 6.7 | 8.1 | 2.5 | no |
| Uqcrc1 | 6.6 | 8.9 | 5.0 | Yes |
| Atp5a1 | 9.1 | 11.1 | 3.8 | Yes |
| Atp6v0c | 7.4 | 9.2 | 3.4 | no |
| Ndufab1 | 6.4 | 7.4 | 2.1 | no |
| Atp6v1d | 5.5 | 6.8 | 2.5 | Yes |
| Ndufs2 | 6.9 | 9.7 | 6.8 | Yes |
| Ndufa10 | 5.9 | 8.3 | 5.3 | Yes |
| Atp5b | 9.3 | 11.9 | 6.4 | Yes |
| Atp6v0e2 | 5.9 | 10.1 | 19 | Yes |
| Lhpp | 2.1 | 5.3 | 9.1 | Yes |
| Atp5c1 | 7.1 | 9.5 | 5.1 | Yes |
| Ndufa9 | 5.5 | 7.0 | 2.8 | Yes |
| Ndufc2 | 5.9 | 7.0 | 2.1 | no |
| Sdhc | 6.0 | 8.0 | 3.7 | Yes |
| Atp6v1g1 | 6.8 | 8.3 | 2.9 | Yes |
| Atp6v1a | 7.3 | 9.4 | 4.2 | Yes |
| Atp6v1e1 | 6.2 | 8.0 | 3.3 | Yes |
| Ppa2 | 5.8 | 8.7 | 7.4 | Yes |
| Sdha | 7.6 | 9.7 | 4.5 | Yes |
| Atp6v1c1 | 5.2 | 7.6 | 5.2 | Yes |
| Ppa1 | 5.2 | 8.6 | 11 | Yes |
| Ndufs3 | 6.2 | 7.2 | 1.9 | no |
| Atp6v0b | 7.7 | 8.2 | 1.4 | no |
| Ndufs7 | 5.4 | 6.5 | 2.1 | no |
| Cox7c | 3.8 | 3.9 | 1.1 | no |
| Atp5l | 0.4 | 2.8 | 5.1 | no |
| Sdhb | 5.7 | 6.0 | 1.2 | no |
| Sdhd | 6.1 | 6.6 | 1.4 | no |
| Atp5d | 6.2 | 7.6 | 2.7 | no |
| Ndufv1 | 6.4 | 7.9 | 2.8 | no |
| Ndufb7 | 5.2 | 6.9 | 3.3 | no |
| Ndufa2 | 5.6 | 7.5 | 3.8 | Yes |
| Ndufs6 | 4.6 | 6.5 | 3.6 | Yes |
| Atp5e | 6.3 | 7.7 | 2.5 | no |
| Ndufa11 | 4.4 | 5.7 | 2.5 | no |
| Ndufa7 | 5.8 | 7.6 | 3.3 | no |
| Atp5g3 | 7.6 | 9.1 | 3.0 | Yes |
| Cyc1 | 6.2 | 7.8 | 3.0 | Yes |
| Atp5g1 | 5.2 | 7.3 | 4.3 | Yes |
| Uqcrq | 5.7 | 8.1 | 5.4 | Yes |
| Ndufb8 | 6.4 | 9.0 | 6.0 | Yes |
| Ndufb9 | 5.9 | 8.3 | 5.5 | Yes |
| Cox4i1 | 7.6 | 9.4 | 3.4 | Yes |
| Ndufb10 | 5.7 | 7.1 | 2.5 | no |
| Atp5o | 6.9 | 8.6 | 3.3 | Yes |
| Ndufs4 | 5.5 | 6.4 | 1.9 | no |
| Ndufv2 | 6.2 | 7.4 | 2.4 | no |
| Cox6c | 6.6 | 9.2 | 5.8 | Yes |
| Ndufa5 | 5.2 | 7.5 | 4.7 | Yes |
| Ndufb5 | 6.1 | 7.8 | 3.4 | Yes |
| Ndufb4 | 3.4 | 5.6 | 4.5 | Yes |
| Atp5j | 6.7 | 8.1 | 2.7 | no |
| Ndufc1 | 5.6 | 7.4 | 3.4 | Yes |
| Cox7b | 5.9 | 7.5 | 3.1 | Yes |
| Ndufa6 | 5.2 | 7.1 | 3.8 | Yes |
| Ndufb3 | 4.8 | 7.2 | 5.4 | Yes |
| Uqcrb | 5.5 | 8.3 | 6.7 | Yes |
| Cox5a | 6.2 | 8.2 | 4.0 | Yes |
| Atp5h | 7.0 | 9.0 | 4.0 | Yes |
| Ndufa4 | 7.0 | 10.5 | 12 | Yes |
| Atp6v1g2 | 3.5 | 4.2 | 1.6 | no |
| Cox17 | 4.6 | 6.0 | 2.6 | no |
| Uqcr11 | 5.1 | 6.4 | 2.4 | no |
| Ndufv3 | 6.0 | 7.6 | 3.2 | Yes |
| Ndufa8 | 4.8 | 6.1 | 2.5 | no |
| Cox5b | 6.3 | 8.1 | 3.4 | Yes |
| Cox6a1 | 6.6 | 8.6 | 4.2 | Yes |
| Cox7a2 | 6.2 | 7.9 | 3.1 | Yes |
| Ndufb2 | 5.5 | 7.3 | 3.6 | Yes |
| Atp5k | 5.6 | 7.4 | 3.6 | Yes |
| Cox8a | 7.0 | 8.9 | 3.6 | Yes |
| Ndufa1 | 5.1 | 7.4 | 4.7 | Yes |
| Ndufa3 | 5.4 | 6.6 | 2.3 | no |
| Cox6b1 | 6.4 | 8.2 | 3.4 | Yes |
| Ndufb6 | 4.8 | 6.5 | 3.2 | Yes |
| Ndufs5 | 5.1 | 7.0 | 3.8 | Yes |
| Atp5j2 | 5.8 | 7.6 | 3.5 | Yes |
| Uqcr10 | 5.1 | 6.9 | 3.7 | no |
| Atp5g2 | -2.7 | -2.7 | -1.0 | no |
| Cox6a2 | -2.7 | -2.7 | -1.0 | no |
| Cox15 | 4.5 | 5.1 | 1.6 | no |
| Uqcrc2 | 7.0 | 7.4 | 1.3 | no |

Unexpectedly, given their position at a key branch point between OXPHOS and lactate production, changes in expression of *Ldha* and *Ldhb* were not statistically significantly greater than 2-fold – although both exhibited similar increasing trends of 2.2-fold (not significant at 2-fold cut-off) and 1.5-fold, respectively. The LDH reaction is rapid and generally in equilibrium[168], so it is likely these enzymes are able to support a large increase in flux through to lactate over this maturation period without a great increase in their expression.

Outside of the canonical glycolytic pathway, an interesting upregulated gene was *Bpgm*, which encodes bisphopshoglycerate mutase. This enzyme is expressed in erythrocytes, where it catalyses the production of 2,3-bisphosphoglycerate (2,3-BPG) from the glycolytic intermediate 1,3-bisphosphoglycerate. 2,3-BPG allosterically decreases the affinity of haemoglobin (Hb) for oxygen[169]. *Bpgm* has not been studied in the retina to my knowledge. Speculatively, its expression in rods might improve oxygen delivery by increasing the local concentration of 2,3-BPG and decreasing the oxygen affinity of Hb in the choroid or retinal vessels. This would require transport 2,3-BPG out of the retina, into blood vessels, and into erythrocytes. Alternatively, aerobic glycolysis has been proposed to reflect a metabolic state in which demand for $NAD^+$ is elevated relative to demand for ATP[42]. A detour in the glycolytic pathway via the *Bpgm* reaction circumvents production of an ATP molecule[170]. It is plausible that such a means of decreasing ATP production while maintaining other functions of glycolysis (if they exist), might be beneficial to a cell in such a state. These hypotheses are speculative, and investigation is needed to determine whether *Bpgm* plays a meaningful role in rod glucose metabolism.

Similar to glycolytic genes, at least one isoform of an enzyme at every step of the TCA cycle displayed an increasing trend over rod maturation, and many exhibited statistically significant increases (Figure 4.1 B). This was expected. Rods are known for their high rate of mitochondrial oxidative phosphorylation in addition to a high rate of lactate production. Equally noteworthy were observations regarding the genes that decreased in expression. Succinyl-CoA ligase is a TCA cycle enzyme comprised of an invariable alpha subunit encoded by *Suclg1* and one of two isoforms of a beta subunit, *Suclg2* or *Sucla2*[171]. The former produces GTP in the reaction it catalyses, and its expression significantly decreased from P2 to P28, whereas the latter produces ATP, and its expression (along with the expression of the invariable subunit) significantly increased. Rods may therefore favour production of ATP rather than GTP at this step of the TCA cycle. Secondly, isocitrate dehydrogenase (Idh) is another TCA cycle enzyme. Idh2 (homodimer) is $NADP^+$-dependent and Idh3 (2 x Idh3a, Idh3b, Idh3g heterotetramer) is $NAD^+$-dependent (as mentioned above, Idh1 localises to the cytoplasm and is therefore not a TCA cycle enzyme). Expression of *Idh2* significantly decreased in rods from P2 to P28. This is interesting as it may suggest that rods have a particular reliance on Idh3 and $NAD^+$ at this step of the TCA cycle. This is not a novel suggestion, and these data agree well with previous

observations[120]. Mutations in *IDH3A* and *IDH3B* are associated with retinitis pigmentosa in human patients possibly due to this reliance on $NAD^+$-dependent Idh[119,120,172]. It is worth noting that *Idh2* mRNA is not entirely absent from rods – see the present data and ref[172].

Assessing the OXPHOS gene set, expression of most OXPHOS genes increased from P2 to P28, consistent with a general upregulation of OXPHOS as photoreceptors mature (Figure 4.1 D). A large subgroup of these genes reached their maximal expression level at P10 without clearly increasing further between P10 and P28. This is in contrast to the sets of glycolytic and TCA cycle genes, most of which did not peak in expression until P28. The group of OXPHOS genes peaking at P10 appeared to largely comprise subunits of the ETC complexes. This increase from P6 to P10 fits well with data regarding the postnatal development of photoreceptors in the mouse, in particular the morphogenesis of the mitochondria-dense ellipsoid region[161].

## *Developing Müller cells*

Chronologically, the following dataset was not analysed at this point in the project, but it is relevant to discuss here as it makes a useful comparison with the maturing photoreceptor data. In 2020, VandenBosch et al.[2] published bulk RNA-seq data from FACS-isolated Müller cells (from *Rlbp-creER:flox-stop-tdTomato* mice) or progenitors (from *Sox2-GFP* mice) at several points from P2 to adulthood. Counts were downloaded from GEO (accession number: GSE137318) and processed similarly to previous datasets (see methods for detail). Heatmaps were generated showing changes in gene expression over development from P2 retinal progenitors to adult Müller cells. No differential expression analysis was performed due to the absence of repeats of each age group[173]. Nevertheless, it was useful to qualitatively assess changes in expression over development. Heatmaps were generated showing changes from P2 to adult Müller cells (Figure 4.2). Tables alongside heatmaps show expression values for the P2 and adult samples, and the fold-change between these two groups.

Many glycolytic genes increased in expression from P2 progenitors to adult Müller cells, and those where an increase was not obvious, such as *Gpi1* and *Tpi1*, were not at key regulatory steps of the pathway and did not exhibit low read counts so would be unlikely to cause a glycolytic bottleneck despite not increasing in expression to the same extent as other genes (Figure 4.1 A). These results show that Müller cells likely increase their glycolytic capacity as they develop. However, unlike in the maturing rod cell data above, the expression of two enzymes canonically important for aerobic glycolysis, *Hk2* and *Ldha*, decreased over Müller cell development, although a moderate level of expression of both genes remained in adult cells. Isoforms of these genes not typically involved in aerobic glycolysis, *Hk1* and *Ldhb*, increased in expression. Another point of interest was the high

upregulation of *Aldoc* in Müller cells. This gene was also upregulated in rods but to a lesser extent. It encodes an isoform of the glycolytic enzyme aldolase, but isoform-specific functions that may be important in Müller cells are unknown. *Pkm* was entirely absent from the Müller cell dataset – this is discussed below.

In contrast to rod photoceptors, Müller cells downregulated the majority of TCA cycle and OXPHOS genes over development, albeit by small fold-changes in most cases (Figure 4.2 A and B). This is not entirely surprising. Müller cells are long, radially oriented cells, and much of their length resides in the central and inner retina where oxygen tension is low. They likely have less access to oxygen, and have lower ATP demand than photoreceptors, hence a lower level of OXPHOS is consistent with this.

**Figure 4.2 Metabolic gene expression in RNA-seq data from developing mouse Müller cells (data from VandenBosch et al. 2020). A-C.** VandenBosch et al.[2] performed RNA-seq on FACS-isolated Sox2-GFP retinal progenitor cells (P2 group) and *Rlbp-creER:flox-stop-tdTomato* developing mouse Müller cells (P8, P12, Adult groups). The table of trimmed counts was downloaded from Gene Expression Omnibus under accession number GSE137318. Counts were TMM-normalised and log2-transformed. **Left Panels:** Heatmaps were generated (from z-scores across each row) showing changes in expression of each gene over development. **Right Panels:** Tables were generated showing normalised log2 counts per million for P2 and P28 groups, as well as the fold-change between these two groups. Lists of genes under each heading were obtained from the Gene Set Enrichment Analysis (GSEA) Molecular Signatures Database (MSigDB).

## A Glycolysis and Gluconeogenesis

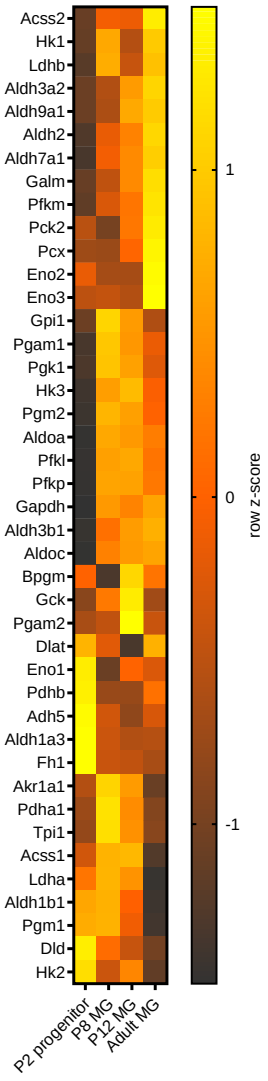


| | P2 log2 cpm | Adult log2 cpm | Fold change |
|---|---|---|---|
| Acss2 | 5.4 | 5.9 | 1.4 |
| Hk1 | 6.5 | 7.3 | 1.7 |
| Ldhb | 7.1 | 7.6 | 1.4 |
| Aldh3a2 | 5.6 | 8.1 | 5.7 |
| Aldh9a1 | 5.7 | 6.8 | 2.1 |
| Aldh2 | 4.5 | 7.9 | 11 |
| Aldh7a1 | 5.8 | 7.3 | 2.7 |
| Galm | 2.1 | 6.1 | 16 |
| Pfkm | 6.2 | 7.7 | 3.0 |
| Pck2 | 4.5 | 5.6 | 2.2 |
| Pcx | 5.6 | 7.0 | 2.6 |
| Eno2 | 5.3 | 6.3 | 1.9 |
| Eno3 | 4.2 | 4.5 | 1.2 |
| Gpi1 | 7.9 | 8.1 | 1.2 |
| Pgam1 | 6.7 | 8.0 | 2.5 |
| Pgk1 | 8.5 | 9.1 | 1.6 |
| Hk3 | -1.6 | 0.9 | 5.5 |
| Pgm2 | 6.0 | 6.8 | 1.7 |
| Aldoa | 8.4 | 9.4 | 2.1 |
| Pfkl | 7.6 | 8.6 | 2.0 |
| Pfkp | 6.6 | 8.7 | 4.3 |
| Gapdh | 7.4 | 9.8 | 5.3 |
| Aldh3b1 | -1.6 | 3.9 | 47.0 |
| Aldoc | 2.1 | 10.4 | 320 |
| Bpgm | 5.9 | 5.9 | 1.0 |
| Gck | 3.2 | 3.2 | 1.0 |
| Pgam2 | 0.0 | 0.1 | 1.0 |
| Dlat | 5.7 | 5.7 | -1.0 |
| Eno1 | 9.8 | 8.8 | -2.0 |
| Pdhb | 6.6 | 6.5 | -1.1 |
| Adh5 | 7.1 | 6.7 | -1.3 |
| Aldh1a3 | 5.7 | 0.3 | -43 |
| Fh1 | 6.1 | 5.0 | -2.1 |
| Akr1a1 | 8.0 | 7.8 | -1.1 |
| Pdha1 | 6.1 | 6.1 | -1.0 |
| Tpi1 | 8.7 | 8.6 | -1.0 |
| Acss1 | 1.9 | 1.0 | -1.8 |
| Ldha | 9.6 | 8.3 | -2.4 |
| Aldh1b1 | 0.2 | -1.7 | -3.6 |
| Pgm1 | 4.8 | 4.3 | -1.5 |
| Dld | 7.0 | 6.2 | -1.7 |
| Hk2 | 5.7 | 4.7 | -1.9 |

## B TCA Cycle

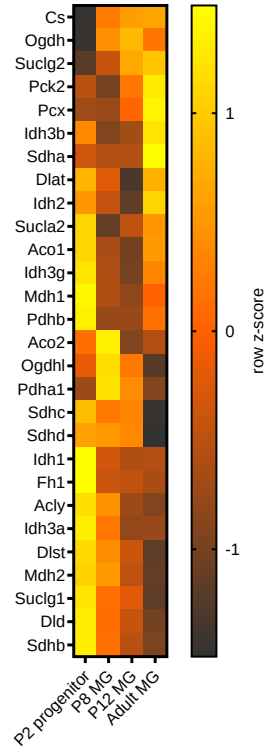


| | P2 log2 cpm | Adult log2 cpm | Fold change |
|---|---|---|---|
| Cs | 8.0 | 8.4 | 1.3 |
| Ogdh | 7.3 | 7.4 | 1.1 |
| Suclg2 | 5.1 | 5.7 | 1.5 |
| Pck2 | 4.5 | 5.6 | 2.2 |
| Pcx | 5.6 | 7.0 | 2.6 |
| Idh3b | 7.1 | 7.2 | 1.1 |
| Sdha | 7.7 | 8.2 | 1.4 |
| Dlat | 5.7 | 5.7 | -1.0 |
| Idh2 | 6.8 | 6.9 | 1.1 |
| Sucla2 | 6.1 | 6.0 | -1.1 |
| Aco1 | 7.0 | 6.9 | -1.0 |
| Idh3g | 6.7 | 6.5 | -1.1 |
| Mdh1 | 7.9 | 7.5 | -1.3 |
| Pdhb | 6.6 | 6.5 | -1.1 |
| Aco2 | 7.7 | 7.6 | -1.1 |
| Ogdhl | 4.8 | 4.2 | -1.6 |
| Pdha1 | 6.1 | 6.1 | -1.0 |
| Sdhc | 6.3 | 6.0 | -1.3 |
| Sdhd | 6.2 | 5.6 | -1.6 |
| Idh1 | 7.2 | 6.4 | -1.7 |
| Fh1 | 6.1 | 5.0 | -2.1 |
| Acly | 8.6 | 7.6 | -2.0 |
| Idh3a | 6.1 | 5.2 | -2.0 |
| Dlst | 7.3 | 6.5 | -1.8 |
| Mdh2 | 7.7 | 6.6 | -2.0 |
| Suclg1 | 6.1 | 5.3 | -1.7 |
| Dld | 7.0 | 6.2 | -1.7 |
| Sdhb | 6.7 | 5.8 | -1.8 |

## C OXPHOS

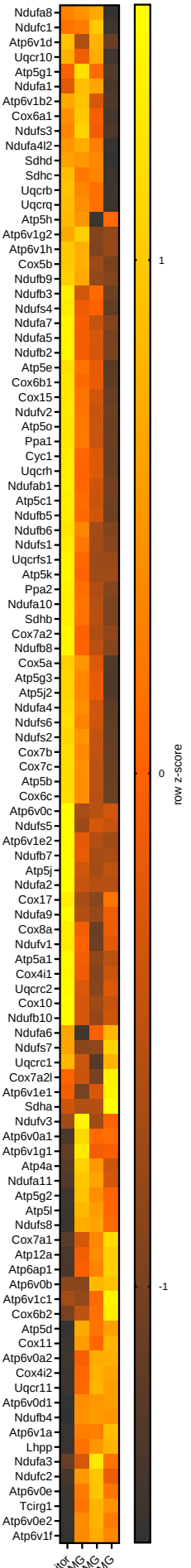


| | P2 log2 cpm | Adult log2 cpm | Fold change |
|---|---|---|---|
| Ndufa8 | 5.0 | 4.9 | -1.1 |
| Ndufc1 | 4.6 | 4.3 | -1.2 |
| Atp6v1d | 5.6 | 5.5 | -1.1 |
| Uqcr10 | 5.0 | 4.6 | -1.4 |
| Atp5g1 | 5.1 | 4.7 | -1.3 |
| Ndufa1 | 4.4 | 4.0 | -1.3 |
| Atp6v1b2 | 7.6 | 7.3 | -1.2 |
| Cox6a1 | 6.2 | 5.8 | -1.3 |
| Ndufs3 | 5.8 | 5.5 | -1.2 |
| Ndufa4l2 | 6.9 | 2.4 | -22 |
| Sdhd | 6.2 | 5.6 | -1.6 |
| Sdhc | 6.3 | 6.0 | -1.3 |
| Uqcrb | 5.3 | 4.7 | -1.5 |
| Uqcrq | 5.5 | 4.9 | -1.5 |
| Atp5h | 6.3 | 6.2 | -1.1 |
| Atp6v1g2 | 3.7 | 3.5 | -1.2 |
| Atp6v1h | 6.4 | 6.1 | -1.2 |
| Cox5b | 5.7 | 5.4 | -1.2 |
| Ndufb9 | 5.8 | 5.3 | -1.4 |
| Ndufb3 | 4.8 | 4.5 | -1.2 |
| Ndufs4 | 6.0 | 5.6 | -1.3 |
| Ndufa7 | 5.4 | 5.2 | -1.1 |
| Ndufa5 | 4.6 | 3.8 | -1.7 |
| Ndufb2 | 4.9 | 4.1 | -1.7 |
| Atp5e | 6.3 | 5.5 | -1.7 |
| Cox6b1 | 6.5 | 5.9 | -1.5 |
| Cox15 | 5.7 | 5.2 | -1.3 |
| Ndufv2 | 6.3 | 5.5 | -1.8 |
| Atp5o | 7.0 | 5.7 | -2.5 |
| Ppa1 | 6.0 | 4.0 | -4.1 |
| Cyc1 | 6.7 | 6.3 | -1.3 |
| Uqcrh | 6.6 | 5.6 | -2.0 |
| Ndufab1 | 5.3 | 3.8 | -2.8 |
| Atp5c1 | 7.5 | 6.7 | -1.8 |
| Ndufb5 | 5.8 | 5.1 | -1.6 |
| Ndufb6 | 4.8 | 3.8 | -2.0 |
| Ndufs1 | 6.6 | 6.1 | -1.4 |
| Uqcrfs1 | 6.6 | 6.2 | -1.4 |
| Atp5k | 5.2 | 4.2 | -1.9 |
| Ppa2 | 5.4 | 4.3 | -2.2 |
| Ndufa10 | 6.3 | 5.1 | -2.2 |
| Sdhb | 6.7 | 5.8 | -1.8 |
| Cox7a2 | 6.0 | 4.9 | -2.1 |
| Ndufb8 | 5.9 | 4.9 | -1.9 |
| Cox5a | 6.0 | 4.7 | -2.4 |
| Atp5g3 | 7.5 | 6.6 | -1.9 |
| Atp5j2 | 5.7 | 5.1 | -1.5 |
| Ndufa4 | 6.3 | 5.3 | -1.9 |
| Ndufs6 | 4.5 | 4.0 | -1.4 |
| Ndufs2 | 7.2 | 6.7 | -1.4 |
| Cox7b | 5.8 | 5.1 | -1.6 |
| Cox7c | 4.6 | 3.6 | -1.9 |
| Atp5b | 9.7 | 8.6 | -2.1 |
| Cox6c | 6.3 | 5.5 | -1.7 |
| Atp6v0c | 6.5 | 4.4 | -4.3 |
| Ndufs5 | 4.7 | 1.2 | -11 |
| Atp6v1e2 | 1.9 | -2.2 | -17 |
| Ndufb7 | 5.7 | 5.0 | -1.7 |
| Atp5j | 6.9 | 6.1 | -1.7 |
| Ndufa2 | 5.7 | 5.2 | -1.4 |
| Cox17 | 4.4 | 3.9 | -1.4 |
| Ndufa9 | 6.0 | 5.9 | -1.1 |
| Cox8a | 6.7 | 6.5 | -1.2 |
| Ndufv1 | 6.6 | 6.3 | -1.3 |
| Atp5a1 | 9.5 | 8.9 | -1.5 |
| Cox4i1 | 7.5 | 7.3 | -1.2 |
| Uqcrc2 | 7.7 | 7.2 | -1.4 |
| Cox10 | 4.1 | 3.6 | -1.4 |
| Ndufb10 | 6.0 | 5.2 | -1.7 |
| Ndufa6 | 4.9 | 4.9 | 1.0 |
| Ndufs7 | 5.4 | 5.5 | 1.1 |
| Uqcrc1 | 7.0 | 7.0 | -1.0 |
| Cox7a2l | 6.5 | 6.6 | 1.0 |
| Atp6v1e1 | 6.3 | 6.5 | 1.1 |
| Sdha | 7.7 | 8.2 | 1.4 |
| Ndufv3 | 5.9 | 5.9 | 1.1 |
| Atp6v0a1 | 7.1 | 7.4 | 1.2 |
| Atp6v1g1 | 6.2 | 6.4 | 1.1 |
| Atp4a | -1.0 | -0.8 | 1.2 |
| Ndufa11 | 4.7 | 4.8 | 1.1 |
| Atp5g2 | 5.9 | 6.5 | 1.6 |
| Atp5l | 4.5 | 5.5 | 2.1 |
| Ndufs8 | 4.7 | 5.0 | 1.2 |
| Cox7a1 | -1.3 | 0.3 | 3.0 |
| Atp12a | -2.2 | -0.1 | 4.3 |
| Atp6ap1 | 7.2 | 8.2 | 2.0 |
| Atp6v0b | 6.4 | 6.6 | 1.1 |
| Atp6v1c1 | 5.7 | 6.1 | 1.3 |
| Cox6b2 | 0.9 | 4.2 | 10 |
| Atp5d | 6.2 | 6.5 | 1.2 |
| Cox11 | 2.5 | 4.0 | 2.9 |
| Atp6v0a2 | 6.2 | 7.6 | 2.7 |
| Cox4i2 | 5.5 | 7.6 | 4.3 |
| Uqcr11 | 4.8 | 5.4 | 1.5 |
| Atp6v0d1 | 6.8 | 7.2 | 1.3 |
| Ndufb4 | 3.8 | 4.5 | 1.7 |
| Atp6v1a | 7.1 | 7.4 | 1.2 |
| Lhpp | 1.6 | 6.5 | 31 |
| Ndufa3 | 4.5 | 4.6 | 1.1 |
| Ndufc2 | 5.7 | 5.8 | 1.0 |
| Atp6v0e | 4.5 | 5.3 | 1.7 |
| Tcirg1 | 3.7 | 5.8 | 4.3 |
| Atp6v0e2 | 7.1 | 7.8 | 1.6 |
| Atp6v1f | 5.2 | 5.6 | 1.3 |

## *Comparison of Müller cell and rod datasets*

To clearly determine the differing metabolic specialisations of Müller cells and rods, the maturing Müller cell dataset of VandenBosch et al.[2] was compared more directly with the maturing rod dataset of Kim et al.[1] The datasets were from entirely different studies, so no statistical comparison was made, but a qualitative comparison was useful for exploration and development of new hypotheses.

An obvious idea would be to directly compare expression levels of genes in adult rods with those in adult Müller cells, but such a comparison would be problematic given the data were from separate studies, each performed with different techniques. Instead, changes in gene expression from P2 to adulthood in each study could be calculated, and these differences could be compared between studies, providing a degree of internal control. This would be especially informative if the cells at the earliest timepoint in each study, P2, were transcriptomically similar, as then the changes would reflect divergence of each cell type from a similar starting population. In the study of Kim et al., rod precursor cells were the target population at P2, and they were isolated from *Nrl*p-GFP mice. In the study of VandenBosch et al., retinal progenitor cells were the target population at P2, and they were isolated from *Sox2*-GFP mice. Rod precursor cells (and Müller cells) derive from retinal progenitor cells, and P2 is at the peak of rod precursor genesis in mice[174], so a high degree of similarity is likely between *Sox2*-positive and *Nrl*-positive populations at P2.

To gauge the similarity of the P2 populations, the mean normalised expression of each gene in the Kim et al. dataset was plotted against its expression in the VandenBosch et al. dataset (Figure 4.3 A). Promisingly, the data were strongly correlated with high $R^2$ (0.84). The mean P28 rod data were then plotted against the adult Müller cell data, and as expected, the $R^2$ of the linear regression was much lower (0.36), reflecting transcriptomic divergence of the two cell types over maturation (Figure 4.3 B). Sets of marker genes for rods and Müller cells behaved largely as expected in these comparisons, changing from quite closely correlated at P2 to dispersed in the expected directions in the mature populations (Figure 4.3 C and D). Finally, plots were generated after filtering for a set of metabolic genes comprised of the glycolysis and gluconeogenesis, TCA cycle, and OXPHOS gene sets used above. These followed the same trends as the full transcriptomes, with a strong correlation at P2 (0.78), but only a weak correlation at P28 (0.36). Together, this justifies qualitatively comparing changes in gene expression over development between each study. In all of these analyses, normalisation was performed on each dataset individually.

Genes that diverged in expression over maturation between rods and Müller cells were of interest. To identify these, the fold-change from P2 to adulthood was calculated for each gene in each cell type, then the difference between the fold-changes was used to order the genes. Before assessing

metabolic genes, this approach was validated to discover functionally important genes by checking the overall top 10 divergent genes (Figure 4.4 A). They included several in which mutations are known to cause retinal disease (*Gnat1*[175], *Slc24a1*[176], *Guca1b*[177], *Pde6a*[178-180]), where experimental mutation or knockout causes retinal disease (*Aqp4*[181], *Cds1*[182,183]), or which are useful as specific retinal cell markers (*Mlc1*[184,185]). Interestingly, the gene that diverged in expression by the greatest magnitude between rods and Müller cells, *Abca8a*, which encodes an ATP-binding cassette transporter, has previously been identified as enriched in Müller cells[186], but, to my knowledge, remains unstudied in the retina.

Metabolic genes were then selected using the glycolysis/gluconeogenesis, TCA cycle and OXPHOS sets as above. The top 15 divergent metabolic genes that relatively increased in rods were identified, as well as the top 15 that relatively increased in Müller cells. *Hk2* and *Hk1* exhibited the greatest increase in expression in rods relative to Müller cells (Figure 4.4 B). They have been discussed above, and this further emphasises their importance in rods. Other glycolytic genes in this group included *Eno1*, *Aldoa* and *Gapdh*. These are not classically regarded as rate-determining enzymes of glycolysis[187], but their upregulation is generally consistent with the view that rods are able to sustain a high glycolytic rate. Interestingly, recent studies indicate that Gapdh may be rate-limiting in the context of aerobic glycolysis[188,189], so its potential importance in control of rod metabolism should not be overlooked. Also, anti-Eno1 antibodies may contribute to disease in patients with autoimmune and cancer-associated retinopathies[190-192]. While this may relate to its catalytic role in glycolysis, Eno1 also has several other functions to be considered[193]. Further study is needed to better characterise its roles in rods.

Regarding non-glycolytic genes, *Ndufs5* and *Nduf4a* were upregulated in rods (Figure 4.4 B) and encode subunits of the mitochondrial ETC complex I. These genes may play important roles in rod metabolism which have yet to be investigated. Two other genes of interest upregulated in rods were *Ppa1* and *Ppa2*, which encode inorganic pyrophosphatases. Pyrophosphate is generated in many biochemical reactions, notably in biosynthetic pathways, and its rapid hydrolysis, catalysed by pyrophosphatase, renders reactions that produce pyrophosphate effectively irreversible[194]. Pyrophosphatases are ubiquitous enzymes, but the relative upregulation of *Ppa1* and *Ppa2* in rods reflects the high metabolic rate and biosynthetic demand of these cells, and these genes may therefore be particularly important for retinal function. It has also been proposed that high pyrophosphatase activity may facilitate rapid cGMP metabolism during phototransduction[195]. Again, further research is needed to determine the importance of these proteins in rods, where they remain largely unstudied.

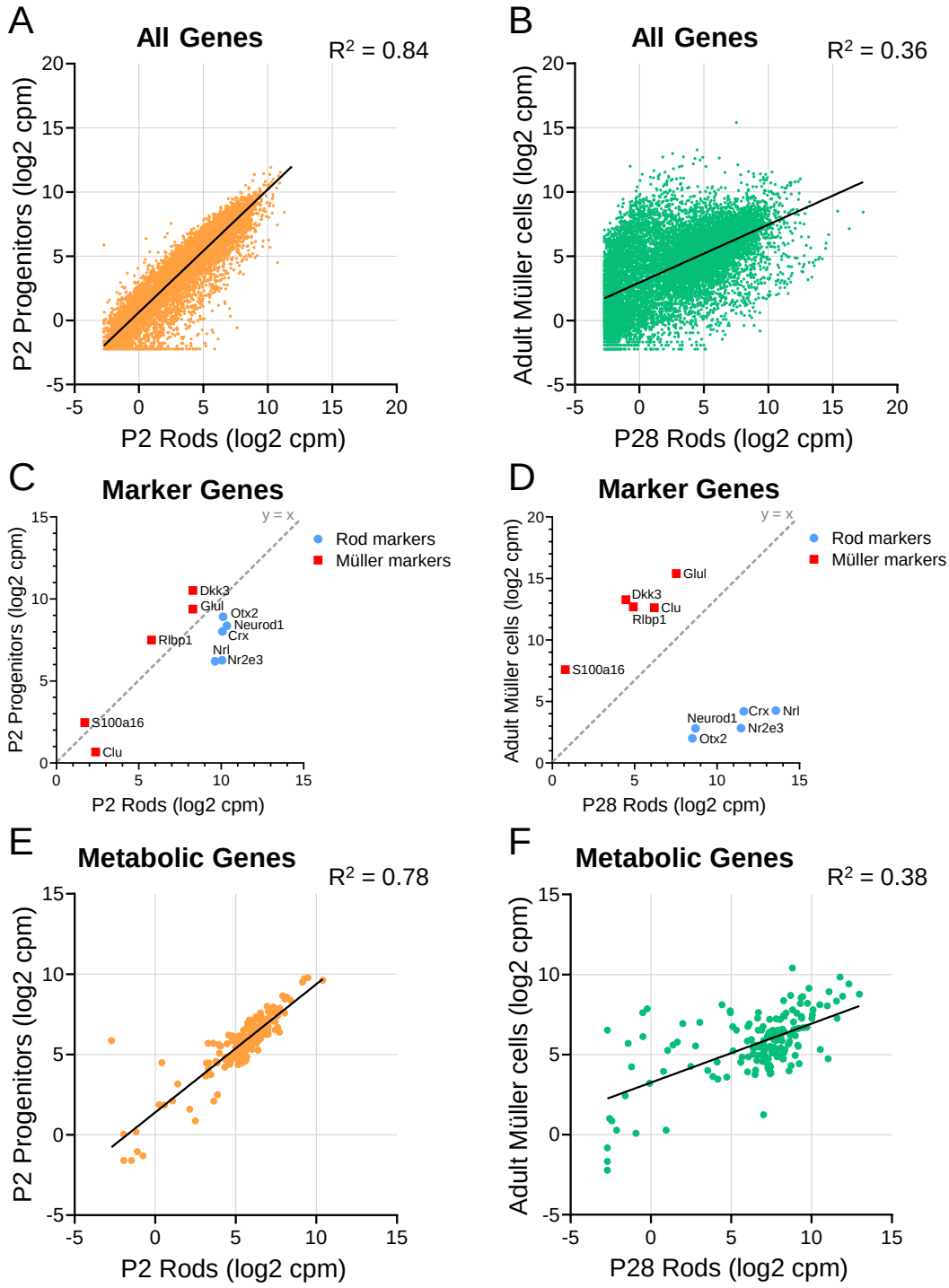


**Figure 4.3 Broad comparison of the developing photoreceptor RNA-seq data of Kim et al. 2016 and the developing Müller cell RNA-seq data of VandenBosch et al. 2020.** Normalised log2 counts per million were calculated separately for each dataset. **A.** The mean P2 values and **B.** the mean P28 values for all genes (that were present in both datasets) from the Kim et al.[1] dataset were plotted against their respective values in the VandenBosch et al.[2] dataset. A line was fitted using R, and the $R^2$ of the regression is indicated. **C, D.** Same as A and B, but showing only a selection of Müller cell and rod marker genes as indicated. Instead of a linear regression, the line y = x is displayed to indicate an ideal correlation. **E, F.** Same as A and B, but showing only a selection of metabolic genes comprised of lists of genes involved in glycolysis and gluconeogenesis, the tricarboxylic acid cycle and oxidative phosphorylation which were obtained from the Gene Set Enrichment Analysis (GSEA) Molecular Signatures Database (MSigDB).

A

**Top 10 overall divergent genes**

| | | Rod P2 $log_2$ cpm | Rod P28 $log_2$ cpm | Müller P2 $log_2$ cpm | Müller Adult $log_2$ cpm | Fold-change difference |
|---|---|---|---|---|---|---|
| 1 | Abca8a | -2.7 | 3.3 | -2.2 | 12.0 | -19000 |
| 2 | Gnat1 | 2.6 | 16.3 | 1.2 | 7.1 | 13000 |
| 3 | Slc24a1 | -0.3 | 13.2 | -1.8 | 4.5 | 11000 |
| 4 | Guca1b | -0.4 | 12.7 | -0.3 | 4.2 | 8800 |
| 5 | Kcnj14 | -1.1 | 11.1 | -2.2 | 3.1 | 4400 |
| 6 | Mlc1 | 0.7 | 1.9 | -1.6 | 10.5 | -4300 |
| 7 | Clu | 2.4 | 6.2 | 0.7 | 12.6 | -4000 |
| 8 | Aqp4 | -2.2 | 2.5 | -0.6 | 10.9 | -2800 |
| 9 | Pde6a | 2.6 | 14.0 | -1.0 | 4.9 | 2600 |
| 10 | Cds1 | 0.3 | 11.3 | 0.9 | 3.0 | 2100 |

B

**Top 10 divergent metabolic genes, up in rods**

| | | Rod P2 $log_2$ cpm | Rod P28 $log_2$ cpm | Müller P2 $log_2$ cpm | Müller Adult $log_2$ cpm | Fold-change difference |
|---|---|---|---|---|---|---|
| 1 | Hk2 | 3.6 | 11.0 | 5.7 | 4.7 | 180 |
| 2 | Hk1 | 5.5 | 11.6 | 6.5 | 7.3 | 68 |
| 3 | Atp6v0e2 | 5.9 | 10.1 | 7.1 | 7.8 | 17 |
| 4 | Ndufs5 | 5.1 | 7.0 | 4.7 | 1.2 | 15 |
| 5 | Ppa1 | 5.2 | 8.6 | 6.0 | 4.0 | 15 |
| 6 | Ndufa4 | 7.0 | 10.5 | 6.3 | 5.3 | 14 |
| 7 | Eno1 | 9.5 | 13.0 | 9.8 | 8.8 | 13 |
| 8 | Aldoa | 8.4 | 12.3 | 8.4 | 9.4 | 13 |
| 9 | Gapdh | 7.6 | 11.8 | 7.4 | 9.8 | 13 |
| 10 | Ppa2 | 5.8 | 8.7 | 5.4 | 4.3 | 9.5 |

C

**Top 10 divergent metabolic genes, up in Müller cells**

| | | Rod P2 $log_2$ cpm | Rod P28 $log_2$ cpm | Müller P2 $log_2$ cpm | Müller Adult $log_2$ cpm | Fold-change difference |
|---|---|---|---|---|---|---|
| 1 | Aldoc | 3.6 | 8.8 | 2.1 | 10.4 | -280 |
| 2 | Ndufa4l2 | 6.1 | -1.6 | 6.9 | 2.4 | -190 |
| 3 | Suclg2 | 4.0 | -1.4 | 5.1 | 5.7 | -44 |
| 4 | Aldh3b1 | -1.5 | 0.8 | -1.6 | 3.9 | -42 |
| 5 | Cox4i2 | 4.1 | -0.5 | 5.5 | 7.6 | -28 |
| 6 | Cox6b2 | 2.5 | -1.2 | 0.9 | 4.2 | -23 |
| 7 | Aldh2 | 3.3 | -0.2 | 4.5 | 7.9 | -22 |
| 8 | Lhpp | 2.1 | 5.3 | 1.6 | 6.5 | -21 |
| 9 | Galm | 1.1 | -0.5 | 2.1 | 6.1 | -19 |
| 10 | Idh2 | 5.9 | 2.0 | 6.8 | 6.9 | -16 |

D

**Hypoxia inducible factors**

| | Rod P2 $log_2$ cpm | Rod P28 $log_2$ cpm | Müller P2 $log_2$ cpm | Müller Adult $log_2$ cpm | Fold-change difference |
|---|---|---|---|---|---|
| Hif1a | 8.9 | 11.3 | 9.0 | 7.6 | 7.7 |
| Epas1 (HIF2a) | 3.7 | 7.5 | 3.8 | 9.4 | -35 |

**Figure 4.4 Comparison of metabolic gene expression in the developing photoreceptor RNA-seq data of Kim et al.[1] 2016 and the developing Müller cell RNA-seq data of VandenBosch et al.[2] 2020.** Normalised log2 counts per million were calculated separately for each dataset. The fold-change from P2 to Adult (P28 for the photoreceptor dataset) of each gene was calculated within each dataset. The difference between these fold-changes was then calculated for each gene. This difference was used to find genes which diverged greatly in expression over development of each cell type. **A.** Table of the overall top 10 genes ordered by decreasing absolute fold-change difference. Expression (normalised log2 counts per million [cpm]) at P2 and Adult (or P28) in each dataset is also displayed. **B, C.** Genes were filtered for those present in the list of metabolic genes defined above. Tables show B. the top 10 metabolic genes which relatively increased in expression in rods and C. the top 10 metabolic genes which relatively increased in expression in Müller cells. D. Table shows the expression and fold-change difference for the genes encoding HIF-1α (*Hif1a*) and HIF-2α (*Epas1*).

Another gene that did not appear in this list, but which was likely relatively upregulated in rods, was *Pkm.* It was entirely absent from the Müller cell dataset (searched using 27 variations of the gene name). Initially, this was thought to most likely be due to low or zero expression. However, *Pkm* exhibited the 28$^{th}$ highest counts of all genes at P2 in the rod dataset, so it would be surprising if it was not present at all at P2 in the Müller cell precursors (retinal progenitor cells) given the general similarity of these populations (Figure 4.3 A). Furthermore, there was rod contamination of the Müller cell population in the VandenBosch data, reflected in the non-zero presence of rod marker genes in Figure 4.3 D. Some *Pkm* reads, at least from contaminating rods, would therefore be expected. To investigate further, *Pkm* expression was checked in other mouse RNA-seq datasets including a P2 retinal progenitor cell dataset[196] (accession number: GSE99818), a P1 and P4 developing Müller cell dataset[197] (accession number: GSE86199), and a dataset containing retinal progenitors and acutely isolated adult (2-month-old and 1.5-year-old) Müller cells[198] (accession number: GSE124532). In all of these groups, *Pkm* ranked in the top 200 features in counts (not shown). While this confirms the anomalous nature of its total absence from the VandenBosch dataset, it does not necessarily mean that *Pkm* is expressed in Müller cells. It is expressed so highly in rods (see Figure 4.1 A) that, in each Müller cell dataset, the number of *Pkm* reads relative to reads of rod marker genes was similar to that observed in rods themselves (determined using the dataset of Kim et al.[1]) so it is plausible that all the *Pkm* reads were actually derived from non-Müller cell types such as rods in these studies. Even if *Pkm* is expressed at the RNA level in Müller cells, reportedly, no isoform of pyruvate kinase is appreciably expressed at the protein level *in vivo*[54].

The relevance of contamination of the intended population by other cell types extends beyond *Pkm*. However, by comparing differences in the change of expression of genes over development between rod-enriched (Kim et al. data) and Müller-enriched (VandenBosch et al. data) groups, this should reveal important differences between the cell types, even if the imperfect separation of cell types confounds the direction or magnitude of changes for some genes.

The gene that increased by the greatest amount in Müller cells relative to rods was *Aldoc* (Figure 4.4 C). As stated above, it encodes an isoform of aldolase, which catalyses a reversible non-rate-limiting step of glycolysis, and its role in Müller cells has not been investigated. No other genes in the main glycolysis pathway made this list, which, when contrasted to the rod list, further supports the idea of a higher rate of glycolysis in rods than Müller cells.

The differences in expression of mitochondrial ETC complex subunits was interesting. Expression of *Nduf4al2* decreased in both Müller cells and rods, but a greater level of expression was retained in adult Müller cells. Nduf4al2 is induced by hypoxia-inducible factor 1 (HIF-1) and acts to decrease the

activity of the ETC complex I under low oxygen conditions[199]. Furthermore, expression of *Cox4i2* increased in Müller cells over development whereas expression in rods decreased to almost zero. Cox4i2 is a subunit of the ETC complex IV which optimises respiratory activity under hypoxic conditions, leading to greater $O_2$ consumption in hypoxia than if the alternative Cox4i1 is expressed, and likely decreased production of reactive oxygen species[200]. *Cox4i2* is induced by HIF-1 and HIF-2[200]. While HIF-1α and HIF-2α are mainly regulated at the protein level, it was confirmed that both were expressed at the RNA level in both Müller cells and rods. It is noteworthy that *Epas1* (*Hif2a*) RNA increased in Müller cells relative to rods over development whereas *Hif1a* exhibited the opposite trend. These data support a more detailed characterisation of the specific roles of the HIFs in Müller cell metabolism. They may be involved in less overt ways than, for example, the canonical widespread upregulation of glycolytic genes.

*Lhpp* encodes a histidine phosphatase that was upregulated in Müller cells over development relative to rods. Lhpp expression can downregulate PI3K/Akt/mTOR signalling[201-203] and can impede glycolysis by inducing ubiquitination and degradation of PKM2[204]. This aligns with the proposed low pyruvate kinase expression in Müller cells, and it may call into question the importance of PI3K/Akt signalling for Müller cell metabolism *in vivo*. Whether Lhpp actually carries out these functions in Müller cells, however, has not been studied, and it should be noted that read counts also increased in rods, just to a lesser degree, so this proposal is not black and white, but warrants investigation.

Müller cells relatively increased expression of *Suclg2*, the GTP-producing isoform of succinyl-CoA synthetase. This largely reflected its decreased expression in rods but indicates that Müller cells likely produce more GTP at this step of the TCA cycle than rods. Interestingly, although it was not present in this top 10 table, Müller cells also relatively increased expression of *Pck2*. This encodes a mitochondrial isoform of phosphoenolpyruvate carboxykinase, which uses GTP to produce phosphoenolpyruvate from oxaloacetate (the cytosolic isoform, *Pck1*, which is involved in gluconeogenesis, was not expressed in either cell type). A network involving these genes in pancreatic beta cells detects glucose availability to control insulin secretion[205-207]. It is possible that Müller cells repurpose a similar network to sense glucose availability and respond in some manner, perhaps to regulate their own metabolism or the metabolism of surrounding cells.

## *Validation with an independent dataset*

To provide further validation for the hypotheses discussed above, and to ensure they were not based on anomalies in either dataset, expression of multiple relevant genes was assessed in another RNA-seq dataset. As a small part of a large study in 2020, Hoang et al. performed RNA-seq on FACS-isolated

mouse Müller cells after induction of retinal damage[136]. GFP-positive cells were isolated from retinas of GLASTCreERT2;Sun1-sGFP mice (after tamoxifen treatment). In these mice, inducible Cre was controlled by the *Glast* (*Slc1a3*) promoter (a Müller-specific gene in the retina), which upon expression removed a floxxed transcriptional blocker from Sun1-GFP[136,208]. The dataset included groups of control undamaged P60 GFP-positive Müller cells, well as the complementary GFP-negative populations. The table of fragments per kilobase per million mapped reads (FPKM) values was downloaded, filtered for only these control groups, and heatmaps and tables were generated showing expression of relevant genes (Figure 4.5). No differential expression analysis was performed as raw count values were not available. Given the high proportion of rods in the mouse retina, the GFP-negative populations were likely dominated by rods. This is demonstrated by the relatively high expression of Müller cell marker genes in the GFP-positive groups, and high expression of rod marker genes in the GFP-negative groups (Figure 4.5 A). Note, though, that there was a moderate degree of rod contamination of GFP-positive groups 1 and 2 based on the expression of rod markers in these groups. Although not perfect, as at least at least a quarter of GFP-negative cells would have been retinal cell types other than rods, a comparison of GFP-positive and GFP-negative groups is similar to a comparison of Müller cells and rods, and it provided independent validation for the comparison of datasets above.

Expression of the two sets of divergent genes defined above was assessed. Due to the rod contamination of GFP-positive groups 1 and 2, it is useful to mainly consider GFP-positive groups 3 and 4 in Figure 4.5 B. In this case, it is clear that most genes in this set followed the same trend of relatively high expression in rod-enriched compared to Müller-enriched groups. Genes that did not follow the same trend included *Eno1*, *Gapdh*, and *Ppa2*. The latter two were similarly expressed in both groups, but confusingly, *Eno1* strongly displayed the opposite trend to above in this dataset. Eno1 is one of the most commonly identified differentially expressed proteins and mRNAs across unrelated proteomics and microarray experiments[209]. It is unclear if this is an artifactual nuisance or a genuine reflection of a biological role, perhaps as a cell stress sensor[209]. Despite this possible nuisance behaviour, it would still be useful to investigate its role in the retina given the presence of autoantibodies in retinopathies as discussed above[190-192]. Overall, the trends observed for most genes in this set were consistent with the conclusions above.

A

**Rod and Müller cell marker genes**

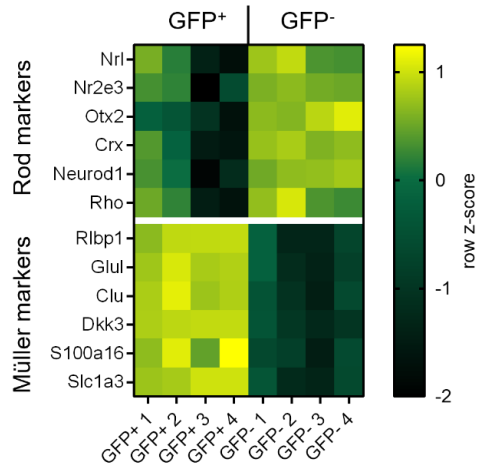


| | Mean GFP+ FPKM | Mean GFP- FPKM |
|---|---|---|
| Nrl | 43.0 | 155.5 |
| Nr2e3 | 28.5 | 118.9 |
| Otx2 | 15.7 | 124.0 |
| Crx | 27.7 | 157.2 |
| Neurod1 | 16.2 | 107.2 |
| Rho | 608.4 | 2278.7 |
| Rlbp1 | 1614.1 | 124.4 |
| Glul | 8404.0 | 733.0 |
| Clu | 876.1 | 92.5 |
| Dkk3 | 2029.3 | 203.4 |
| S100a16 | 56.4 | 3.9 |
| Slc1a3 | 751.7 | 49.2 |

B

**Top 10 divergent metabolic genes, up in rods**

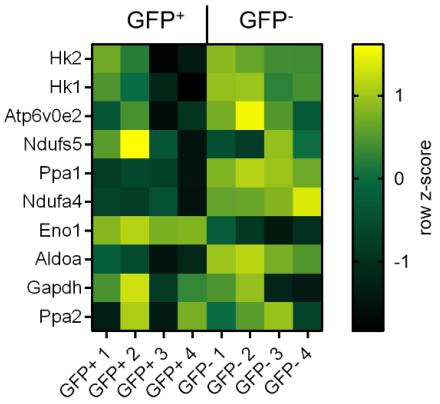


| | Mean GFP+ FPKM | Mean GFP- FPKM |
|---|---|---|
| Hk2 | 14.0 | 32.5 |
| Hk1 | 59.8 | 162.7 |
| Atp6v0e2 | 56.5 | 88.7 |
| Ndufs5 | 8.0 | 6.7 |
| Ppa1 | 21.0 | 38.4 |
| Ndufa4 | 18.3 | 74.5 |
| Eno1 | 488.1 | 110.3 |
| Aldoa | 199.5 | 462.8 |
| Gapdh | 545.0 | 501.1 |
| Ppa2 | 20.2 | 22.1 |

C

**Top 10 divergent metabolic genes, up in Müller cells**

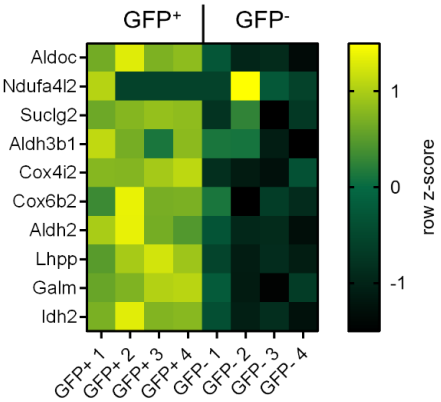


| | Mean GFP+ FPKM | Mean GFP- FPKM |
|---|---|---|
| Aldoc | 205.5 | 68.5 |
| Ndufa4l2 | 0.1 | 0.4 |
| Suclg2 | 14.8 | 3.2 |
| Aldh3b1 | 1.7 | 0.5 |
| Cox4i2 | 48.2 | 4.3 |
| Cox6b2 | 44.4 | 8.4 |
| Aldh2 | 110.6 | 15.7 |
| Lhpp | 28.2 | 5.8 |
| Galm | 19.7 | 2.3 |
| Idh2 | 49.5 | 12.6 |

**Figure 4.5 Analysis of metabolic gene expression in the Müller cell RNA-seq data of Hoang et al. 2020.** Hoang et al. performed RNA-seq on mouse Müller cells FACS-isolated from GLASTCreERT2;Sun1-sGFP mice after tamoxifen treatment. The table containing FPKM values was downloaded from Gene Expression Omnibus under accession number GSE135406 and filtered for only the control postnatal day 60 GFP-positive ($GFP^+$) and GFP-negative (GFP-) groups. Heatmaps (using z-scores by row) and tables of mean FPKM were generated showing **A.** rod and Müller cell marker genes, **B.** the list of top 10 genes which relatively increased in expression in rods in Figure 4.4, and **C.** the list of top 10 genes which relatively increased in expression in Müller cells in Figure 4.4.

The consistency with the previous comparison was better for the set of genes that were relatively upregulated in Müller cells (Figure 4.5 C). In this case, the only gene in the set that did not display the same trend as above was *Ndufa4l2*, which was not appreciably expressed in either the GFP-positive or GFP-negative population. However, given that *Cox4i2* was highly expressed in Müller cells in both datasets, it would still be of interest to investigate the potential regulation of ETC activity by HIFs. Overall, this dataset displays similar differences in gene expression between rods (or a rod-dominated population) and Müller cells to the previous analysis of datasets of Kim et al. and VandenBosch et al., and thus further validates the conclusions from this analysis.

## *Rationale for changing experimental model*

Müller cells provided an excellent starting point for metabolic experiments, where inhibitors could be tested, and assays optimised. However, as discussed above, there was an expanding body of evidence in favour of photoreceptors being responsible for most lactate production *in vivo*[14,50,54,117,210,211]. There also appeared to be significant differences between Müller cells in culture and *in vivo*. One main such difference, as discussed, was the expression of pyruvate kinase, which is present at the protein level in culture[114] but absent or low *in vivo*[54]. Moreover, a 2003 study analysed changes in the abundance of proteins as Müller cells adapted to culture conditions and found that expression levels of several metabolic genes including aldolase C and aldehyde dehydrogenase 2 were rapidly downregulated in culture[212]. These two genes, in particular, were identified above as diverging greatly over development between Müller cells and photoreceptors, and therefore likely play major roles in defining the metabolic identity of Müller cells *in vivo*. The fact that Müller cells upregulated the expression of many glycolytic genes over development suggests an increase in glycolytic capacity; however, it is actually unclear if they are able to undertake complete glycolysis and produce lactate *in vivo*. In the reported absence of any pyruvate kinase, the fate of glucose once reaching phosphoenolpyruvate is unclear. Explanations for this and the metabolic features and interdependencies of different retinal cell types have been proposed, and a complete discussion of retinal metabolic pathways and cell-cell interactions is presented in the final discussion section. Cultured Müller cells, while undoubtedly useful for studying certain facets of Müller cell biology, do not adequately replicate their glucose metabolism *in vivo*. These were the major reasons for transitioning to metabolic experiments on rat retinal explants in the following section of this thesis.

# 5. Results: Rat retinal explants

## *Rat retinal explants as an experimental model*

Rat retinal explants were chosen as an alternative experimental model to the Müller cells used in the preceding section of this thesis for several reasons. Firstly, and importantly, the explants contain photoreceptors, which cannot be cultured alone in a sufficiently physiologically normal state for metabolic experiments. Secondly, they maintain intracellular interactions which are important for retinal glucose metabolism[53,125,211]. Thirdly, there was a large body of past research demonstrating their utility in metabolic studies[5,6,10,50,54,213-216]. And, finally, a source of fresh scavenged rat explants was readily available, permitting screening of inhibitors of many candidate drivers of aerobic glycolysis – although explants are not amenable to a truly high-throughput screening approach. Downsides to the use of explants included a limited experimental timeframe over which the explants could be kept alive *ex vivo*, as well as a more restricted set of experimental techniques than if working with cell lines. For example, while treatments with inhibitors remained possible, a targeted gene knockout or knockdown, if needed, for instance if no inhibitor was available, would have required generation of a mouse strain or the use of adenoviral transductions with limited penetrance.

## *Optimising explant culture conditions*

Before assessing potential drivers of aerobic glycolysis, initial experiments aimed to optimise explant culture conditions. Explants were cultured in minimal essential medium (MEM, Gibco 11090) containing 5.56 mM glucose and supplemented with 0.8 mM L-glutamine, 100 U/mL penicillin and 100 µg/mL streptomycin. This medium was selected in order to closely match blood concentrations of glucose, glutamine and other nutrients.

A potential drawback of the experiments in Results part 1 was that the immortalised rMC-1 cell line was necessarily cultured in medium containing FBS in order to maintain cell growth and survival. Explants do not have the same requirements for growth and long-term culture, and inclusion of FBS may aberrantly activate signalling pathways and alter metabolism. The effect on lactate production by including FBS in the medium was therefore tested. Explants were cultured in medium with or without 10% FBS, and secreted lactate was measured over time (Figure 5.1 A). Inclusion of serum did not alter lactate production, demonstrating that exogenous growth factors were unnecessary for the maintenance of aerobic glycolysis over sixteen hours. Therefore, no serum was included in explant medium in subsequent experiments.

The rate of lactate production decreased over time in both groups, which was not entirely surprising, and was probably due to decreasing substrate availability, accumulation of metabolic waste products,

and/or cell death. The latter possibility was a concern as it would greatly limit the useful timeframe for experiments. To determine what was the major cause of this decrease in the rate of lactate production, an experiment was performed where culture medium was changed every eight hours in order to remove waste and refresh nutrient availability (Figure 5.1 B). This changing of medium dramatically reduced the time-dependent decrease in lactate production, with approximately linear lactate production being observed over sixteen hours and confirmed that the original decrease was not due to rapid, widespread cell death. Subsequent experiments were not extended beyond sixteen hours to ensure explants were not in a stressed metabolic state.

Experiments were then designed to target specific pathways that are likely drivers of the Warburg effect using the battery of inhibitors originally used for the treatment of cultured Müller cells described in Chapter 3. A series of events must occur after treating with an inhibitor before an effect on lactate production can be observed. This includes entry of the inhibitor into cells (photoreceptors are directly exposed to the medium, meaning this likely occurs more readily for these cells than those in internal layers), inhibition of the target protein, then target-specific effects which may include post-translational modification of proteins, turnover of proteins, or potentially transcription and translation of new proteins. As such, the time between first treatment and a detectable change in lactate production is unknown and variable depending on the mechanisms involved. The experiments on rMC-1 cells showed significant effects within an eight-hour total timeframe. Given retinal explants are a thicker, complex tissue, a timeline was chosen of initial treatment for 5 h followed by a change of medium and further treatment for 11 h, then collection of media for lactate assays. This increased the chance of detecting delayed effects on lactate production – although it cannot be ruled out that effects were missed which may have needed longer to manifest.

Firstly, glucose consumption and lactate production by vehicle-treated retinas were measured over the 11 h accumulation period (Figure 5.1 C). If it is assumed that all lactate is derived from glucose in the medium, approximately 92% of glucose consumed was converted to lactate over this period, which is similar to previous studies on rat retinal explants[6]. Direct inhibition of lactate dehydrogenase with oxamate almost completely abolished lactate production, as expected, and showed that an inhibitor could penetrate the tissue and exert its effect in the chosen experimental timeframe (Figure 5.1 D).

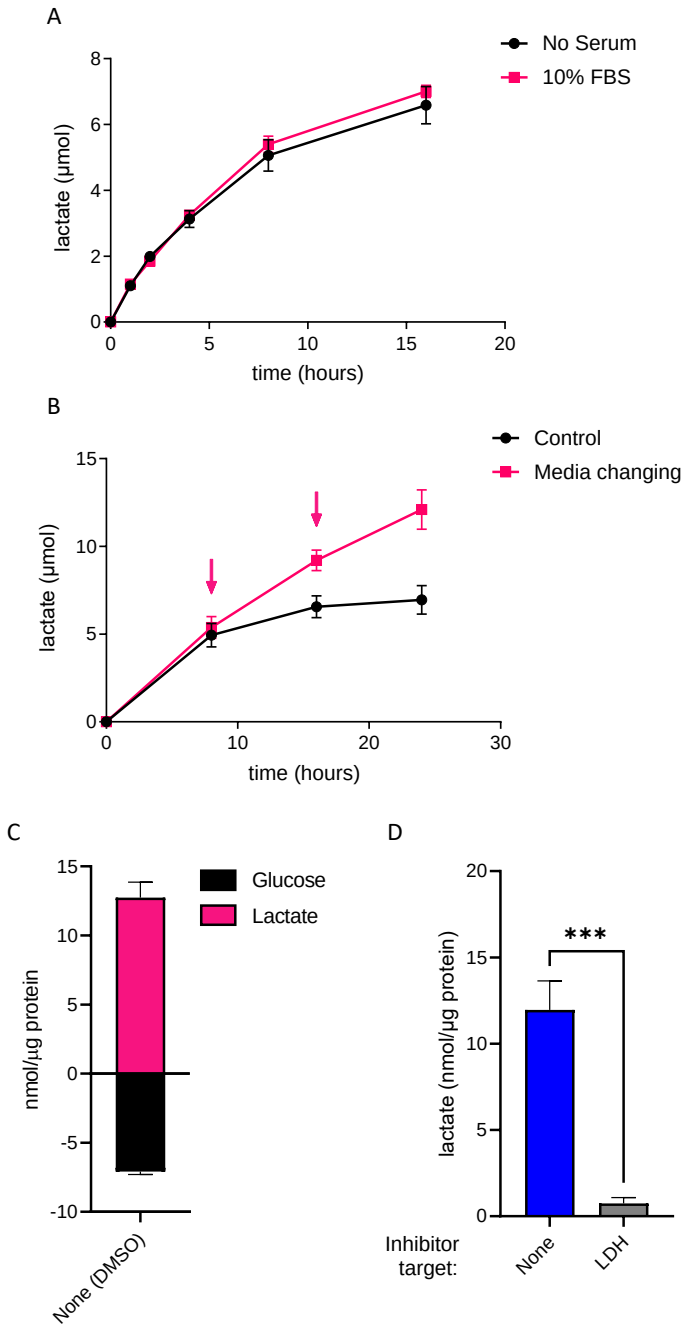


**Figure 5.1 Optimisation and validation of rat retinal explant culture conditions. A.** Rat retinal explants were isolated, and each placed in 1 mL of MEM containing 5.56 mM D-glucose and 0.8 mM L-glutamine, plus or minus supplementation with 10% foetal bovine serum (FBS), then explants were cultured in a humidified, 37 °C incubator in an atmosphere of 5% $CO_2$ in air. Samples of media were taken for analysis at each time point indicated and a colourimetric assay was used to quantify L-lactate. **B.** Retinal explants were cultured as in A, without FBS, and medium was replaced with fresh medium every 8 h (arrows) or left for the full duration without replacement. Samples were taken for measurement of lactate at timepoints indicated. **C.** Rat retinal explants were cultured for 5 h (without FBS) in medium containing DMSO (1:1000), medium was replaced, and retinas cultured for a further 11 h (with DMSO). L-lactate and D-glucose were then measured in media using colourimetric assays. **D.** Explants were cultured and treated as C with the lactate dehydrogenase (LDH) inhibitor oxamate (100 mM), or left untreated. Lactate was measured in media at the end of the experiment. All graphs show mean ± SD from three independent experiments with at least two retinas per group per experiment. Data were normalised to total protein extracted from retinal explants at the end of experiments. Statistical analysis in D was by unpaired Student's t-test. *** indicates $p < 0.001$.

## *Common signalling pathways do not drive aerobic glycolysis in the rat retina*

Small-molecule inhibitors were used to investigate the roles of several pathways in driving lactate production in explants. Initially, as was the approach for the experiments on rMC-1 cells, candidate drivers were selected based on their known roles in driving aerobic glycolysis in cancer cells, as well as their effects on cultured Müller cells. Firstly, explants were treated with inhibitors of PI3K, each at two different concentrations – a standard concentration based on assessment of previous literature, and which was effective in rMC-1 cells, as well as a 2-fold higher concentration (Figure 5.2 A). No significant change in lactate production was observed, although there was a trend of decreased lactate production with increased inhibitor concentration. This was not consistent with the results obtained in rMC-1 cells, where both PI3K inhibitors decreased lactate production by approximately 50% (Figure 3.2 B), confirming the rMC-1 cells were not an ideal model of whole retinal metabolism, although an effect specifically on Müller cells in the explants may have been overshadowed by other cell types. Explants were then treated with inhibitors of Akt or Rac1 which, as expected given the lack of effect of PI3K inhibition, also caused no change in lactate production (Figure 5.2 B). The explants were treated with a MEK inhibitor. In rMC-1 cells, inhibition of MEK1 caused a small decrease in lactate production (Figure 3.2 A), but no such effect was observed in retinal explants (Figure 5.2 B).

mTORC1 is a master integrator of nutrient sensing and metabolism and can be activated by various stimuli. It can promote aerobic glycolysis by mechanisms such as increasing HIF-1 activity[217,218]. However, its inhibition in explants with two different inhibitors caused no change in lactate production (Figure 5.2 C).

Wingless/Int (Wnt) signalling is another pathway that can drive aerobic glycolysis in cancer cells[219,220]. In the retina, Wnt-driven aerobic glycolysis has been proposed to contribute to age-related exudative macular degeneration[221], although mechanistic detail for this hypothesis is unclear. Aerobic glycolysis is a normal phenomenon in the retina, and it has not been shown that altered Wnt signalling affects aerobic glycolysis in the retina. To assess whether Wnt signalling drives basal aerobic glycolysis in the retina, explants were treated with an inhibitor of tankyrase which is known to increase degradation of beta-catenin and inhibit Wnt pathway activity[222] (Figure 5.2 D). However, the tankyrase inhibitor had no effect on lactate production in the explants, consistent with Wnt signalling not being a major driver of basal aerobic glycolysis.

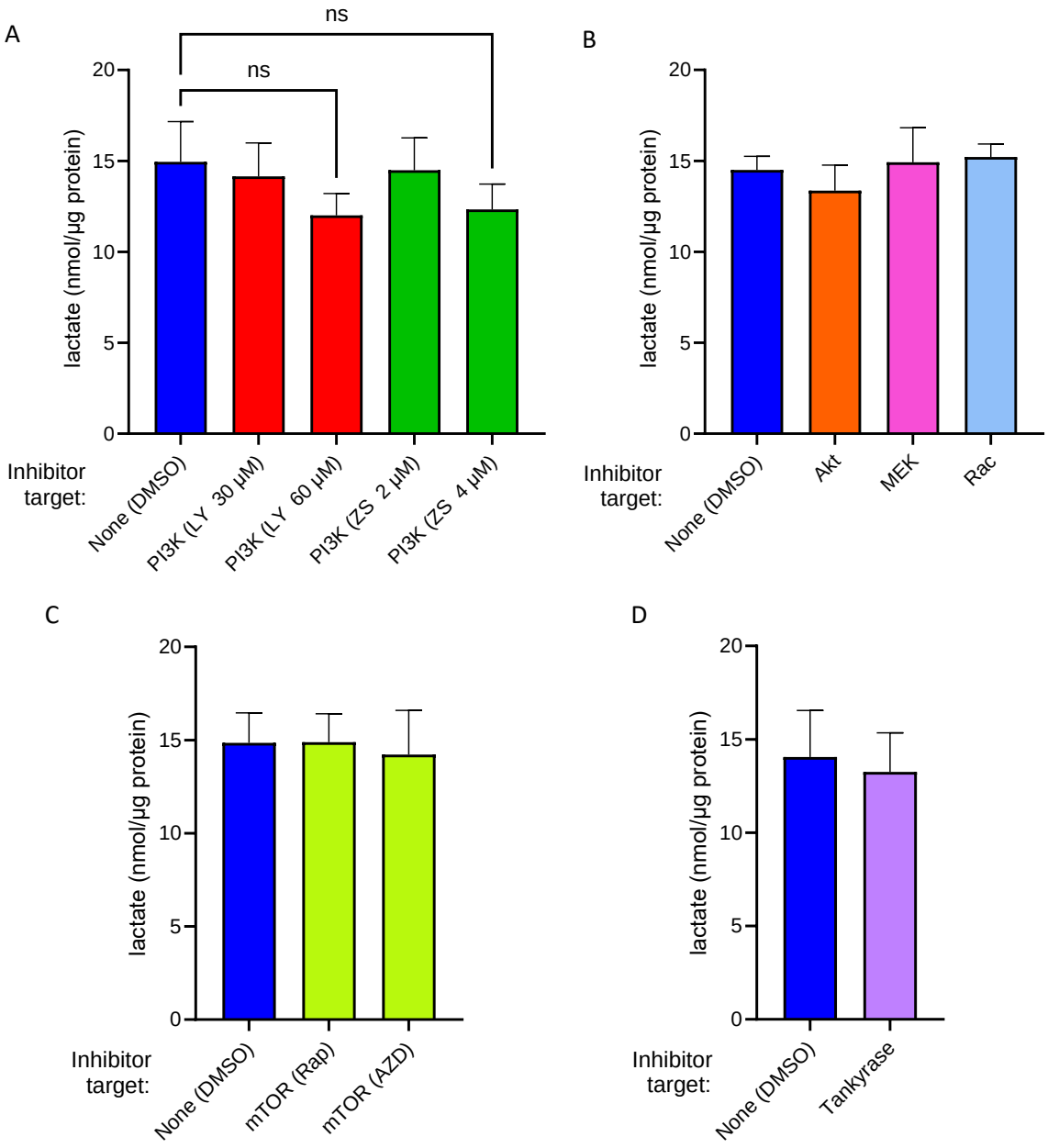


**Figure 5.2 Effect of signalling pathway inhibitors on lactate production in rat retinal explants.** Rat retinal explants were isolated and cultured in MEM containing 5.56 mM D-glucose, 0.8 mM L-glutamine, and inhibitor of the indicated protein (or DMSO as vehicle) in a humidified 37 °C incubator in an atmosphere of 5% $CO_2$ in air. Retinas were treated for 5 h then medium was replaced, and retinas were cultured for a further 11 h. L-lactate was measured in media at the end using a colourimetric assay. Inhibitors used were **A.** PI3K inhibitors LY294002 (LY) (30 µM or 60 µM) or ZSTK474 (ZS) (2 µM or 4 µM), or vehicle (DMSO, 1:1000) **B.** Akt inhibitor MK-2206 (10 µM), MEK1 inhibitor PD98059 (30 µM) or Rac1 inhibitor NSC23766 (50 µM), or vehicle (DMSO, 1:600) **C.** mTOR inhibitors Rapamycin (Rap) (100 nM) or AZD8055 (AZD) (300 nM), or vehicle (DMSO, 1:1000) and **D.** Tankyrase/Wnt signalling inhibitor XAV939 (10 µM), or vehicle (DMSO, 1:1000). Data were normalised to total protein extracted from retinal explants at the end of experiments. All graphs show mean ± SD from three independent experiments with at least two retinas per group per experiment. Statistical analyses for A-C were Dunnet's multiple comparisons tests comparing each group to DMSO, and for D was Student's unpaired t-test. No change was significant at $P < 0.05$. ns: not significant.

## *FGFR signalling does not drive aerobic glycolysis in the rat retina*

FGFR activation can stimulate multiple major signalling pathways with diverse, context-dependent cellular effects including upregulation of glycolysis[223-226]. In addition, FGFR1 can directly phosphorylate PKM2[227], LDHA[228], and pyruvate dehydrogenase kinase 1[229], altering their activities to promote aerobic glycolysis. Importantly, in mouse retinal explants, it was shown that inhibitors of FGFR significantly decreased lactate production, and it was further proposed that FGF2 released by the RPE activates FGFR signalling in photoreceptors, driving aerobic glycolysis[50]. It was hypothesised here that the same is true in the rat retina.

Rat retinal explants were treated with the FGFR inhibitor, PD173074, at three concentrations (Figure 5.3 A). There was a trend toward decreased lactate production with increasing inhibitor concentration, but no statistically significant change in lactate production occurred. In contrast, the magnitude of the decrease in lactate production reported in the mouse retina was very large, approximately 80% with 20 µM PD173074[50].

To assess whether the difference in results was due to particularities of experimental conditions, the experiment was also performed under conditions that much more closely matched the prior publication on mouse explants, including a similar experimental treatment timeline, and incubation in B-27- and N-2-supplemented Neurobasal A medium containing 25 mM glucose under an atmosphere of 95% $O_2$ and 5% $CO_2$ (Figure 5.3 B). The increased oxygen level caused a modest decrease in lactate production and inhibition of FGFR caused a further small but significant decrease. This was of similar magnitude to the non-significant change observed at this concentration of inhibitor under the original experimental conditions (Figure 5.3 A) – the statistical significance attained in this case may simply reflect a decrease in variation between repeats rather than a major difference in actual metabolic drivers caused by the change in experimental conditions. These results support a role for FGFR in driving aerobic glycolysis in the rat retina, albeit of much lower magnitude than in the mouse retina. However, literature indicated that PD173074 is effective in inhibiting FGFR in cell culture at the lowest concentration used here of 0.1 µM[230-233], where no decrease in lactate production was observed (Figure 5.3 A). It was therefore possible that the need for much higher concentrations (5 or 20 µM) to observe changes in lactate production here and in the study by Chinchore et al.[50] indicate that off-target or toxic effects may be responsible.

To confirm the actual concentration required for the PD173074 to take effect on FGFR, western blots were performed for phosphorylated forms of fibroblast growth factor receptor substrate 2 (P-FRS2) (at position Y436) and P-ERK1/2 (at positions T202 and Y204 in ERK1 and T185 and Y187 of ERK2), proteins in the FGFR signalling pathway, the phosphorylation states of which reflect pathway activity

(Figure 5.3 C). However, phosphorylation of either protein was not detected in the retina even in the absence of inhibitor (see far left lane). This indicated that FGFR signalling was likely inactive or minimally active in the rat retinal explants and further implied that lactate production was probably not driven by FGFR. Given the hypothesis proposed by Chinchore et al.[50] that FGF2 released by the RPE activates FGFR in photoreceptors, foreseeably, the continued presence of RPE-derived FGF2 may have been required for maintenance of FGFR signalling in the retina. To test this, eyecup and retina were incubated intact together before separation for western blots. In the same experiment, separated eyecup and retina were treated with hFGF2 at several concentrations (Figure 5.3 C). In all cases, phosphorylated forms of FRS2 and ERK1/2, indicative of active FGFR signalling, were detected only in the eyecup. The absence of detectable FGF pathway activity in the retina, and minimal effect of PD173074 on lactate production led to the conclusion that FGFR signalling is unlikely to be a major driver of basal aerobic glycolysis in the rat retina.

**Figure 5.3 Investigating FGFR signalling as a driver of aerobic glycolysis in rat retinal explants. A.** Explants were cultured in 1 mL of MEM with 5.56 mM D-glucose and 0.8 mM L-glutamine in a humidified 37 °C incubator in an atmosphere of 5% $CO_2$ in air for 5 h in the presence of FGFR inhibitor PD173074 (0.1 µM, 5 µM or 20 µM) or vehicle (DMSO, 1:1000), medium was replaced, and explants treated for a further 11 h. L-lactate was then measured in media. **B.** Explants were cultured in 1 mL of Neurobasal A medium with 25 mM D-glucose and 2 mM glutaMAX supplemented with 0.2% B-27 and 0.1% N-2 in a humidified 37 °C incubator in an atmosphere of either 5% $CO_2$ in air, or 95% $O_2$ and 5% $CO_2$ for 6 h in the presence, where indicated, of PD173074 (20 µM) or vehicle (DMSO, 1:1000). Medium was removed and replaced with 1 mL of Kreb's Ringer's solution without inhibitor. Explants were cultured for 30 min under the same atmosphere. L-lactate was then measured in solution. Data in A and B were normalised to total protein extracted from retinas at the end of each experiment. A and B each show the mean ± SD of three independent experiments. A was analysed by Dunnet's multiple comparisons test comparing to DMSO. B was analysed by Tukey's multiple comparisons test. * indicates $P < 0.05$, ** indicates $P < 0.01$. **C.** Rat retinal explants and eyecups were cultured either intact together, or after separation as indicated, under the same conditions as A for 1 h in the presence of the stated concentration of human FGF2 (hFGF2). rMC-1 cells treated with hFGF2 were included as a positive control. Western blots performed for the indicated proteins. P- indicates specific detection of the phosphorylated form of the protein; P-FRS2 at position Y436, P-ERK1 at positions T202 and Y204, and P-ERK2 at positions T185 and Y187. **D.** Expression of FGFR-related genes was assessed in the developing rod RNA-seq data of Kim et al.[1]. The effective counts table was downloaded (GSE74660), counts were summed to the gene level, normalised and $log_2$-transformed. Differential expression (DE) by greater than 2-fold between the P2 and P28 groups was tested using limma (requiring a Benjamini-Hochberg corrected P-value of < 0.05). A heatmap (using z-scores by row from $log_2$ counts per million [cpm] values) and table were generated showing changes in gene expression over development. Red or blue in the table indicates direction of change. **E.** Expression of FGFR-related genes was assessed in the adult mouse whole retina and retinal pigment epithelium (RPE) RNA-seq data of Kallestad et al.[3]. The table of counts was downloaded (GSE135415). Counts were TMM-normalised and differential expression by greater than 2-fold was tested using limma (requiring a Benjamini-Hochberg corrected P-value of < 0.05). A heatmap and table were generated as for D.

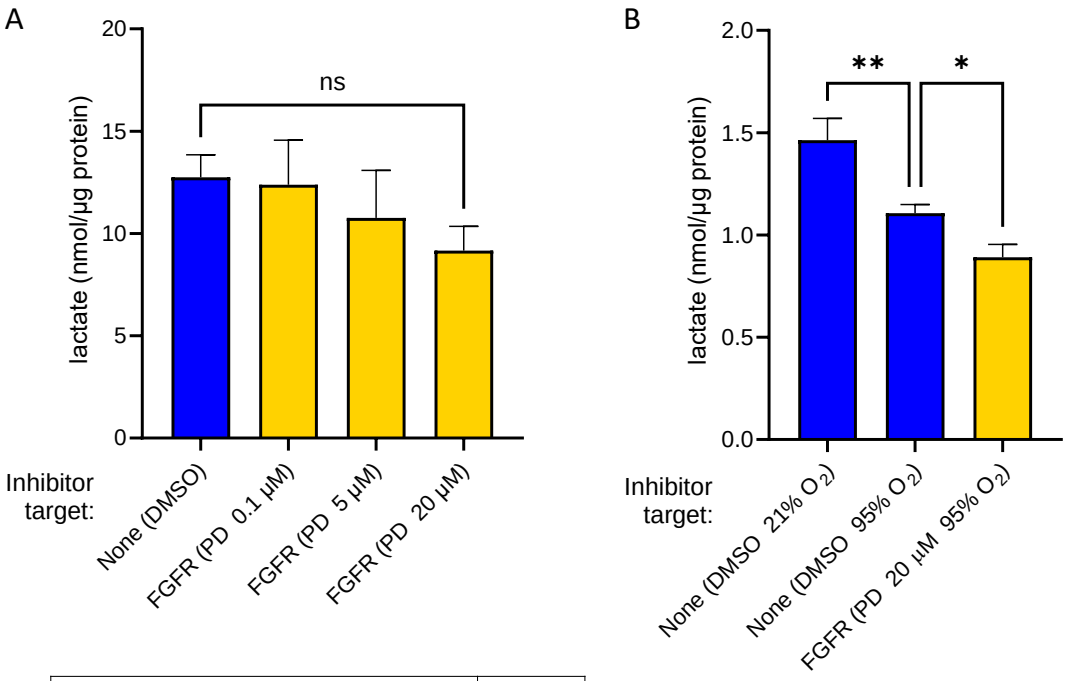


C

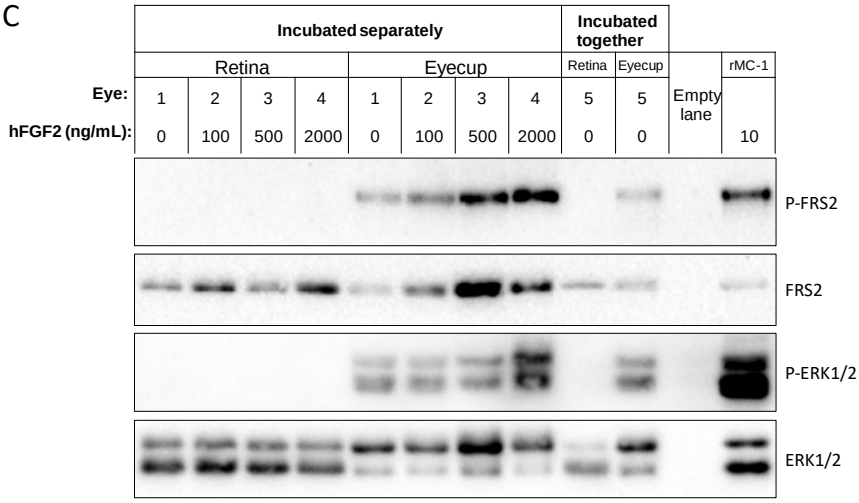


D

## Maturing rods

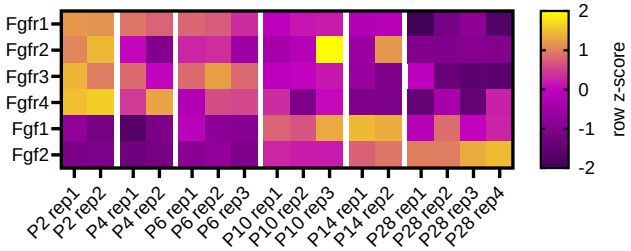


| | P2 avg log2 cpm | P28 avg log 2 cpm | Fold-change | Significant > 2-fold DE |
|---|---|---|---|---|
| Fgfr1 | 4.7 | -0.6 | -39 | Yes |
| Fgfr2 | -0.3 | -2.7 | -5.4 | no |
| Fgfr3 | 2.1 | -0.9 | -7.7 | Yes |
| Fgfr4 | 0.2 | -2.0 | -4.9 | Yes |
| Fgf1 | -1.4 | 0.2 | 3.1 | no |
| Fgf2 | -2.2 | 3.8 | 61 | Yes |

E

## Retina vs RPE

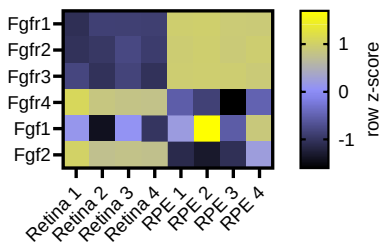


| | Retina avg log2 cpm | RPE avg log2 cpm | Fold-change | Significant > 2-fold DE |
|---|---|---|---|---|
| Fgfr1 | 4.6 | 6.7 | 4.3 | yes |
| Fgfr2 | 2.1 | 7.5 | 43 | yes |
| Fgfr3 | 0.4 | 7.6 | 140 | yes |
| Fgfr4 | 0.6 | -1.5 | -4.1 | yes |
| Fgf1 | 5.6 | 5.7 | 1.1 | no |
| Fgf2 | 4.3 | 3.4 | -1.9 | no |

As a final means of investigating the discrepancy between our FGFR-inhibition results and the published mouse data, two mouse RNA-seq datasets were explored. Firstly, expression of FGFR-related genes was assessed in the maturing mouse photoreceptor dataset of Kim et al.[1] which was analysed in the previous section. Expression of *Fgfr1-4* all decreased over the course of rod maturation, although interestingly, expression of *Fgf2* increased (Figure 5.3 D). The second dataset analysed was from a 2019 study by Kallestad et al.[3] In this study, RNA-seq was performed on samples from mouse and baboon retina and RPE at various timepoints post-mortem. Expression of FGFR-related genes was assessed in the zero-timepoint (fresh tissue) mouse retina and RPE groups, with differential expression testing (> 2-fold threshold) performed between the two groups. *Fgfr1-3* were more highly expressed in the RPE than in the retina with only *Fgfr4* showing the opposite trend (Figure 5.3 E). Additionally, FGF2 was more highly expressed in the retina than the RPE (although not significantly by greater than 2-fold). RNA levels do not necessarily correlate with protein levels, and many factors contribute to FGFR signalling, but these data collectively do not favour the hypothesis that FGF2 released by the RPE drives aerobic glycolysis in the retina. The data appear more consistent with the results above indicating higher FGFR signalling activity in the RPE than the retina. Previous studies have indicated a role for FGFR signalling in RPE function, but this remains poorly characterised[234,235].

## *Investigating transcriptional drivers of aerobic glycolysis in rods*

So far, candidate drivers of aerobic glycolysis were chosen for testing based on their established roles in driving aerobic glycolysis in cancer cells – but none of those tested displayed a role in the retina. Therefore, an alternative approach was used to identify new candidate pathways. In the rod RNA-seq dataset of Kim et al.[1], the mRNA levels of many glycolytic and TCA cycle genes increased similarly over rod maturation, reflecting a transcriptional program of upregulated expression of metabolic genes in rods. Therefore, the expression of a list of transcription factors was assessed in this dataset, with the aim of finding factors that exhibited an expression profile that matched or preceded the increase in metabolic genes and hence may be responsible for upregulation of these metabolic genes.

A list of transcription factors was obtained using the Mouse Genome Informatics (MGI) database Gene Ontology Browser to retrieve genes under the molecular function term, “transcription regulator activity > DNA-binding transcription factor activity”. There were 1352 unique transcription factors under this term. Some were either not appreciably expressed (< 1 cpm on average at P2 and P28) or were not found in the rod dataset, leaving a list of 863 genes. Most of these factors decreased in expression over rod maturation, although a small group increased (Figure 5.4 A). To narrow down the

list of candidate metabolic drivers, the list was filtered for genes with a positive fold-change from P2 to P28 which was statistically significantly greater than 2-fold. A resulting shortlist of 43 genes was obtained. It was ordered by fold-change, and a heatmap and corresponding table was generated for these genes (Figure 5.4 B). Expression of a set of key glycolytic genes is shown at the bottom of the heatmap for reference. Genes were evaluated individually for potential roles in driving aerobic glycolysis based on published literature.

**Figure 5.4 Changes in expression of transcription factors over rod development in the RNA-seq data of Kim et al. 2016.** A list of transcription factors was obtained from the Gene Set Enrichment Analysis (GSEA) Molecular Signatures Database (MSigDB) by filtering for genes under the heading "transcription regulator activity > DNA-binding transcription factor activity". Expression of unique genes in the list was assessed in the RNA-seq data of Kim et al.[1] which was obtained from developing rods FACS-isolated at the indicated post-natal ages. Briefly, the effective counts table was downloaded (GSE74660), counts were summed to the gene level, normalised and $\log_2$-transformed. Differential expression (DE) by greater than 2-fold between the P2 and P28 groups was tested using limma (requiring a Benjamini-Hochberg corrected P-value of < 0.05). **A.** A heatmap (using z-scores by row from $\log_2$ counts per million [cpm] values) was generated showing changes in expression of all genes in the list over development. **B.** Genes in A that were statistically significantly expressed more highly at P28 than P2 by greater than 2-fold were selected and a heatmap (z-scores) and corresponding table were generated showing changes in expression over rods development.

A

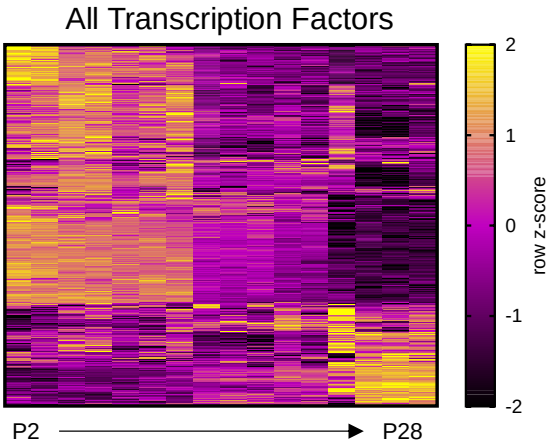


B

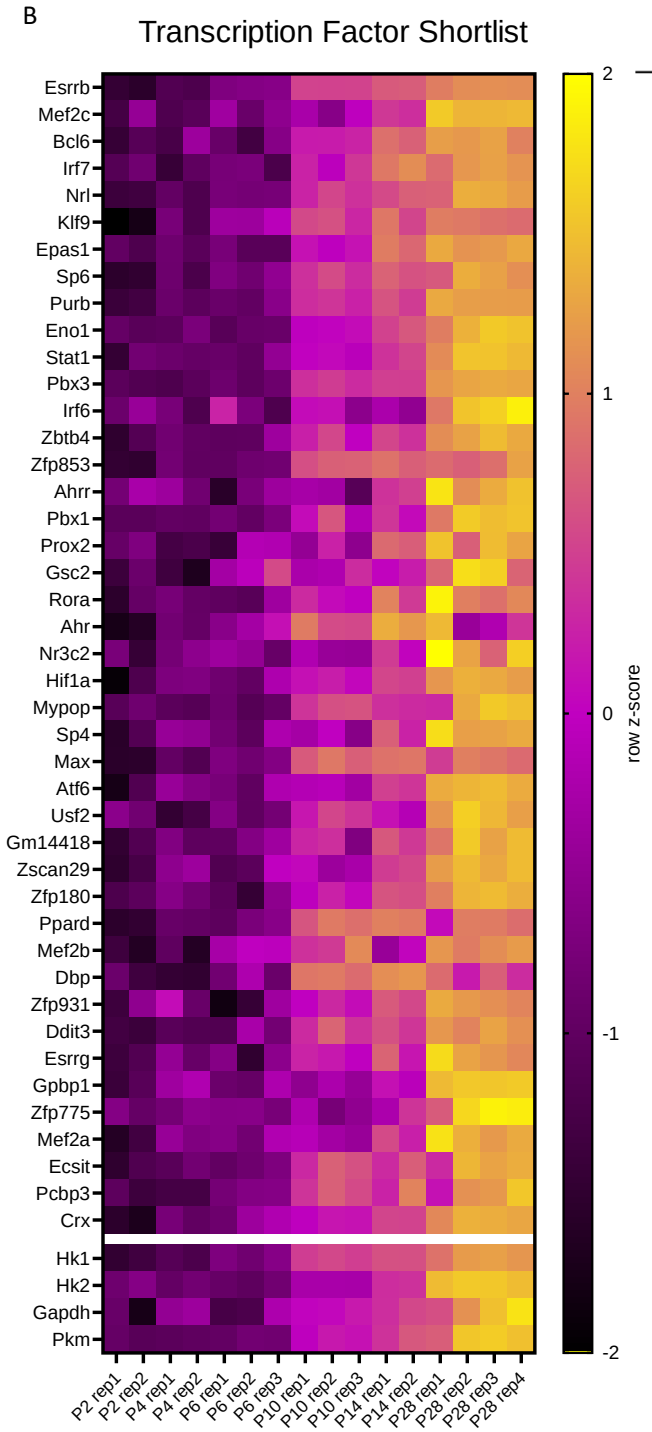


| | P2 avg log2 cpm | P28 avg log 2 cpm | Fold-change | Significant > 2-fold DE |
|---|---|---|---|---|
| Esrrb | -0.2 | 10.7 | 1822.0 | Yes |
| Mef2c | -0.9 | 8.5 | 676.4 | Yes |
| Bcl6 | -0.8 | 3.4 | 18.8 | Yes |
| Irf7 | -0.1 | 4.1 | 18.0 | Yes |
| Nrl | 9.6 | 13.6 | 15.3 | Yes |
| Klf9 | 3.8 | 7.6 | 14.0 | Yes |
| Epas1 | 3.7 | 7.5 | 13.5 | Yes |
| Sp6 | 1.2 | 4.7 | 12.0 | Yes |
| Purb | 8.2 | 11.8 | 11.8 | Yes |
| Eno1 | 9.5 | 13.0 | 11.2 | Yes |
| Stat1 | 3.2 | 6.6 | 10.8 | Yes |
| Pbx3 | 4.5 | 7.9 | 10.8 | Yes |
| Irf6 | -1.9 | 1.3 | 9.3 | Yes |
| Zbtb4 | 5.5 | 8.6 | 8.7 | Yes |
| Zfp853 | -1.0 | 1.8 | 6.9 | Yes |
| Ahrr | 1.7 | 4.5 | 6.9 | Yes |
| Pbx1 | 7.0 | 9.8 | 6.9 | Yes |
| Prox2 | 0.1 | 2.8 | 6.5 | Yes |
| Gsc2 | -2.1 | 0.5 | 6.1 | Yes |
| Rora | 6.8 | 9.3 | 5.6 | Yes |
| Ahr | 2.3 | 4.7 | 5.4 | Yes |
| Nr3c2 | 1.2 | 3.6 | 5.4 | Yes |
| Hif1a | 8.9 | 11.3 | 5.3 | Yes |
| Mypop | 0.7 | 3.0 | 5.0 | Yes |
| Sp4 | 6.8 | 9.1 | 5.0 | Yes |
| Max | 5.5 | 7.8 | 4.8 | Yes |
| Atf6 | 6.0 | 8.1 | 4.4 | Yes |
| Usf2 | 6.6 | 8.8 | 4.3 | Yes |
| Gm14418 | 2.4 | 4.5 | 4.2 | Yes |
| Zscan29 | 4.4 | 6.5 | 4.2 | Yes |
| Zfp180 | 4.9 | 6.9 | 4.0 | Yes |
| Ppard | 4.4 | 6.4 | 3.9 | Yes |
| Mef2b | -0.8 | 1.1 | 3.9 | Yes |
| Dbp | 2.5 | 4.5 | 3.8 | Yes |
| Zfp931 | 3.3 | 5.2 | 3.6 | Yes |
| Ddit3 | 4.4 | 6.2 | 3.5 | Yes |
| Esrrg | 5.5 | 7.3 | 3.5 | Yes |
| Gpbp1 | 7.3 | 9.1 | 3.5 | Yes |
| Zfp775 | 3.1 | 4.9 | 3.4 | Yes |
| Mef2a | 6.1 | 7.8 | 3.4 | Yes |
| Ecsit | 3.9 | 5.6 | 3.4 | Yes |
| Pcbp3 | 7.2 | 8.9 | 3.2 | Yes |
| Crx | 10.1 | 11.6 | 2.9 | Yes |

## *A possible role for estrogen-related receptor beta*

The gene that exhibited by far the greatest fold-increase from P2 to P28 was *Esrrb*, which encodes estrogen-related receptor β (ERRβ). ERRβ is a member of the NR3B group of orphan nuclear receptors which also includes ERRα and γ[236,237] (the latter, encoded by *Esrrg*, was also present in the shortlist of upregulated transcription factors). These transcription factors display ligand-independent constitutive transactivation activity, binding DNA at estrogen-related response elements (ERREs) as well as classic estrogen response elements (EREs). ERRβ is known to have roles in metabolic regulation and pluripotency[236-238]. Onishi et al. knocked out *Esrrb* in mouse rod photoreceptors using Cre under the control of a rhodopsin promoter[239]. Rod photoreceptors degenerated over time and mRNA levels of rod-specific genes, including several involved in glycolysis, were lower in the knockout. However, no measurements of metabolic flux, such as lactate production rate, were reported. We therefore sought to expand the findings with measurements of lactate production in rat retinal explants, and further investigate the potential role of ERRβ in retinal aerobic glycolysis.

Rat retinal explants were treated with two different inhibitors of ERRs, diethylstilbestrol (DES)[240] and 4-hydroxytamoxifen (4-OHT)[241], and lactate production was measured (Figure 5.5 A). Promisingly, treatment with DES caused an approximately 40% decrease in lactate production, but 4-OHT caused no significant change. It was unexpected that both inhibitors did not have a similar effect, although some evidence indicated that 4-OHT may not be a strong inhibitor of ERRβ in a cellular context[236,241]. We sought to confirm the ability of each inhibitor to target ERRβ – specifically the rat isoform – and to gauge their toxicity using dual luciferase reporter assays in cell lines. Two different cell lines, rMC-1 and HEK 293T, were used to control for cell type-specific differences in inhibition or toxicity. In these assays, an SV40 promoter with or without the additional presence of a 3xERRE enhancer element drove firefly luciferase expression (pGL3 promoter 3xERRE[242]). A plasmid from which Renilla luciferase was constitutively expressed (RL-TK) provided an internal control for overall transcriptional activity in all samples. Co-transfection of a plasmid encoding constitutively expressed rat ERRβ (pTwist EF1α puro rEsrrb) induced firefly luciferase expression in both cell lines, as expected (Figure 5.5 B). Whilst both inhibitors decreased firefly in a dose-dependent manner, they also decreased expression of the constitutive Renilla luciferase, which indicated a general downregulation of transcription rather than specific inhibition of ERRβ. There was no concentration of either inhibitor in either cell line at which firefly decreased without a corresponding decrease in Renilla. It is most likely that the inhibitors were toxic to the cells at a lower concentration than required to inhibit ERRβ, which is indicative of off-target effects. Indeed, toxicity was visually evident in the form of rounded morphology and detachment of cells from the well surface. It is also possible that the inhibitors were specific for ERRs but that one or more ERRs were required for survival of both cell types. The question of the

involvement of ERRβ in driving aerobic glycolysis in the retina would be best addressed by a genetic targeting approach.

It remains likely, based on the published data showing that *Esrrb* knockout decreased expression of some glycolytic genes, that ERRβ is at least partly responsible for driving aerobic glycolysis in the retina, but this was not able to be confirmed from the present set of experiments. It would be ideal to examine lactate production and other measures of metabolic flux in rod-specific ERRβ-knockout retinas in the future. A rod-specific inducible-Cre mouse would also be useful for this experiment and similar experiments so that genes can be knocked out and metabolic roles determined in the adult retina, avoiding confounding factors around possible developmental roles of targeted genes.

Further experiments to test other potential drivers of aerobic glycolysis in the retina have yet to be performed. However, other relevant findings and potential new hypotheses from the analysis of transcription factors in the RNA-seq data are discussed below.

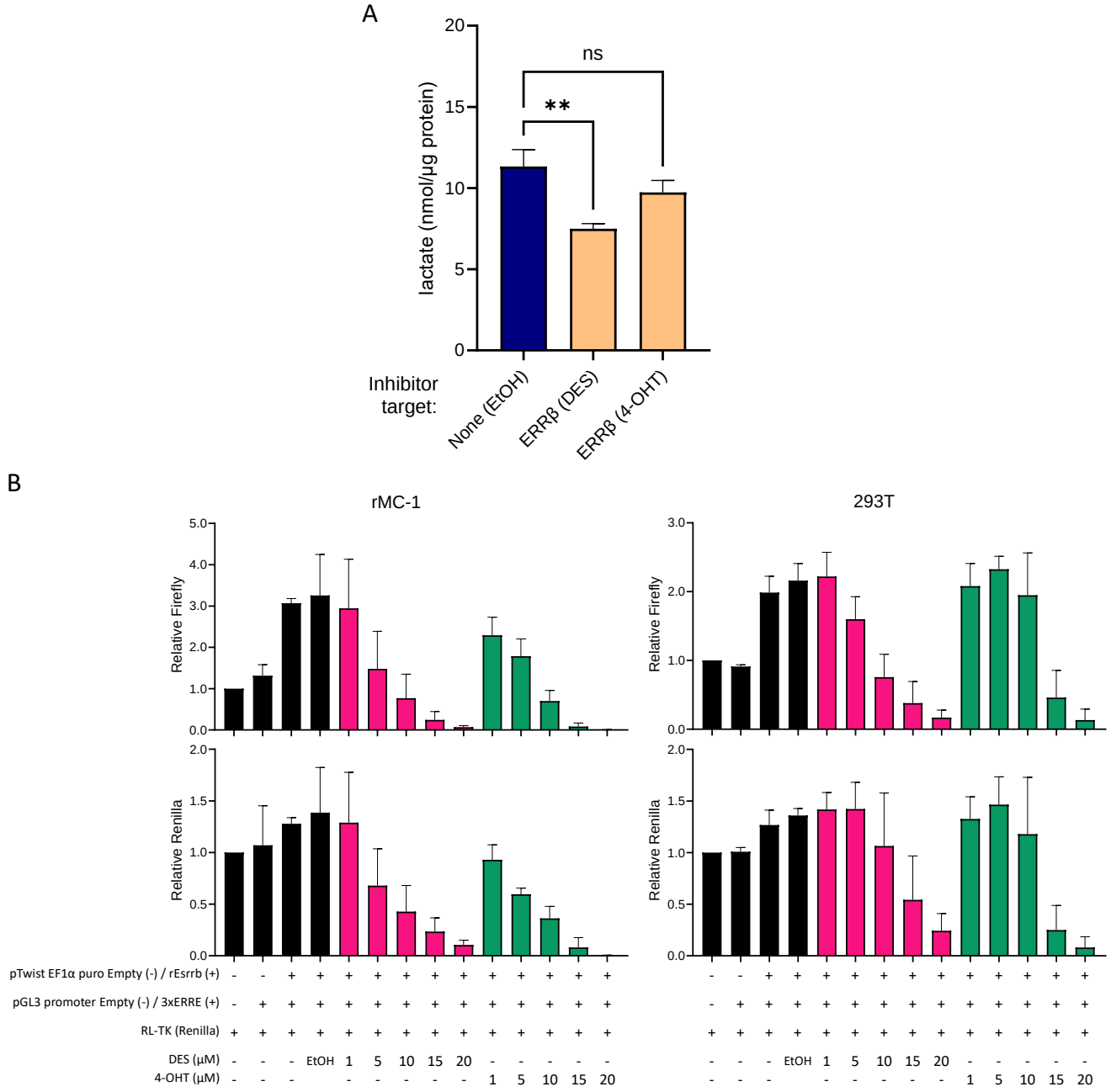


**Figure 5.5 Investigating estrogen-related receptor beta as a driver of aerobic glycolysis in rat retinal explants. A.** Rat retinal explants were cultured in MEM with 5.56 mM D-glucose and 0.8 mM L-glutamine in a humidified 37 °C incubator in an atmosphere of 5% $CO_2$ in air for 5 h in the presence of one of two inhibitors of estrogen related receptors (ERR), diethylstilbestrol (DES) (20 µM) or 4-hydroxytamoxifen (4-OHT) (10 µM), or vehicle (EtOH, 1:1000). Medium was replaced and cells were treated with inhibitor for a further 11 h. L-lactate was measured in media at the end of the experiment using a colourimetric assay. Total protein was quantified after experiments and used to normalise lactate values. Data show the mean ± SD from three independent experiments and were analysed using Dunnet's multiple comparisons test comparing each treatment group to DMSO. ** indicates $P < 0.01$. ns: not significant. **B.** rMC-1 cells were co-transfected with plasmid encoding rat ERRβ (*rEsrrb*) under control of a constitutive EF-1α promoter (or the same empty plasmid) in order to drive firefly luciferase (FF) expression from a pGL3 promoter plasmid, where firefly was controlled by an SV40 promoter and 3xERRE enhancer element (or empty plasmid lacking the enhancer) and the RL-TK plasmid encoding constitutively expressed Renilla luciferase. At the same time as transfection, cells were treated with DES or 4-OHT at the indicated concentration. Dual luciferase assays were performed 16 h after transfection/treatment. Data shown are the mean ± SD from three independent experiments, each performed in triplicate, after normalisation of each experiment to the first control group.

## *Transcriptional drivers of aerobic glycolysis in rods – future hypotheses*

The genes in the transcription factor shortlist with perhaps the best-established roles in driving glycolysis were *Hif1a* and *Epas1* (*Hif2a*). Early in this project, these genes were among the most promising hypothesised drivers of retinal aerobic glycolysis due to the strength of evidence for their roles in driving glycolysis in other contexts[243-246]. However, a series of studies was published showing that knockout of either HIF-1α[247] or HIF-2α[248], or dual knockout of both proteins[248] in mouse rods, and knockout of HIF-1α or dual knockout of HIF-1α and HIF-2α in cones[249] had no overt effect on retinal function. While any measurements of metabolic flux were not reported, it would be expected that a major disruption to glycolysis would manifest significant functional defects. It was therefore considered unlikely that the HIFs were major drivers of aerobic glycolysis in photoreceptors. Recent work by another student in our laboratory using HIF inhibitors is consistent with this view (David Hansman, unpublished).

STAT1 (*Stat1)*, which was upregulated over the course of rod maturation, is another possible transcriptional driver of glycolytic and other metabolic genes in rods. It has been shown to promote transcription of metabolic genes in squamous cell carcinoma[250]. However, there is immunostaining evidence to suggest that STAT1 is not expressed (or lowly expressed) at the protein level in mouse photoreceptors[251]. Furthermore, in the rd10 model of retinal degeneration, STAT1 protein and mRNA levels increased concurrent with photoreceptor loss and large decreases in the abundance of glycolytic enzymes, which is inconsistent with a role for STAT1 as a main driver of expression of these enzymes[252]. There is currently no direct evidence linking STAT1 to metabolic control in the retina. For these reasons, we elected to focus attention instead on ERRβ. A potential role of STAT1 in retinal metabolism, however, cannot be excluded without investigation.

The roles of transcription factors can be unexpected and context dependent. A surprisingly large number of shortlisted transcription factors that increased in expression over rod maturation have been shown in studies in various contexts to downregulate glycolysis. For example, Bcl6, a transcriptional repressor commonly dysregulated in lymphoma[253,254], has been reported to directly repress glycolytic gene expression in some T cell subtypes[255]. Irf7 has recently been shown to inhibit aerobic glycolysis in osteosarcoma by a mechanism involving repression of PKM2 expression[256]. Similarly, Irf6 represses transcription of PKM2 and GLUT1, and its upregulation in glioma decreases aerobic glycolysis and tumour xenograft growth[257]. However, PKM2 expression increased by more than 8-fold over rod maturation. Overexpression of RORα (*Rora*) decreases aerobic glycolysis in hepatoma[258]. Pparδ (*Ppard*) may decrease expression of glycolytic genes including Hk2 in mouse muscle[259]. Sp6 (also known as Klf14) can downregulate glycolysis in macrophages by inhibiting

transcription of Hk2[260] and its overexpression can also downregulate glycolysis in colon cancer cells[261]. However, Hk2 exhibited the greatest increase in expression of any glycolytic gene over rod maturation.

It is intriguing that so many transcription factors upregulated over rod maturation have reported roles in downregulating glycolytic genes – the implications are unclear given that rods clearly upregulate expression of most glycolytic genes. These transcription factors might play a balancing role in the retina to limit or control the rate of glycolysis, or they may function entirely differently in the retina than in these other contexts, perhaps promoting glycolytic gene expression via interactions with an alternative set of coactivators, corepressors, and other proteins. In either case, the upregulation of these transcription factors is of interest for rod metabolism and has yet to be investigated.

Klf9 can decrease aerobic glycolysis in squamous cell carcinoma by downregulating expression of 6-phosphofructo-2-kinase/fructose-2,6-bisphosphatase 3 (*PFKFB3*)[262]. *Pfkfb1-4* encode protein isoforms with dual enzymatic activity, able to catalyse the phosphorylation and hydrolysis of the C2 position of fructose-6-P at separate active sites. They therefore both produce and remove fructose-2,6-bisphosphate, a strong allosteric activator of the rate-limiting glycolytic enzyme, phosphofructokinase 1 (Pfk1). Unlike the transcription factors above, in the case of Klf9, its upregulation was consistent with the change in *Pfkfb3* expression in rods, which was downregulated over maturation (although it is not known if this was related to *Klf9* expression) (Figure 5.6). Most interestingly, despite the fact that the isoforms *Pfkfb3* and *4* are more commonly associated with aerobic glycolysis[263], it was noted that the isoform *Pfkfb2* was by far the most highly upregulated in rods – all others were downregulated. It is likely that Pfkfb2 plays an important role in controlling glycolysis in rods which has yet to be investigated. There is no isoform-specific inhibitor of Pfkfb2 available, so such a study would be best approached with genetic targeting. All Pfkfb isoforms are inhibited by ATP and by TCA cycle intermediates including succinate and citrate, especially strongly by the latter[264]. Pfkfb2 is regulated by post-translational modifications such as phosphorylation of specific residues by Akt, PKA or AMPK. These modifications increase its kinase activity in specific ways to drive glycolysis[265-267]. For example, amino acids increase Pfkfb2 activity in cancer cell lines and cardiomyocytes via activation of Akt and phosphorylation of Pfkfb2, leading to increased glucose uptake and lactate production[268]. The data we collected showed no constitutive requirement for Akt activity in driving lactate production in rat explants (Figure 5.2 B), but it would be important to test for roles of other known regulators of Pfkfb2.

It is possible that classic photoreceptor-specific lineage-determining transcription factors such as Nrl or Crx may directly upregulate expression of glycolytic genes. Nrl is a rod-specific transcription factor. In mice, its knockout results in rod-less retinas which are instead cone dominant. However, microarray

comparison of $Nrl^{+/+}$ and $Nrl^{-/-}$ mouse retinas has been performed and did not reveal any glycolytic genes that were significantly differentially expressed between the two groups[269]. It is therefore unlikely that Nrl directly regulates these genes. Interestingly though, *Pfkfb2* was among the only differentially expressed genes in this study with an obvious link to glycolysis. It was downregulated at maturity in the Nrl knockout, further suggesting a likely unique importance in rods.

As a final consideration, components of glycolysis and glucose metabolism pathways may be post-transcriptionally regulated. Analyses of RNA-seq data cannot account for such regulation of protein stability or activity. In future, proteomics, phospho-proteomics and metabolomics, or combined multi-omics approaches may shed light on pathways of regulation of retinal metabolism that are not apparent at the RNA level.

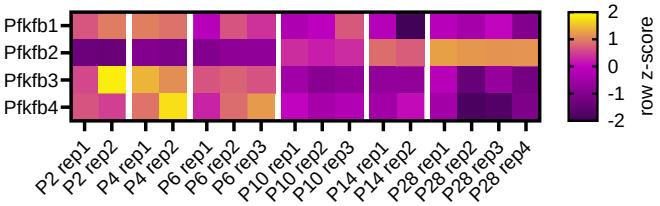


| | P2 Avg log2 cpm | P28 Avg log2 cpm | Fold change | Significant > 2-fold DE |
|---|---|---|---|---|
| Pfkfb1 | 1.6 | 0.8 | -1.7 | no |
| Pfkfb2 | 5.8 | 10.5 | 26 | Yes |
| Pfkfb3 | 4.1 | 1.9 | -4.7 | Yes |
| Pfkfb4 | 3.0 | 1.3 | -3.3 | no |

**Figure 5.6 Changes in expression of Pfkfb genes over rod development in the RNA-seq data of Kim et al. 2016.** Expression of Pfkfb genes was assessed in the RNA-seq data of Kim et al.[1] which was obtained from developing rods FACS-isolated at the indicated post-natal ages. Briefly, the effective counts table was downloaded from Gene Expression Omnibus (GEO) under accession number GSE74660, counts were summed to the gene level, normalised and $\log_2$-transformed. Differential expression (DE) by greater than 2-fold between the P2 and P28 groups was tested using limma (requiring a Benjamini-Hochberg corrected P-value of < 0.05). A heatmap (using z-scores by row from $\log_2$ counts per million [cpm] values) and corresponding table were generated showing changes in expression of genes over development.

# 6. Discussion

# *Müller cell metabolism*

## *Conclusions from rMC-1 cell experiments*

The main findings from the research presented in Chapter 3 were firstly that PI3K and Rac1 drive lactate production in rMC-1 cells, with inhibition of either reducing lactate production by approximately 50%. MEK1 also drives lactate production but to a lesser extent than PI3K and Rac1. Secondly, this role for PI3K is entirely independent of Akt, as Akt inhibition had no effect on lactate production. This is the first direct implication of the signalling pathways and components in mediated aerobic glycolysis in cultured Müller cells.

It will be important to follow up these findings to determine the molecular mechanisms responsible for driving glycolysis downstream of these proteins in rMC-1 cells. In MCF10A mammary epithelial cells, PI3K leads to activation of Rac1, cytoskeletal remodelling and release of the glycolytic enzyme, Aldolase A, from an inactive F-actin-bound form to an active soluble form[149]. Whether PI3K and Rac1 act in the same pathway to drive lactate production in rMC-1 cells could not be determined from the set of experiments performed in this thesis, and given the differences between the cultured and *in vivo* cells, additional experiments were not pursued as part of this thesis. However, all necessary proteins for this mechanism are expressed in rMC-1, SIRMu-1 and primary cultured rat Müller cells (not shown) based on our laboratory's RNA-seq data presented at the end of Chapter 3, so it is possible that a similar mechanism is responsible. While of interest, the physiological relevance of the findings presented in Chapter 3 are of questionable significance given the differences between the cultured and *in vivo* Müller cells.

## *Differences between culture and in vivo*

A pertinent point of difference between Müller cells in culture and *in vivo* is the expression of pyruvate kinase. Initial evidence that no isoform of PK is expressed in Müller cells *in vivo* was published in a 2014 study by Lindsay et al.[54]. Further studies employing immunological methods to detect PKM1 and PKM2 have also since failed to detect either protein in Müller cells in rats or mice, although a small amount of PKM2 may be expressed in marmoset Müller cells[50,117]. On the other hand, in our laboratory, Thaksaon Kittipassorn showed by western blot that all three cultured Müller cell types investigated in this project, including primary cells, express PKM2[114], and this is consistent with the analysis of RNA-seq data from the three Müller cell types presented in Figure 3.7 A, which showed expression of *Pkm* (PKM1 and PKM2 are encoded by splice variants of the *Pkm* gene). *Pklr*, which encodes other isoforms of PK, was also not expressed in culture. In this project, the expression of *Pkm*

at the RNA-level *in vivo* was assessed in a published single-cell RNA-seq dataset and several bulk Müller cell RNA-seq datasets where the cells used were freshly isolated; however, it was not possible to discriminate reads that derived from Müller cells from those that derived from contaminating rods or other cells. In future, assessment of *Pkm* expression at the RNA level in Müller cells *in vivo* may be more reliably made using a method that does not rely on perfect separation of cell types, such as RNA fluorescence *in situ*-hybridisation. It is, however, likely that *Pkm* is expressed lowly in Müller cells relative to rods at the RNA level *in vivo*, which would be consistent with its low or absent expression at the protein level.

The consequences of the absence of PK are not entirely clear. The same paper that reported the lack of PK also reported the lack of the aspartate glutamate carrier in Müller cells[54]. This carrier is an essential component of the malate aspartate shuttle (MAS), which indirectly transports NADH generated by glycolysis into the mitochondrial matrix where it can be oxidised by passing electrons to the ETC. The inability of Müller cells to utilise the MAS may imply a proclivity to oxidise cytosolic NADH by lactate dehydrogenase which would fit with a high level of aerobic glycolysis. But, also lacking PK, Müller cells are unlikely able to readily produce pyruvate from glucose, rendering the metabolic scheme at play more enigmatic. It is possible that Müller cells express a small amount of PK, but this is much less than is present in photoreceptors[54]. Müller cells store glycogen and there is some evidence in amphibians they can perform gluconeogenesis[270,271]. Given this, they might be considered a glucose depot for retinal neurons, able to store and release glucose, only minimally catabolising it themselves.

There is, however, also the possibility that Müller cells maintain pyruvate production in the absence of PK by utilising a non-canonical glycolytic pathway. For example, there is evidence that some cancer cells can utilise the phosphate group of phosphoenolpyruvate to phosphorylate a specific histidine residue on the glycolytic enzyme PGAM1, a reaction that yields pyruvate[272]. This may be able to occur continuously due to the release of inorganic phosphate from the phosphorylated PGAM1. In regard to Müller cells, this idea has also been proposed by Rajala[210], but it has not been tested to my knowledge. It is unclear how such a scheme would benefit the Müller cells over expression of PK.

Although it has not been explicitly shown, it can be assumed that PKM2 expression and/or stability must rapidly increase as Müller cells adapt to primary culture, and there is evidence of changes in expression of several other proteins involved in glucose metabolism[212]. It would be useful to determine the timescale over which these changes occur, the regulatory mechanisms involved, as well as other metabolic changes. While we no longer consider cultured Müller cells to be an ideal model of retinal aerobic glycolysis, the importance of Müller cells in the metabolic network in the retina remains

unquestionable. An essential new goal for Müller cell research is to develop a cell line or culture method that better models Müller cell metabolism *in vivo*. It would be interesting to knock out *Pkm* entirely (both PKM1 and PKM2) for the purpose of generating a Müller cell line for study that more closely represents *in vivo* metabolism. However, this would be a heavy-handed intervention that may affect metabolic responses in subsequent experiments. The change in PKM2 expression in culture highlights the fact that common culture conditions for Müller cells *in vitro* must differ to the physiological environment *in vivo*, so it would be important to first reassess the commonly used culture conditions and attempt to determine conditions that support Müller cells in a state that better reflects their metabolic roles *in vivo*.

## *Proposed changes for future Müller cell experiments*

There are several factors that may be involved in inducing metabolic changes in Müller cells during adaptation to cell culture including the loss of protein-protein interactions and signalling connections with surrounding cells, changes in the available fuel sources and partial pressure of oxygen *in vitro* compared to *in vivo*, and gain of non-physiological proliferative signals from serum. Intercellular signalling may be difficult to accurately replicate *in vitro*. In the case of the interaction between rods and cones, the secretion of a protein termed rod-derived cone viability factor by rods has been shown to stimulate aerobic glycolysis in cones[13]. A similar but opposite relationship may exist between rods and Müller cells, or between another cell type and Müller cells.

Fuel sources and oxygen availability, on the other hand, are easily manipulated and there is an increasing body of literature on which changes to culture media can be rationally based. For example, it has been suggested that Müller cells, rather than producing lactate, may net consume lactate released by photoreceptors to power OXPHOS[54], and/or, as speculated above, to generate glucose. Aspartate is also reportedly a preferred fuel of Müller cells[54]. Any changes, however, should be implemented not because Müller cells are able use a particular supplied fuel, but only because they have been shown to do so, or likely do so, *in vivo*. For example, clearly Müller cells can consume glucose to produce lactate *in vitro*, but it is unlikely they have a high capacity to do this *in vivo*. Given photoreceptors have primary access to glucose that diffuses through the RPE (Müller cells also have access via the subretinal space) it is likely that Müller cells *in vivo* exist in an environment where lactate is more abundant than glucose extracellularly over most of the length of the cell. In addition, one of the major functions of Müller cells *in vivo* is the uptake of glutamate released by neurons, which they convert to glutamine and return to neurons[273]. In cell culture, it is normal to grow cells in medium containing high concentrations of glutamine in order to support rapid growth, and no glutamate,

opposing this major function of Müller cells. Perhaps Müller cells should be cultured in medium containing glutamate and lactate rather than glutamine and glucose. The inner retina of the rat and other mammals, especially in darkness, can reach oxygen levels lower than that used in typical cell culture[106,108,274,275], so it would be equally important to also assess the effects of varying levels of hypoxia on Müller cell metabolism.

Serum in culture medium contains growth factors that are well-known to activate signalling pathways that affect metabolism. Its inclusion is generally necessary to maintain survival and proliferation of cultured cells. It was included in the culture medium in all experiments in Chapter 3 except the Seahorse assay. Proliferation is necessary to realise many of the advantages that cultured cells have over other methods, but it is non-physiological in the case of Müller cells. To improve the usefulness of Müller cell cultures for metabolic studies, after plating for an experiment it may be necessary to transition them from a growth-supporting medium to a physiological serum-free or defined medium for an empirically determined minimum period of time before undertaking experiments. Metabolic changes induced by immortalisation by viral oncogene transduction are possibly not fully mitigatable with changes to culture medium, but this would need to be experimentally tested. Primary cells and spontaneously immortalised lines such as the SIRMu-1[128], MIO-M1[276], or QMMuC-1[277] lines may be more amenable to reversal of metabolic changes. The degree to which metabolic changes can be reversed by changes to culture media needs to be tested.

Ultimately, the only way to perfectly model physiological Müller cell metabolism is to perform experiments *in vivo*, but such experiments are often impracticable for many reasons including expense and time constraints, the impossibility of broad screening approaches, the dominant metabolism of photoreceptors in the retina which may overshadow metabolic changes in other cell types, a relatively limited range of experimental techniques compared to *in vitro*, and the limited set of tools available for species other than mice. However, with the rapid development of single-cell omics technologies, it may be possible in the not-too-distant future to obtain metabolomic data, including metabolic flux, from single cells *in vivo*. While *in vivo* studies will remain the gold standard for translation to clinical practice, it may be possible to significantly improve the physiological relevance of studies on cultured Müller cells with simple changes to culture media, warranting further investigation.

# *Rat retina metabolism*

## *Conclusions from rat retinal explant experiments*

Inhibitors of PI3K, Akt, mTOR, Rac1, MEK1 or Wnt signalling had no significant effect on lactate production in rat retinal explants. Under the conditions used for these inhibitors, inhibition of FGFR also had no significant effect on lactate production, although there was a trend towards decreased lactate production with increasing inhibitor concentration. Under culture conditions that matched a previous publication where the same FGFR inhibitor was shown to cause a large decrease in lactate production in mouse retinal explants[50], FGFR inhibition caused a small but significant decrease in lactate production at a high inhibitor concentration. However, any FGFR signalling activity in the explants was below the level of detection by western blot for P-FRS2 or P-ERK1/2, suggesting the decrease in lactate production may have been due to off-target effects of the inhibitor. In contrast, FGFR signalling was active in the eyecup. Two different ERR inhibitors had different effects on lactate production. Diethylstilbestrol decreased lactate production by approximately 40% whereas 4-hydroxytamoxifen caused no significant change. Follow-up experiments indicated the decrease caused by diethylstilbestrol was most likely due to toxic effects of the inhibitor likely to be unrelated to ERR inhibition. Overall, no strong evidence was found to indicate that any of the proteins or pathways investigated drive aerobic glycolysis in the rat retina; however, the data collected for FGFR and ERR inhibitors have important implications in revealing potential species-specific differences in drivers of retinal aerobic glycolysis or in calling into question the conclusions derived from some published results.

Many tested inhibitors caused no change in lactate production. While the fact that oxamate, which inhibits LDH directly, abolished lactate production, and the fact that the ratio of glucose consumed to lactate produced approximately matched published data spoke to the soundness of the explant model, there are factors to consider before the lack of effect of inhibitors can be confidently attributed to a genuine lack of involvement of these proteins in driving aerobic glycolysis.

Firstly, P-Akt (not shown) and P-ERK1/2 (Figure 5.3 C) were extremely lowly expressed and inconsistently detectable at all in western blots using rat explant extracts which is consistent with neither pathway having a constitutive role in driving aerobic glycolysis. While the activity of Rac1 was not directly measured, the reported mechanism via which Rac1 modulates aerobic glycolysis occurs downstream of PI3K so it is also unlikely to play a constitutive role. The basal activity of mTOR and Wnt changes as a consequence of treatment with their inhibitors were not directly assessed but it is likely the inhibitors were able to access the tissue and exert effects. Photoreceptors in retinal explants are directly exposed to the culture medium, so deep permeation of the inner layers of tissue is not

expected to be required for an inhibitor to exert effects on photoreceptors and therefore lactate production. Furthermore, rapamycin has been shown to exert autophagy-related effects in mouse retinal explants at the concentration used in this project (100 nM)[278]. To my knowledge, there are no reports of AZD8055 treatment of retinal explants, but in multiple cell lines it effectively inhibits mTORC1 and 2 at concentrations orders of magnitude below the 300 nM used in this project[279,280]. In neuronal cultures, 100 nM AZD8055 effectively inhibits mTOR[281]. Considering 3D cultures, 100 nM AZD8055 is also effective in tumour organoids[282]. The Wnt signalling inhibitor XAV939 has similarly not been used to treat retinal explants to my knowledge, but it has been used successfully to inhibit signalling in the chick retina *in vivo*, injected intravitreally at a predicted initial concentration in the vitreous of 3.2 µM, which is below the 10 µM used in the culture media in this project. It effectively inhibits Wnt signalling in cell culture at 1 µM[222]. In addition to these data, clearly oxamate was able to access the tissue and inhibit LDH. The high concentration of oxamate used (100 mM) is necessary due to the polar nature of the molecule which renders it poorly cell-permeable[283], but the concentration used to treat explants is similar to that required to treat cell monolayers; 50 mM oxamate significantly decreased lactate production in rMC-1 cells (Figure 3.2 A). Finally, recent unpublished data from a current member of the laboratory has found effects of chemical inhibition of another pathway on lactate production, so, while the pharmacokinetics of each inhibitor differs, there was no general problem of tissue accessibility of inhibitors.

Depending on the potential mechanisms at play, it is possible that the treatment time was not sufficiently long to observe effects on lactate production. However, in rMC-1 cells, inhibitors of PI3K, Akt and MEK1 had abolished pathway activity within 40 min of treatment and the inhibitors of PI3K, Rac1 and MEK1 exerted effects on lactate production in rMC-1 cells in a much shorter time period (8 h) than the explant treatment duration (16 h). Many effects of Akt on glucose metabolism are proposed to occur via post-translational regulation of proteins[144-147], which would likely result in rapid metabolic effects. In the study that first reported the mechanism via which Rac1 modulates glycolysis, metabolic effects of inhibitors of PI3K and Akt were evident in Seahorse assays within just 1 h of treatment. In a separate experiment in the same study, effects of the Rac inhibitor NSC23766 were evident in under 4 h (less time is probably required based on the PI3K inhibitor result, but no shorter treatment was reported in the paper for this inhibitor)[149]. mTORC1 promotes glycolysis through mechanisms that more likely predominantly involve transcription and translation and may require protein turnover – decreased lactate production involving these mechanisms has been reported after 18 h of treatment[284]. As ERRβ is a transcription factor, the mechanism via which it modulates glycolysis is proposed to involve gene transcription, so turnover of proteins in glucometabolic pathways would be required to observe effects on lactate production after its inhibition. This is relevant mainly to 4-

hyroxytamoxifen treatment, where no significant effect was observed (Figure 5.5 A). For diethylstilbestrol, the decrease in lactate production was not able to be attributed to inhibition of ERRβ. In mouse retinal explants, cell death upon treatment with these inhibitors is evident after 2 d *in vitro* (it may have been evident but not tested earlier)[239]. Wnt signalling is also mediated predominantly via transcriptional modulation[219,220,285]. The half-life of many glycolytic enzymes is less than the 16 h treatment timeframe (although may depend on the cell type), and there is some evidence that their half-life is inversely correlated with flux through the pathway[286], so the half-lives may be low in photoreceptors given enzyme expression and pathway flux is high, although this would need to be tested.

In summary, it is likely that the chosen treatment time of 16 h was sufficiently long to observe effects on lactate production, but the possibility that a longer treatment was required cannot be definitively ruled out where mechanisms necessitated protein turnover, especially where possible effects were small. Longer treatment times would require reassessment of culture conditions and further optimisation to determine conditions that maintain linear lactate production, cell survival, and ideally function, for times beyond 16 h *ex vivo*.

## *Explant culture conditions*

There is a diverse spectrum of conditions published for the maintenance of retinal explants *ex vivo*, and a broad range of durations over which different research groups extend experiments. In some cases, explants have been reported to survive for up to 17 days *ex vivo*[287]. Generally, prenatal or early postnatal retinas survive for longer *ex vivo* probably due to the activity of growth and developmental pathways[288]. The aims of this project, however, necessitated the use of adult retinas. There were several considerations made in deciding upon the culture conditions used in this project, and these were generally made to maintain the metabolism and metabolic drivers unchanged from *in vivo*, while balancing the capacity to readily screen many candidate pathways and to perform different treatments in parallel.

### *Culture medium*

The culture medium used in this project was MEM containing 5.56 mM D-glucose supplemented with 0.8 mM L-glutamine, 100 U/mL penicillin and 100 µg/mL streptomycin. It contained sodium bicarbonate, which is essential for maintenance of retinal function and metabolism *ex vivo*[289]. Many recent studies utilising retinal explants have used either DMEM or Neurobasal A as the base

medium[288,290]. One study using human retinal explants found no difference in gross appearance between retinas cultured in DMEM placed directly in medium versus those cultured in Neurobasal A on tissue culture inserts, though more extensive comparison was not performed[290]. In this project, rather than selecting a medium to maximise long-term survival, it was considered more important to use a medium that contained approximately physiological levels of key nutrients which would minimise the chance of altering metabolism and metabolic drivers. For this reason, MEM was chosen as the base medium. DMEM was not used as it contains four-fold higher concentrations of most amino acids and vitamins compared to MEM which makes DMEM useful for maximising growth of cancer cells and minimising changes of medium but less physiological. Neurobasal and Neurobasal A media are formulated to maximise the survival of prenatal and adult neurons in culture, respectively[291]. These media were designed for situations where only neurons were present, which is not the case for the culture of retinal explants. Serum and defined supplements such as B-27 or N-2 were not included in the medium as they contain components including corticosterone, progesterone and insulin which may affect glucose metabolism[292,293]. In the case of serum, the presence and concentrations of growth factors are unknown and batch dependent. Importantly, the absence of serum did not cause a decrease in lactate production over the 16 h culture period (Figure 5.1 A).

A detailed comparison would be required to conclusively determine the most appropriate culture medium, with reference to data collected *in vivo*, but it is likely that the MEM based medium used in this project maintained the explants in a sufficiently metabolically normal state for valid conclusions to be drawn about the role of each investigated pathway in driving aerobic glycolysis, keeping in mind the caveats above regarding treatment times. At the start of the set of experiments on retinal explants in this project, MEM was validated to support approximately linear lactate production over sixteen hours (Figure 5.1 B), and the level of lactate production was unchanged by inclusion of 10% FBS (Figure 5.1 A). This reflects stable and autonomous lactate production without the requirement for exogenous growth factors over the experimental period. Furthermore, the rate of lactate production did not appear to vary greatly from immediately after isolation of the explants consistent with continuous production from *in vivo* to *ex vivo* rather than reflecting a major change in production rates due to explant isolation.

*Oxygen tension*

Metabolic experiments that utilise retinal explants are sometimes performed in hyperoxic conditions, commonly in an atmosphere of 95% oxygen and 5% $CO_2$[5,6,50,294,295]. This is not universal, however, with recent studies by major contributors to the field also having used conditions of 5% $CO_2$ in air[12,54,211,296-299], which were the conditions used for all experiments in this project except where stated in Figure 5.3 B. The use of hyperoxic conditions arose from multiple studies in the 1900s. Winkler showed that

20% oxygen was not adequate to maintain ATP content at the level of freshly isolated retinas in rat retinal explants[6,295]. Ames et al. showed that 40% oxygen was the minimum level needed to attain maximal electrical responses of rabbit retinal explants to light[5]. Winkler suggested that the requirement for hyperoxic conditions was due to a limit of diffusion of oxygen into the tissue in the absence of the physiological blood supply to the inner retina[6]. This is possible, but it has also been argued that oxygen consumption can reach non-physiologically high rates if it is provided in excess[5].

Some species possess mechanisms that limit retinal hyperoxia. In the cat and rat, when ventilated with hyperoxic gas mixtures, the inner retinal oxygen level rises disproportionately less than the choroidal oxygen level[4]. This is possibly due in part to a mechanism that decreases retinal blood flow under hyperoxia[4,300]. The guinea pig appears to have actually evolved a mechanism to limit choroidal oxygen level; when anesthetised guinea pigs were ventilated with increasing levels of oxygen, choroidal $PO_2$ rose a relatively tiny amount compared to systemic arterial $PO_2$[4]. Systemic hyperoxia is clearly not a natural occurrence, so these mechanisms, in a physiological setting, are proposed to act in response to small changes in oxygen level in order to maintain oxygen availability within a tight range[4]. In contrast to these species, the rabbit retina does not show any similar adaptations; the retinal oxygen profile instead rises in parallel with increases in arterial oxygen level[4]. The fact that several species, including rat, have evolved mechanisms apparently to limit large increases in retinal oxygen tension adds reason for not performing all experiments under hyperoxia.

In this project, where 5% $CO_2$ in air was used, no increase in the rate of lactate production was observed over time in culture, we have not been able to detect HIF-1α in western blots from explant extracts (not shown), and a current PhD candidate in our laboratory has shown that chemical inhibition of HIF results in no change in lactate production (David Hansman, unpublished). Together, these data indicate that the explants are probably not hypoxic under the conditions used, or the hypoxia is mild and not adequate to activate the canonical hypoxia signalling pathways. The evidence is nevertheless strong that 20% oxygen is inadequate to maintain ATP content at fresh levels in rat retinal explants[6,295], so both sides of this issue have merit. Had a pathway been identified that drove lactate production in this project, follow-up would have included performing experiments under hyperoxia to test for differential effects, as well as functional analysis by electroretinogram with oxygen tension raised if necessary. As a future study, it would be valuable to measure the oxygen profile through the depth of retinal explants incubated in different oxygen tensions to determine a level that results in a profile most similar to that *in vivo*[105]. Oxygen levels could then be paired with functional analyses. If a normal level of electrical function did not align with the most physiological oxygen level, it may indicate a deficiency in another component of the medium, which would require further investigation. For example, it would be interesting to assess the effects of including β-

hydroxybutyrate in the culture medium, which has been proposed to fuel retinal metabolism[301]. This would be a major undertaking, requiring separate optimisation for any given species.

### *What drives aerobic glycolysis in the rat retina?*

From the experiments performed in this project, in can be concluded that PI3K, Akt, Rac1 and MEK1 do not play a major role in driving aerobic glycolysis in the adult rat retina. The result of Akt inhibition agrees with a previous study that also reported no change in lactate production upon Akt inhibition in rat retinal explants[294]. The treatment duration in the earlier study was much shorter than in the present project so the result obtained here greatly bolsters the confidence in this conclusion. FGFR does not play a major role in aerobic glycolysis in the rat retina despite its reported role in the mouse retina. FGFR may play a small role but given that neither P-FRS2 nor P-ERK1/2 was detected in rat retinal explants (Figure 5.3 C), and given the high concentration of PD173074 used, it is possible that the small decrease in lactate production observed (Figure 5.3 B) was due to off-target or toxic effects. Inhibition of Wnt signalling caused no decrease in lactate production so it is highly unlikely to play a major role in driving aerobic glycolysis. However, given that this pathway would putatively act on glycolysis through a mechanism requiring protein turnover, it is possible that the treatment time needs to be extended to observe an effect. The situation is the same for ERRβ. In this case, the decrease in lactate production caused by diethylstilbestrol was likely due to off-target toxic effects. 4-OHT caused no significant change in lactate production over the 16 h of treatment, but there is a possibility that a longer treatment may have been needed to observe an effect of ERRβ inhibition.

The RNA-seq analyses in Chapter 4 revealed potential novel characteristics of retinal metabolism and Müller cell metabolism worth investigation. The analysis of transcription factors that increased in expression correlatively with glycolytic genes in rods in Chapter 5 revealed surprisingly few strong candidate drivers of aerobic glycolysis. Instead, many of the factors identified have known roles in downregulating glycolysis. Perhaps, in light of this, it is worthwhile instead investigating the roles of particular co-activators, co-repressors or patterns of epigenetic modifications in the retina which may differ in function to other contexts.

Diverse pharmacological agents that target metabolism, including those pathways investigated in this project, have been trialled for the treatment of cancers[302] but, to my knowledge, the only case where a strong deleterious effect on the retina was found was an inhibitor of monocarboxylate transporter 1 (MCT1)[302-304], which is canonically required for lactate export[305] but also succinate export in the retina[306]. This case emphasises the importance of metabolism for retinal function. As the number of studies targeting potential driver pathways of aerobic glycolysis increases without adverse effects

observed on the retina, it becomes increasingly likely that aerobic glycolysis in the retina is driven by a mechanism that is distinct from the classic driver pathways characteristic of cancers, but this is not a conjecture that can be made with certainty until the molecular drivers of aerobic glycolysis in the retina are discovered. In summary, from this project, major drivers of aerobic glycolysis in the rat retina at the molecular level remain undetermined, but several likely pathways have been ruled out.

# 7. Review: Why does the mammalian retina exhibit aerobic glycolysis?

## *Why does the mammalian retina exhibit aerobic glycolysis?*

Despite the existence of aerobic glycolysis in the retina being known since Warburg's work in the 1920s[7], there is no consensus as to the fundamental reason for it. The experiments in this project were not designed to directly address the question of why the retina exhibits aerobic glycolysis, but an answer would likely reveal clues as to what drives aerobic glycolysis at the molecular level and would also provide a basis for the rational design of therapies that modulate retinal metabolism. It is an important outstanding question under the theme of the project. The following discussion explores and expands ideas in the literature that have been proposed in the retinal or cancer metabolism fields and weighs logic and evidence for and against each. Hypotheses relate to intercellular shuttling of lactate, biosynthesis, ATP production and management of reactive oxygen species (ROS), among others, although there is significant overlap of ideas between these.

## *Intercellular lactate shuttling*

The first possibility to consider is that lactate is produced by a cell type for the primary purpose of fuelling OXPHOS in another cell type. This was the idea in the ANLS model, where Müller cells were proposed to produce lactate to feed photoreceptors[44]. However, the mammalian retina as a whole, depending on the species and conditions, exports as lactate on the order of 80-90% of the glucose that it consumes[6]. It seems implausible that a cell type would have evolved to produce lactate in such excess of that required if the main driving force was to fuel another cell type. Photoreceptors are the most energetically demanding retinal cell type[5], and there is now a convincing body of evidence to indicate they are the main, albeit not necessarily the only, lactate producers in the retina[14,50,54,117,210,211]. They are also uniquely vulnerable to inhibition of glycolysis[213] and there is a cell-autonomous requirement for aerobic glycolysis in photoreceptors[50]. These observations indicate that lactate is predominantly a metabolic endpoint in the retina. It is still possible that a portion of lactate produced in the retina may be consumed by certain cell types. It is interesting to note that lactate consumption by the RPE may supress its consumption of glucose, thereby increasing glucose supply to the photoreceptors[211]. But, given net lactate production is so high – including *in vivo* or when explants are cultured with the eyecup and RPE present[50,307,308], only a small proportion of lactate must be consumed, and it is highly likely that there is another underlying reason for aerobic glycolysis.

## *Biosynthesis*

A common and plausible suggestion is that aerobic glycolysis in photoreceptors supports the anabolic demands of outer segment biosynthesis by supplying macromolecular precursors, which parallels the idea that it supports anabolism in cancer cells[37,50]. The main evidence is that disruption of glycolysis by pharmacological or genetic targeting of glycolytic enzymes decreases outer segment length[50]. However, outer segment damage may not result exclusively from primary defects of anabolism[309,310]. The hypothesis also suffers the same pitfall as in the context of cancer – why export as lactate such a large proportion of the glucose consumed? Why not use the glucose to synthesise precursors, rather than waste such a large proportion on lactate production? The hypothesis remains plausible but requires a more complete explanation for the high rate of lactate efflux as well as direct evidence showing that a substantial proportion of carbon that comprises macromolecules in the retina derives from glucose. In various proliferating mammalian cells that exhibit aerobic glycolysis, only a small proportion of cell biomass derives from glucose, with most biomass instead deriving from amino acids when they are available, suggesting the direct incorporation of glycolytic intermediates into macromolecules is not likely to be the primary role of aerobic glycolysis in these cells[38]. Similar experiments should be performed on the retina to determine the likely importance of aerobic glycolysis for outer segment biosynthesis.

Aerobic glycolysis and high proliferation rates or high rates of biosynthesis undeniably co-occur frequently[37]. It is possible that aerobic glycolysis supports anabolism primarily by means other than directly supplying intermediate metabolites for incorporation into macromolecules. This is a current area of research in cell metabolism from a broader perspective than retinal metabolism alone[35]. It is at the core of the question of why proliferating cells exhibit aerobic glycolysis and, to my knowledge, there is currently no complete explanation. There is evidence that aerobic glycolysis is a metabolic state that occurs when demand for $NAD^+$ is heightened relative to demand for ATP[42]. Exactly how aerobic glycolysis benefits a cell in such a state is not clear. This idea and its relation to the retina is discussed in detail below.

## *Rapid ATP production*

The most obvious product of glycolysis that has not been discussed so far is ATP. It is possible that ATP production is the primary purpose of aerobic glycolysis in the retina. This is initially counterintuitive given the inefficiency of aerobic glycolysis in terms of molecules of ATP produced per glucose consumed, but there are scenarios where aerobic glycolysis could be elevated for the purpose of ATP production. Despite being inefficient, glycolysis is proposed to be able to produce ATP more rapidly

than OXPHOS[39]. Dynamic changes in ATP demand that cannot be met sufficiently rapidly by OXPHOS might require ATP production by aerobic glycolysis – a situation where, regardless of the oxidative capacity of the cell, the responsiveness of OXPHOS to changes in ATP demand is too slow to maintain required functions. This has been proposed as a reason for aerobic glycolysis in some cancer cells which may use glycolysis to power membrane transporters and use OXPHOS to power base processes such as the synthesis of macromolecules[40]. In hippocampal neurons, a similar idea has been proposed where a transient burst of aerobic glycolysis in response to stimulation rapidly meets increased ATP demand[311], although it is also recognised that aerobic glycolysis cannot supply the full ATP demand of ion pumping in neurons[312].

Experiments on retinas do not clearly match this hypothesis. Lactate is produced continually and at a similarly high rate under both steady state light-adaptation and dark-adaptation where the major energy-consuming processes are largely different[5,6,10,313] and there is no obvious process that would cause fluctuations in ATP demand warranting the high rate of aerobic glycolysis observed. In response to flickering light, which would be expected to induce rapidly fluctuating ATP demand due to the large difference in energy consumption between light and darkness[5,313], glucose consumption and lactate production do increase but by a small amount relative to the total rate of each[314]. The study that demonstrated the requirement of aerobic glycolysis for membrane transporters in cancer found that treatment with ouabain, which inhibits the Na,K ATPase, greatly decreased aerobic glycolysis without affecting OXPHOS[40]. This differs from findings in the retina, where treatment with ouabain or strophanthidin, another Na,K ATPase inhibitor, has been found to decrease both aerobic glycolysis and OXPHOS in rats and rabbits[5,10,315]. These observations indicate that most aerobic glycolysis in the retina is probably not for the purpose of generating ATP at a rate that cannot be intrinsically met by OXPHOS.

## *Was it anaerobic glycolysis all along?*

The discussion so far has assumed that oxygen supply is sufficient to meet ATP demand but is this true? It is possible that the retina consumes the maximum amount of oxygen available to it from the circulation for ATP production, but that it is advantageous to the animal to use even more ATP, in excess of that which can be maximally produced aerobically. Regarding terminology, in this case, lactate production in the retina would be better considered anaerobic glycolysis despite the fact that oxygen supply is abundant. Many studies have measured the oxygen level and oxygen consumption of retinal layers in various mammals *in vivo* using microelectrodes. In the cat, which is similarly vascularised to the rat, mouse, monkey and human, the oxygen level reaches effectively zero in the

outer nuclear layer in darkness[108]. In the rat, the retinal oxygen distribution never reaches zero but drops to a low of approximately 5.2 mm Hg in the IPL in darkness[274,275]. The perifoveal region of the macaque retina reaches a similar minimum in darkness in the zone of the photoreceptor inner segments[106]. In the guinea pig, which has avascular retinas, the inner retina is essentially anoxic[103,316]. It is clear that the retina in each of these species in darkness consumes all or almost all oxygen supplied by the choroid. Lactate production by photoreceptors could validly be considered anaerobic glycolysis in darkness *in vivo* in some mammalian species.

In light, however, the retina requires 3 to 4-fold less ATP than in darkness[313], retinal oxygen consumption is considerably lower, and the oxygen distribution for these species does not dip nearly as low, yet lactate production changes relatively little between these states[6,10], with most of the difference in ATP production accounted for by a change in the rate of OXPHOS[5,6,108,317]. The magnitude of changes in oxygen consumption and lactate production in darkness and light varies between species and experimental conditions, but there is generally no consistent preference for a decrease in either aerobic glycolysis or OXPHOS specifically. Why would a decrease in ATP demand not initially be met by a large decrease in the inefficient mode of ATP production, aerobic glycolysis? Does this reflect imperfect development of regulatory mechanisms to limit glucose usage when ATP demand declines, or is there a benefit to maintaining a high rate of aerobic glycolysis when ATP demand is not maximal? These questions are unanswered. However, it is clear that at least in light, lactate production certainly occurs aerobically.

## *Molecular crowding*

Anoxic regions in darkness are not a universal phenomenon among retinas of different mammalian species as shown by the oxygen distributions of the macaque[106] and rat[275], possibly indicating a constraint on the respiratory rate other than oxygen availability in some species. Within any cell, there is a finite volume that can be dedicated to ATP production as opposed to other processes. A flux balance analysis model of glycolysis and OXPHOS in a mammalian cell was developed which accounted for this finite solvent capacity[318]. It predicted that, as glucose uptake increases from zero, mitochondria increasingly occupy cell volume until they occupy the entire cell volume available for ATP production. As glucose uptake increases beyond this point, cells were predicted to rapidly increase ATP production via aerobic glycolysis and gradually decrease OXPHOS as the capacity of glycolysis to utilise more of the available glucose outweighs its lower ATP yield per glucose. In this model, aerobic glycolysis maximises ATP production above a threshold rate of glucose uptake. This is because glycolysis alone is able to produce more ATP per unit volume than OXPHOS despite producing

less ATP per glucose[318]. The model was confirmed to fit well with metabolic measurements on cell lines, and several similar models agree with the general findings[319-321].

Maximising highly inefficient consumption of a resource for a small benefit is an effective strategy for cells in competition, but, in a multicellular organism, efficient use of resources by most cells is generally beneficial[39]. There is a clear link here to cancer metabolism, where cancer cells are no longer in cooperation with the organism but in competition with the organism and each other, and therefore a selfish but maximised metabolism benefits the cancer[39]. It is foreseeable that the retina as a key sensory organ is of such importance to the fitness of the animal that it is afforded the ability to maximise ATP production by using a mix of aerobic glycolysis and OXPHOS despite the inefficiency. Higher photoreceptor densities, which require narrow photoreceptor morphology, must necessarily limit the cytoplasmic volume of photoreceptors. Perhaps mammalian photoreceptors are adapted to maximise ATP production from available glucose while balancing the advantage of narrow morphology with the disadvantage of inefficient metabolism, striking a species-dependent sweet spot where all or almost all available oxygen is consumed. This line of thinking is not without counter arguments, though: As above, if aerobic glycolysis is primarily required for ATP production, why would the retina not respond to the decreased ATP demand in light with a decrease in lactate production in preference to a decrease in OXPHOS?

### *Limited respiratory capacity*

Staying under the theme of ATP production, two important studies have indicated there may be little to no spare mitochondrial respiratory capacity in the mouse retina[298,322]. Kooragayala et al[322] proposed that demand for ATP in the retina exceeds the maximal capacity for its production by mitochondria, so aerobic glycolysis is used to supplement ATP production[322].

In the studies by Du et al[298] and Kooragayala et al[322], mouse retinal explants (either pieces or punch biopsies in the respective studies) were treated with the mitochondrial uncoupler, FCCP, and oxygen consumption was found to remain almost unchanged from the basal rate. A point to consider with these experiments, however, is that they were performed using air-equilibrated medium where oxygen may have been limiting. In the study by Kooragayala et al., wild-type, Rpgrip1$^{-/-}$ and Nrl$^{-/-}$ retinas each exhibited approximately the same maximum oxygen consumption rate despite having different numbers, types and functional capacities of photoreceptors. It is possible this equality was coincidental but it could reflect a limit of oxygen availability under the experimental conditions. In the study by Du et al., which differed methodologically, there was one important piece of evidence indicating that $O_2$ was not limiting: FCCP-treated P11 and P12 mouse retinas displayed $O_2$ consumption

rates well above those of FCCP-treated adult retinas, which indicates the $O_2$ consumption rate of the adult retinas was likely below the limit of $O_2$ diffusion. However, it is also possible that oxygen may have more ready access to the inner retinal layers when photoreceptors have yet to fully develop.

The contribution of photoreceptors to oxygen consumption is not relatively so large as to render the contribution of the inner retina negligible[315,317], so the results of Du et al.[298] and Kooragayala et al[322] also imply the highly surprising finding that not only photoreceptors but most or all mouse retinal cell types have little spare respiratory capacity. Du et al.[298] further found that non-photoreceptor cells of the mouse retina actually do have spare respiratory capacity but this is lost when mature photoreceptors are present. The reason for this is unclear – the simplest explanation is that there is a limit of oxygen accessibility to the inner retina when mature photoreceptors are present, rather than a retina-wide alteration to mitochondrial respiratory capacity.

It is also relevant to note that the rabbit retina, *ex vivo*, consumes more oxygen in darkness in medium equilibrated with 40% or 95% $O_2$ compared to 20% $O_2$[5], indicating that mitochondria in the rabbit retina do not operate at maximal respiratory capacity at 20% oxygen. The cat retina, *in vivo*, reportedly consumes more oxygen in light/hyperoxia than in darkness/normoxia[307], so this is potentially also the case in the cat; however, another study found no difference in oxygen consumption between dark-adapted normoxic and hyperoxic cat retinas[323]. Several other studies have assessed the effects of hyperoxia on retinal oxygen distribution or consumption but only in light, where oxygen consumption and ATP demand are submaximal, so unchanged oxygen consumption in hyperoxia in these studies does not necessarily reflect a respiratory limit[109,324-326]. In summary, it would be useful to substantiate the findings of Du et al[298] and Kooragayala et al[322] with experiments performed on multiple species and under hyperoxia in darkness to assess species-specific differences and to confirm that the observed limit of oxygen consumption reflects mitochondrial respiratory capacity and not another phenomenon such as a limit of oxygen availability. As discussed above, limited oxygen availability, especially in darkness, may be a physiological reality in many species, but the distinction between mitochondria operating at maximal capacity in an environment where oxygen is abundant versus operating at the limit of oxygen availability may have different metabolic implications.

If these findings of limited respiratory capacity are confirmed, one interpretation is that aerobic glycolysis is necessary to meet ATP demand in excess of that which can be met by the mitochondrial capacity[322]. But why not generate more mitochondria? Possibly *in vivo* there is insufficient unused oxygen to make this energetically favourable – a co-occurring limit of mitochondrial capacity and oxygen availability – or possibly molecular crowding constraints would mean this strategy would

decrease ATP yield. These lines of thought integrate into the discussions of oxygen availability, molecular crowding and maximisation of ATP production above.

### *Mitochondrial uncoupling, ROS management, and $NAD^+$ regeneration*

Interesting alternative reasons for, and implications of, the limited respiratory capacity in the retina were investigated by Du et al[298]. They found that treatment with oligomycin, which inhibits ATP synthase (Figure 7.1), caused only a 50% decrease in oxygen consumption, indicating that oxygen consumption by retinal mitochondria is unusually highly uncoupled from ATP production. The authors went on to elucidate intriguing mechanisms via which calcium signalling may control metabolic flux in darkness versus light. The proteins or mechanisms responsible, and the reason for uncoupling in the retina, are unknown. I analysed the developing rod RNA seq data of Kim et al.[1] for expression of the uncoupling proteins UCP1-5 (not shown). UCP4 and UCP5 were the most highly expressed in rods throughout postnatal development and at P28. These isoforms are expressed in various cell populations in the central nervous system but they are less well-studied than UCP1-3[327].

One recognised function of uncoupling is to decrease production of reactive oxygen species (ROS)[328]. See a recent review by Hass and Barnstable for a comprehensive discussion of uncoupling in relation to the retina[327]. The ETC is a significant contributor to ROS production as electrons can leak from various points of the chain to molecular oxygen, forming superoxide[329]. ROS production is particularly high when the mitochondrial membrane potential is high or when the $NAD^+$ to NADH ratio is low in the mitochondrial matrix[330]. Mild uncoupling dissipates a fraction of the membrane potential resulting in decreased production of ROS. Aerobic glycolysis may be rationalisable in the context of minimising ROS production. In the simple sense, aerobic glycolysis could shift a portion of the ATP production burden away from respiration, thereby decreasing ETC activity and ROS production[331]. Interestingly, overexpression of UCP4 in PC12 cells has been shown to increase glucose uptake and lactate production, and to decrease dependence on OXPHOS for ATP production[332]. There is not yet any experimental evidence for this hypothesis in the retina, but it warrants investigation.

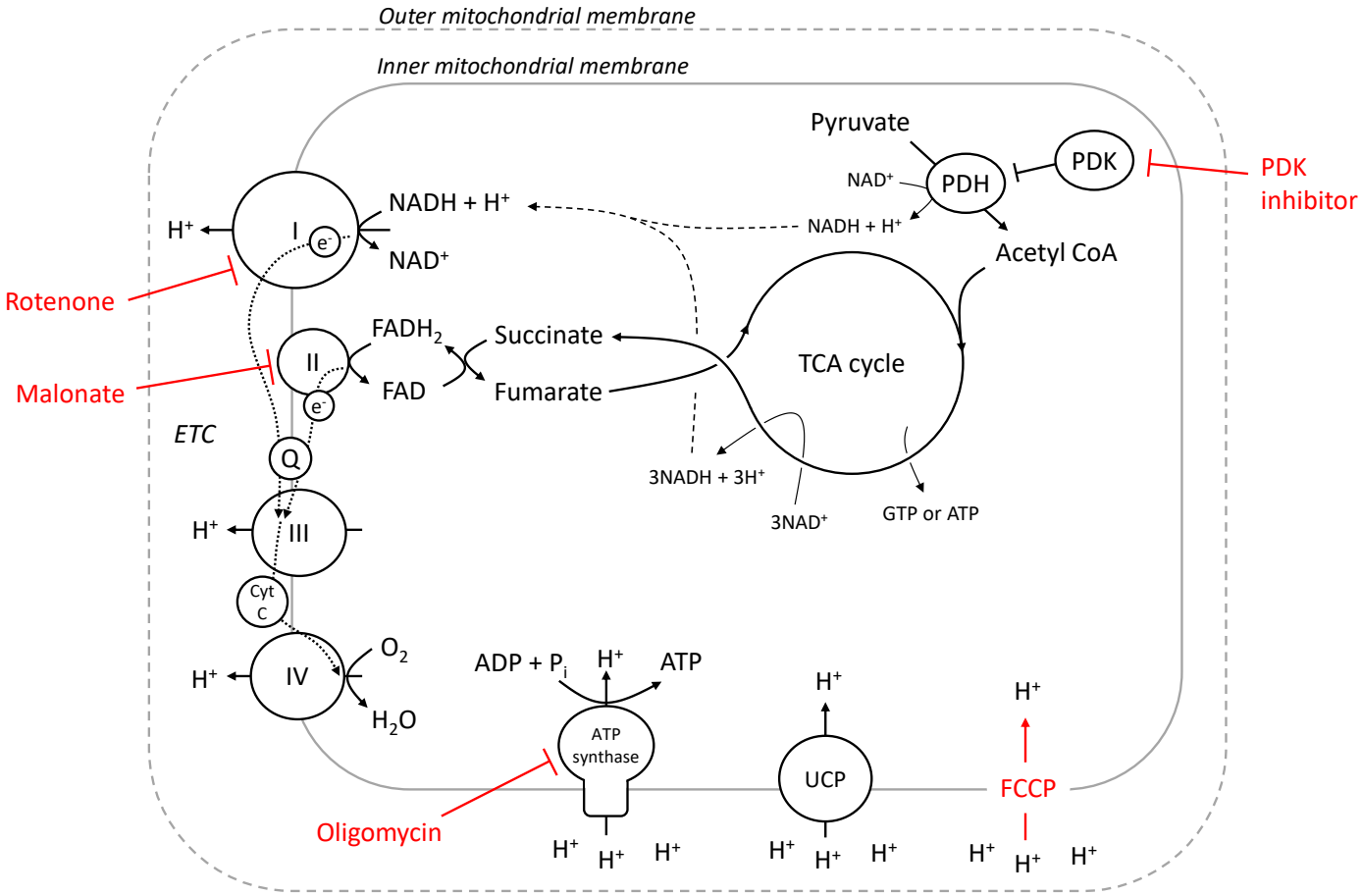


**Figure 7.1 Oxidative phosphorylation, highlighting particular inhibitors.** In oxidative phosphorylation (OXPHOS), pyruvate is converted to acetyl CoA which fuels the tricarboxylic acid (TCA) cycle. The TCA cycle and other reactions contribute to generating NADH. Electrons are passed from NADH to the Electron Transport Chain (ETC) complex I. Succinate, which is produced in the TCA cycle, passes electrons to ETC complex II via reduction of FAD. Both complex I and complex II pass electrons to Coenzyme Q (Q) which passes them to complex III. They are then passed to complex IV via cytochrome C (Cyt C). Complex IV reduces molecular oxygen to produce water. In the reactions at complexes I, III and IV, protons are transferred from the mitochondrial matrix to the intermembrane space, generating a proton gradient and electrical potential difference across the inner membrane. This energy drives production of ATP as electrons return to the matrix through ATP synthase. Uncoupling proteins (UCP) can dissipate this gradient by permitting passage of protons back to the matrix uncoupled from ATP synthesis. The chemical uncoupler carbonyl cyanide-p-trifluoromethoxyphenylhydrazone (FCCP), and several inhibitors relevant to the text are highlighted in red. PDH: Pyruvate dehydrogenase, PDK: Pyruvate dehydrogenase kinase.

There also exist other potential reasons for uncoupling and aerobic glycolysis. Du et al. proposed that the high level of uncoupling in the retina may relate to biosynthesis, but a mechanism was not proposed[298]. Recent studies of cancer metabolism provide some leads and indicate that additional ATP production by glycolysis may actually be undesirable. This relates to the idea introduced above that aerobic glycolysis is driven by high $NAD^+$ demand relative to ATP demand, which was outlined in a study by Luengo et al. using cancer cell lines[42]. The $NAD^+$ to NADH ratio is intimately related to biosynthesis via synthesis of aspartate, serine and purine nucleotides[333-335]. Aspartate, serine and $NAD^+$ availability can be limiting for proliferation of cancer cells[42,333-336]. Luengo et al.[42] treated cancer cells with an inhibitor of pyruvate dehydrogenase kinase to decrease aerobic glycolysis. This diverted pyruvate away from lactate production and into the TCA cycle by increasing pyruvate dehydrogenase activity (Figure 7.1). It decreased the $NAD^+$ to NADH ratio, aspartate level and proliferation rate. Notably, uncoupling the mitochondrial proton gradient with FCCP (Figure 7.1) resulted in a substantial degree of rescue of each of these effects. FCCP treatment alone was shown to increase proliferation of one cell type. These results suggest that a key role of the respiratory chain in these cells, which ordinarily undertake aerobic glycolysis, is $NAD^+$ regeneration. The rate at which $NAD^+$ can be regenerated may be limited by the rate of ATP turnover. As stated above, a low $NAD^+$ to NADH ratio in the mitochondrial matrix can lead to high rates of ROS production[330]. Given that the retina engages in aerobic glycolysis, the unexpectedly high degree of uncoupling of retinal mitochondria may be an evolved mechanism to enable a high rate of $NAD^+$ regeneration relative to ATP synthesis, facilitating both biosynthesis and redox homeostasis.

Aerobic glycolysis from glucose to lactate has a net neutral effect on the $NAD^+$ to NADH ratio[42]. As recognised by Luengo et al.[42], it remains unclear why cells in a state of high $NAD^+$ demand opt to increase glucose uptake and glycolytic NADH production to a rate where NADH reoxidation seemingly cannot be met by mitochondria via the MAS and respiratory chain, necessitating conversion of pyruvate to lactate. Their observations therefore do not reveal a complete explanation for aerobic glycolysis. It is nevertheless apparent that cells engaging in aerobic glycolysis benefit from interventions that increase the $NAD^+$ to NADH ratio. Most directly, supplementing normal glucose-containing medium with pyruvate greatly benefited cells in the Luengo et al. study, almost completely rescuing the proliferative defect caused by PDK inhibition in many cell lines, in some cases increasing proliferation even in the absence of PDK inhibition[42]. Supplementation with lactate, which would favour NADH production by its conversion to pyruvate, instead caused the opposite effect. It would be interesting to assess the potential neuroprotective benefit of supplying the retina with both glucose and pyruvate compared to glucose alone in disease models.

A striking result from the Du et al. study which showed uncoupling of retinal mitochondria was that, in the presence of oligomycin, inhibition of ETC complex I with rotenone (Figure 7.1) resulted in almost complete abolition of the remaining oxygen consumption whereas inhibition of complex II (succinate dehydrogenase) with malonate (Figure 7.1) resulted in no decrease in oxygen consumption beyond that induced by oligomycin[298]. Rotenone alone eliminates all retinal oxygen consumption even in the absence of oligomycin[322]. To my knowledge, the effect of malonate alone on retinal oxygen consumption has not been reported, but these results indicate a likely minimal role for complex II in driving oxygen consumption in the retina. Consistent with this, a recent study found evidence that the complex II reaction may actually operate in reverse in the retina, consuming fumarate on net to produce succinate, which may then be exported and oxidised in the RPE[299]. Succinate is a metabolic end product of anaerobic metabolism in certain contexts[337]. Net reversal of the complex II reaction renders fumarate a terminal electron acceptor in hypoxia, a physiological occurrence recently delineated in detail by Spinelli et al.[338]

Regarding the retina, it was proposed that the complex II reaction operates in the reverse direction due to limited oxygen availability[299]. Most experiments in this study were performed under 21% oxygen. The direction of the complex II reaction is closely linked to oxygen availability[338], and this was indeed shown to be true in the retina with differences in relative levels of fumarate and succinate observed depending on the oxygen tension used. However, the assumption in this study was that 21% $O_2$ was not only sufficient but provided a greater supply of oxygen than that *in vivo*. This is counter to conventional wisdom for *ex vivo* culture of retinal explants[5,6]. For accurate interpretation of these results, and all retinal metabolic studies using explants, it is vital to determine whether 21% oxygen *in vitro* is physiologically equivalent to retinal oxygen availability *in vivo*. Whether a cell type could or would engage a metabolic scheme involving reversal of the complex II reaction if oxygen were not limiting for respiration is not known.

Whether it only occurs under hypoxic stress, or whether it occurs continually in the retina physiologically, reversal of the complex II reaction is likely to play an important role in $NAD^+$ regeneration by allowing the deposition of electrons at complex I to continue when oxygen is limiting or to elevate the rate at which this can occur above that which can be attained with oxygen as the only terminal electron acceptor.

## *Glycolysis-function relationship*

It is possible that ATP from aerobic glycolysis is needed to power a specific, as-yet-undetermined cellular process. Many studies have sought to investigate the link between aerobic glycolysis and

retinal function but any specific process that exclusively requires ATP from glycolysis has remained elusive[5,6,10]. The observation that ouabain decreases both OXPHOS and glycolysis likely indicates that glycolytic ATP provides a portion of the ATP consumed by the Na,K ATPase. However, there is no evidence that glycolytic ATP is specifically required for this process. The weight of evidence does not currently indicate that OXPHOS-derived and glycolysis-derived ATP fuel separate processes.

It might be hypothesised that the morphology of photoreceptors, with mitochondria mostly located in the inner segment necessitates non-mitochondrial ATP production in distal regions. However, photoreceptors in vascular retinas contain mitochondria at their synaptic terminals, so there can be local ATP production by OXPHOS to fuel synaptic functions[339]. Also, the synaptic terminal is enriched with creatine kinase and synaptic functions in avascular retinas rely on the flow of phosphocreatine from the inner segment to the synaptic terminal[340]. At the other end of the cell, if aerobic glycolysis was absolutely required to power phototransduction processes in the outer segments, the rate of aerobic glycolysis would be expected to be low in darkness and to increase dramatically in light unless there is a complementary process requiring approximately the same level of ATP production from glycolysis in darkness. This is possible but seems unlikely. Furthermore, the distributions of glycolytic enzymes suggest the inner segments are the site of most glycolysis[14,50,54,117,156,157].

Winkler performed a seminal study relating metabolism to function using rat retinal explants in 1981[10]. Photoreceptor function, as measured by fast PIII amplitude, was completely lost within 30 minutes of transition from medium containing 5 mM glucose to no glucose[10]. Decline of function was slowed when 10 mM pyruvate was supplied in the absence of glucose but the photoreceptor response was still halved within 90 minutes[10]. Therefore, OXPHOS using pyruvate alone cannot support photoreceptor function. The retinal ATP level after incubation with 10 mM pyruvate alone was unchanged from that in the presence of 5 mM glucose after 30 minutes whereas fast PIII amplitude had declined by almost 40% over this period. The unchanged level of ATP does not necessarily reflect unchanged ATP production, but it is possible that this indicates functional decline in the absence of glycolysis might be independent of an ATP deficit.

The results of a study by Chertov et al. have interesting implications for the role of glycolysis in photoreceptors[12]. Mouse retinal explants were incubated in the presence of glucose, the absence of glucose, or in the absence of glucose but the presence of a mixture of mitochondrial fuels. In contrast to the study by Winkler, the ATP level after 90 minutes had dropped greatly and equally with mitochondrial fuels or no substrate as compared to glucose. This study used atmospheric oxygen tension, whereas Winkler used 95% oxygen, which may explain the difference in ATP maintenance, or it may indicate a difference between rat and mouse retinas. The key point is that, in the Chertov et al.

study, ATP level did not correlate with photoreceptor survival. Photoreceptors died rapidly over 90 minutes in the absence of glucose but survived equally well in the presence of mitochondrial fuels alone as glucose alone despite the difference in ATP level. Chertov et al. concluded that photoreceptor death in the absence of glucose was therefore not due to ATP deficiency.

Mitochondrial fuels were unable to sustain photoreceptor survival as well as glucose over an extended experimental period of 8 h[12]. The requirement of glycolysis for long-term survival was attributed to it supplying biosynthetic building blocks, though this was not shown directly. While photoreceptors do have the biosynthetic burden of outer segment renewal which other cell types do not, the outer segments are only renewed at a rate of approximately 10% of their length per day[341]. It would be surprising if there is such an unyielding requirement for an uninterrupted supply of biosynthetic precursors that their absence leads to cell death within eight hours. More recent experiments by Chinchore et al. have shown that inhibition of glycolysis *in vivo* leads to decreased photoreceptor outer segment length but not widespread death of photoreceptors[50]. It is difficult to directly compare these studies as a variety of metabolic substrates and survival factors may be present *in vivo* that were not present in the experiments of Chertov. et al., and the intervention in the Chinchore et al. study was not as severe as removing glucose entirely, but the results indicate that photoreceptors are able to survive for an extended duration with severely shortened outer segments due to inhibition of glycolysis (as discussed above, whether the shortening of outer segments is due to a lack of biosynthetic precursors has not been shown directly).

An interesting finding in the study by Chertov et al.[12] which was not discussed was that the mitochondrial fuel mix induced a slight increase in retinal oxygen consumption yet a large decrease in the $NAD^+$ to NADH ratio. This seems to indicate the normal rate of oxidation of NADH cannot be met by respiration alone in the absence of glucose. This finding is in line with the idea that aerobic glycolysis benefits cells in a state of high $NAD^+$ demand, but it is not clear at the mechanistic level how aerobic glycolysis provides this benefit. It should also be noted that the mitochondrial membrane potential was lower with mitochondrial fuels alone than with glucose alone despite the higher oxygen consumption with the former. There is still much to understand about the respiratory chain, the roles of uncoupling and how these aspects of metabolism link with glycolysis, as well as how particular metabolic perturbations lead to dysfunction or cell death, and how metabolism can be modulated in a targeted manner to counter dysfunction and restore health.

## *Conclusions*

Despite aerobic glycolysis being observed and highly studied for a century, there is still no complete understanding of how it benefits cells. It is commonly, although not exclusively, associated with proliferation, or in some cases an uncommonly high biosynthetic demand without proliferation. Photoreceptors fall into the latter group. There is some evidence that inhibition of glycolysis causes an anabolic deficit of outer segment biosynthesis but there is no direct evidence that glycolytic intermediates form a substantial fraction of photoreceptor biomass – it would be very valuable to test this. Other mechanisms via which aerobic glycolysis benefits anabolic processes comprise an exciting current active field of cell metabolism research.

The metabolic situation in photoreceptors is complicated by the fact that they must maintain a continuous high rate of ATP synthesis for function in addition to their biosynthetic burden. Glycolysis is necessary for a large portion of ATP production in photoreceptors. Mostly, this is due to its production of pyruvate which feeds the TCA cycle and OXPHOS. Glycolysis itself generates less ATP than OXPHOS in photoreceptors; however, current evidence cannot conclusively rule out that ATP production is the main, or at least an essential, role of aerobic glycolysis in the retina.

It seems that the mammalian retina has evolved to use the maximum amount of fuel and oxygen available to it to gain every ounce of functional capability it can. This has led to it being uniquely vulnerable to diseases that affect the supply or utilisation of oxygen and nutrients. If we can elucidate, in detail, the specific uses of fuel sources and roles of metabolic pathways in the retina, it will undoubtedly reveal new opportunities for treatment of debilitating visual diseases.

In ruling out several candidate pathways, the work in this thesis has contributed to our understanding of the molecular pathways that drive aerobic glycolysis in the retina. Discovery of the pathways responsible may shed light on the reason for aerobic glycolysis in the retina and, importantly, will provide targets for the development of therapeutics that modulate metabolism in the fight against retinal disease.

# Appendices

# *Appendix 1: Example full western blots*

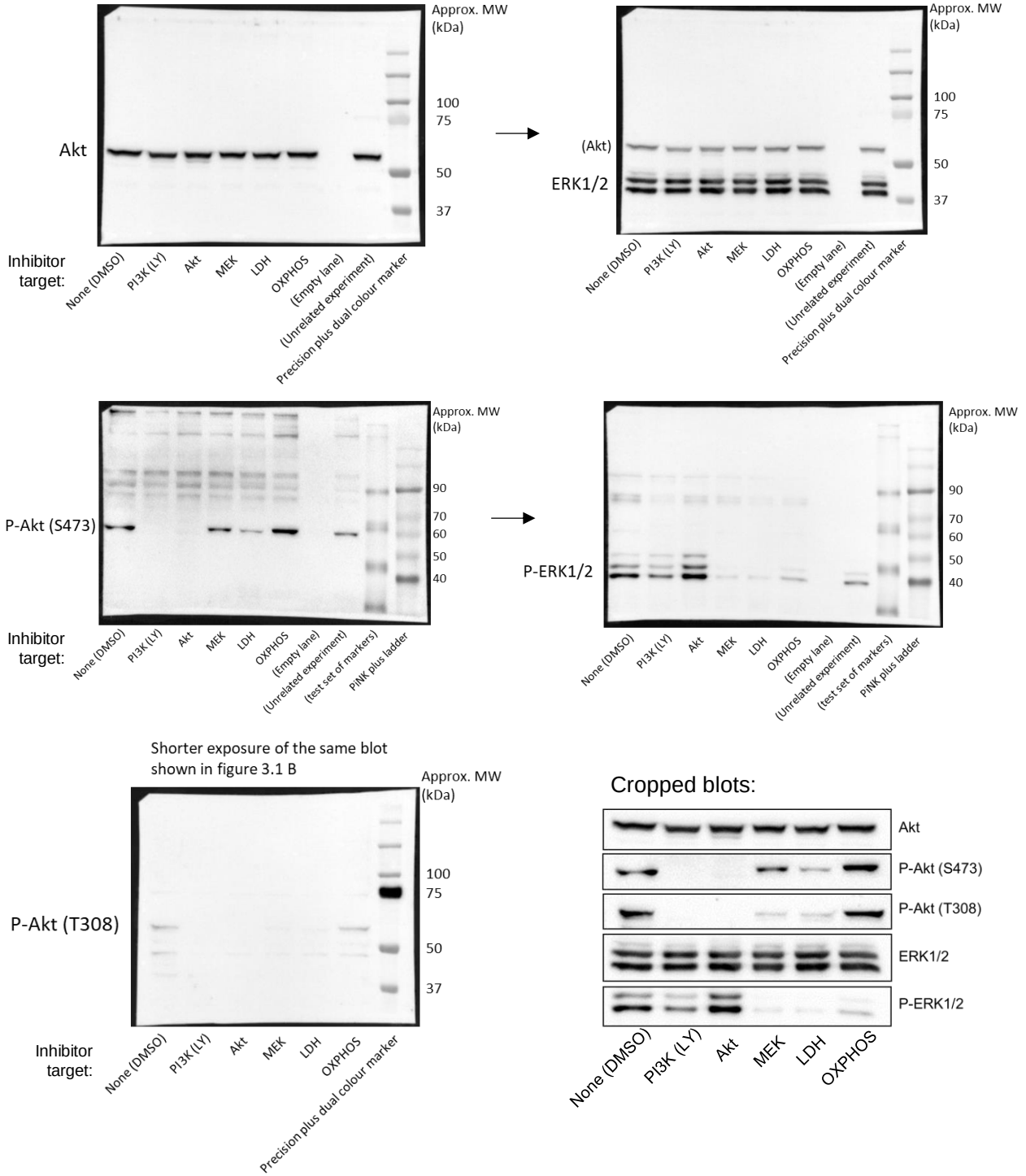


**Figure A.1 Full western blots for Figure 3.1 B.** rMC-1 cells were treated with PI3K inhibitor LY294002 (LY) (30 µM), Akt inhibitor MK-2206 (10 µM), MEK inhibitor PD98059 (30 µM), lactate dehydrogenase (LDH) inhibitor oxamate (50 mM), oxidative phosphorylation (OXPHOS) inhibitor Antimycin A (1 µM), or vehicle (DMSO, 1:1000) for 2 h, then culture medium was changed, and cells treated for a further 6 h before extracts were taken for western blots for the target protein indicated. P-Akt indicates detection of phosphorylation of Akt at the positions stated. P-ERK1/2 indicates detection of phosphorylation of ERK1, at positions T202 and Y204, and ERK2, at positions T185 and Y187. Arrows indicate sequential probing of the same membrane for a different target.

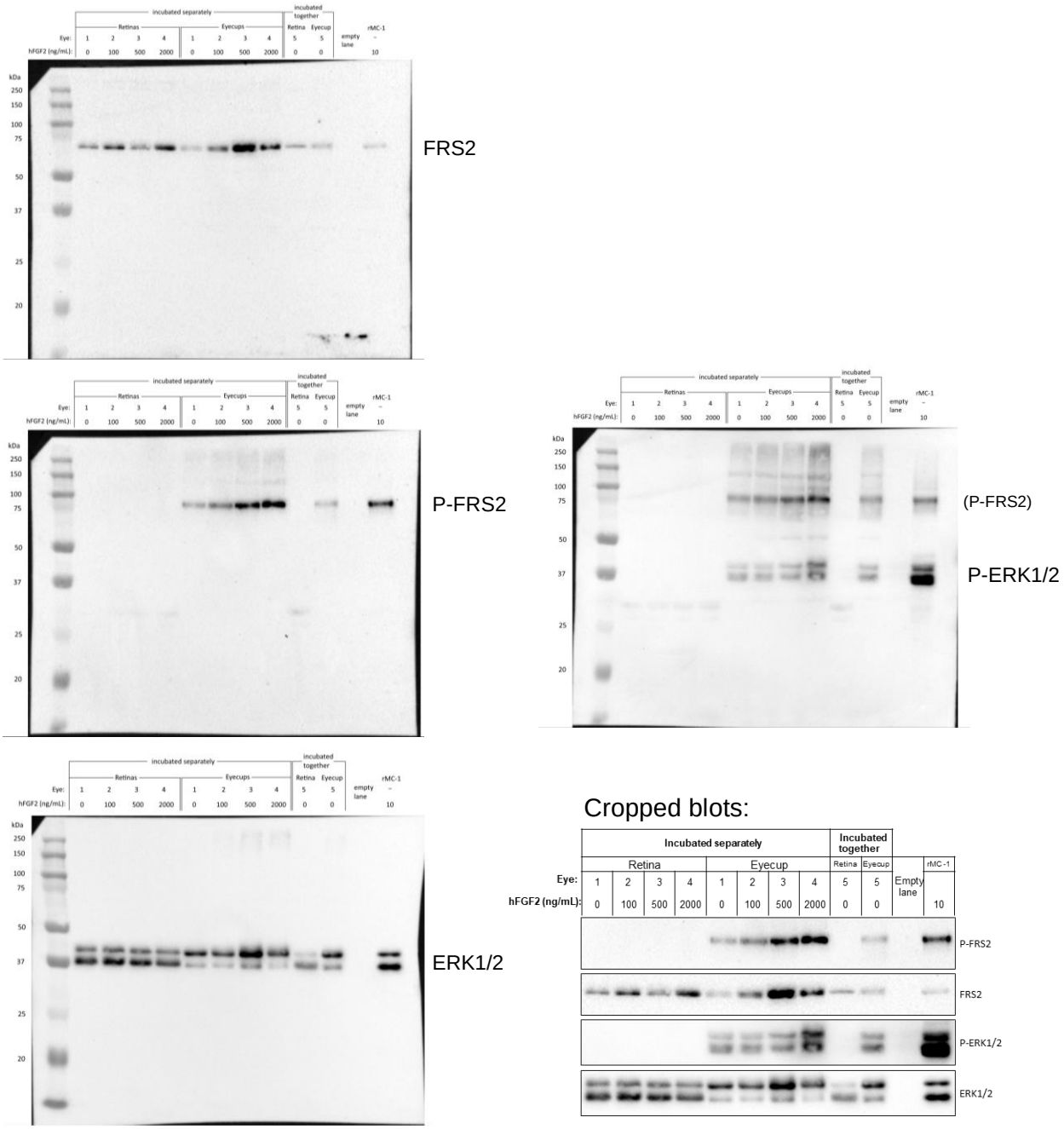


**Figure A.2 Full western blots for Figure 5.3 C.** Rat retinal explants and eyecups were cultured in 1 mL of MEM with 5.56 mM D-glucose and 0.8 mM L-glutamine in a humidified 37 °C incubator in an atmosphere of 5% CO2 in air for 1 h in the presence of the stated concentration of human fibroblast growth factor 2 (hFGF2). rMC-1 cells treated with hFGF2 were included as a positive control. Protein extracts were prepared, and western blots performed for the indicated target proteins. Arrows indicate sequential probing of the same membrane for a different target. Precision plus dual color marker was used in all blots.

# *Appendix 2: Characterization of the novel spontaneously immortalized rat Müller cell line SIRMu-1*

See over page.

# Statement of Authorship

| | |
|---|---|
| Title of Paper | Characterization of the novel spontaneously immortalised rat Müller cell line SIRMu-1 |
| Publication Status | ☑ Published ☐ Accepted for Publication<br>☐ Submitted for Publication ☐ Unpublished and Unsubmitted work written in manuscript style |
| Publication Details | Kittipassorn T, Haydinger CD, Wood JPM, Mammone T, Casson RJ, Peet DJ. Characterization of the novel spontaneously immortalized rat Müller cell line SIRMu-1. Exp Eye Res. 2019 Apr;181:127-135. doi: 10.1016/j.exer.2019.01.013. Epub 2019 Jan 21. PMID: 30677389. |

## Candidate (Co-Author)

| | | | |
|---|---|---|---|
| Name of Co-Author (Candidate) | Cameron D Haydinger | | |
| Contribution to the Paper | Planned experiments. Interpreted the results. Analysed data for and generated Figure 4 and Supplementary Figure S1. Wrote parts of the manuscript: the methods for analysing mRNA sequencing data (subsection 2.7 in the Materials and Methods section), and together with the primary author, Thaksaon Kittipassorn, the results of the mRNA sequencing (subsection 3.4 in the results section). Reviewed and edited the manuscript. | | |
| Overall percentage (%) | 15 | | |
| Certification: | This paper reports on original research I conducted during the period of my Higher Degree by Research candidature and is not subject to any obligations or contractual agreements with a third party that would constrain its inclusion in this thesis. | | |
| Signature | | Date | |

## Other Author Contributions

By signing the Statement of Authorship, each author certifies that:

i. the candidate's stated contribution to the publication is accurate (as detailed above);

ii. permission is granted for the candidate in include the publication in the thesis; and

iii. the sum of all author contributions is equal to 100%

| | | | |
|---|---|---|---|
| Name of Primary Author | Thaksaon Kittipassorn | | |
| Contribution to the Paper | Conceived the project. Planned experiments. Established, isolated and maintained the SIRMu-1 cell line in culture. Conducted most of the experimental work. Interpreted the results. Generated Table 2, Figure 1, Figure 2, Figure 3 and Figure 4D. Contributed to Table 1, Figure 4 and Supplementary Figure S1. Wrote most of the manuscript. Reviewed and edited the manuscript.<br>% Contribution: 65 | | |
| Signature | | Date | 18/5/2022 |

| | | | |
|---|---|---|---|
| Name of Co-Author | John PM Wood | | |
| Contribution to the Paper | Planned experiments. Provided primary cell cultures. Together with the author, Thaksaon Kittipassorn, conducted experiments for Figure 3. Interpreted the results. Reviewed and edited the manuscript. | | |
| Signature | | Date | 180522 |

| Name of Co-Author | Teresa Mammone | | |
|---|---|---|---|
| Contribution to the Paper | Provided primary cell cultures. Together with the author, Thaksaon Kittipassorn, contributed to Table 1. Reviewed and edited the manuscript. | | |
| Signature | | Date | 20/05/2022 |

| Name of Co-Author | Robert J Casson | | |
|---|---|---|---|
| Contribution to the Paper | Conceived and supervised the project. Planned experiments. Interpreted the results. Reviewed and edited the manuscript. | | |
| Signature | | Date | 18 May 2022 |

| Name of Co-Author | Daniel J Peet | | |
|---|---|---|---|
| Contribution to the Paper | Conceived and supervised the project. Planned experiments. Interpreted the results. Reviewed and edited the manuscript. | | |
| Signature | | Date | 27/4/2022 |

Experimental Eye Research 181 (2019) 127–135

Contents lists available at ScienceDirect

Experimental Eye Research

journal homepage: www.elsevier.com/locate/yexer

# Characterization of the novel spontaneously immortalized rat Müller cell line SIRMu-1

Thaksaon Kittipassorn[a,1], Cameron D. Haydinger[a], John P.M. Wood[b], Teresa Mammone[b], Robert J. Casson[b], Daniel J. Peet[a,*]

[a] School of Biological Sciences, Molecular Life Sciences Building, University of Adelaide, Adelaide, SA, 5005, Australia
[b] Department of Ophthalmology and Visual Sciences, Adelaide Health and Medical Sciences Building, University of Adelaide, Adelaide, SA, 5000, Australia

ARTICLE INFO

*Keywords:*
Müller cell
Spontaneously immortalized cell
SIRMu-1
Retina
Cell culture

ABSTRACT

Müller cells (MCs) play a crucial role in the retina, and cultured MC lines are an important tool with which to study MC function. Transformed MC lines have been widely used; however, the transformation process can also lead to unwanted changes compared to the primary cells from which they were derived. To provide an alternative experimental tool, a novel monoclonal spontaneously immortalized rat Müller cell line, SIRMu-1, was derived from primary rat MCs and characterized. Immunofluorescence, western blotting and RNA sequencing demonstrate that the SIRMu-1 cell line retains similar characteristics to cultured primary MCs in terms of expression of the MC markers cellular retinaldehyde-binding protein, glutamine synthetase, S100, vimentin and glial fibrillary acidic protein at both the mRNA and protein levels. Both the cellular morphology and overall transcriptome of the SIRMu-1 cells are more similar to primary rat MCs than the commonly used rMC-1 cells, a well-described, transformed rat MC line. Furthermore, SIRMu-1 cells proliferate rapidly, have an effectively indefinite life span and a high transfection efficiency. The expression of Y chromosome specific genes confirmed that the SIRMu-1 cells are derived from male MCs. Thus, the SIRMu-1 cell line represents a valuable experimental tool to study roles of MCs in both physiological and pathological states.

## 1. Introduction

Müller cells (MCs) are the major type of glial cell of the vertebrate retina. They have diverse functions, including mechanical support of the neural retina, removal of neurotransmitters from the extracellular space, spatial buffering of potassium cations, storage of glycogen, and possible transfer of substrates for cellular metabolic reactions to neighboring neurons (Bringmann et al., 2006; Vecino et al., 2016). Since they span the entire thickness of the retina, MCs have also been proposed to guide light through other retinal layers to photoreceptors in the outer nuclear layer, reducing light scattering and increasing visual acuity (Franze et al., 2007; Labin and Ribak, 2010). MCs undergo reactive gliosis in retinal diseases and injuries (Bringmann et al., 2006; Vecino et al., 2016). Stressed MCs have also been shown to dedifferentiate into multipotent progenitor cells which can subsequently differentiate into retinal neurons, including photoreceptors (Bringmann et al., 2006; Jadhav et al., 2009; Jayaram et al., 2014; Lawrence et al., 2007; Ramirez et al., 2012; Vecino et al., 2016). Experimental systems using cultured primary MCs enable detailed biochemical analysis of this important cell type, and allow chemical and genetic manipulation (Linser and Moscona, 1979; Sarthy, 1985; Savage et al., 1988). However, analysis of primary cells is restricted by difficulties in acquiring and maintaining the cells, slow proliferation rates, early senescence, and low transfection efficiency (Roque et al., 1997; Sarthy et al., 1998).

As an alternative to primary MCs, numerous studies use immortalized MCs, which proliferate rapidly, do not senesce and are relatively easy to maintain and manipulate. These immortalized MCs have been largely generated by transformation of primary cells with viral oncogenes. The rMC-1 and the RMC HPV-16 E6/E7 rat MC lines, for example, were immortalized by transfecting primary MCs with simian virus 40 (SV40) DNA and by transducing with human papillomavirus (HPV) type 16 E6 and E7 viral construct, respectively (Roque et al., 1997; Sarthy et al., 1998). However, the transformation process can alter other characteristics in addition to proliferation and life span

* Corresponding author.
*E-mail addresses:* thaksaon.kit@mahidol.ac.th (T. Kittipassorn), cameron.haydinger@adelaide.edu.au (C.D. Haydinger), john.wood2@sa.gov.au (J.P.M. Wood), teresa.mammone@adelaide.edu.au (T. Mammone), robert.casson@adelaide.edu.au (R.J. Casson), daniel.peet@adelaide.edu.au (D.J. Peet).
[1] Other affiliation/permanent address. Department of Physiology, Faculty of Medicine Siriraj Hospital, Mahidol University, 2 Wanglang Road, Bangkoknoi, Bangkok, 10700, Thailand.

https://doi.org/10.1016/j.exer.2019.01.013
Received 5 October 2018; Received in revised form 10 January 2019; Accepted 10 January 2019
Available online 21 January 2019

**List of abbreviations**

| | |
|---|---|
| CMF-HBSS | calcium- and magnesium-free Hank's balanced salt solution |
| cpm | count per million reads |
| CRALBP | cellular retinaldehyde-binding protein |
| DAPI | 4′,6-diamidino-2-phenylindole dihydrochloride |
| DEGs | differentially expressed genes |
| FBS | fetal bovine serum |
| FDR | false discovery rate |
| GFAP | glial fibrillary acidic protein |
| GO | gene ontology |
| GS | glutamine synthetase |
| HBSS | Hank's balanced salt solution |
| HPV | human papillomavirus |
| MCs | Müller cells |
| MEM | minimal essential medium |
| mRNA-seq | mRNA sequencing |
| NG2 | neuron glial antigen-2 |
| PBS-HS | horse serum in phosphate-buffered saline |
| PEI | polyethylenimine |
| RPE | retinal pigmented epithelial |
| RPKM | reads per kilobase per million |
| SIRMu | spontaneously immortalized rat Müller cells |
| SIRMu-1 | spontaneously immortalized rat Müller cell line |
| SV40 | simian virus 40 |

compared to primary cells, such as cellular morphology (Sarthy et al., 1998) and metabolism (Bissell et al., 1972). Hence, spontaneously immortalized cell lines which have not been intentionally transformed by exogenous reagents often retain a greater similarity to primary cells than transformed cells, and therefore serve as more relevant experimental tools.

To provide an alternative and valuable model for MC research, we established and characterized a novel spontaneously immortalized rat Müller cell line, SIRMu-1. The MC-like characteristics of this monoclonal line are described in relation to primary rat MCs and the commonly-used transformed rat MC line rMC-1 (Sarthy et al., 1998), including cellular morphology, expression of MC and other retinal cell marker proteins, a comprehensive transcriptomic analysis and transfection efficiency.

## 2. Materials and methods

### 2.1. Primary rat mixed retinal, MC and retinal pigmented epithelial (RPE) cell cultures

Sprague-Dawley rats were used for the generation of primary MC cultures. Handling of these animals conformed to the Australian Code of Practice for the Care and Use of Animals for Scientific Purposes 2004, and the ARVO Statement for the Use of Animals in Ophthalmic and Vision Research. Mixed retinal cell cultures consisting of neurons, photoreceptors and glial cells were prepared from litters of 2–4 day post-natal pups using a trypsin-mechanical digest method as described previously (Wood et al., 2003, 2005). Briefly, freshly dissected rat pup retinas were incubated for 5 min in a shaking water bath in sterile incubation medium (5.4 mM KCl, 116 mM NaCl, 0.096 mM $NaH_2PO_4{\cdot}2H_2O$, 19.5 mM glucose, 0.15 mM $MgSO_4$, 23.8 mM $NaHCO_3$, 3 g/L bovine serum albumin, 10 mg/L phenol red) containing 0.1 mg/ml trypsin. After allowing tissue to settle for an additional 5 min, the trypsin/incubation medium was removed and replaced with incubation medium containing 1000 U DNAse (bovine pancreas, type II), soybean trypsin inhibitor (type I-S, 0.667 mg/ml) and 0.19 mM $MgSO_4$. After a further 5 min, trituration was carried out with a flame-rounded glass pipette until all tissue had been dissociated. After a brief centrifugation (180 g/5 min/4 °C) dissociated retinal cells were resuspended and then grown in minimal essential medium (MEM, +Earle's Salts, -L-glutamine, #11090, Life Technologies Australia, Scoresby, VIC, Australia) containing 10% fetal bovine serum (FBS), 87 mg/L gentamicin sulfate, 2.2 mg/L amphotericin B, 25 mM glucose and 2 mM L-glutamine. 25 mM glucose was used to facilitate attachment of primary cells in mixed retinal cell cultures. Cultures were maintained in a humidified incubator at 37 °C, 5% $CO_2$ without disruption for 7 days, and then continuously maintained with medium changed every 3 days for 28–42 days until almost all other cell types died and detached from the culture vessel surface, leaving predominantly MCs (Osborne, 1990; Wood et al., 2005). Once isolated, MC cultures were grown as above but with 20% FBS, and used at passage numbers 2–4 for experiments.

Production of primary RPE cell cultures was based on a method described previously (Mayerson et al., 1985). Litters of 10–12 day old Dark Agouti rat pups were used to generate cultures. Briefly, enucleated eyes from pups were washed in Hank's balanced salt solution (HBSS with 1.26 mM $CaCl_2$, 0.49 mM $MgCl_2.6H_2O$, 0.41 mM $MgSO_4.7H_2O$, #14025-092, Life Technologies Australia), containing 50 µg/ml gentamicin and 100 µg/ml kanamycin. Intact eyes were subsequently incubated in HBSS containing 100 U/ml collagenase and 50 U/ml hyaluronidase for 60 min followed by incubation in calcium- and magnesium-free HBSS (CMF-HBSS) containing 1 mg/ml trypsin for 60 min. Eyes were transferred to growth medium (MEM containing 2 mM L-glutamine, gentamicin/kanamycin as above, and 20% FBS), where they were opened via a circumferential incision immediately below the ora serrata and the anterior segment, and vitreous and retina were discarded. RPE sheets were brushed out of eye-cups in fresh growth medium, rinsed and incubated in CMF-HBSS containing 1 mg/ml trypsin for 5 min. RPE cells were mechanically dissociated, centrifuged (180 g/5 min/4 °C) and adjusted to 1000 cells/$mm^3$ in growth medium. Cultures were maintained in growth medium and were used at passage number 2 for experiments.

### 2.2. Establishment of a spontaneously immortalized rat MC line and monoclonal isolation

Rapidly-proliferating, spontaneously immortalized cells were derived from primary MCs in a mixed retinal cell culture and cultured in MEM containing 20% FBS (unless otherwise stated), 25 mM glucose and 2 mM glutamine at 37 °C with 5% $CO_2$. Cells were cultured in 25 mM glucose to keep the growth conditions consistent with the primary retinal cultures. A monoclonal line was isolated from these cells by 2 sequential rounds of single cell cloning by serial dilution. For each round, 4000 cells were added to well A1 of a 96-well plate. Serial ½ dilutions were performed vertically down the first column on the plate (wells A1-A8). Each of these wells were then serially diluted ½ horizontally across the plate. Culture medium was added to each well to give a final volume of 200 µl, and plates incubated for 14–20 days. Single clones were selected as a single colony of growth at the highest dilutions across the plate. After 2 sequential rounds of single cell isolation 8 monoclonal lines were generated, all of which retained a similar morphology to primary MCs and a rapid proliferation. One was expanded and named the spontaneously immortalized rat Müller cell line SIRMu-1. SIRMu-1 cells of passage numbers 6–22 were used for experiments.

### 2.3. Culture of the rMC-1 cell line

The rMC-1 cells were a kind gift of Dr Vijay Sarthy (Northwestern University, Chicago, IL, USA), obtained from Dr Binoy Appukuttan (Flinders University, Adelaide, SA, Australia), and maintained under

the same conditions as the SIRMu-1 line but with 10% FBS. Cells of passage numbers 23–34 were used for experiments.

### 2.4. Immunocytochemical analysis

Immunofluorescence was performed as previously described (Wood et al., 2012) with minor modifications as outlined below. Cells seeded on coverslips, coated with 0.2% gelatin in phosphate-buffered saline (PBS), were fixed with 4% paraformaldehyde/PBS for 20 min, washed with PBS, permeabilized by incubating in 0.1% triton X-100/PBS for 15 min at room temperature, washed with PBS, and blocked with 3.3% (v/v) horse serum/PBS (PBS-HS) for 15 min at room temperature. Primary antibody incubation was performed overnight at room temperature using antibodies diluted in PBS-HS against vimentin, SV40 T-antigen, S100, glial fibrillary acidic protein (GFAP), rhodopsin, blue cone opsin, tau, CD11b, neuron glial antigen-2 (NG2), and RPE65 (Table 1). The following day, cells were incubated for 1 h at room temperature with secondary antibodies (1:250 to 1:500 dilutions; Life Technologies Australia): anti-mouse Alexa Fluor 594 (#A11005, #A21203), anti-rabbit Alexa Fluor 594 (#A21207), anti-rabbit Alexa Fluor 488 (#A21206), and anti-goat Alexa Fluor 594 (#A11058) antibodies. Nuclear counterstaining was performed with 500 ng/mL 4′,6-diamidino-2-phenylindole dihydrochloride (DAPI; #D8417, Sigma-Aldrich, Castle Hill, NSW, Australia). Cell coverslips were mounted onto glass slides with a fluorescence-protecting mounting medium (ProLong Gold Antifade Mountant, #P10144, Life Technologies Australia) and visualized using fluorescence microscopy (Nikon Eclipse Ti microscope, Nikon Australia, Rhodes, NSW, Australia).

### 2.5. Western blotting

Protein lysates were prepared in whole cell extract buffer (20 mM HEPES pH 7.8, 0.42 M NaCl, 0.5% Igepal, 25% glycerol, 0.2 mM EDTA, 1.5 mM $MgCl_2$ with freshly added 1 mM DTT, 1 mM PMSF, 2 μg/mL aprotinin, 4 μg/mL bestatin, 5 μg/mL leupeptin, and 1 μg/ml pepstatin), and quantified by Bio-rad protein assay (#5000006, Bio-Rad Laboratories, Gladesville, NSW, Australia). Equivalent amounts of total protein were separated on 10% SDS-PAGE and transferred to nitrocellulose membranes using a Trans-Blot Turbo Transfer System (Bio-Rad Laboratories). Membranes were blocked with 10% (w/v) skimmed milk in PBS containing 0.1% nonionic detergent (TWEEN20, #P1379, Sigma-Aldrich) for 1 h at room temperature, incubated overnight at 4 °C with primary antibodies for glutamine synthetase (GS), cellular retinaldehyde-binding protein (CRALBP), and α-tubulin (Table 1) diluted in 2% skimmed milk in 0.1%TWEEN20/PBS, and detected using horseradish peroxidase-conjugated secondary antibodies (goat anti-mouse IgG, #31430, Life Technologies Australia, and goat anti-rat IgG, #ab6845, Abcam, Melbourne, VIC, Australia; both at 1:5000 dilution) and visualized using chemiluminescence and a Bio-Rad ChemiDoc Imaging system (Bio-Rad Laboratories).

### 2.6. mRNA sequencing (mRNA-seq)

Primary MCs, SIRMu-1 and rMC-1 cells were trypsinised, pelleted and RNA extracted with a *mir*Vana miRNA Isolation Kit (#AM1561, Life Technologies Australia). RNA samples (4 biological replicates of primary MCs of passage numbers 3–4, 5 of SIRMu-1 cells of passage numbers 6–20, and 3 of rMC-1 cells of passage numbers 23–26 (Table 1 in Kittipassorn et al., 2019)) were submitted to the Australian Cancer Research Foundation (ACRF) Cancer Genomics Facility (Adelaide, SA, Australia), quality determined with an Agilent RNA 6000 Nano kit (#5067-1511, Agilent Technologies, Santa Clara, CA, USA) on an Agilent 2100 bioanalyzer and concentrations determined using a Qubit RNA HS assay kit (#Q32852, Life Technologies Australia). 5 ng of enriched polyA RNA was used for library preparation by a KAPA stranded RNAseq HyperPrep kit (#KK8544, KAPA, Cape Town, South Africa). Briefly, RNA was fragmented (approximate insert length: 200 base-pairs) and converted to cDNA, followed by end-repair and A-tailing. Adapters compatible with Illumina sequencing were ligated to the cDNA with an approximate adapter to molar insert ratio of 200:1, and a post-ligation clean-up to remove excess adapters performed. The libraries were amplified with 10 cycles of PCR and cleaned with 1× ratio of beads. Library sizes and yields were confirmed using an Agilent High Sensitivity DNA kit (#5067-4626, Agilent Technologies) with an Agilent 2100 bioanalyzer and diluted to 4 nM stocks. Libraries were pooled in equimolar ratios and sequenced on an Illumina NextSeq 500 system using a 75 cycle high output kit (#FC-404-2005, Illumina, San Diego, CA, USA).

### 2.7. Analysis of mRNA-seq data

Sequencing reads were mapped to the reference rat genome (Rnor_6.0) using the STAR algorithm (Dobin et al., 2013). Raw count data were imported into R. Genes that were either not expressed or expressed at very low levels (not detected at greater than one count per million reads (cpm) for all samples of at least one group) were filtered out of the analysis. Counts for the remaining genes (10,236 genes) were normalized to library size and composition using the "TMM" method in Bioconductor's EdgeR package (McCarthy et al., 2012; Robinson et al., 2010). The TMM-normalized data were used for generation of the multidimensional scaling plot.

Differential expression was determined using Bioconductor's Limma package which employs a linear modelling approach (Ritchie et al., 2015). A fold-change threshold of 5 with a Benjamini-Hochberg corrected P-value of $< 0.05$ defined whether a gene was differentially expressed (Benjamini and Hochberg, 1995). Gene ontology (GO) analysis was also performed. Overrepresentation of GO-slim biological process terms (PANTHER annotation version 13.1, released 2018-02-03) among lists of differentially expressed genes, relative to the *Rattus norvegicus* reference list, was assessed using the PANTHER statistical overrepresentation test (released 2017-12-05) (Mi et al., 2017). Fisher's exact test with false discovery rate (FDR) correction was used, and terms with a FDR $< 0.05$ were considered overrepresented.

For generation of the heatmap showing expression of MC marker genes, TMM-normalized count data were further normalized to transcript length (downloaded from the Ensembl database, release 91 (Zerbino et al., 2018), Rnor_6.0, INSDC Assembly GCA_000001895.4) to obtain reads per kilobase per million (RPKM) for each gene, and log-transformed by taking $\log_2$ (RPKM + 1).

**Table 1**
Primary antibodies used in the present study.

| Target protein | Species | Source[a] | Cat. No./clone | Dilution |
|---|---|---|---|---|
| vimentin | mouse | DAKO | V9 | 1:500$^{IF}$ |
| SV40 T-antigen | mouse | Abcam | AB16879 | 1:50$^{IF}$ |
| S100 | rabbit | Sigma-Aldrich | S2644 | 1:50$^{IF}$ |
| GFAP | rabbit | DAKO | Z033429 | 1:100$^{IF}$ |
| GS | mouse | BD Bioscience | 610517 | 1:250$^{WB}$ |
| CRALBP | mouse | Life Technologies | MA1-813 | 1:250$^{WB}$ |
| α-tubulin | rat | Novus Biologicals | NB600-506 | 1:2000$^{WB}$ |
| rhodopsin | mouse | Abcam | AB3267 | 1:1000$^{IF}$ |
| blue cone opsin | goat | Santa Cruz | SC-14363 | 1:2000$^{IF}$ |
| Tau | rabbit | DAKO | A0024 | 1:5000$^{IF}$ |
| CD11b | mouse | Ab D Serotec | MCA275R | 1:500$^{IF}$ |
| NG2 | rabbit | Merk Millipore | AB5320 | 1:1000$^{IF}$ |
| RPE65 | mouse | Santa Cruz | SC-53489 | 1:1000$^{IF}$ |

[a] Source location: Abcam, Melbourne, VIC, Australia; Ab D Serotec, Kidlington, UK; BD Bioscience, Franklin Lakes, NJ, USA; DAKO, Sydney, NSW, Australia; Life Technologies Australia, Scoresby, Victoria, Australia; Merk Millipore, North Ryde, NSW, Australia; Novus Biologicals, Littleton, CO, USA; Santa Cruz Biotechnology, Paso Robles, CA, USA; Sigma-Aldrich, Castle Hill, NSW, Australia, $^{IF}$dilution used for immunofluorescence; $^{WB}$dilution used for western blotting.

### 2.8. Transfection efficiency

SIRMu-1 and rMC-1 cells were seeded into a 24-well plate (20,000 cells per well), and transfected 20–24 h later with a plasmid encoding nuclear Tomato fluorescence protein (500 ng per well) using either FuGENE HD (#E2311, Promega Australia, Alexandria, NSW, Australia), FuGENE 6 (#E2692, Promega Australia), Lipofectamine 2000 (#11668019, Life Technologies Australia) or Polyethylenimine (PEI) (#23966-1, Polysciences, Warrington, PA, USA) according to the manufacturers' instructions, at a transfection reagent:DNA ratio of 3:1. 24 h after transfection the cells were labelled with Hoechst 33342 nuclear stain (NucBlue Live ReadyProbes Reagent, #R37605, Life Technologies Australia) and imaged using fluorescence microscopy (Nikon Eclipse Ti microscope, Nikon Australia). Transfection efficiency was calculated from proportions of Tomato fluorescence-positive transfected cells to total cell numbers indicated by nuclear staining. Cell counts were performed on three different fields of vision for each sample using the Fiji (a distribution of ImageJ) software (Schindelin et al., 2012). Data are presented as mean ± SD of 3 independent experiments.

## 3. Results

### 3.1. Establishment and initial characterization of spontaneously immortalized rat Müller cells

Primary MC cultures were generated by continuous culturing for 28–42 days of mixed retinal cells derived from neonatal rat retinas, resulting in the loss of retinal neurons and other cell types to leave an almost homogeneous population of MCs (Osborne, 1990; Wood et al., 2005). The cultured primary MCs were typically large, flat and adherent with a unique "ghost-like" morphology, and a large nucleus (Fig. 1A) (Roque et al., 1997; Sarthy, 1985; Sarthy et al., 1998; Vecino et al., 2016; Wood et al., 2005). Primary rat MCs proliferate with a doubling time of approximately 7 days and typically senesce after 4 to 8 divisions.

After 28 days of culturing a batch of neonatal rat mixed retinal cells, a visible colony of rapidly-proliferating cells was observed. These large cells had a similar morphology to primary MCs (Fig. 1A). The proliferating cells were passaged and continued to rapidly proliferate beyond 12 weeks, well after the time which primary MCs would typically senesce (Sarthy, 1985). The doubling time of these cells was approximately 2–3 days, and they retained a MC-like morphology. As these cells had survived for more than 12 weeks *in vitro*, had been derived under the commonly-used conditions to generate primary MC cultures and had a characteristic morphology of MCs, it was hypothesized that they originated from primary MCs, and not another retinal cell type. These cells were maintained in culture, being passaged at 1:10 every 5–7 days. After 30 passages (approximately 7 months) these cells still proliferated rapidly and maintained a morphology similar to primary MCs (data not shown). Arising from primary cultures without having been transformed, they were named spontaneously immortalized rat Müller cells (SIRMu).

Initial characterization was performed on early passage number cells (passage number 6) to confirm that these SIRMu cells display common features of MCs. Analysis by immunocytochemistry clearly shows that the MC marker vimentin is expressed in the cytoplasm of every cell, similar to primary MCs and the transformed rMC-1 cell line (Fig. 1B). Since the SIRMu cells were established while the transformed rMC-1 cells were being cultured in the same facility, it was important to confirm that the SIRMu cells were unique, and not simply a potential contamination of primary MCs with rMC-1 cells, although the smaller, more elongated and spindle-like morphology of the rMC-1 cells (Fig. 1A) indicated that such a contamination was unlikely. Hence, the SIRMu cells were labelled for expression of the SV40 T-antigen used to generate the rMC-1 cells (Sarthy et al., 1998). Fig. 1C shows that as expected the rMC-1 cells label strongly for the nuclear SV40 T-antigen, while both the primary MCs and the SIRMu cells do not show any staining, demonstrating that the SIRMu cells are a unique line of spontaneously immortalized cells. These SIRMu cells have now been continuously cultured for more than 32 months and passaged over 140 times (greater than 400 population doublings), consistent with

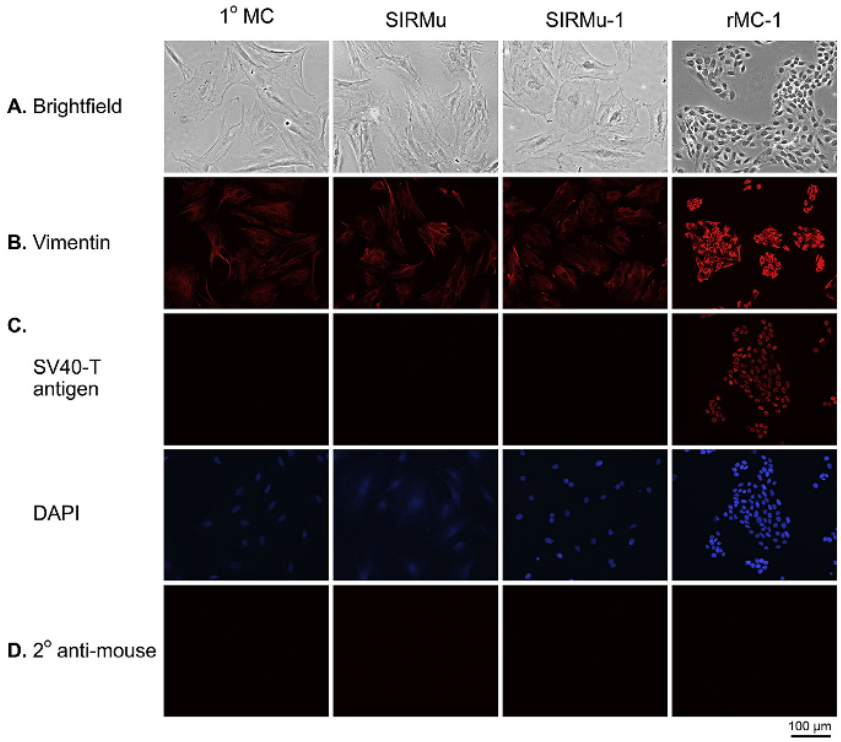


**Fig. 1.** Initial characterization of SIRMu and SIRMu-1 cells. Immunocytochemistry was performed on primary (1°) MCs, SIRMu, SIRMu-1 and rMC-1 cells. (**A**) Phase contrast images of cells fixed with 4% paraformaldehyde/PBS. Cells were labelled with primary antibodies targeting (**B**) vimentin and (**C**) SV40 T-antigen. (**D**) Anti-mouse Alexa Fluor 594 secondary (2°) antibody control, in the absence of primary antibody, for B and C. DAPI was used for nuclear staining. Scale bar = 100 µm and applies to all images.

effectively indefinite growth (Pirisi et al., 1987; Roque et al., 1997).

### 3.2. Monoclonal isolation of the SIRMu cells

To ensure purity of this spontaneously immortalized line, we generated a single monoclonal line by performing 2 sequential rounds of cell cloning by serial dilution on the SIRMu cells (from passage 9 of the original preparation). The first passage after the first serial dilution was defined as passage number 1 for the isolated monoclonal line. This monoclonal line had a similar proliferation rate and morphology to the original culture, and was named SIRMu-1. Immunocytochemistry demonstrated that the monoclonal SIRMu-1 cells do not express the SV40 T-antigen and hence were not derived from rMC-1 cells (Fig. 1C).

The SIRMu-1 cell line has been cultured in both 10% and 20% FBS, with estimated doubling times of 36 and 30 h, respectively. To date, it has been passaged over 40 times and has retained a similar morphology to primary MCs.

### 3.3. Marker protein expression of the SIRMu-1 cells

To validate that the SIRMu-1 cells were derived from MCs, immunocytochemistry was performed on primary MCs, SIRMu-1 and rMC-1 cells to detect expression of the commonly used MC markers vimentin and S100, in addition to the glial cell marker GFAP (Lewis et al., 1988; Limb et al., 2002; Roque et al., 1997; Sarthy et al., 1998) (Figs. 1B, 2A and 2B). The SIRMu-1 cells express all of these markers at similar levels to the primary MCs and the rMC-1 cells. Western blotting analysis of two other MC markers, which are associated with mature MCs, GS (Ji et al., 2017; Linser and Moscona, 1979; Sarthy, 1985) and CRALBP (Bunt-Milam and Saari, 1983; Sarthy et al., 1998) (Fig. 2D) show that both the SIRMu-1 and the rMC-1 cells express GS, but at a lower level compared to primary MCs, and that all 3 cell lines express a low level of CRALBP.

In addition to MCs, other retinal cell types can be present in mixed retinal cultures, including rod and cone photoreceptors, neurons, astrocytes, microglia, pericytes, and RPE cells (Wood et al., 2005, 2012). To confirm that the SIRMu-1 cells were not derived from other non-MC cell types, immunofluorescence was performed for expression of rhodopsin (a marker of rod photoreceptors), blue cone opsin (cone photoreceptors), tau (neurons), CD11b (microglia), NG2 (pericytes), and RPE65 (RPE cells) (Fig. 3). In contrast to mixed retinal cultures, in which distinct populations of cells positively label for rhodopsin, blue cone opsin, tau, CD11b and NG2, the SIRMu-1 cells do not show expression of any of these markers, with the exception of NG2 where low levels of staining slightly above background are visible (Fig. 3A–E). As expected, cultured primary rat RPE cells express RPE65, while the SIRMu-1 cells do not (Fig. 3I). Finally, although rat retinal astrocytes can also be immunoreactive to vimentin, S-100, GFAP and GS (Derouiche and Rauen, 1995; Mansour et al., 2008; Vecino et al., 2016), in culture they have a characteristic star shape with a smaller nucleus (Vecino et al., 2016) that is distinct from primary MCs and the SIRMu-1 cells, and they do not express the MC-specific marker CRALBP observed in the SIRMu-1 cells (Fig. 2D). Hence, it is clear that the SIRMu-1 were not derived from astrocytes. Taken together these data strongly support the hypothesis that the SIRMu-1 cells originated from primary MCs rather than any other retinal cell type, and that they retain MC-like characteristics, including their distinct morphology and the expression of MC marker proteins.

### 3.4. Transcriptomic analysis of the SIRMu-1, primary MCs, and the rMC-1

To further characterize the SIRMu-1 cell line, the transcriptomes of the SIRMu-1, primary MC and rMC-1 cells were analysed using mRNA-seq. RNA was isolated from 5 biological replicates of SIRMu-1 cells, 4 of primary MCs, and 3 of the rMC-1. To control for potential differences in gene expression between cell types being due to differences in culture media, 2 out of the 5 SIRMu-1 RNA samples were isolated from cells grown in the presence of the antibiotic gentamicin and the antifungal amphotericin B, to match the culture conditions of the primary MCs, whereas the other 3 samples were isolated from SIRMu-1 cells grown in the absence of these drugs, which is the usual culture condition of SIRMu-1 and rMC-1 cells. The total RNA was polyA enriched, barcoded and sequenced, with 44–84 million reads per sample (60 million average). Transcripts from 10,236 different genes were detected at significant levels in all cells.

Analysis of the sequences obtained showed that on average 98.25% of reads per sample (range of 97.91–98.47%) mapped successfully to the rat genome, confirming that all three lines are of rat origin. Based on overall gene expression, a multidimensional scaling plot shows clustering of the RNA-seq samples (Fig. 4A). Three distinct clusters of samples are evident, each representing one of the distinct cell types, indicating that the sequencing results were consistent among replicates within the same cell groups. Importantly, the multidimensional scaling plot demonstrates that the transcriptome of the SIRMu-1 cells is more similar to the transcriptome of the primary MCs than the rMC-1 transcriptome is to the primary MCs. These data also demonstrate that there are no large differences in gene expression profiles between all of the 5 SIRMu-1 samples, including the 2 samples derived from cells cultured in medium with gentamicin and amphotericin B, indicating that the two

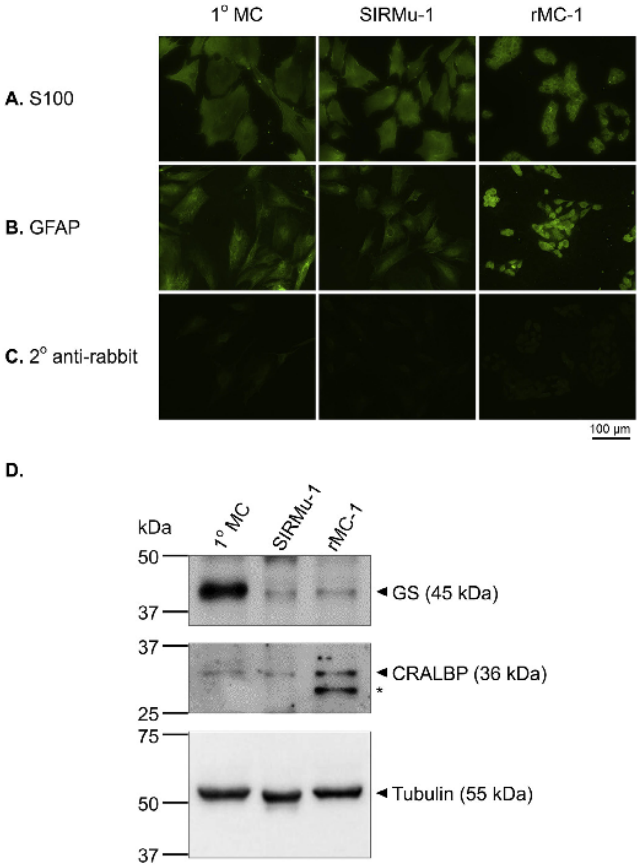


**Fig. 2.** Expression of MC markers in SIRMu-1 cells. Immunocytochemistry was performed on primary (1°) MCs, SIRMu-1 and rMC-1 cells, labelled for (**A**) S100 and (**B**) glial fibrillary acidic protein (GFAP). (**C**) Anti-rabbit Alexa Fluor 488 secondary (2°) antibody control, in the absence of primary antibody, for A and B. Scale bar = 100 µm and applies to all images. (**D**) Western blots of 1° MCs, SIRMu-1 and rMC-1 cells, probed for glutamine synthetase (GS) and cellular retinaldehyde-binding protein (CRALBP). Expected band size of each protein is shown in brackets. Arrows indicate target protein bands and asterisks indicate non-specific bands.

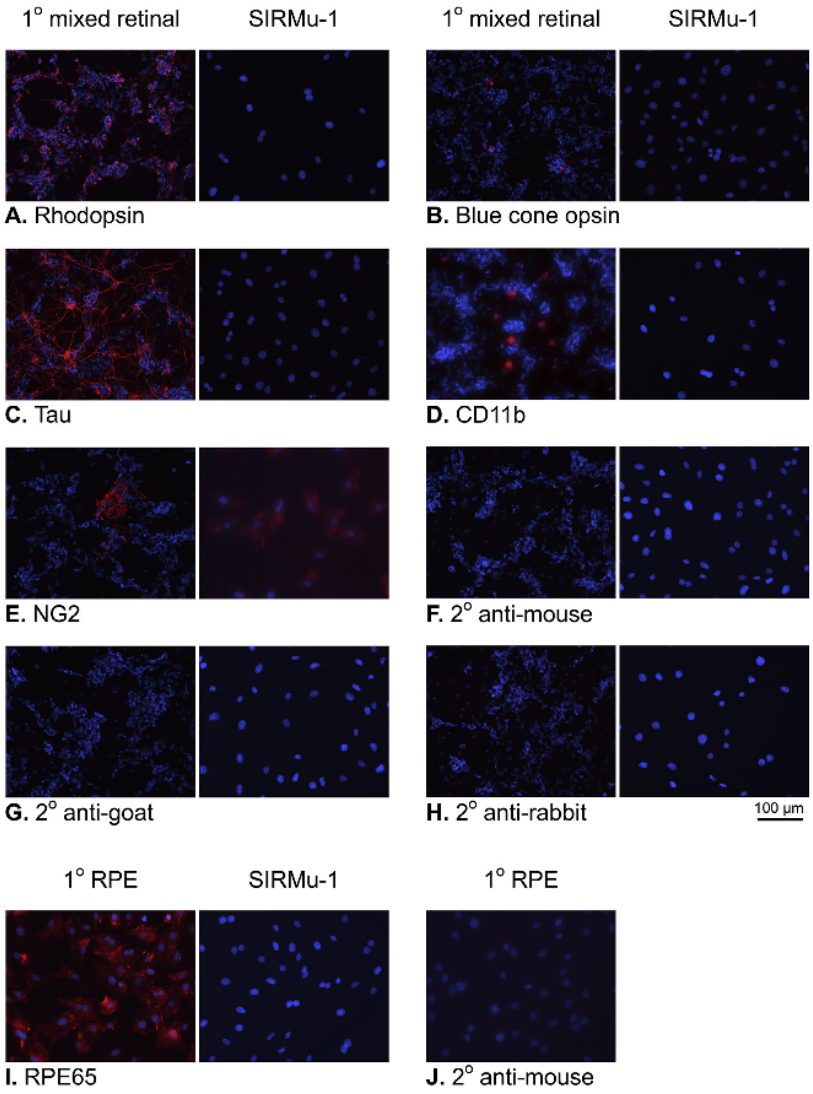


**Fig. 3.** Immunocytochemical analysis of retinal cell markers on SIRMu-1 cells. Primary (1°) mixed retinal cultures and SIRMu-1 cells were labelled for (**A**) rhodopsin, (**B**) blue cone opsin, (**C**) tau, (**D**) CD11b and (**E**) NG2. (**F**) Anti-mouse Alexa Fluor 594 secondary (2°) antibody control, in the absence of primary antibody, for A and D. (**G**) Anti-goat Alexa Fluor 594 secondary antibody control for B. (**H**) Anti-rabbit Alexa Fluor 594 secondary antibody control for C and E. (**I**) 1° retinal pigmented epithelial (RPE) cells and SIRMu-1 cells were stained for RPE65. (**J**) Anti-mouse Alexa Fluor 594 secondary antibody control for 1° RPE in I. See F for SIRMu-1 anti-mouse secondary antibody control. DAPI was used for nuclear staining. Scale bar = 100 µm and applies to all images.

drugs in the growth medium do not have a major effect on the transcriptome.

Transcriptomic differences between groups were further examined by comparing differentially expressed genes (DEGs) between each of the two immortalized cell lines and the primary MCs. Genes that were expressed at very low levels or not expressed in all groups were first filtered out of the analysis, leaving 10,236 genes that were tested for differential expression. Genes that were upregulated or downregulated greater than 5-fold compared to the primary MCs were considered differentially expressed. A total of 10,036 genes (98% of the 10,236 expressed genes) were not differentially expressed in the SIRMu-1 cell line compared to the primary MCs, with 200 genes differentially expressed. Among these 200 DEGs, 13 genes were upregulated and 187 were downregulated (Fig. 4B). In comparison, for the rMC-1 cells 9304 genes (91%) were not differentially expressed compared to the primary MCs, but 932 genes were, with 314 upregulated and 618 downregulated (Fig. 4B). These data indicate that both the SIRMu-1 and rMC-1 cell lines have a similar transcriptome to the primary MCs, but that the SIRMu-1 cells are more closely related to the primary MCs than are the rMC-1 cells.

Interestingly, among the 200 DEGs in the SIRMu-1 compared to primary MCs and the 932 DEGs in the rMC-1 compared to primary MCs, there were 126 genes in common (Supplementary Fig. S1A, Supplementary Table S1). For the remainder of the DEGs, 74 genes were differentially expressed uniquely in the SIRMu-1 cells, while 806 genes were differentially expressed uniquely in the rMC-1 cells (Supplementary Fig. S1A, Supplementary Table S1). To assess functional differences between each immortalized cell line and primary MCs, GO analyses were performed using the PANTHER classification system. The lists of genes differentially expressed in both cell lines with respect to primary MCs were classified by GO-Slim biological process terms, and statistically overrepresented terms were determined by comparison to their frequency in a reference rat genome. There were no statistically significantly (FDR $< 0.05$) overrepresented biological process terms among the 74 genes differentially expressed between SIRMu-1 cells and primary MCs, nor among the 126 genes differentially expressed in both cell lines compared to primary MCs, possibly due in part to the relatively low number of genes in these two groups. However, there was significant overrepresentation of terms among the 806 genes differentially expressed between rMC-1 cells and primary MCs. The top 10 such terms by fold-enrichment are shown in Supplementary Fig. S1B. Consistent with being a highly-proliferative transformed cell line, a large proportion of the DEGs in rMC-1 cells are involved in DNA replication and cell division-related processes.

Next, expression of the transcripts encoding the MC marker proteins were examined. The SIRMu-1 cells express similar levels of transcripts

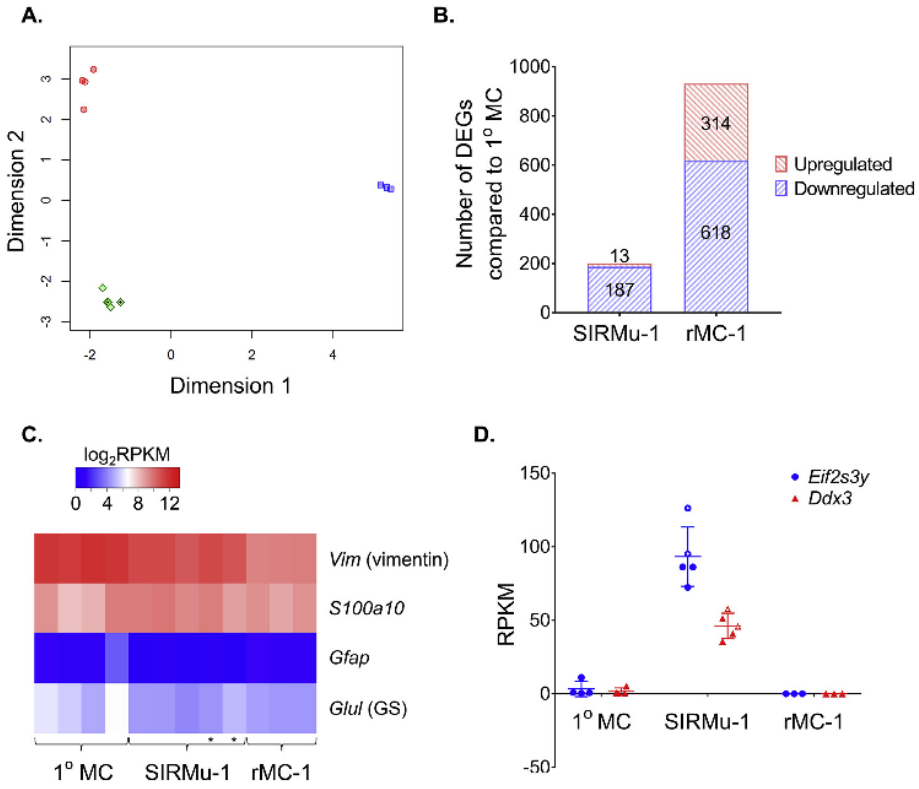


**Fig. 4.** mRNA sequencing of MCs. (**A**) Multidimensional scaling plot of normalized data for 12 RNA-seq samples. Red circles: primary (1°) MCs (4 biological replicates), Blue squares: rMC-1s (3 replicates), Green diamonds: SIRMu-1s (5 replicates). 2 SIRMu-1 samples grown in the presence of the antibiotic gentamicin and the antifungal amphotericin B are indicated by black dots. (**B**) Bar graph showing numbers of significantly differentially expressed genes (DEGs) which were either upregulated or downregulated at a fold-change of greater than 5 in SIRMu-1 and rMC-1 cells compared to 1° MCs. (**C**) Heatmap showing expression levels of MC marker genes. SIRMu-1 samples grown in the presence of gentamicin and amphotericin B are indicated by asterisks. RPKM, reads per kilobase per million. (**D**) Quantification of mRNA expression levels of two Y chromosome specific genes, *Eif2s3y* (blue circles) and *Ddx3* (red triangles), in the 3 MC lines. Expression level expressed in reads per kilobase per million (RPKM). Horizontal lines represent means and error bars ± SD. SIRMu-1 samples grown in the presence of gentamicin and amphotericin B are indicated by white dots.

encoding vimentin, S100, and GFAP to the primary MCs and rMC-1 cells, with transcripts encoding GFAP expressed at low levels (Fig. 4C). SIRMu-1 and rMC-1 cells also express GS transcripts, but at a lower level compared to the primary MCs (Fig. 4C). All cell types express CRALBP transcripts at very low levels with an average of 0.06, 0.15, and 1.16 cpm in primary MCs, SIRMu-1 and rMC-1 cells, respectively. These results are consistent with protein expression from immunocytochemical and western blotting analyses (Figs. 1, 2 and 4C). The relatively small difference in GS mRNA levels observed between primary MCs and the two immortalized lines shown in Fig. 4C is not of the same magnitude as the greater difference in protein levels demonstrated by western blotting in Fig. 2D, which is likely to be a consequence of post-transcriptional regulation.

Importantly, SIRMu-1 and rMC-1 cells express very low to undetectable levels of transcripts encoding rhodopsin, blue cone opsin, tau, CD11b, and RPE65, markers used in the immunofluorescence analysis that are characteristic of other retinal cell types including rod and cone photoreceptors, neurons, microglia, and RPE cells. Of note, while SIRMu-1 cells express transcripts encoding NG2, a pericyte marker, the levels are many fold lower than the vimentin transcripts in these cells (Fig. 4C), and primary MCs and rMC-1 cells also express NG2 at low levels. Together these data show that the SIRMu-1 cells display a MC-like transcriptomic profile, and also authenticate the MC characteristics of the rMC-1 cells used in the present study.

Finally, we examined the expression of gender-specific genes between the three different MC types. Compared to primary MCs, which were derived from mixed litters presumed to contain both male and female pups, the SIRMu-1 cells show an upregulation of two Y chromosome-specific genes, *Eif2s3y* and *Ddx3* (Fig. 4D), consistent with the SIRMu-1 cell line originating from a male pup. In contrast, *Eif2s3y* and *Ddx3* were not expressed at significant levels in the rMC-1 cell samples (Fig. 4D), nor were any other Y chromosome-specific genes, consistent with the rMC-1 cell line being derived from a female rat.

### 3.5. Transfection efficiency

One key advantage of most immortalized cell lines is high transfection efficiency with standard transfection reagents, such as cationic lipids, compared to primary cells. To determine transfection efficiency of the SIRMu-1 cell line, various commercially-available lipid-based transfection reagents were used to transfect SIRMu-1 cells with a fluorescence reporter gene, and transfection efficiency was measured using fluorescence microscopy (Table 2). The transfection efficiency of the SIRMu-1 cells is between 7 and 14%, which is similar to that achieved with the rMC-1 cells (6–24%), and approximately 10-fold higher than what we observed with the primary MCs (1.9%).

## 4. Discussion

Immortalized rat MC lines generated via transformation, such as rMC-1 (Sarthy et al., 1998), RMC HPV-16 E6/E7 (Roque et al., 1997) and TR-MUL5 (Tomi et al., 2003), have been used extensively for the analysis of MC function. Similar to the spontaneously immortalized human MC line MIO-M1 (Limb et al., 2002) and the spontaneously immortalized murine MC line QMMuC-1 (Augustine et al., 2018) serving as an alternative model for studying human and mouse MCs, respectively, the spontaneously immortalized SIRMu-1 cells described

**Table 2**
Transfection efficiency of SIRMu-1 and rMC-1 cells.

| Transfection reagent | SIRMu-1[a] | rMC-1[a] |
|---|---|---|
| FuGENE HD | 14 ± 7 | 16 ± 1 |
| FuGENE 6 | 7 ± 6 | 6 ± 2 |
| Lipofectamine 2000 | 13 ± 3 | 24 ± 6 |
| PEI[b] | 12 ± 2 | 15 ± 2 |

[a] Data are presented as mean ± SD of % transfection efficiency from 3 independent experiments.
[b] PEI, polyethylenimine.

here provide an alternative system for investigating MC function in rat cells not transformed with viral oncogenes. Although the mechanism of spontaneous immortalization remains to be ascertained, the SIRMu-1 cells appear capable of proliferating indefinitely.

SIRMu-1 cells, like transformed rMC-1 cells, display key characteristics of primary MCs, including the expression of an array of well-characterized MC marker proteins (Figs. 1B and 2) and genes (Fig. 4C). The presence of transcripts encoding the MC markers vimentin, GS and CRALBP (Fig. 4C) in all 3 types of MCs investigated in the present study is consistent with published reports on rat and mouse MC transcriptomes (Roesch et al., 2008; Ueno et al., 2017; Zhao et al., 2015). Furthermore, the lack of expression of key markers indicative of other major retinal cell types (Fig. 3) supports the conclusion that SIRMu-1 cells were derived from primary MCs.

Of note, the results are also consistent with the SIRMu-1 cells having been derived from mature MCs. The SIRMu-1 cells originated from a rat mixed retinal culture made from 2 to 4 day post-natal pups. While the generation of MCs is spread over a long period of retinal development between embryonic day 18 and post-natal day 12, in the rat retina one of the major peaks of MC genesis is between post-natal days 2–4 (Rapaport et al., 2004), where we produce mixed retinal cultures. At post-natal days 2–4, 50% of MCs have developed (Rapaport et al., 2004), supporting the presence of a significant proportion of mature MCs in these cultures. More importantly, similar to the primary MCs and the rMC-1 cells derived from adult rats, the SIRMu-1 cells express CRALBP and GS, which are markers associated with mature MCs (Bunt-Milam and Saari, 1983; Ji et al., 2017; Linser and Moscona, 1979; Sarthy, 1985; Sarthy et al., 1998). The SIRMu-1 cells also display a characteristic cellular morphology of cultured primary adult rat MCs. (Roque et al., 1997; Sarthy, 1985; Sarthy et al., 1998).

While most MC markers were expressed at similar levels when comparing the two immortalized lines and the primary MCs, at both the mRNA and protein levels, the SIRMu-1 and the rMC-1 cell lines express GS at a lower level than the primary MCs (Figs. 2D and 4C). GS catalyzes the conversion of glutamate to glutamine in MCs, playing an important role in the neurotransmitter recycling process, an essential function of MCs in support of retinal neurons (Bringmann et al., 2006; Vecino et al., 2016). The decreased GS expression levels may reflect changes due to extended propagation in culture in the absence of retinal neurons, consistent with previous studies (Germer et al., 1997; Hauck et al., 2003; Lewis et al., 1989, 1999; Roque et al., 1997). Similarly, this may also explain the low expression levels of the MC marker CRALBP in all 3 types of MCs investigated (Fig. 2D). CRALBP in MCs *in vivo* is involved in the recycling of photopigments derived from photoreceptors (Das et al., 1992); the absence of functional light-sensitive photoreceptors and prolonged culture likely leads to a decrease in CRALBP expression (Hauck et al., 2003; Lewis et al., 1989; Pfeffer et al., 2016). In addition, our finding that the cultured MCs express GFAP (Figs. 2B and 4C) is consistent with a number of published studies (Limb et al., 2002; Roque et al., 1997; Sarthy et al., 1998). Given that expression of GFAP can be induced in MCs under reactive gliosis and/or during injury or stress (Bringmann et al., 2006), the presence of GFAP in the SIRMu-1 cell cultures and cultured MCs in other studies above likely reflects differences in culturing MCs compared to their *in vivo* retinal environment. However, the relatively low GFAP expression levels in all 3 MC types in this study suggest that the culture conditions employed do not cause major stress to the cells.

Overall, the transcriptome of the SIRMu-1 cells closely resembles the transcriptome of primary MCs. The rMC-1 cells are also transcriptomically similar to the primary MCs but to a lesser degree than are the SIRMu-1 cells. While the rMC-1 cells do have a greater number of genes showing differential expression when compared to the primary MCs than the SIRMu-1 cells (Fig. 4B), this may be in part a function of the more consistent gene expression profiles among the independent rMC-1 samples (revealed in the close clustering for rMC-1 samples in Fig. 4A). Not surprisingly, genes encoding proteins involved in DNA replication and cell cycle/division were overrepresented in the rapidly-proliferating rMC-1 transcriptomes compared to the primary MCs (Supplementary Fig. S1B). In contrast, DNA replication and cell cycle/division were not overrepresented in the list of genes differentially expressed between the rapidly-proliferating SIRMu-1 cells and the primary MCs, even when the stringency of differential expression was reduced to 2-fold (data not shown). This may reflect differences between transformation with viral oncogenes and the spontaneous immortalization observed here on cell proliferation, or it may be that a transcriptomic analysis of more SIRMu-1 samples is required to detect significant changes in expression of genes contributing to cellular proliferation. Furthermore, the rMC-1 cells were derived from adult rats (Sarthy et al., 1998) which may contribute to the bigger transcriptomic differences observed here between these cells and the primary neonatal rat MCs used in this study, compared to between the SIRMu-1 and the primary MCs. It is important to note, however, that the SIRMu-1 cells retaining the distinct large, flat, ghost-like shape are morphologically similar to both cultured primary adult rat MCs (Roque et al., 1997; Sarthy, 1985; Sarthy et al., 1998) and cultured primary neonatal rat MCs (Wood et al., 2005) (Fig. 1A), in contrast to the smaller, fibroblast-like morphology of the rMC-1 cells (Sarthy et al., 1998) (Fig. 1A). Given the well-established sex-related differences in retinal function (Chaychi et al., 2015; Wagner et al., 2008), the male genotype of SIRMu-1 cells compared to the female genotype of rMC-1 cells (Fig. 4D) also represents another important difference. It is also noteworthy that while the SIRMu-1 cells are transcriptomically and morphologically similar to primary MCs, other metabolic or functional properties of these cells are not compared.

In summary, we present the establishment and characterization of the SIRMu-1 cell line, which to our knowledge is the first spontaneously immortalized cell line derived from primary rat MCs. SIRMu-1 cells display similar morphology and gene expression profiles to primary MCs, but proliferate more rapidly, have an effectively indefinite life span, and are more amenable to transfection. Thus, these SIRMu-1 cells comprise a valuable new tool for investigation of MC function and roles in retinal health and disease.

## Data accessibility

The RNA-seq data discussed in this article have been deposited in NCBI Gene Expression Omnibus (Edgar et al., 2002) and are accessible through GEO ID: GSE123161. (https://www.ncbi.nlm.nih.gov/geo/query/acc.cgi?acc=GSE123161).

## Declarations of interest for all authors

None.

## Funding

This work was supported by a project grant from the National Health and Medical Research Council of Australia (109932). The funding source has no involvement in the conduct of experiments, data analysis and interpretation, the preparation of the manuscript and the decision to submit the work for publication.

## Author contributions

T.K. conceived the project, planned experiments, carried out experimental work, interpreted the results, and wrote the paper. C.D.H. planned experiments, interpreted the results, and wrote the paper. J.P.M.W. planned experiments, provided primary cell cultures, carried out experimental work, interpreted the results, and edited the paper. T.M. provided primary cell cultures, and edited the paper. R.J.C. and D.J.P. conceived and supervised the project, planned experiments, interpreted the results, and edited the paper.

## Acknowledgements

The authors thank Joel Geoghegan, Andreas Schreiber, Wendy Parker and Ming Lin (ACRF Cancer Genomics Facility, Adelaide, SA, Australia) for their assistance with the RNA-seq, and members of the Peet and Whitelaw laboratories and Onruedee Khantisitthiporn (University of Adelaide, SA, Australia) for helpful discussion and technical assistance.

## Appendix A. Supplementary data

Supplementary data to this article can be found online at https://doi.org/10.1016/j.exer.2019.01.013.

## References

Augustine, J., Pavlou, S., O'Hare, M., Harkin, K., Stitt, A., Curtis, T., Xu, H., Chen, M., 2018. Characterization of a spontaneously immortalized murine muller glial cell line QMMuC-1. Invest. Ophthalmol. Vis. Sci. 59, 1666–1674.
Benjamini, Y., Hochberg, Y., 1995. Controlling the false discovery rate: a practical and powerful approach to multiple testing. J. Roy. Stat. Soc. B (Method) 57, 289–300.
Bissell, M.J., Hatie, C., Rubin, H., 1972. Patterns of glucose metabolism in normal and virus-transformed chick cells in tissue culture. J. Natl. Cancer Inst. 49, 555–565.
Bringmann, A., Pannicke, T., Grosche, J., Francke, M., Wiedemann, P., Skatchkov, S.N., Osborne, N.N., Reichenbach, A., 2006. Muller cells in the healthy and diseased retina. Prog. Retin. Eye Res. 25, 397–424.
Bunt-Milam, A.H., Saari, J.C., 1983. Immunocytochemical localization of two retinoid-binding proteins in vertebrate retina. J. Cell Biol. 97, 703–712.
Chaychi, S., Polosa, A., Lachapelle, P., 2015. Differences in retinal structure and function between aging male and female sprague-dawley rats are strongly influenced by the estrus cycle. PLoS One 10, e0136056.
Das, S.R., Bhardwaj, N., Kjeldbye, H., Gouras, P., 1992. Muller cells of chicken retina synthesize 11-cis-retinol. Biochem. J. 285 (Pt 3), 907–913.
Derouiche, A., Rauen, T., 1995. Coincidence of L-glutamate/L-aspartate transporter (GLAST) and glutamine synthetase (GS) immunoreactions in retinal glia: evidence for coupling of GLAST and GS in transmitter clearance. J. Neurosci. Res. 42, 131–143.
Dobin, A., Davis, C.A., Schlesinger, F., Drenkow, J., Zaleski, C., Jha, S., Batut, P., Chaisson, M., Gingeras, T.R., 2013. STAR: ultrafast universal RNA-seq aligner. Bioinformatics 29, 15–21.
Edgar, R., Domrachev, M., Lash, A.E., 2002. Gene Expression Omnibus: NCBI gene expression and hybridization array data repository. Nucleic Acids Res. 30, 207–210.
Franze, K., Grosche, J., Skatchkov, S.N., Schinkinger, S., Foja, C., Schild, D., Uckermann, O., Travis, K., Reichenbach, A., Guck, J., 2007. Muller cells are living optical fibers in the vertebrate retina. Proc. Natl. Acad. Sci. U. S. A 104, 8287–8292.
Germer, A., Jahnke, C., Mack, A., Enzmann, V., Reichenbach, A., 1997. Modification of glutamine synthetase expression by mammalian Muller (glial) cells in retinal organ cultures. Neuroreport 8, 3067–3072.
Hauck, S.M., Suppmann, S., Ueffing, M., 2003. Proteomic profiling of primary retinal Muller glia cells reveals a shift in expression patterns upon adaptation to in vitro conditions. Glia 44, 251–263.
Jadhav, A.P., Roesch, K., Cepko, C.L., 2009. Development and neurogenic potential of Muller glial cells in the vertebrate retina. Prog. Retin. Eye Res. 28, 249–262.
Jayaram, H., Jones, M.F., Eastlake, K., Cottrill, P.B., Becker, S., Wiseman, J., Khaw, P.T., Limb, G.A., 2014. Transplantation of photoreceptors derived from human Muller glia restore rod function in the P23H rat. Stem Cells Transl. Med. 3, 323–333.
Ji, H.P., Xiong, Y., Zhang, E.D., Song, W.T., Gao, Z.L., Yao, F., Sun, H., Zhou, R.R., Xia, X.B., 2017. Which has more stem-cell characteristics: muller cells or Muller cells derived from in vivo culture in neurospheres? Am. J. Transl. Res. 9, 611–619.
Kittipassorn, T., Haydinger, C.D., Wood, J.P.M., Mammone, T., Casson, R.J., Peet, D.J., 2018. RNA sequencing data of cultured primary rat Müller cells, the spontaneously immortalized rat Müller cell line, SIRMu-1, and the SV40-transformed rat Müller cell line, rMC-1. Submitted to Elsevier, Data in Brief.
Labin, A.M., Ribak, E.N., 2010. Retinal glial cells enhance human vision acuity. Phys. Rev. Lett. 104, 158102.
Lawrence, J.M., Singhal, S., Bhatia, B., Keegan, D.J., Reh, T.A., Luthert, P.J., Khaw, P.T., Limb, G.A., 2007. MIO-M1 cells and similar muller glial cell lines derived from adult human retina exhibit neural stem cell characteristics. Stem Cell. 25, 2033–2043.
Lewis, G., Mervin, K., Valter, K., Maslim, J., Kappel, P.J., Stone, J., Fisher, S., 1999. Limiting the proliferation and reactivity of retinal Muller cells during experimental retinal detachment: the value of oxygen supplementation. Am. J. Ophthalmol. 128, 165–172.
Lewis, G.P., Erickson, P.A., Guerin, C.J., Anderson, D.H., Fisher, S.K., 1989. Changes in the expression of specific Muller cell proteins during long-term retinal detachment. Exp. Eye Res. 49, 93–111.
Lewis, G.P., Kaska, D.D., Vaughan, D.K., Fisher, S.K., 1988. An immunocytochemical study of cat retinal Muller cells in culture. Exp. Eye Res. 47, 855–868.
Limb, G.A., Salt, T.E., Munro, P.M., Moss, S.E., Khaw, P.T., 2002. In vitro characterization of a spontaneously immortalized human Muller cell line (MIO-M1). Invest. Ophthalmol. Vis. Sci. 43, 864–869.
Linser, P., Moscona, A.A., 1979. Induction of glutamine synthetase in embryonic neural retina: localization in Muller fibers and dependence on cell interactions. Proc. Natl. Acad. Sci. U. S. A 76, 6476–6480.
Mansour, H., Chamberlain, C.G., Weible 2nd, M.W., Hughes, S., Chu, Y., Chan-Ling, T., 2008. Aging-related changes in astrocytes in the rat retina: imbalance between cell proliferation and cell death reduces astrocyte availability. Aging Cell 7, 526–540.
Mayerson, P.L., Hall, M.O., Clark, V., Abrams, T., 1985. An improved method for isolation and culture of rat retinal pigment epithelial cells. Invest. Ophthalmol. Vis. Sci. 26, 1599–1609.
McCarthy, D.J., Chen, Y., Smyth, G.K., 2012. Differential expression analysis of multifactor RNA-Seq experiments with respect to biological variation. Nucleic Acids Res. 40, 4288–4297.
Mi, H., Huang, X., Muruganujan, A., Tang, H., Mills, C., Kang, D., Thomas, P.D., 2017. PANTHER version 11: expanded annotation data from Gene Ontology and Reactome pathways, and data analysis tool enhancements. Nucleic Acids Res. 45, D183–D189.
Osborne, N.N., 1990. Stimulatory and inhibitory actions of excitatory amino acids on inositol phospholipid metabolism in rabbit retina. Evidence for a specific quisqualate receptor subtype associated with neurones. Exp. Eye Res. 50, 397–405.
Pfeffer, B.A., Xu, L., Porter, N.A., Rao, S.R., Fliesler, S.J., 2016. Differential cytotoxic effects of 7-dehydrocholesterol-derived oxysterols on cultured retina-derived cells: dependence on sterol structure, cell type, and density. Exp. Eye Res. 145, 297–316.
Pirisi, L., Yasumoto, S., Feller, M., Doniger, J., DiPaolo, J.A., 1987. Transformation of human fibroblasts and keratinocytes with human papillomavirus type 16 DNA. J. Virol. 61, 1061–1066.
Ramirez, M., Hernandez-Montoya, J., Sanchez-Serrano, S.L., Ordaz, B., Ferraro, S., Quintero, H., Pena-Ortega, F., Lamas, M., 2012. GABA-mediated induction of early neuronal markers expression in postnatal rat progenitor cells in culture. Neuroscience 224, 210–222.
Rapaport, D.H., Wong, L.L., Wood, E.D., Yasumura, D., LaVail, M.M., 2004. Timing and topography of cell genesis in the rat retina. J. Comp. Neurol. 474, 304–324.
Ritchie, M.E., Phipson, B., Wu, D., Hu, Y., Law, C.W., Shi, W., Smyth, G.K., 2015. Limma powers differential expression analyses for RNA-sequencing and microarray studies. Nucleic Acids Res. 43, e47.
Robinson, M.D., McCarthy, D.J., Smyth, G.K., 2010. edgeR: a Bioconductor package for differential expression analysis of digital gene expression data. Bioinformatics 26, 139–140.
Roesch, K., Jadhav, A.P., Trimarchi, J.M., Stadler, M.B., Roska, B., Sun, B.B., Cepko, C.L., 2008. The transcriptome of retinal Muller glial cells. J. Comp. Neurol. 509, 225–238.
Roque, R.S., Agarwal, N., Wordinger, R.J., Brun, A.M., Xue, Y., Huang, L.C., Nguyen, L.P., Shay, J.W., 1997. Human papillomavirus-16 E6/E7 transfected retinal cell line expresses the Muller cell phenotype. Exp. Eye Res. 64, 519–527.
Sarthy, P.V., 1985. Establishment of Muller cell cultures from adult rat retina. Brain Res. 337, 138–141.
Sarthy, V.P., Brodjian, S.J., Dutt, K., Kennedy, B.N., French, R.P., Crabb, J.W., 1998. Establishment and characterization of a retinal Muller cell line. Invest. Ophthalmol. Vis. Sci. 39, 212–216.
Savage, F.J., Day, J.E., Hogg, P., Grierson, I., 1988. Tissue culture of retinal glial cells. Eye 2 (Suppl. l), S164–S179.
Schindelin, J., Arganda-Carreras, I., Frise, E., Kaynig, V., Longair, M., Pietzsch, T., Preibisch, S., Rueden, C., Saalfeld, S., Schmid, B., Tinevez, J.Y., White, D.J., Hartenstein, V., Eliceiri, K., Tomancak, P., Cardona, A., 2012. Fiji: an open-source platform for biological-image analysis. Nat. Methods 9, 676–682.
Tomi, M., Funaki, T., Abukawa, H., Katayama, K., Kondo, T., Ohtsuki, S., Ueda, M., Obinata, M., Terasaki, T., Hosoya, K., 2003. Expression and regulation of L-cystine transporter, system xc-, in the newly developed rat retinal Muller cell line (TR-MUL). Glia 43, 208–217.
Ueno, K., Iwagawa, T., Ochiai, G., Koso, H., Nakauchi, H., Nagasaki, M., Suzuki, Y., Watanabe, S., 2017. Analysis of Muller glia specific genes and their histone modification using Hes1-promoter driven EGFP expressing mouse. Sci. Rep. 7, 3578.
Vecino, E., Rodriguez, F.D., Ruzafa, N., Pereiro, X., Sharma, S.C., 2016. Glia-neuron interactions in the mammalian retina. Prog. Retin. Eye Res. 51, 1–40.
Wagner, H., Fink, B.A., Zadnik, K., 2008. Sex- and gender-based differences in healthy and diseased eyes. Optometry 79, 636–652.
Wood, J.P., Chidlow, G., Graham, M., Osborne, N.N., 2005. Energy substrate requirements for survival of rat retinal cells in culture: the importance of glucose and monocarboxylates. J. Neurochem. 93, 686–697.
Wood, J.P., Mammone, T., Chidlow, G., Greenwell, T., Casson, R.J., 2012. Mitochondrial inhibition in rat retinal cell cultures as a model of metabolic compromise: mechanisms of injury and neuroprotection. Invest. Ophthalmol. Vis. Sci. 53, 4897–4909.
Wood, J.P., Schmidt, K.G., Melena, J., Chidlow, G., Allmeier, H., Osborne, N.N., 2003. The beta-adrenoceptor antagonists metipranolol and timolol are retinal neuroprotectants: comparison with betaxolol. Exp. Eye Res. 76, 505–516.
Zerbino, D.R., Achuthan, P., Akanni, W., Amode, M.R., Barrell, D., Bhai, J., Billis, K., Cummins, C., Gall, A., Girón, C.G., Gil, L., Gordon, L., Haggerty, L., Haskell, E., Hourlier, T., Izuogu, O.G., Janacek, S.H., Juettemann, T., To, J.K., Laird, M.R., Lavidas, I., Liu, Z., Loveland, J.E., Maurel, T., McLaren, W., Moore, B., Mudge, J., Murphy, D.N., Newman, V., Nuhn, M., Ogeh, D., Ong, C.K., Parker, A., Patricio, M., Riat, H.S., Schuilenburg, H., Sheppard, D., Sparrow, H., Taylor, K., Thormann, A., Vullo, A., Walts, B., Zadissa, A., Frankish, A., Hunt, S.E., Kostadima, M., Langridge, N., Martin, F.J., Muffato, M., Perry, E., Ruffier, M., Staines, D.M., Trevanion, S.J., Aken, B.L., Cunningham, F., Yates, A., Flicek, P., 2018. Ensembl 2018. Nucleic Acids Res. 46, D754–D761.
Zhao, M., Andrieu-Soler, C., Kowalczuk, L., Paz Cortes, M., Berdugo, M., Dernigoghossian, M., Halili, F., Jeanny, J.C., Goldenberg, B., Savoldelli, M., El Sanharawi, M., Naud, M.C., van Ijcken, W., Pescini-Gobert, R., Martinet, D., Maass, A., Wijnholds, J., Crisanti, P., Rivolta, C., Behar-Cohen, F., 2015. A new CRB1 rat mutation links Muller glial cells to retinal telangiectasia. J. Neurosci. Official J. Soc. Neurosci. 35, 6093–6106.

# *Appendix 3: RNA sequencing data of cultured primary rat Müller cells, the spontaneously immortalized rat Müller cell line, SIRMu-1, and the SV40-transformed rat Müller cell line, rMC-1*

See over page.

# Statement of Authorship

| | |
|---|---|
| Title of Paper | RNA sequencing data of cultured primary rat Müller cells, the spontaneously immortalized rat Müller cell line, SIRMu-1, and the SV40-transformed rat Müller cell line, rMC-1. |
| Publication Status | ☑ Published ☐ Accepted for Publication<br>☐ Submitted for Publication ☐ Unpublished and Unsubmitted work written in manuscript style |
| Publication Details | Kittipassorn T, Haydinger CD, Wood JPM, Mammone T, Casson RJ, Peet DJ. RNA sequencing data of cultured primary rat Müller cells, the spontaneously immortalized rat Müller cell line, SIRMu-1, and the SV40-transformed rat Müller cell line, rMC-1. Data Brief. 2019 Mar 7;23:103721. doi: 10.1016/j.dib.2019.103721. PMID: 31372369; PMCID: PMC6660449. |

## Co-Author (Candidate)

| | | | |
|---|---|---|---|
| Name of Co-Author (Candidate) | Cameron D Haydinger | | |
| Contribution to the Paper | Planned experiments. Prepared and submitted mRNA sequencing data to the NCBI Gene Expression Omnibus (GEO) repository. Reviewed and edited the manuscript. | | |
| Overall percentage (%) | 15 | | |
| Certification: | This paper reports on original research I conducted during the period of my Higher Degree by Research candidature and is not subject to any obligations or contractual agreements with a third party that would constrain its inclusion in this thesis. | | |
| Signature | | Date | |

## Primary and Other Co-Author Contributions

By signing the Statement of Authorship, each author certifies that:

i. the candidate's stated contribution to the publication is accurate (as detailed above);
ii. permission is granted for the candidate in include the publication in the thesis; and
iii. the sum of all author contributions is equal to 100%

| | | | |
|---|---|---|---|
| Name of Primary Author | Thaksaon Kittipassorn | | |
| Contribution to the Paper | Conceived the project. Planned experiments and conducted experimental work. Generated Table 1. Contributed to preparing mRNA sequencing data for submission to the NCBI GEO repository. Wrote the manuscript. Reviewed and edited the manuscript.<br>% Contribution: 65 | | |
| Signature | | Date | 18/5/2022 |

| | | | |
|---|---|---|---|
| Name of Co-Author | John PM Wood | | |
| Contribution to the Paper | Planned experiments. Provided primary cell cultures. Reviewed and edited the manuscript. | | |
| Signature | | Date | 180522 |

| Name of Co-Author | Teresa Mammone | | |
|---|---|---|---|
| Contribution to the Paper | Provided primary cell cultures. Reviewed and edited the manuscript. | | |
| Signature | | Date | 20/05/2022 |

| Name of Co-Author | Robert J Casson | | |
|---|---|---|---|
| Contribution to the Paper | Conceived and supervised the project. Planned experiments. Reviewed and edited the manuscript. | | |
| Signature | | Date | 18 May 2022 |

| Name of Co-Author | Daniel J Peet | | |
|---|---|---|---|
| Contribution to the Paper | Conceived and supervised the project. Planned experiments. Reviewed and edited the manuscript. | | |
| Signature | | Date | 27/4/2022 |

Data in brief 23 (2019) 103721

Contents lists available at ScienceDirect

Data in brief

journal homepage: www.elsevier.com/locate/dib

Data Article

# RNA sequencing data of cultured primary rat Müller cells, the spontaneously immortalized rat Müller cell line, SIRMu-1, and the SV40-transformed rat Müller cell line, rMC-1

Thaksaon Kittipassorn [a, 1], Cameron D. Haydinger [a], John P.M. Wood [b], Teresa Mammone [b], Robert J. Casson [b], Daniel J. Peet [a, *]

[a] School of Biological Sciences, Molecular Life Sciences Building, University of Adelaide, Adelaide, SA 5005, Australia
[b] Department of Ophthalmology and Visual Sciences, Adelaide Health and Medical Sciences Building, University of Adelaide, Adelaide, SA 5000, Australia

ARTICLE INFO

*Article history:*
Received 12 January 2019
Received in revised form 23 January 2019
Accepted 25 January 2019
Available online 7 March 2019

ABSTRACT

Müller cells (MCs), the major type of glial cell of the vertebrate retina, have a vital role in retinal physiology and pathology. They provide structural and functional support for retinal neurons, including photoreceptors, and are implicated in various retinal diseases. Primary and immortalized MCs are important experimental tools for MC research. Here we present high throughput RNA sequencing data of 3 populations of cultured rat MCs: primary cells, the spontaneously immortalized rat MC line, SIRMu-1, and the SV40-transformed rat MC line, rMC-1. These data were deposited in NCBI Gene Expression Omnibus (GEO ID: GSE123161). For data analysis, interpretation and discussion, please refer to the research article, "Characterization of the novel spontaneously immortalized rat Müller cell line SIRMu-1" (Kittipassorn et al., 2019). This dataset is valuable for gaining insight

* Corresponding author.
*E-mail addresses:* thaksaon.kit@mahidol.ac.th (T. Kittipassorn), cameron.haydinger@adelaide.edu.au (C.D. Haydinger), john.wood2@sa.gov.au (J.P.M. Wood), teresa.mammone@adelaide.edu.au (T. Mammone), robert.casson@adelaide.edu.au (R.J. Casson), daniel.peet@adelaide.edu.au (D.J. Peet).
[1] Other affiliation/permanent address. Department of Physiology, Faculty of Medicine Siriraj Hospital, Mahidol University, 2 Wanglang Road, Bangkoknoi, Bangkok 10700, Thailand.

https://doi.org/10.1016/j.dib.2019.103721

into gene expression profiles of different types of cultured MCs and the roles of MCs in health and disease.



Specifications table

| | |
|---|---|
| Subject area | *Biology, Ophthalmology* |
| More specific subject area | *Retinal Müller cell (MC) gene expression* |
| Type of data | *In the article*<br>• *RNA sample information table*<br><br>*In NCBI Gene Expression Omnibus*<br>• *Raw: fastq files (one per sample)*<br>• *Processed: csv files (one per sample) containing reads per gene (un-normalized and before any filtering)*<br>• *Summary: tsv file containing TMM-normalized* log2 *counts per million reads (cpm) for all samples* |
| How data was acquired | *mRNA sequencing by an Illumina NextSeq 500 system* |
| Data format | *Raw and processed data* |
| Experimental factors | *3 different populations of cultured MCs* |
| Experimental features | *Total RNA was extracted from cultured primary rat MC cells, the spontaneously immortalized rat MC line, SIRMu-1 [1], and the SV40-transformed rat MC line, rMC-1 [2]. cDNA libraries were prepared from enriched polyA RNA and sequenced.* |
| Data source location | *Adelaide, Australia* |
| Data accessibility | *Data available in the article and in NCBI Gene Expression Omnibus [3] (GEO ID:* GSE123161*) (https://www.ncbi.nlm.nih.gov/geo/query/acc.cgi?acc=GSE123161).* |
| Related research article | *Kittipassorn, T., Haydinger, C.D., Wood, J.P.M., Mammone, T., Casson, R.J., Peet, D.J., Characterization of the novel spontaneously immortalized rat Müller cell line SIRMu-1, Exp. Eye. Res. 181 (2019) 127-135. https://doi.org/10.1016/j.exer.2019.01.013 [1]* |

**Value of the data**

- Commonly and differentially expressed genes can be identified between 3 distinct MC populations, providing invaluable information about the similarity between the different cells, as well as important functional differences.
- The rat MC transcriptomic data can be compared with MCs from a range of species from other published analyses to elucidate unique and similar gene expression patterns, signaling pathways and functions of MCs in different organisms.
- The ability to determine the origin and nature of a novel cell line.
- The data facilitate informed selection based on gene expression of appropriate MC lines to be used as an experimental tool.

## 1. Data

The data presented here are mRNA sequencing analyses of 3 populations of cultured rat MCs: primary cells, the novel spontaneously immortalized rat MC line, SIRMu-1 [1], and the SV40-transformed rat MC line, rMC-1 [2]. RNA samples were extracted from 4 biological replicates of primary MCs, 5 biological replicates of SIRMu-1 cells, and 3 biological replicates of rMC-1 cells. Table 1 in this article provides details on each sample, including the passage number and growth conditions of cells from which the samples were isolated. The data relating to this article are stored in NCBI Gene Expression Omnibus [3] (GEO ID: GSE123161), including: fastq files containing raw sequencing reads (one per sample, 12 in total); csv files containing numbers of reads per gene (un-normalized and

**Table 1**
RNA sample information.

| Cell type | Sample name | Source | Passage no.[a] of cells used for RNA extraction | Gentamicin and amphotericin B present in culture medium? |
|---|---|---|---|---|
| Primary MC | P1T1_4 | First litter, culture tray 1 | 4 | Yes |
| | P1T2_4 | First litter, culture tray 2 | 4 | Yes |
| | P2a_3 | Second litter | 3 | Yes |
| | P3b_3 | Third litter | 3 | Yes |
| SIRMu-1 | S4_6 | A frozen vial, passage no. 4 | 6 | No |
| | S4_11 | Same as S4_6 | 11 | No |
| | S4_11A | Same as S4_6 | 11 | Yes |
| | S10_11 | A frozen vial, passage no. 10 | 11 | No |
| | S10_20A | Same as S10_11 | 20 | Yes |
| rMC-1 | R22_23 | A frozen vial, passage no. 22 | 23 | No |
| | R22_26 | Same as R22_23 | 26 | No |
| | R24_26 | A frozen vial, passage no. 24 | 26 | No |

[a] No., number.

unfiltered, one per sample, 12 in total); a tsv file containing TMM-normalized log2 counts per million reads for all 12 samples. Please refer to the related research article [1] for details on data processing.

## 2. Experimental design, materials and methods

### 2.1. Cell culture

Primary rat MC cultures were prepared as described previously [1]. Briefly, mixed retinal cultures, consisting of retinal neurons and glial cells, were generated from 2 to 4 day post-natal Sprague-Dawley rat pups. Handling of these animals complied with the Australian Code of Practice for the Care and Use of Animals for Scientific Purposes 2004, and the ARVO Statement for the Use of Animals in Ophthalmic and Vision Research. The cultures were maintained in minimal essential medium (MEM, +Earle's Salts, -L-glutamine, #11090, Life Technologies Australia, Scoresby, VIC, Australia) containing 10% fetal bovine serum (FBS), 87 mg/L gentamicin sulfate, 2.2 mg/L amphotericin B, 25 mM glucose and 2 mM L-glutamine. 25 mM glucose is routinely used in our laboratories with neurons/glial cultures as a lower glucose concentration can lead to problems with cell attachment. After 7 days without any disturbance, the medium of the mixed retinal cultures was changed and the cultures were maintained for 28–42 days with medium changed every 3 days until almost all other cells died, leaving a near homogenous population of MCs. The isolated primary MCs were cultured in the same medium as above but with 20% FBS and passaged at 1:2 when confluent, approximately every 7 days. The SIRMu-1 cell line was cultured in the same medium as the primary MCs with the exception of gentamicin and amphotericin B (unless otherwise stated), and was passaged at 1:4 every 3–4 days. For the rMC-1 cell line (a kind gift of Dr Vijay Sarthy, Northwestern University, Chicago, IL, USA, obtained from Dr Binoy Appukuttan, Flinders University, Adelaide, SA, Australia), the same medium as the SIRMu-1 cells was used but with 10% FBS. rMC-1 cells were passaged at 1:10 every 2–3 days.

### 2.2. RNA extraction

Total RNA was extracted from 4 biological replicates of primary MCs, 5 replicates of SIRMu-1 cells, and 3 replicates of rMC-1 cells (Table 1), using a mirVana miRNA Isolation Kit (#AM1561, Life Technologies Australia) according to the manufacturer's instructions. The antibiotic gentamicin and the antifungal amphotericin B are routinely used to culture primary MCs to prevent contamination as the cells come directly from animals, but these drugs are not used for the culture of immortalized cells. To control for potential differences in transcriptome due to the absence or presence of gentamicin and amphotericin B in culture medium, 2 of the 5 SIRMu-1 samples were extracted from cells grown in

medium containing the two drugs, while the other 3 SIRMu-1 samples and all rMC-1 samples were from cells grown without the drugs (Table 1).

### 2.3. Library preparation and mRNA sequencing

RNA samples were submitted to the Australian Cancer Research Foundation (ACRF) Cancer Genomics Facility (Adelaide, SA, Australia). Sample quality was determined on an Agilent 2100 bioanalyzer with an Agilent RNA 6000 Nano kit (#5067-1511, Agilent Technologies, Santa Clara, CA, USA) to confirm that RIN values were above 7 (unless concentrations too low to accurately determine RIN), and concentrations determined using a Qubit RNA HS assay kit (#Q32852, Life Technologies Australia). Libraries were prepared by a KAPA stranded RNAseq HyperPrep kit (#KK8544, KAPA, Cape Town, South Africa) using 5 ng of enriched polyA RNA. RNA was fragmented (approximate insert length: 200 basepairs) and converted to cDNA. End-repair and A-tailing were then performed. Adapters compatible with Illumina sequencing were ligated to the cDNA using a concentration of 1.5 μM with an approximate adapter to molar insert ratio of 200:1. Next, a post-ligation clean-up was carried out to remove excess adapters. The libraries were amplified with 10 cycles of PCR and cleaned with 1X ratio of beads. Library yields and sizes were confirmed on an Agilent 2100 bioanalyzer with an Agilent High Sensitivity DNA kit (#5067-4626, Agilent Technologies) and diluted to 4 nM stocks. Libraries were pooled in equimolar ratios and sequenced using a 75 cycle high output kit (#FC-404-2005, Illumina, San Diego, CA, USA) on an Illumina NextSeq 500 system.

## Acknowledgements

The authors thank Joel Geoghegan, Andreas Schreiber, Ming Lin, and Wendy Parker (ACRF Cancer Genomics Facility, Adelaide, SA, Australia) for their assistance with the RNA sequencing. This work was supported by a National Health and Medical Research Council of Australia project grant (1099932). The funding source has no involvement in the conduct of experiments, data collection, manuscript preparation and the decision to submit the work for publication.

## Transparency document

Transparency document associated with this article can be found in the online version at https://doi.org/10.1016/j.dib.2019.103721.

## References

[1] T. Kittipassorn, C.D. Haydinger, J.P.M. Wood, T. Mammone, R.J. Casson, D.J. Peet, Characterization of the novel spontaneously immortalized rat Müller cell line SIRMu-1, Exp. Eye Res. 181 (2019) 127–135. https://doi.org/10.1016/j.exer.2019.01.013.
[2] V.P. Sarthy, S.J. Brodjian, K. Dutt, B.N. Kennedy, R.P. French, J.W. Crabb, Establishment and characterization of a retinal Müller cell line, Investig. Ophthalmol. Vis. Sci. 39 (1) (1998) 212–216.
[3] R. Edgar, M. Domrachev, A.E. Lash, Gene Expression Omnibus: NCBI gene expression and hybridization array data repository, Nucleic Acids Res. 30 (1) (2002) 207–210. https://doi.org/10.1093/nar/30.1.207.

# *Appendix 4: Müller RNA-seq: insulin signalling pathway*

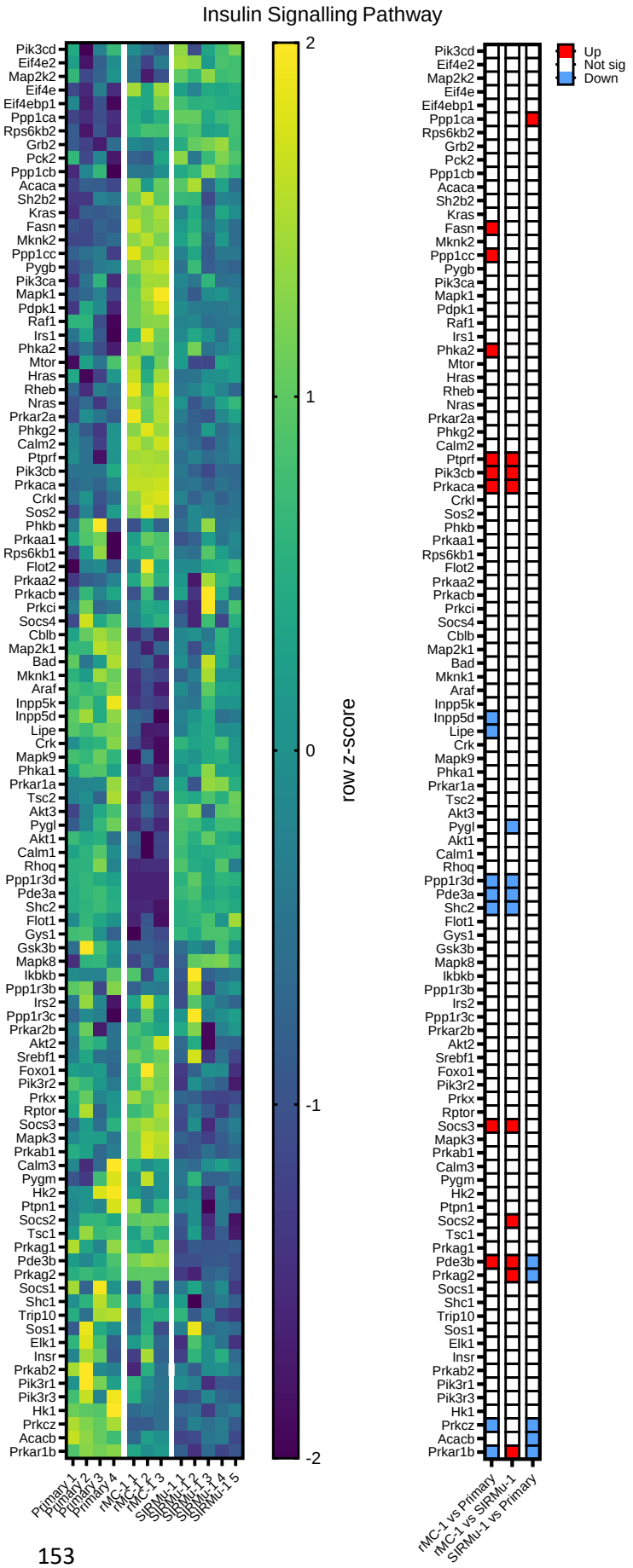


**Figure A.3 RNA-seq: Differences in expression of insulin signalling pathway genes between cultured Müller cell types.** RNA-sequencing was performed on cultured Müller cell types indicated. **Left panel:** A heatmap was generated from log2 normalised counts per million (with z-scores calculated across each row) to show differences in expression of genes involved in insulin signalling between cultured Müller cell types. **Right Panel:** Genes that were significantly differentially expressed (Benjamini-Hochberg corrected P-value of < 0.05) by greater than 2-fold between each pair of cell types are indicated. The list of genes was obtained from the Gene Set Enrichment Analysis (GSEA) Molecular Signatures Database (MSigDB). "Up" indicates significantly higher expression in the first-named cell type. "Down" indicates significantly lower expression in the first-named cell type.

# *Appendix 5: ERRβ expression vector insert sequence*

pTwist EF1α puro rEsrrb insert sequence encoding rat estrogen-related receptor β:

ATGTCGTCCGAAGACAGGCACCTGGGCTCTAGCTGCGGCTCCTTCATCAAGACGGAGCCATCTAGCCC
ATCCTCGGGCATTGATGCCCTCAGCCACCACAGCCCCAGCGGCTCGTCGGACGCCAGCGGTGGCTTTG
GCATGGCCCTGGGCACCCACGCCAACGGTCTGGACTCTCCGCCTATGTTCGCAGGTGCGGGGCTGGGA
GGCAACCCGTGTCGCAAGAGCTACGAGGACTGTACTAGCGGTATCATGGAGGACTCGGCCATCAAGTG
CGAGTACATGCTTAACGCCATCCCCAAGCGCCTGTGCCTCGTGTGCGGGGACATTGCTTCTGGCTACC
ACTATGGAGTGGCCTCCTGCGAGGCTTGCAAGGCGTTCTTCAAGAGAACCATTCAAGGAAACATCGAA
TACAGCTGCCCTGCCACCAACGAGTGTGAGATCACCAAACGGAGGCGCAAGTCCTGTCAGGCCTGCCG
GTTCATGAAATGCCTCAAAGTGGGGATGCTGAAGGAAGGCGTGCGCCTTGACCGGGTGCGAGGAGGCC
GCCAGAAGTACAAGAGACGGCTGGATTCGGAGAACAGCCCCTACCTGAGCTTACAGATTTCCCCGCCT
GCTAAAAAGCCATTGACTAAGATTGTCTCGTATCTACTGGTGGCCGAGCCGGACAAGCTGTACGCTAT
GCCTCCCGACGATGTGCCTGAAGGGGATATCAAGGCCCTGACCACTCTCTGTGACTTGGCAGATCGGG
AGCTTGTGTTCCTCATTAGCTGGGCCAAGCACATCCCAGGTTTCTCCAACCTGACACTCGGGGACCAG
ATGAGCCTGCTGCAGAGTGCCTGGATGGAGATCCTCATCCTGGGCATCGTGTACCGCTCGCTTCCCTA
TGATGACAAGCTGGCATACGCGGAGGACTATATCATGGATGAGGAACACTCTCGCCTGGTGGGGCTGC
TGGAGCTTTACCGAGCCATCTTGCAGCTCGTACGCAGGTACAAGAAGCTCAAGGTGGAGAAGGAAGAG
TTTGTGATGCTCAAAGCCCTGGCCCTTGCCAACTCAGATTCAATGTACATCGAGAACCTGGAGGCTGT
GCAGAAGCTTCAGGACCTGCTGCATGAGGCGCTGCAGGACTATGAGCTGAGCCAGCGCCATGAGGAGC
CACGGAGGGCGGGCAAGCTGCTGTTGACACTGCCCCTGCTGCGGCAGACGGCAGCCAAAGCCGTCCAG
CACTTCTACAGTGTGAAACTGCAGGGCAAGGTGCCCATGCACAAACTCTTCCTGGAGATGCTGGAGGC
CAAGGTGTGA

1302 bp

Final plasmid:

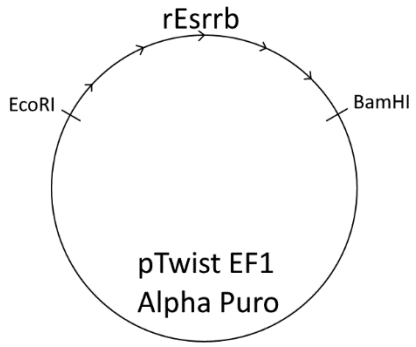

# References

1. Kim JW, Yang HJ, Oel AP *et al.* Recruitment of Rod Photoreceptors from Short-Wavelength-Sensitive Cones during the Evolution of Nocturnal Vision in Mammals. *Dev Cell* 2016; **37**: 520-32.
2. VandenBosch LS, Wohl SG, Wilken MS *et al.* Developmental changes in the accessible chromatin, transcriptome and Ascl1-binding correlate with the loss in Müller Glial regenerative potential. *Sci Rep* 2020; **10**: 13615.
3. Kallestad L, Blackshaw S, Khalil AM, Palczewski K. Tissue- and Species-Specific Patterns of RNA metabolism in Post-Mortem Mammalian Retina and Retinal Pigment Epithelium. *Scientific Reports* 2019; **9**: 14821.
4. Yu DY, Cringle SJ. Oxygen distribution and consumption within the retina in vascularised and avascular retinas and in animal models of retinal disease. *Prog Retin Eye Res* 2001; **20**: 175-208.
5. Ames A, 3rd, Li YY, Heher EC, Kimble CR. Energy metabolism of rabbit retina as related to function: high cost of Na+ transport. *J Neurosci* 1992; **12**: 840-53.
6. Winkler BS. A quantitative assessment of glucose metabolism in the rat retina. *Les Seminaries ophthalmologiques d'IPSEN* 1995; **tome 6 (ed. Y. Christen, M. Doly, M.T. Droy-Lefaix) Elsevier, Paris**: 78-96.
7. Warburg O, Posener K, Negelein E. On the metabolism of carcinoma cells. *Biochem Z* 1924; **152**: 309-44.
8. Ng SK, Wood JP, Chidlow G *et al.* Cancer-like metabolism of the mammalian retina. *Clinical and Experimental Ophthalmology* 2015; **43**: 367-76.
9. Warburg O. The Metabolism of Carcinoma Cells. *The Journal of Cancer Research* 1925; **9**: 148-63.
10. Winkler BS. Glycolytic and oxidative metabolism in relation to retinal function. *J Gen Physiol* 1981; **77**: 667-92.
11. Ames A, 3rd, Gurian BS. Effects of glucose and oxygen deprivation on function of isolated mammalian retina. *J Neurophysiol* 1963; **26**: 617-34.
12. Chertov AO, Holzhausen L, Kuok IT *et al.* Roles of glucose in photoreceptor survival. *J Biol Chem* 2011; **286**: 34700-11.
13. Aït-Ali N, Fridlich R, Millet-Puel G *et al.* Rod-Derived Cone Viability Factor Promotes Cone Survival by Stimulating Aerobic Glycolysis. *Cell* 2015; **161**: 817-32.
14. Petit L, Ma S, Cipi J *et al.* Aerobic Glycolysis Is Essential for Normal Rod Function and Controls Secondary Cone Death in Retinitis Pigmentosa. *Cell reports* 2018; **23**: 2629-42.
15. Cheng SY, Cipi J, Ma S *et al.* Altered photoreceptor metabolism in mouse causes late stage age-related macular degeneration-like pathologies. *Proc Natl Acad Sci U S A* 2020; **117**: 13094-104.
16. Léveillard T, Philp NJ, Sennlaub F. Is Retinal Metabolic Dysfunction at the Center of the Pathogenesis of Age-related Macular Degeneration? *Int J Mol Sci* 2019; **20**.
17. Chan KKW, Tang F, Tham CCY, Young AL, Cheung CY. Retinal vasculature in glaucoma: a review. *BMJ Open Ophthalmol* 2017; **1**: e000032.
18. Casson RJ, Han G, Ebneter A *et al.* Glucose-induced temporary visual recovery in primary open-angle glaucoma: a double-blind, randomized study. *Ophthalmology* 2014; **121**: 1203-11.
19. Duh EJ, Sun JK, Stitt AW. Diabetic retinopathy: current understanding, mechanisms, and treatment strategies. *JCI Insight* 2017; **2**.
20. Elliott WH, Elliott DC. *Biochemistry and molecular biology*, Third edn. New York: Oxford University Press, 2005.
21. Kornberg MD. The immunologic Warburg effect: Evidence and therapeutic opportunities in autoimmunity. *Wiley Interdiscip Rev Syst Biol Med* 2020; **12**: e1486.
22. Everts B, Amiel E, van der Windt GJ *et al.* Commitment to glycolysis sustains survival of NO-producing inflammatory dendritic cells. *Blood* 2012; **120**: 1422-31.

23. Peng M, Yin N, Chhangawala S, Xu K, Leslie CS, Li MO. Aerobic glycolysis promotes T helper 1 cell differentiation through an epigenetic mechanism. *Science* 2016; **354**: 481-4.
24. Chang CH, Curtis JD, Maggi LB, Jr. *et al.* Posttranscriptional control of T cell effector function by aerobic glycolysis. *Cell* 2013; **153**: 1239-51.
25. Koppenol WH, Bounds PL, Dang CV. Otto Warburg's contributions to current concepts of cancer metabolism. *Nat Rev Cancer* 2011; **11**: 325-37.
26. Warburg O. On the origin of cancer cells. *Science* 1956; **123**: 309-14.
27. Lim HY, Ho QS, Low J, Choolani M, Wong KP. Respiratory competent mitochondria in human ovarian and peritoneal cancer. *Mitochondrion* 2011; **11**: 437-43.
28. Funes JM, Quintero M, Henderson S *et al.* Transformation of human mesenchymal stem cells increases their dependency on oxidative phosphorylation for energy production. *Proc Natl Acad Sci U S A* 2007; **104**: 6223-8.
29. Fantin VR, St-Pierre J, Leder P. Attenuation of LDH-A expression uncovers a link between glycolysis, mitochondrial physiology, and tumor maintenance. *Cancer Cell* 2006; **9**: 425-34.
30. Weinhouse S. On respiratory impairment in cancer cells. *Science* 1956; **124**: 267-9.
31. LeBleu VS, O'Connell JT, Gonzalez Herrera KN *et al.* PGC-1α mediates mitochondrial biogenesis and oxidative phosphorylation in cancer cells to promote metastasis. *Nat Cell Biol* 2014; **16**: 992-1003, 1-15.
32. Tan AS, Baty JW, Dong LF *et al.* Mitochondrial genome acquisition restores respiratory function and tumorigenic potential of cancer cells without mitochondrial DNA. *Cell Metab* 2015; **21**: 81-94.
33. Viale A, Pettazzoni P, Lyssiotis CA *et al.* Oncogene ablation-resistant pancreatic cancer cells depend on mitochondrial function. *Nature* 2014; **514**: 628-32.
34. Weinberg F, Hamanaka R, Wheaton WW *et al.* Mitochondrial metabolism and ROS generation are essential for Kras-mediated tumorigenicity. *Proc Natl Acad Sci U S A* 2010; **107**: 8788-93.
35. Liberti MV, Locasale JW. The Warburg Effect: How Does it Benefit Cancer Cells? *Trends Biochem Sci* 2016; **41**: 211-8.
36. Gatenby RA, Gillies RJ. Why do cancers have high aerobic glycolysis? *Nat Rev Cancer* 2004; **4**: 891-9.
37. Vander Heiden MG, Cantley LC, Thompson CB. Understanding the Warburg effect: the metabolic requirements of cell proliferation. *Science* 2009; **324**: 1029-33.
38. Hosios AM, Hecht VC, Danai LV *et al.* Amino Acids Rather than Glucose Account for the Majority of Cell Mass in Proliferating Mammalian Cells. *Dev Cell* 2016; **36**: 540-9.
39. Pfeiffer T, Schuster S, Bonhoeffer S. Cooperation and competition in the evolution of ATP-producing pathways. *Science* 2001; **292**: 504-7.
40. Epstein T, Xu L, Gillies RJ, Gatenby RA. Separation of metabolic supply and demand: aerobic glycolysis as a normal physiological response to fluctuating energetic demands in the membrane. *Cancer Metab* 2014; **2**: 7.
41. Lardner A. The effects of extracellular pH on immune function. *J Leukoc Biol* 2001; **69**: 522-30.
42. Luengo A, Li Z, Gui DY *et al.* Increased demand for NAD(+) relative to ATP drives aerobic glycolysis. *Mol Cell* 2021; **81**: 691-707.e6.
43. Baden T, Euler T, Berens P. Understanding the retinal basis of vision across species. *Nat Rev Neurosci* 2020; **21**: 5-20.
44. Poitry-Yamate CL, Poitry S, Tsacopoulos M. Lactate released by Müller glial cells is metabolized by photoreceptors from mammalian retina. *J Neurosci* 1995; **15**: 5179-91.
45. Winkler BS, Pourcho RG, Starnes C, Slocum J, Slocum N. Metabolic mapping in mammalian retina: a biochemical and 3H-2-deoxyglucose autoradiographic study. *Exp Eye Res* 2003; **77**: 327-37.
46. Tsacopoulos M, Poitry-Yamate CL, MacLeish PR, Poitry S. Trafficking of molecules and metabolic signals in the retina. *Prog Retin Eye Res* 1998; **17**: 429-42.

47. Winkler BS, Arnold MJ, Brassell MA, Puro DG. Energy metabolism in human retinal Muller cells. *Invest Ophthalmol Vis Sci* 2000; **41**: 3183-90.
48. Bringmann A, Pannicke T, Grosche J *et al.* Müller cells in the healthy and diseased retina. *Prog Retin Eye Res* 2006; **25**: 397-424.
49. Wong-Riley MT. Energy metabolism of the visual system. *Eye Brain* 2010; **2**: 99-116.
50. Chinchore Y, Begaj T, Wu D, Drokhlyansky E, Cepko CL. Glycolytic reliance promotes anabolism in photoreceptors. *Elife* 2017; **6**.
51. Wubben TJ, Pawar M, Smith A, Toolan K, Hager H, Besirli CG. Photoreceptor metabolic reprogramming provides survival advantage in acute stress while causing chronic degeneration. *Sci Rep* 2017; **7**: 17863.
52. Rajala A, Wang Y, Brush RS *et al.* Pyruvate kinase M2 regulates photoreceptor structure, function, and viability. *Cell Death Dis* 2018; **9**: 240.
53. Viegas FO, Neuhauss SCF. A Metabolic Landscape for Maintaining Retina Integrity and Function. *Front Mol Neurosci* 2021; **14**: 656000.
54. Lindsay KJ, Du J, Sloat SR *et al.* Pyruvate kinase and aspartate-glutamate carrier distributions reveal key metabolic links between neurons and glia in retina. *Proc Natl Acad Sci U S A* 2014; **111**: 15579-84.
55. Grünert U, Martin PR. Cell types and cell circuits in human and non-human primate retina. *Prog Retin Eye Res* 2020: 100844.
56. Lukowski SW, Lo CY, Sharov AA *et al.* A single-cell transcriptome atlas of the adult human retina. *Embo j* 2019; **38**: e100811.
57. Macosko EZ, Basu A, Satija R *et al.* Highly Parallel Genome-wide Expression Profiling of Individual Cells Using Nanoliter Droplets. *Cell* 2015; **161**: 1202-14.
58. Morrow EM, Belliveau MJ, Cepko CL. Two phases of rod photoreceptor differentiation during rat retinal development. *J Neurosci* 1998; **18**: 3738-48.
59. Hoang QV, Linsenmeier RA, Chung CK, Curcio CA. Photoreceptor inner segments in monkey and human retina: mitochondrial density, optics, and regional variation. *Vis Neurosci* 2002; **19**: 395-407.
60. Young RW, Droz B. The renewal of protein in retinal rods and cones. *J Cell Biol* 1968; **39**: 169-84.
61. Arshavsky VY, Lamb TD, Pugh EN, Jr. G proteins and phototransduction. *Annu Rev Physiol* 2002; **64**: 153-87.
62. Molday RS, Molday LL. Molecular properties of the cGMP-gated channel of rod photoreceptors. *Vision Res* 1998; **38**: 1315-23.
63. Spencer M, Detwiler PB, Bunt-Milam AH. Distribution of membrane proteins in mechanically dissociated retinal rods. *Invest Ophthalmol Vis Sci* 1988; **29**: 1012-20.
64. Young RW. The renewal of photoreceptor cell outer segments. *J Cell Biol* 1967; **33**: 61-72.
65. Young RW, Bok D. Participation of the retinal pigment epithelium in the rod outer segment renewal process. *J Cell Biol* 1969; **42**: 392-403.
66. Hall MO, Bok D, Bacharach AD. Biosynthesis and assembly of the rod outer segment membrane system. Formation and fate of visual pigment in the frog retina. *J Mol Biol* 1969; **45**: 397-406.
67. Anderson DH, Fisher SK, Steinberg RH. Mammalian cones: disc shedding, phagocytosis, and renewal. *Invest Ophthalmol Vis Sci* 1978; **17**: 117-33.
68. Steinberg RH. Phagocytosis by pigment epithelium of human retinal cones. *Nature* 1974; **252**: 305-7.
69. Bibb C, Young RW. Renewal of fatty acids in the membranes of visual cell outer segments. *J Cell Biol* 1974; **61**: 327-43.
70. Heitzmann H. Rhodopsin is the predominant protein of rod outer segment membranes. *Nat New Biol* 1972; **235**: 114.

71. Bibb C, Young RW. Renewal of glycerol in the visual cells and pigment epithelium of the frog retina. *J Cell Biol* 1974; **62**: 378-89.
72. Young RW. The renewal of rod and cone outer segments in the rhesus monkey. *J Cell Biol* 1971; **49**: 303-18.
73. Besharse JC, Hollyfield JG, Rayborn ME. Photoreceptor outer segments: accelerated membrane renewal in rods after exposure to light. *Science* 1977; **196**: 536-8.
74. Korenbrot JI, Fernald RD. Circadian rhythm and light regulate opsin mRNA in rod photoreceptors. *Nature* 1989; **337**: 454-7.
75. Besharse JC, Iuvone PM. Circadian clock in Xenopus eye controlling retinal serotonin N-acetyltransferase. *Nature* 1983; **305**: 133-5.
76. Bok D. Retinal photoreceptor-pigment epithelium interactions. Friedenwald lecture. *Invest Ophthalmol Vis Sci* 1985; **26**: 1659-94.
77. Shen W, Fruttiger M, Zhu L *et al.* Conditional Müllercell ablation causes independent neuronal and vascular pathologies in a novel transgenic model. *J Neurosci* 2012; **32**: 15715-27.
78. Dubois-Dauphin M, Poitry-Yamate C, de Bilbao F, Julliard AK, Jourdan F, Donati G. Early postnatal Müller cell death leads to retinal but not optic nerve degeneration in NSE-Hu-Bcl-2 transgenic mice. *Neuroscience* 2000; **95**: 9-21.
79. Maw MA, Kennedy B, Knight A *et al.* Mutation of the gene encoding cellular retinaldehyde-binding protein in autosomal recessive retinitis pigmentosa. *Nat Genet* 1997; **17**: 198-200.
80. Reichenbach A, Bringmann A. *Müller Cells in the Healthy and Diseased Retina*, 1st ed. 2010. edn. New York, NY: Springer New York, 2010.
81. Reichenbach A, Robinson SR. The involvement of Müller cells in the outer retina. In: Djamgoz MBA, Archer SN, Vallerga S, eds.*The involvement of Müller cells in the outer retina*, Dordrecht: Springer Netherlands, 1995; 395-416.
82. Omri S, Omri B, Savoldelli M *et al.* The outer limiting membrane (OLM) revisited: clinical implications. *Clin Ophthalmol* 2010; **4**: 183-95.
83. Peynshaert K, Devoldere J, Minnaert AK, De Smedt SC, Remaut K. Morphology and Composition of the Inner Limiting Membrane: Species-Specific Variations and Relevance toward Drug Delivery Research. *Curr Eye Res* 2019; **44**: 465-75.
84. Reichenbach A, Ziegert M, Schnitzer J *et al.* Development of the rabbit retina. V. The question of 'columnar units'. *Brain Res Dev Brain Res* 1994; **79**: 72-84.
85. Lu YB, Franze K, Seifert G *et al.* Viscoelastic properties of individual glial cells and neurons in the CNS. *Proc Natl Acad Sci U S A* 2006; **103**: 17759-64.
86. Franze K, Grosche J, Skatchkov SN *et al.* Muller cells are living optical fibers in the vertebrate retina. *Proc Natl Acad Sci U S A* 2007; **104**: 8287-92.
87. Rauen T, Rothstein JD, Wässle H. Differential expression of three glutamate transporter subtypes in the rat retina. *Cell Tissue Res* 1996; **286**: 325-36.
88. Rauen T, Taylor WR, Kuhlbrodt K, Wiessner M. High-affinity glutamate transporters in the rat retina: a major role of the glial glutamate transporter GLAST-1 in transmitter clearance. *Cell Tissue Res* 1998; **291**: 19-31.
89. Rauen T. Diversity of glutamate transporter expression and function in the mammalian retina. *Amino Acids* 2000; **19**: 53-62.
90. Harada T, Harada C, Watanabe M *et al.* Functions of the two glutamate transporters GLAST and GLT-1 in the retina. *Proc Natl Acad Sci U S A* 1998; **95**: 4663-6.
91. Matsui K, Hosoi N, Tachibana M. Active role of glutamate uptake in the synaptic transmission from retinal nonspiking neurons. *J Neurosci* 1999; **19**: 6755-66.
92. Higgs MH, Lukasiewicz PD. Glutamate uptake limits synaptic excitation of retinal ganglion cells. *J Neurosci* 1999; **19**: 3691-700.
93. Hasegawa J, Obara T, Tanaka K, Tachibana M. High-density presynaptic transporters are required for glutamate removal from the first visual synapse. *Neuron* 2006; **50**: 63-74.

94. Pow DV, Crook DK. Direct immunocytochemical evidence for the transfer of glutamine from glial cells to neurons: use of specific antibodies directed against the d-stereoisomers of glutamate and glutamine. *Neuroscience* 1996; **70**: 295-302.
95. Pow DV, Robinson SR. Glutamate in some retinal neurons is derived solely from glia. *Neuroscience* 1994; **60**: 355-66.
96. Bui BV, Hu RG, Acosta ML, Donaldson P, Vingrys AJ, Kalloniatis M. Glutamate metabolic pathways and retinal function. *J Neurochem* 2009; **111**: 589-99.
97. Newman EA, Frambach DA, Odette LL. Control of extracellular potassium levels by retinal glial cell K+ siphoning. *Science* 1984; **225**: 1174-5.
98. Kusaka S, Puro DG. Intracellular ATP activates inwardly rectifying K+ channels in human and monkey retinal Müller (glial) cells. *J Physiol* 1997; **500 ( Pt 3)**: 593-604.
99. Nagelhus EA, Horio Y, Inanobe A *et al.* Immunogold evidence suggests that coupling of K+ siphoning and water transport in rat retinal Müller cells is mediated by a coenrichment of Kir4.1 and AQP4 in specific membrane domains. *Glia* 1999; **26**: 47-54.
100. Kuwabara T, Cogan DG. Retinal glycogen. *Arch Ophthalmol* 1961; **66**: 680-8.
101. Germer A, Biedermann B, Wolburg H *et al.* Distribution of mitochondria within Müller cells--I. Correlation with retinal vascularization in different mammalian species. *J Neurocytol* 1998; **27**: 329-45.
102. Germer A, Schuck J, Wolburg H, Kuhrt H, Mack AF, Reichenbach A. Distribution of mitochondria within Müller cells--II. Post-natal development of the rabbit retinal periphery in vivo and in vitro: dependence on oxygen supply. *J Neurocytol* 1998; **27**: 347-59.
103. Yu DY, Cringle SJ, Alder VA, Su EN, Yu PK. Intraretinal oxygen distribution and choroidal regulation in the avascular retina of guinea pigs. *Am J Physiol* 1996; **270**: H965-73.
104. Wangsa-Wirawan ND, Linsenmeier RA. Retinal oxygen: fundamental and clinical aspects. *Arch Ophthalmol* 2003; **121**: 547-57.
105. Yu DY, Cringle SJ, Alder VA, Su EN. Intraretinal oxygen distribution in rats as a function of systemic blood pressure. *Am J Physiol* 1994; **267**: H2498-507.
106. Birol G, Wang S, Budzynski E, Wangsa-Wirawan ND, Linsenmeier RA. Oxygen distribution and consumption in the macaque retina. *Am J Physiol Heart Circ Physiol* 2007; **293**: H1696-704.
107. Ahmed J, Braun RD, Dunn R, Jr., Linsenmeier RA. Oxygen distribution in the macaque retina. *Invest Ophthalmol Vis Sci* 1993; **34**: 516-21.
108. Linsenmeier RA. Effects of light and darkness on oxygen distribution and consumption in the cat retina. *J Gen Physiol* 1986; **88**: 521-42.
109. Pournaras CJ, Riva CE, Tsacopoulos M, Strommer K. Diffusion of O2 in the retina of anesthetized miniature pigs in normoxia and hyperoxia. *Exp Eye Res* 1989; **49**: 347-60.
110. Yu DY, Cringle SJ. Oxygen distribution in the mouse retina. *Invest Ophthalmol Vis Sci* 2006; **47**: 1109-12.
111. Volland S, Esteve-Rudd J, Hoo J, Yee C, Williams DS. A comparison of some organizational characteristics of the mouse central retina and the human macula. *PLoS One* 2015; **10**: e0125631.
112. Provis JM, Dubis AM, Maddess T, Carroll J. Adaptation of the central retina for high acuity vision: cones, the fovea and the avascular zone. *Prog Retin Eye Res* 2013; **35**: 63-81.
113. Chong NH, Keonin J, Luthert PJ *et al.* Decreased thickness and integrity of the macular elastic layer of Bruch's membrane correspond to the distribution of lesions associated with age-related macular degeneration. *Am J Pathol* 2005; **166**: 241-51.
114. Kittipassorn T. Investigating the Warburg effect and the role of pyruvate kinase M2 in retinal Müller glial cells. In.*Investigating the Warburg effect and the role of pyruvate kinase M2 in retinal Müller glial cells*, Vol. PhD, Adelaide: University of Adelaide, 2019.
115. Xu Y, Ola MS, Berkich DA *et al.* Energy sources for glutamate neurotransmission in the retina: absence of the aspartate/glutamate carrier produces reliance on glycolysis in glia. *J Neurochem* 2007; **101**: 120-31.

116. Haydinger CD, Kittipassorn T, Peet DJ. Power to see-Drivers of aerobic glycolysis in the mammalian retina: A review. *Clin Exp Ophthalmol* 2020; **48**: 1057-71.
117. Casson RJ, Wood JPM, Han G, Kittipassorn T, Peet DJ, Chidlow G. M-type pyruvate kinase isoforms and lactate dehydrogenase a in the mammalian retina: Metabolic implications. *Invest Ophthalmol Vis Sci* 2016; **57**: 66-80.
118. Hamel C. Retinitis pigmentosa. *Orphanet J Rare Dis* 2006; **1**: 40.
119. Pierrache LHM, Kimchi A, Ratnapriya R *et al.* Whole-Exome Sequencing Identifies Biallelic IDH3A Variants as a Cause of Retinitis Pigmentosa Accompanied by Pseudocoloboma. *Ophthalmology* 2017; **124**: 992-1003.
120. Hartong DT, Dange M, McGee TL, Berson EL, Dryja TP, Colman RF. Insights from retinitis pigmentosa into the roles of isocitrate dehydrogenases in the Krebs cycle. *Nat Genet* 2008; **40**: 1230-4.
121. Wang F, Wang Y, Zhang B *et al.* A missense mutation in HK1 leads to autosomal dominant retinitis pigmentosa. *Invest Ophthalmol Vis Sci* 2014; **55**: 7159-64.
122. Zhang L, Sun Z, Zhao P *et al.* Whole-exome sequencing revealed HKDC1 as a candidate gene associated with autosomal-recessive retinitis pigmentosa. *Hum Mol Genet* 2018; **27**: 4157-68.
123. Country MW. Retinal metabolism: A comparative look at energetics in the retina. *Brain Res* 2017; **1672**: 50-7.
124. Blasiak J, Petrovski G, Veréb Z, Facskó A, Kaarniranta K. Oxidative stress, hypoxia, and autophagy in the neovascular processes of age-related macular degeneration. *Biomed Res Int* 2014; **2014**: 768026.
125. Pan WW, Wubben TJ, Besirli CG. Photoreceptor metabolic reprogramming: current understanding and therapeutic implications. *Commun Biol* 2021; **4**: 245.
126. Punzo C, Kornacker K, Cepko CL. Stimulation of the insulin/mTOR pathway delays cone death in a mouse model of retinitis pigmentosa. *Nat Neurosci* 2009; **12**: 44-52.
127. Wallsh JO, Gallemore RP. Anti-VEGF-Resistant Retinal Diseases: A Review of the Latest Treatment Options. *Cells* 2021; **10**.
128. Kittipassorn T, Haydinger CD, Wood JPM, Mammone T, Casson RJ, Peet DJ. Characterization of the novel spontaneously immortalized rat Müller cell line SIRMu-1. *Exp Eye Res* 2019; **181**: 127-35.
129. Bradford MM. A rapid and sensitive method for the quantitation of microgram quantities of protein utilizing the principle of protein-dye binding. *Anal Biochem* 1976; **72**: 248-54.
130. Kittipassorn T, Haydinger CD, Wood JPM, Mammone T, Casson RJ, Peet DJ. RNA sequencing data of cultured primary rat Müller cells, the spontaneously immortalized rat Müller cell line, SIRMu-1, and the SV40-transformed rat Müller cell line, rMC-1. *Data Brief* 2019; **23**: 103721.
131. R Core Team. R: A language and environment for statistical computing. In.*R: A language and environment for statistical computing*, Vienna, Austria: R Foundation for Statistical Computing, 2021.
132. Robinson MD, McCarthy DJ, Smyth GK. edgeR: a Bioconductor package for differential expression analysis of digital gene expression data. *Bioinformatics* 2010; **26**: 139-40.
133. Robinson MD, Oshlack A. A scaling normalization method for differential expression analysis of RNA-seq data. *Genome Biol* 2010; **11**: R25.
134. Ritchie ME, Phipson B, Wu D *et al.* limma powers differential expression analyses for RNA-sequencing and microarray studies. *Nucleic Acids Res* 2015; **43**: e47.
135. Soneson C, Love MI, Robinson MD. Differential analyses for RNA-seq: transcript-level estimates improve gene-level inferences. *F1000Res* 2015; **4**: 1521.
136. Hoang T, Wang J, Boyd P *et al.* Gene regulatory networks controlling vertebrate retinal regeneration. *Science* 2020; **370**.
137. Sarthy VP, Brodjian SJ, Dutt K, Kennedy BN, French RP, Crabb JW. Establishment and characterization of a retinal Muller cell line. *Invest Ophthalmol Vis Sci* 1998; **39**: 212-6.

138. Winkler BS, Sauer MW, Starnes CA. Modulation of the Pasteur effect in retinal cells: implications for understanding compensatory metabolic mechanisms. *Exp Eye Res* 2003; **76**: 715-23.
139. Winkler BS, Sauer MW, Starnes CA. Effects of L-glutamate/D-aspartate and monensin on lactic acid production in retina and cultured retinal Müller cells. *J Neurochem* 2004; **89**: 514-25.
140. Kusner LL, Sarthy VP, Mohr S. Nuclear translocation of glyceraldehyde-3-phosphate dehydrogenase: a role in high glucose-induced apoptosis in retinal Muller cells. *Invest Ophthalmol Vis Sci* 2004; **45**: 1553-61.
141. Papa S, Choy PM, Bubici C. The ERK and JNK pathways in the regulation of metabolic reprogramming. *Oncogene* 2019; **38**: 2223-40.
142. Gharbi SI, Zvelebil MJ, Shuttleworth SJ *et al.* Exploring the specificity of the PI3K family inhibitor LY294002. *Biochem J* 2007; **404**: 15-21.
143. Barthel A, Okino ST, Liao J *et al.* Regulation of GLUT1 gene transcription by the serine/threonine kinase Akt1. *J Biol Chem* 1999; **274**: 20281-6.
144. Rathmell JC, Fox CJ, Plas DR, Hammerman PS, Cinalli RM, Thompson CB. Akt-directed glucose metabolism can prevent Bax conformation change and promote growth factor-independent survival. *Mol Cell Biol* 2003; **23**: 7315-28.
145. Pastorino JG, Hoek JB, Shulga N. Activation of Glycogen Synthase Kinase 3β Disrupts the Binding of Hexokinase II to Mitochondria by Phosphorylating Voltage-Dependent Anion Channel and Potentiates Chemotherapy-Induced Cytotoxicity. *Cancer Res* 2005; **65**: 10545-54.
146. Roberts DJ, Tan-Sah VP, Smith JM, Miyamoto S. Akt phosphorylates HK-II at Thr-473 and increases mitochondrial HK-II association to protect cardiomyocytes. *J Biol Chem* 2013; **288**: 23798-806.
147. Deprez J, Vertommen D, Alessi DR, Hue L, Rider MH. Phosphorylation and activation of heart 6-phosphofructo-2-kinase by protein kinase B and other protein kinases of the insulin signaling cascades. *J Biol Chem* 1997; **272**: 17269-75.
148. Zhong H, Chiles K, Feldser D *et al.* Modulation of hypoxia-inducible factor 1alpha expression by the epidermal growth factor/phosphatidylinositol 3-kinase/PTEN/AKT/FRAP pathway in human prostate cancer cells: implications for tumor angiogenesis and therapeutics. *Cancer Res* 2000; **60**: 1541-5.
149. Hu H, Juvekar A, Lyssiotis CA *et al.* Phosphoinositide 3-Kinase Regulates Glycolysis through Mobilization of Aldolase from the Actin Cytoskeleton. *Cell* 2016; **164**: 433-46.
150. Al-Khallaf H. Isocitrate dehydrogenases in physiology and cancer: biochemical and molecular insight. *Cell Biosci* 2017; **7**: 37.
151. Bunik V, Kaehne T, Degtyarev D, Shcherbakova T, Reiser G. Novel isoenzyme of 2-oxoglutarate dehydrogenase is identified in brain, but not in heart. *Febs j* 2008; **275**: 4990-5006.
152. Sen T, Sen N, Noordhuis MG *et al.* OGDHL is a modifier of AKT-dependent signaling and NF-κB function. *PLoS One* 2012; **7**: e48770.
153. Jiao Y, Li Y, Fu Z *et al.* OGDHL Expression as a Prognostic Biomarker for Liver Cancer Patients. *Dis Markers* 2019; **2019**: 9037131.
154. Dai W, Xu L, Yu X *et al.* OGDHL silencing promotes hepatocellular carcinoma by reprogramming glutamine metabolism. *J Hepatol* 2020; **72**: 909-23.
155. Liu Y, Meng F, Wang J *et al.* A Novel Oxoglutarate Dehydrogenase-Like Mediated miR-214/TWIST1 Negative Feedback Loop Inhibits Pancreatic Cancer Growth and Metastasis. *Clin Cancer Res* 2019; **25**: 5407-21.
156. Rajala RV, Rajala A, Kooker C, Wang Y, Anderson RE. The Warburg Effect Mediator Pyruvate Kinase M2 Expression and Regulation in the Retina. *Sci Rep* 2016; **6**: 37727.
157. Rueda EM, Johnson JE, Jr., Giddabasappa A *et al.* The cellular and compartmental profile of mouse retinal glycolysis, tricarboxylic acid cycle, oxidative phosphorylation, and ~P transferring kinases. *Mol Vis* 2016; **22**: 847-85.

158. Haque A, Engel J, Teichmann SA, Lönnberg T. A practical guide to single-cell RNA-sequencing for biomedical research and clinical applications. *Genome Med* 2017; **9**: 75.
159. Shekhar K, Lapan SW, Whitney IE *et al.* Comprehensive Classification of Retinal Bipolar Neurons by Single-Cell Transcriptomics. *Cell* 2016; **166**: 1308-23.e30.
160. Hafemeister C, Satija R. Normalization and variance stabilization of single-cell RNA-seq data using regularized negative binomial regression. *Genome Biol* 2019; **20**: 296.
161. De Robertis E. Morphogenesis of the retinal rods; an electron microscope study. *J Biophys Biochem Cytol* 1956; **2**: 209-18.
162. Caley DW, Johnson C, Liebelt RA. The postnatal development of the retina in the normal and rodless CBA mouse: a light and electron microscopic study. *Am J Anat* 1972; **133**: 179-212.
163. Keeler CE, Sutcliffe E, Chaffee EL. A Description of the Ontogenetic Development of Retinal Action Currents in the House Mouse. *Proc Natl Acad Sci U S A* 1928; **14**: 811-5.
164. Arora KK, Pedersen PL. Functional significance of mitochondrial bound hexokinase in tumor cell metabolism. Evidence for preferential phosphorylation of glucose by intramitochondrially generated ATP. *J Biol Chem* 1988; **263**: 17422-8.
165. Gershon TR, Crowther AJ, Tikunov A *et al.* Hexokinase-2-mediated aerobic glycolysis is integral to cerebellar neurogenesis and pathogenesis of medulloblastoma. *Cancer Metab* 2013; **1**: 2.
166. Patra KC, Wang Q, Bhaskar PT *et al.* Hexokinase 2 is required for tumor initiation and maintenance and its systemic deletion is therapeutic in mouse models of cancer. *Cancer Cell* 2013; **24**: 213-28.
167. Anderson M, Marayati R, Moffitt R, Yeh JJ. Hexokinase 2 promotes tumor growth and metastasis by regulating lactate production in pancreatic cancer. *Oncotarget* 2017; **8**: 56081-94.
168. Borst P. The malate-aspartate shuttle (Borst cycle): How it started and developed into a major metabolic pathway. *IUBMB Life* 2020; **72**: 2241-59.
169. Benesch R, Benesch RE. The effect of organic phosphates from the human erythrocyte on the allosteric properties of hemoglobin. *Biochem Biophys Res Commun* 1967; **26**: 162-7.
170. Cho J, King JS, Qian X, Harwood AJ, Shears SB. Dephosphorylation of 2,3-bisphosphoglycerate by MIPP expands the regulatory capacity of the Rapoport-Luebering glycolytic shunt. *Proc Natl Acad Sci U S A* 2008; **105**: 5998-6003.
171. Dobolyi A, Ostergaard E, Bagó AG *et al.* Exclusive neuronal expression of SUCLA2 in the human brain. *Brain Struct Funct* 2015; **220**: 135-51.
172. Findlay AS, Carter RN, Starbuck B *et al.* Mouse Idh3a mutations cause retinal degeneration and reduced mitochondrial function. *Dis Model Mech* 2018; **11**.
173. Conesa A, Madrigal P, Tarazona S *et al.* A survey of best practices for RNA-seq data analysis. *Genome Biol* 2016; **17**: 13.
174. Swaroop A, Kim D, Forrest D. Transcriptional regulation of photoreceptor development and homeostasis in the mammalian retina. *Nat Rev Neurosci* 2010; **11**: 563-76.
175. Naeem MA, Chavali VR, Ali S *et al.* GNAT1 associated with autosomal recessive congenital stationary night blindness. *Invest Ophthalmol Vis Sci* 2012; **53**: 1353-61.
176. Riazuddin SA, Shahzadi A, Zeitz C *et al.* A mutation in SLC24A1 implicated in autosomal-recessive congenital stationary night blindness. *Am J Hum Genet* 2010; **87**: 523-31.
177. Sato M, Nakazawa M, Usui T, Tanimoto N, Abe H, Ohguro H. Mutations in the gene coding for guanylate cyclase-activating protein 2 (GUCA1B gene) in patients with autosomal dominant retinal dystrophies. *Graefes Arch Clin Exp Ophthalmol* 2005; **243**: 235-42.
178. Sothilingam V, Garcia Garrido M, Jiao K *et al.* Retinitis pigmentosa: impact of different Pde6a point mutations on the disease phenotype. *Hum Mol Genet* 2015; **24**: 5486-99.
179. Li Y, Li R, Dai H, Li G. Novel variants in PDE6A and PDE6B genes and its phenotypes in patients with retinitis pigmentosa in Chinese families. *BMC Ophthalmol* 2022; **22**: 27.

180. Kuehlewein L, Zobor D, Andreasson SO *et al.* Clinical Phenotype and Course of PDE6A-Associated Retinitis Pigmentosa Disease, Characterized in Preparation for a Gene Supplementation Trial. *JAMA Ophthalmol* 2020; **138**: 1241-50.
181. Nicchia GP, Pisani F, Simone L *et al.* Glio-vascular modifications caused by Aquaporin-4 deletion in the mouse retina. *Exp Eye Res* 2016; **146**: 259-68.
182. Wu L, Niemeyer B, Colley N, Socolich M, Zuker CS. Regulation of PLC-mediated signalling in vivo by CDP-diacylglycerol synthase. *Nature* 1995; **373**: 216-22.
183. Inglis-Broadgate SL, Ocaka L, Banerjee R *et al.* Isolation and characterization of murine Cds (CDP-diacylglycerol synthase) 1 and 2. *Gene* 2005; **356**: 19-31.
184. Toutounchian JJ, McCarty JH. Selective expression of eGFP in mouse perivascular astrocytes by modification of the Mlc1 gene using T2A-based ribosome skipping. *Genesis* 2017; **55**.
185. Danjo Y, Shinozaki Y, Natsubori A *et al.* The Mlc1 Promoter Directs Müller Cell-specific Gene Expression in the Retina. *Transl Vis Sci Technol* 2022; **11**: 25.
186. Roesch K, Jadhav AP, Trimarchi JM *et al.* The transcriptome of retinal Müller glial cells. *J Comp Neurol* 2008; **509**: 225-38.
187. Tanner LB, Goglia AG, Wei MH *et al.* Four Key Steps Control Glycolytic Flux in Mammalian Cells. *Cell Syst* 2018; **7**: 49-62.e8.
188. Locasale JW. New concepts in feedback regulation of glucose metabolism. *Curr Opin Syst Biol* 2018; **8**: 32-8.
189. Liberti MV, Dai Z, Wardell SE *et al.* A Predictive Model for Selective Targeting of the Warburg Effect through GAPDH Inhibition with a Natural Product. *Cell Metab* 2017; **26**: 648-59.e8.
190. Adamus G. Are Anti-Retinal Autoantibodies a Cause or a Consequence of Retinal Degeneration in Autoimmune Retinopathies? *Front Immunol* 2018; **9**: 765.
191. Magrys A, Anekonda T, Ren G, Adamus G. The role of anti-alpha-enolase autoantibodies in pathogenicity of autoimmune-mediated retinopathy. *J Clin Immunol* 2007; **27**: 181-92.
192. Weleber RG, Watzke RC, Shults WT *et al.* Clinical and electrophysiologic characterization of paraneoplastic and autoimmune retinopathies associated with antienolase antibodies. *Am J Ophthalmol* 2005; **139**: 780-94.
193. Didiasova M, Schaefer L, Wygrecka M. When Place Matters: Shuttling of Enolase-1 Across Cellular Compartments. *Front Cell Dev Biol* 2019; **7**: 61.
194. Stetten D, Jr. Biosynthesis and pyrophosphate. *Am J Med* 1960; **28**: 867-70.
195. Yang Z, Wensel TG. Inorganic pyrophosphatase from bovine retinal rod outer segments. *J Biol Chem* 1992; **267**: 24634-40.
196. Zibetti C, Liu S, Wan J, Qian J, Blackshaw S. Epigenomic profiling of retinal progenitors reveals LHX2 is required for developmental regulation of open chromatin. *Commun Biol* 2019; **2**: 142.
197. Ueno K, Iwagawa T, Ochiai G *et al.* Analysis of Müller glia specific genes and their histone modification using Hes1-promoter driven EGFP expressing mouse. *Sci Rep* 2017; **7**: 3578.
198. Lin S, Guo J, Chen S. Transcriptome and DNA Methylome Signatures Associated With Retinal Müller Glia Development, Injury Response, and Aging. *Invest Ophthalmol Vis Sci* 2019; **60**: 4436-50.
199. Tello D, Balsa E, Acosta-Iborra B *et al.* Induction of the mitochondrial NDUFA4L2 protein by HIF-1α decreases oxygen consumption by inhibiting Complex I activity. *Cell Metab* 2011; **14**: 768-79.
200. Fukuda R, Zhang H, Kim JW, Shimoda L, Dang CV, Semenza GL. HIF-1 regulates cytochrome oxidase subunits to optimize efficiency of respiration in hypoxic cells. *Cell* 2007; **129**: 111-22.
201. Zheng J, Dai X, Chen H, Fang C, Chen J, Sun L. Down-regulation of LHPP in cervical cancer influences cell proliferation, metastasis and apoptosis by modulating AKT. *Biochem Biophys Res Commun* 2018; **503**: 1108-14.
202. Liu S, Gao W, Lu Y *et al.* As a Novel Tumor Suppressor, LHPP Promotes Apoptosis by Inhibiting the PI3K/AKT Signaling Pathway in Oral Squamous Cell Carcinoma. *Int J Biol Sci* 2022; **18**: 491-506.

203. Sun W, Qian K, Guo K *et al.* LHPP inhibits cell growth and migration and triggers autophagy in papillary thyroid cancer by regulating the AKT/AMPK/mTOR signaling pathway. *Acta Biochim Biophys Sin (Shanghai)* 2020; **52**: 382-9.
204. Chen WJ, Chen LH, Wang J *et al.* LHPP impedes energy metabolism by inducing ubiquitin-mediated degradation of PKM2 in glioblastoma. *Am J Cancer Res* 2021; **11**: 1369-90.
205. Stark R, Kibbey RG. The mitochondrial isoform of phosphoenolpyruvate carboxykinase (PEPCK-M) and glucose homeostasis: has it been overlooked? *Biochim Biophys Acta* 2014; **1840**: 1313-30.
206. Stark R, Pasquel F, Turcu A *et al.* Phosphoenolpyruvate cycling via mitochondrial phosphoenolpyruvate carboxykinase links anaplerosis and mitochondrial GTP with insulin secretion. *J Biol Chem* 2009; **284**: 26578-90.
207. Kibbey RG, Pongratz RL, Romanelli AJ, Wollheim CB, Cline GW, Shulman GI. Mitochondrial GTP regulates glucose-stimulated insulin secretion. *Cell Metab* 2007; **5**: 253-64.
208. Mo A, Mukamel EA, Davis FP *et al.* Epigenomic Signatures of Neuronal Diversity in the Mammalian Brain. *Neuron* 2015; **86**: 1369-84.
209. Petrak J, Ivanek R, Toman O *et al.* Déjà vu in proteomics. A hit parade of repeatedly identified differentially expressed proteins. *Proteomics* 2008; **8**: 1744-9.
210. Rajala RVS. Aerobic Glycolysis in the Retina: Functional Roles of Pyruvate Kinase Isoforms. *Front Cell Dev Biol* 2020; **8**: 266.
211. Kanow MA, Giarmarco MM, Jankowski CS *et al.* Biochemical adaptations of the retina and retinal pigment epithelium support a metabolic ecosystem in the vertebrate eye. *Elife* 2017; **6**.
212. Hauck SM, Suppmann S, Ueffing M. Proteomic profiling of primary retinal Müller glia cells reveals a shift in expression patterns upon adaptation to in vitro conditions. *Glia* 2003; **44**: 251-63.
213. Noell WK. The effect of iodoacetate on the vertebrate retina. *J Cell Comp Physiol* 1951; **37**: 283-307.
214. Graymore C. Metabolism of the developing retina. I. Aerobic and anaerobic glycolysis in the developing rat retina. *Br J Ophthalmol* 1959; **43**: 34-9.
215. Cohen LH, Noell WK. Glucose catabolism of rabbit retina before and after development of visual function. *J Neurochem* 1960; **5**: 253-76.
216. Graymore C. Metabolism of the developing retina. III. Respiration in the developing normal rat retina and the effect of an inherited degeneration of the retinal neuroepithelium. *Br J Ophthalmol* 1960; **44**: 363-9.
217. Cheng SC, Quintin J, Cramer RA *et al.* mTOR- and HIF-1α-mediated aerobic glycolysis as metabolic basis for trained immunity. *Science* 2014; **345**: 1250684.
218. Sun Q, Chen X, Ma J *et al.* Mammalian target of rapamycin up-regulation of pyruvate kinase isoenzyme type M2 is critical for aerobic glycolysis and tumor growth. *Proc Natl Acad Sci U S A* 2011; **108**: 4129-34.
219. Pate KT, Stringari C, Sprowl-Tanio S *et al.* Wnt signaling directs a metabolic program of glycolysis and angiogenesis in colon cancer. *Embo j* 2014; **33**: 1454-73.
220. Yang HY, Shen JX, Wang Y, Liu Y, Shen DY, Quan S. Tankyrase Promotes Aerobic Glycolysis and Proliferation of Ovarian Cancer through Activation of Wnt/β-Catenin Signaling. *Biomed Res Int* 2019; **2019**: 2686340.
221. Vallée A, Lecarpentier Y, Guillevin R, Vallée JN. Aerobic Glycolysis Hypothesis Through WNT/Beta-Catenin Pathway in Exudative Age-Related Macular Degeneration. *J Mol Neurosci* 2017; **62**: 368-79.
222. Huang SM, Mishina YM, Liu S *et al.* Tankyrase inhibition stabilizes axin and antagonizes Wnt signalling. *Nature* 2009; **461**: 614-20.

223. Liu J, Chen G, Liu Z *et al.* Aberrant FGFR Tyrosine Kinase Signaling Enhances the Warburg Effect by Reprogramming LDH Isoform Expression and Activity in Prostate Cancer. *Cancer Res* 2018; **78**: 4459-70.
224. Fumarola C, Cretella D, La Monica S *et al.* Enhancement of the anti-tumor activity of FGFR1 inhibition in squamous cell lung cancer by targeting downstream signaling involved in glucose metabolism. *Oncotarget* 2017; **8**: 91841-59.
225. Babina IS, Turner NC. Advances and challenges in targeting FGFR signalling in cancer. *Nat Rev Cancer* 2017; **17**: 318-32.
226. Lo AK, Dawson CW, Young LS, Ko CW, Hau PM, Lo KW. Activation of the FGFR1 signalling pathway by the Epstein-Barr virus-encoded LMP1 promotes aerobic glycolysis and transformation of human nasopharyngeal epithelial cells. *J Pathol* 2015; **237**: 238-48.
227. Hitosugi T, Kang S, Vander Heiden MG *et al.* Tyrosine phosphorylation inhibits PKM2 to promote the Warburg effect and tumor growth. *Sci Signal* 2009; **2**: ra73.
228. Fan J, Hitosugi T, Chung TW *et al.* Tyrosine phosphorylation of lactate dehydrogenase A is important for NADH/NAD(+) redox homeostasis in cancer cells. *Mol Cell Biol* 2011; **31**: 4938-50.
229. Hitosugi T, Fan J, Chung TW *et al.* Tyrosine phosphorylation of mitochondrial pyruvate dehydrogenase kinase 1 is important for cancer metabolism. *Mol Cell* 2011; **44**: 864-77.
230. Gudernova I, Vesela I, Balek L *et al.* Multikinase activity of fibroblast growth factor receptor (FGFR) inhibitors SU5402, PD173074, AZD1480, AZD4547 and BGJ398 compromises the use of small chemicals targeting FGFR catalytic activity for therapy of short-stature syndromes. *Hum Mol Genet* 2016; **25**: 9-23.
231. Turner N, Pearson A, Sharpe R *et al.* FGFR1 amplification drives endocrine therapy resistance and is a therapeutic target in breast cancer. *Cancer Res* 2010; **70**: 2085-94.
232. Mohammadi M, Froum S, Hamby JM *et al.* Crystal structure of an angiogenesis inhibitor bound to the FGF receptor tyrosine kinase domain. *Embo j* 1998; **17**: 5896-904.
233. Skaper SD, Kee WJ, Facci L, Macdonald G, Doherty P, Walsh FS. The FGFR1 inhibitor PD 173074 selectively and potently antagonizes FGF-2 neurotrophic and neurotropic effects. *J Neurochem* 2000; **75**: 1520-7.
234. Malecaze F, Mascarelli F, Bugra K, Fuhrmann G, Courtois Y, Hicks D. Fibroblast growth factor receptor deficiency in dystrophic retinal pigmented epithelium. *J Cell Physiol* 1993; **154**: 631-42.
235. Rousseau B, Dubayle D, Sennlaub F *et al.* Neural and angiogenic defects in eyes of transgenic mice expressing a dominant-negative FGF receptor in the pigmented cells. *Exp Eye Res* 2000; **71**: 395-404.
236. Divekar SD, Tiek DM, Fernandez A, Riggins RB. Estrogen-related receptor β (ERRβ) - renaissance receptor or receptor renaissance? *Nucl Recept Signal* 2016; **14**: e002.
237. Festuccia N, Owens N, Navarro P. Esrrb, an estrogen-related receptor involved in early development, pluripotency, and reprogramming. *FEBS Lett* 2018; **592**: 852-77.
238. Sone M, Morone N, Nakamura T *et al.* Hybrid Cellular Metabolism Coordinated by Zic3 and Esrrb Synergistically Enhances Induction of Naive Pluripotency. *Cell Metab* 2017; **25**: 1103-17.e6.
239. Onishi A, Peng GH, Poth EM *et al.* The orphan nuclear hormone receptor ERRbeta controls rod photoreceptor survival. *Proc Natl Acad Sci U S A* 2010; **107**: 11579-84.
240. Tremblay GB, Kunath T, Bergeron D *et al.* Diethylstilbestrol regulates trophoblast stem cell differentiation as a ligand of orphan nuclear receptor ERR beta. *Genes Dev* 2001; **15**: 833-8.
241. Coward P, Lee D, Hull MV, Lehmann JM. 4-Hydroxytamoxifen binds to and deactivates the estrogen-related receptor gamma. *Proc Natl Acad Sci U S A* 2001; **98**: 8880-4.
242. Heckler MM, Thakor H, Schafer CC, Riggins RB. ERK/MAPK regulates ERRγ expression, transcriptional activity and receptor-mediated tamoxifen resistance in ER+ breast cancer. *Febs j* 2014; **281**: 2431-42.

243. Semenza GL, Jiang BH, Leung SW *et al.* Hypoxia response elements in the aldolase A, enolase 1, and lactate dehydrogenase A gene promoters contain essential binding sites for hypoxia-inducible factor 1. *J Biol Chem* 1996; **271**: 32529-37.
244. Zhong H, De Marzo AM, Laughner E *et al.* Overexpression of hypoxia-inducible factor 1alpha in common human cancers and their metastases. *Cancer Res* 1999; **59**: 5830-5.
245. Semenza GL. HIF-1 mediates the Warburg effect in clear cell renal carcinoma. *J Bioenerg Biomembr* 2007; **39**: 231-4.
246. Semenza GL. Regulation of metabolism by hypoxia-inducible factor 1. *Cold Spring Harb Symp Quant Biol* 2011; **76**: 347.
247. Thiersch M, Lange C, Joly S *et al.* Retinal neuroprotection by hypoxic preconditioning is independent of hypoxia-inducible factor-1 alpha expression in photoreceptors. *Eur J Neurosci* 2009; **29**: 2291-302.
248. Kast B, Schori C, Grimm C. Hypoxic preconditioning protects photoreceptors against light damage independently of hypoxia inducible transcription factors in rods. *Exp Eye Res* 2016; **146**: 60-71.
249. Samardzija M, Barben M, Todorova V, Klee K, Storti F, Grimm C. Hif1a and Hif2a can be safely inactivated in cone photoreceptors. *Scientific Reports* 2019; **9**: 16121.
250. Pitroda SP, Wakim BT, Sood RF *et al.* STAT1-dependent expression of energy metabolic pathways links tumour growth and radioresistance to the Warburg effect. *BMC Med* 2009; **7**: 68.
251. Samardzija M, Wenzel A, Aufenberg S, Thiersch M, Remé C, Grimm C. Differential role of Jak-STAT signaling in retinal degenerations. *Faseb j* 2006; **20**: 2411-3.
252. Ly A, Merl-Pham J, Priller M *et al.* Proteomic Profiling Suggests Central Role Of STAT Signaling during Retinal Degeneration in the rd10 Mouse Model. *J Proteome Res* 2016; **15**: 1350-9.
253. Phan RT, Dalla-Favera R. The BCL6 proto-oncogene suppresses p53 expression in germinal-centre B cells. *Nature* 2004; **432**: 635-9.
254. Seyfert VL, Allman D, He Y, Staudt LM. Transcriptional repression by the proto-oncogene BCL-6. *Oncogene* 1996; **12**: 2331-42.
255. Oestreich KJ, Read KA, Gilbertson SE *et al.* Bcl-6 directly represses the gene program of the glycolysis pathway. *Nat Immunol* 2014; **15**: 957-64.
256. Li Z, Geng M, Ye X *et al.* IRF7 inhibits the Warburg effect via transcriptional suppression of PKM2 in osteosarcoma. *Int J Biol Sci* 2022; **18**: 30-42.
257. Lu J, Liu X, Zheng J *et al.* Lin28A promotes IRF6-regulated aerobic glycolysis in glioma cells by stabilizing SNHG14. *Cell Death Dis* 2020; **11**: 447.
258. Byun JK, Choi YK, Kang YN *et al.* Retinoic acid-related orphan receptor alpha reprograms glucose metabolism in glutamine-deficient hepatoma cells. *Hepatology* 2015; **61**: 953-64.
259. Fan W, Waizenegger W, Lin CS *et al.* PPARδ Promotes Running Endurance by Preserving Glucose. *Cell Metab* 2017; **25**: 1186-93.e4.
260. Yuan Y, Fan G, Liu Y *et al.* The transcription factor KLF14 regulates macrophage glycolysis and immune function by inhibiting HK2 in sepsis. *Cell Mol Immunol* 2022.
261. Wu G, Yuan S, Chen Z *et al.* The KLF14 Transcription Factor Regulates Glycolysis by Downregulating LDHB in Colorectal Cancer. *Int J Biol Sci* 2019; **15**: 628-35.
262. Xing J, Jia Z, Xu Y *et al.* KLF9 (Kruppel Like Factor 9) induced PFKFB3 (6-Phosphofructo-2-Kinase/Fructose-2, 6-Biphosphatase 3) downregulation inhibits the proliferation, metastasis and aerobic glycolysis of cutaneous squamous cell carcinoma cells. *Bioengineered* 2021; **12**: 7563-76.
263. Yi M, Ban Y, Tan Y, Xiong W, Li G, Xiang B. 6-Phosphofructo-2-kinase/fructose-2,6-biphosphatase 3 and 4: A pair of valves for fine-tuning of glucose metabolism in human cancer. *Mol Metab* 2019; **20**: 1-13.

264. Crochet RB, Kim JD, Lee H *et al.* Crystal structure of heart 6-phosphofructo-2-kinase/fructose-2,6-bisphosphatase (PFKFB2) and the inhibitory influence of citrate on substrate binding. *Proteins* 2017; **85**: 117-24.
265. Lee M, Harley G, Katerelos M *et al.* Mutation of regulatory phosphorylation sites in PFKFB2 worsens renal fibrosis. *Sci Rep* 2020; **10**: 14531.
266. Rider MH, Bertrand L, Vertommen D, Michels PA, Rousseau GG, Hue L. 6-phosphofructo-2-kinase/fructose-2,6-bisphosphatase: head-to-head with a bifunctional enzyme that controls glycolysis. *Biochem J* 2004; **381**: 561-79.
267. Rider MH, van Damme J, Vertommen D, Michel A, Vandekerckhove J, Hue L. Evidence for new phosphorylation sites for protein kinase C and cyclic AMP-dependent protein kinase in bovine heart 6-phosphofructo-2-kinase/fructose-2,6-bisphosphatase. *FEBS Lett* 1992; **310**: 139-42.
268. Rider MH, Hue L. Activation of rat heart phosphofructokinase-2 by insulin in vivo. *FEBS Lett* 1984; **176**: 484-8.
269. Yoshida S, Mears AJ, Friedman JS *et al.* Expression profiling of the developing and mature Nrl-/- mouse retina: identification of retinal disease candidates and transcriptional regulatory targets of Nrl. *Hum Mol Genet* 2004; **13**: 1487-503.
270. Goldman SS. Evidence that the gluconeogenic pathway is confined to an enriched Müller cell fraction derived from the amphibian retina. *Exp Eye Res* 1990; **50**: 213-8.
271. Hurley JB, Lindsay KJ, Du J. Glucose, lactate, and shuttling of metabolites in vertebrate retinas. *J Neurosci Res* 2015; **93**: 1079-92.
272. Vander Heiden MG, Locasale JW, Swanson KD *et al.* Evidence for an alternative glycolytic pathway in rapidly proliferating cells. *Science* 2010; **329**: 1492-9.
273. Bringmann A, Grosche A, Pannicke T, Reichenbach A. GABA and Glutamate Uptake and Metabolism in Retinal Glial (Müller) Cells. *Front Endocrinol (Lausanne)* 2013; **4**: 48.
274. Cringle SJ, Yu DY, Yu PK, Su EN. Intraretinal oxygen consumption in the rat in vivo. *Invest Ophthalmol Vis Sci* 2002; **43**: 1922-7.
275. Yu DY, Cringle SJ. Outer retinal anoxia during dark adaptation is not a general property of mammalian retinas. *Comp Biochem Physiol A Mol Integr Physiol* 2002; **132**: 47-52.
276. Limb GA, Salt TE, Munro PM, Moss SE, Khaw PT. In vitro characterization of a spontaneously immortalized human Müller cell line (MIO-M1). *Invest Ophthalmol Vis Sci* 2002; **43**: 864-9.
277. Augustine J, Pavlou S, O'Hare M *et al.* Characterization of a Spontaneously Immortalized Murine Müller Glial Cell Line QMMuC-1. *Invest Ophthalmol Vis Sci* 2018; **59**: 1666-74.
278. Rodríguez-Muela N, Hernández-Pinto AM, Serrano-Puebla A *et al.* Lysosomal membrane permeabilization and autophagy blockade contribute to photoreceptor cell death in a mouse model of retinitis pigmentosa. *Cell Death Differ* 2015; **22**: 476-87.
279. Chresta CM, Davies BR, Hickson I *et al.* AZD8055 is a potent, selective, and orally bioavailable ATP-competitive mammalian target of rapamycin kinase inhibitor with in vitro and in vivo antitumor activity. *Cancer Res* 2010; **70**: 288-98.
280. Willems L, Chapuis N, Puissant A *et al.* The dual mTORC1 and mTORC2 inhibitor AZD8055 has anti-tumor activity in acute myeloid leukemia. *Leukemia* 2012; **26**: 1195-202.
281. Proenca CC, Stoehr N, Bernhard M *et al.* Atg4b-dependent autophagic flux alleviates Huntington's disease progression. *PLoS One* 2013; **8**: e68357.
282. Calandrini C, van Hooff SR, Paassen I *et al.* Organoid-based drug screening reveals neddylation as therapeutic target for malignant rhabdoid tumors. *Cell reports* 2021; **36**: 109568.
283. Granchi C, Paterni I, Rani R, Minutolo F. Small-molecule inhibitors of human LDH5. *Future Med Chem* 2013; **5**: 1967-91.
284. Düvel K, Yecies JL, Menon S *et al.* Activation of a metabolic gene regulatory network downstream of mTOR complex 1. *Mol Cell* 2010; **39**: 171-83.
285. Zhan T, Rindtorff N, Boutros M. Wnt signaling in cancer. *Oncogene* 2017; **36**: 1461-73.

286. García-Aguilar A, Martínez-Reyes I, Cuezva JM. Changes in the Turnover of the Cellular Proteome during Metabolic Reprogramming: A Role for mtROS in Proteostasis. *J Proteome Res* 2019; **18**: 3142-55.
287. Johnson TV, Martin KR. Development and characterization of an adult retinal explant organotypic tissue culture system as an in vitro intraocular stem cell transplantation model. *Invest Ophthalmol Vis Sci* 2008; **49**: 3503-12.
288. Li Y, Zhang Y, Qi S, Su G. Retinal organotypic culture - A candidate for research on retinas. *Tissue Cell* 2018; **51**: 1-7.
289. Winkler BS. Buffer dependence of retinal glycolysis and ERG potentials. *Exp Eye Res* 1986; **42**: 585-93.
290. Niyadurupola N, Sidaway P, Osborne A, Broadway DC, Sanderson J. The development of human organotypic retinal cultures (HORCs) to study retinal neurodegeneration. *Br J Ophthalmol* 2011; **95**: 720-6.
291. Brewer GJ, Torricelli JR, Evege EK, Price PJ. Optimized survival of hippocampal neurons in B27-supplemented Neurobasal, a new serum-free medium combination. *J Neurosci Res* 1993; **35**: 567-76.
292. Bartová A, Tibagong M, Birmingham MK. Steroid-mediated stimulation of aerobic glycolysis by intact mouse adrenal glands in vitro. *Endocrinology* 1971; **89**: 1142-51.
293. Hopkins BD, Goncalves MD, Cantley LC. Insulin-PI3K signalling: an evolutionarily insulated metabolic driver of cancer. *Nat Rev Endocrinol* 2020; **16**: 276-83.
294. Gardner TW, Abcouwer SF, Losiewicz MK, Fort PE. Phosphatase control of 4E-BP1 phosphorylation state is central for glycolytic regulation of retinal protein synthesis. *Am J Physiol Endocrinol Metab* 2015; **309**: E546-56.
295. Winkler BS, Arnold MJ, Brassell MA, Sliter DR. Glucose dependence of glycolysis, hexose monophosphate shunt activity, energy status, and the polyol pathway in retinas isolated from normal (nondiabetic) rats. *Invest Ophthalmol Vis Sci* 1997; **38**: 62-71.
296. Du J, Cleghorn W, Contreras L *et al.* Cytosolic reducing power preserves glutamate in retina. *Proc Natl Acad Sci U S A* 2013; **110**: 18501-6.
297. Du J, Cleghorn WM, Contreras L *et al.* Inhibition of mitochondrial pyruvate transport by zaprinast causes massive accumulation of aspartate at the expense of glutamate in the retina. *J Biol Chem* 2013; **288**: 36129-40.
298. Du J, Rountree A, Cleghorn WM *et al.* Phototransduction Influences Metabolic Flux and Nucleotide Metabolism in Mouse Retina. *J Biol Chem* 2016; **291**: 4698-710.
299. Bisbach CM, Hass DT, Robbings BM *et al.* Succinate Can Shuttle Reducing Power from the Hypoxic Retina to the O(2)-Rich Pigment Epithelium. *Cell reports* 2020; **31**: 107606.
300. Deutsch TA, Read JS, Ernest JT, Goldstick TK. Effects of oxygen and carbon dioxide on the retinal vasculature in humans. *Arch Ophthalmol* 1983; **101**: 1278-80.
301. Adijanto J, Du J, Moffat C, Seifert EL, Hurle JB, Philp NJ. The retinal pigment epithelium utilizes fatty acids for ketogenesis. *J Biol Chem* 2014; **289**: 20570-82.
302. Stine ZE, Schug ZT, Salvino JM, Dang CV. Targeting cancer metabolism in the era of precision oncology. *Nat Rev Drug Discov* 2022; **21**: 141-62.
303. Halford SER, Jones P, Wedge S *et al.* A first-in-human first-in-class (FIC) trial of the monocarboxylate transporter 1 (MCT1) inhibitor AZD3965 in patients with advanced solid tumours. *Journal of Clinical Oncology* 2017; **35**: 2516-.
304. Allen AE, Martin EA, Greenwood K *et al.* Effects of a monocarboxylate transport 1 inhibitor, AZD3965, on retinal and visual function in the rat. *Br J Pharmacol* 2020; **177**: 4734-49.
305. Han JYS, Kinoshita J, Bisetto S *et al.* Role of monocarboxylate transporters in regulating metabolic homeostasis in the outer retina: Insight gained from cell-specific Bsg deletion. *Faseb j* 2020; **34**: 5401-19.
306. Bisbach CM, Hass DT, Thomas ED, Cherry TJ, Hurley JB. Monocarboxylate Transporter 1 (MCT1) Mediates Succinate Export in the Retina. *Invest Ophthalmol Vis Sci* 2022; **63**: 1.

307. Wang L, Kondo M, Bill A. Glucose metabolism in cat outer retina. Effects of light and hyperoxia. *Invest Ophthalmol Vis Sci* 1997; **38**: 48-55.
308. Wang L, Tornquist P, Bill A. Glucose metabolism in pig outer retina in light and darkness. *Acta Physiol Scand* 1997; **160**: 75-81.
309. Herron WL, Jr., Riegel BW. Production rate and removal of rod outer segment material in vitamin A deficiency. *Invest Ophthalmol* 1974; **13**: 46-53.
310. Farnsworth CC, Dratz EA. Oxidative damage of retinal rod outer segment membranes and the role of vitamin E. *Biochim Biophys Acta* 1976; **443**: 556-70.
311. Díaz-García CM, Mongeon R, Lahmann C, Koveal D, Zucker H, Yellen G. Neuronal Stimulation Triggers Neuronal Glycolysis and Not Lactate Uptake. *Cell Metab* 2017; **26**: 361-74.e4.
312. Yellen G. Fueling thought: Management of glycolysis and oxidative phosphorylation in neuronal metabolism. *J Cell Biol* 2018; **217**: 2235-46.
313. Okawa H, Sampath AP, Laughlin SB, Fain GL. ATP consumption by mammalian rod photoreceptors in darkness and in light. *Curr Biol* 2008; **18**: 1917-21.
314. Wang L, Bill A. Effects of constant and flickering light on retinal metabolism in rabbits. *Acta Ophthalmol Scand* 1997; **75**: 227-31.
315. Medrano CJ, Fox DA. Oxygen consumption in the rat outer and inner retina: light- and pharmacologically-induced inhibition. *Exp Eye Res* 1995; **61**: 273-84.
316. Cringle S, Yu DY, Alder V, Su EN, Yu P. Oxygen consumption in the avascular guinea pig retina. *Am J Physiol* 1996; **271**: H1162-5.
317. Braun RD, Linsenmeier RA, Goldstick TK. Oxygen consumption in the inner and outer retina of the cat. *Invest Ophthalmol Vis Sci* 1995; **36**: 542-54.
318. Vazquez A, Liu J, Zhou Y, Oltvai ZN. Catabolic efficiency of aerobic glycolysis: the Warburg effect revisited. *BMC Syst Biol* 2010; **4**: 58.
319. Shlomi T, Benyamini T, Gottlieb E, Sharan R, Ruppin E. Genome-scale metabolic modeling elucidates the role of proliferative adaptation in causing the Warburg effect. *PLoS Comput Biol* 2011; **7**: e1002018.
320. Vazquez A, Oltvai ZN. Molecular crowding defines a common origin for the Warburg effect in proliferating cells and the lactate threshold in muscle physiology. *PLoS One* 2011; **6**: e19538.
321. Vazquez A, Oltvai ZN. Macromolecular crowding explains overflow metabolism in cells. *Sci Rep* 2016; **6**: 31007.
322. Kooragayala K, Gotoh N, Cogliati T *et al.* Quantification of Oxygen Consumption in Retina Ex Vivo Demonstrates Limited Reserve Capacity of Photoreceptor Mitochondria. *Invest Ophthalmol Vis Sci* 2015; **56**: 8428-36.
323. Linsenmeier RA, Yancey CM. Effects of hyperoxia on the oxygen distribution in the intact cat retina. *Invest Ophthalmol Vis Sci* 1989; **30**: 612-8.
324. Yu DY, Cringle SJ, Alder V, Su EN. Intraretinal oxygen distribution in the rat with graded systemic hyperoxia and hypercapnia. *Invest Ophthalmol Vis Sci* 1999; **40**: 2082-7.
325. Yu DY, Cringle SJ, Su EN. Intraretinal oxygen distribution in the monkey retina and the response to systemic hyperoxia. *Invest Ophthalmol Vis Sci* 2005; **46**: 4728-33.
326. Cringle SJ, Yu DY. Intraretinal oxygenation and oxygen consumption in the rabbit during systemic hyperoxia. *Invest Ophthalmol Vis Sci* 2004; **45**: 3223-8.
327. Hass DT, Barnstable CJ. Uncoupling proteins in the mitochondrial defense against oxidative stress. *Prog Retin Eye Res* 2021; **83**: 100941.
328. Ramsden DB, Ho PW, Ho JW *et al.* Human neuronal uncoupling proteins 4 and 5 (UCP4 and UCP5): structural properties, regulation, and physiological role in protection against oxidative stress and mitochondrial dysfunction. *Brain Behav* 2012; **2**: 468-78.
329. Kudin AP, Malinska D, Kunz WS. Sites of generation of reactive oxygen species in homogenates of brain tissue determined with the use of respiratory substrates and inhibitors. *Biochim Biophys Acta* 2008; **1777**: 689-95.
330. Murphy MP. How mitochondria produce reactive oxygen species. *Biochem J* 2009; **417**: 1-13.

331. Brand KA, Hermfisse U. Aerobic glycolysis by proliferating cells: a protective strategy against reactive oxygen species. *Faseb j* 1997; **11**: 388-95.
332. Liu D, Chan SL, de Souza-Pinto NC *et al.* Mitochondrial UCP4 mediates an adaptive shift in energy metabolism and increases the resistance of neurons to metabolic and oxidative stress. *Neuromolecular Med* 2006; **8**: 389-414.
333. Birsoy K, Wang T, Chen WW, Freinkman E, Abu-Remaileh M, Sabatini DM. An Essential Role of the Mitochondrial Electron Transport Chain in Cell Proliferation Is to Enable Aspartate Synthesis. *Cell* 2015; **162**: 540-51.
334. Sullivan LB, Gui DY, Hosios AM, Bush LN, Freinkman E, Vander Heiden MG. Supporting Aspartate Biosynthesis Is an Essential Function of Respiration in Proliferating Cells. *Cell* 2015; **162**: 552-63.
335. Diehl FF, Lewis CA, Fiske BP, Vander Heiden MG. Cellular redox state constrains serine synthesis and nucleotide production to impact cell proliferation. *Nat Metab* 2019; **1**: 861-7.
336. Sullivan LB, Luengo A, Danai LV *et al.* Aspartate is an endogenous metabolic limitation for tumour growth. *Nat Cell Biol* 2018; **20**: 782-8.
337. Hochachka PW, Owen TG, Allen JF, Whittow GC. Multiple end products of anaerobiosis in diving vertebrates. *Comp Biochem Physiol B* 1975; **50**: 17-22.
338. Spinelli JB, Rosen PC, Sprenger HG *et al.* Fumarate is a terminal electron acceptor in the mammalian electron transport chain. *Science* 2021; **374**: 1227-37.
339. Stone J, van Driel D, Valter K, Rees S, Provis J. The locations of mitochondria in mammalian photoreceptors: relation to retinal vasculature. *Brain Res* 2008; **1189**: 58-69.
340. Linton JD, Holzhausen LC, Babai N *et al.* Flow of energy in the outer retina in darkness and in light. *Proc Natl Acad Sci U S A* 2010; **107**: 8599-604.
341. LaVail MM. Kinetics of rod outer segment renewal in the developing mouse retina. *J Cell Biol* 1973; **58**: 650-61.